UNIVERSITÀ DEGLI STUDI DI SASSARI

SCUOLA DI DOTTORATO IN SCIENZE E TECNOLOGIE CHIMICHE
INDIRIZZO: SCIENZE FARMACEUTICHE
CICLO XXVIII

Polysaccharides as Drug Delivery Systems for different Administration Routes

Andrea Salis

Tutor:

Prof. Paolo Giunchedi

Direttore della Scuola di Dottorato:

Prof. Stefano Enzo

Anno Accademico 2014/2015

CONTENTS:

ABSTRACT

Polysaccharides are biocompatible and biodegradable long carbohydrate molecules organized in repeated monosaccharide units interconnected with glycosidic bonds. These polymers constitute a large source of biomaterials for drug vehicles, controlled drug delivery, tissue engineering etc.

The ionic character and the presence of reactive functional group led them to be good candidates for the development of controlled release formulations. They are well tolerated by living tissues and body cavities due to their biocompatibility and biodegradability. In fact, polysaccharides have been widely proposed as drug delivery devices for many administration routes such as oral, parenteral, ophthalmic, nasal and transdermal route.

Furthermore, polysaccharides can be considered appropriate for tissue engineering thanks to their mechanical and biochemical functions and ability to deliver and foster cells.

The aim of the present work was the development of polysaccharides based platform formulations suitable for the delivery of drugs into specific anatomical districts.

Self-emulsifying pellets can be considered a multiple unit dosage form capable of transferring a lipophilic drug in the gastric fluids dissolved in fine oil droplets. The combined advantages of this composite formulation are improved stability and absorption of lipophilic drugs, lower dose dumping in gastric transit time tank to a smother movement in the gastrointestinal track. Self-emulsifying mixtures (oil/surfactant/drug), in the form of o/w emulsions, consisting of caprylic/capric triglyceride, and three Cremophors (ELP, RH40, and RH60) at 1.5 and 2.3 weight ratios, and two drugs (furosemide and propranolol) of different lipophilicity were prepared and used as wetting liquids for the preparation of microcrystalline cellulose (MCC) pellets.

Properties of emulsions such as droplet size, zeta potential (ζ),viscosity and evaluation of reconstituted emulsions were determined. Furthermore, the characteristics of pellets such as pellet size, shape, friability, tensile strength, disintegration, and drug migration in pellets were evaluated.

An experimental factorial design and 3-way ANOVA was performed in order to assess the effect of drug, surfactant and oil/surfactant ratio on the above-mentioned properties of emulsions and pellets.

The results of these studies revealed that the 3 factors affected droplet size, viscosity and ζ of emulsions and size, shape, and friability of MCC pellets. Drug migration was more evident for the less lipophilic drug (furosemide) and lower oil/surfactant ratio.

Hepatocellular carcinoma (HCC) is a high chemoresistant tumour and localized anticancer therapies play a key role inthe treatment of advanced stages of HCC. Among them, transarterial embolization (TAE) implies the injection of embolic materials in the artery feeding the tumour, which results in ischemia and subsequent tumour necrosis.

Indocyanine green (ICG) loaded chitosan/glycerophosphate (C/GP) thermogelling solutions were prepared with the aim to develop a new platform for the imaging and loco-regional treatment of HCC. ICG was incorporated in these formulations in order to evaluate their potential for the detection of tumours by fluorescence. The technological properties of these systems such as gel formation, gelling time, injectability, gel strength, gelling temperature, biodegradability and in vitro dye release studies were assessed. Ex vivo embolization studies were carried out for a preliminary embolic evaluation by using an isolated bovine liver.

It was detected an increase of gel strengths and gelation rate for formulations with higher cross-link density between C and GP. These behaviours are unexpectedly more evident for C/GP solutions where a gel-like precipitation at 4°C occurred. Solutions with the lowest cross-link density between C and GP were more injectable thanks to a lower resistance to flow. Dye loading did not affect the hydrogel properties. The release of ICG from all C/GP systems analysed was not significant due to a strong electrostatic interaction between C and ICG. Ex vivo studies showed the fast gelation of these formulations in correspondence of the injected site. In conclusion, ICG-loaded C/GP thermo sensitive solutions have the potential for loco regional treatment of HCC following intraoperative fluorescence detection and resection of tumour nodules.

Antiretroviral therapy against HIV infection shows limited efficacy due to poor bioavailability of the corresponding drugs, such as zidovudine (AZT), at HIV reservoir sites. This drawback is quite evident in cerebrospinal fluid (CSF) subarachnoid spaces where macrophages are the only site of HIV replication in the brain. The rationale is that the active efflux transporters extrude zidovudine from the central nervous system (CNS) and macrophages. The prodrug called UDCA-AZT made with the conjugation of AZT to ursodeoxycholic, previously synthesized by our research group, is able to elude the AET systems. Chitosan chloride-based microparticles (CP) loaded with UDCA-AZT were developed for the nasal administration of this molecule as a potential strategy to enhance its uptake into the CNS. This formulation was characterized in terms of size, morphology, density, water uptake and the dissolution rate of UDCA-AZT. In addition, the CP sample was administered to rats via the nasal route. Drug release studies showed the capability of this formulation to release the drug in a relatively short time. Thus, a rapid absorption of the

prodrug after the nasal administration of the CP can be potentially achieved. In vivo studies demonstrated that nasal administration of UDCA-AZT loaded CP microparticles produced detectable amount of this prodrug in the CSF of the rats that could be sufficient to achieve an anti-HIV activity.

Iron excess is considered a key factor in the etiology of neurological disorders, cancer, stroke, muscle diseases, and aging. This toxicity is the consequence of the release of reactive oxygen species (ROS) whose are responsible of oxidative damage to various cell components such as lipid membranes, DNA, and proteins. Iron dysregulation can be overcame using iron chelators such as deferoxamine (DFO). Nevertheless, DFO displays reduced absorption in the gut and short plasma half-life. DFO loaded chitosan/alginate hydrogels were developed with the aim to overcome DFO limitations by using prolonged delivery systems. DFO loaded hydrogel alone or composite systems of chitosan/alginate hydrogels and DFO loaded poly(d,l-lactide-co-glycolide) microspheres were investigated in vitro. The influence of the preparation methods on the performance of composite hydrogels on controlled DFO release was assessed. Among the formulations studied, only the composite hydrogels were able to sustain the release of DFO. In particular, it was observed that the inclusion of microspheres into pre-formed chitosan/alginate hydrogel led to the best platform for the release of this iron chelator: DFO released from microspheres is strongly entrapped in the hydrogel network and, consequently, it is slowly released from the gel matrix by diffusion.

Ocular infections from Gram-positive and Gram-negative bacteria are commonly treated with topical eye drops loaded with ciprofloxacin. This type of formulation displays some drawbacks such as the rapid ocular clearance and frequent administrations are required. To overcome this limit, ciprofloxacin loaded chondroitin sulphate or lambda carrageenan microparticulate controlled release systems were engineered. The ionic interactions between ciprofloxacin and these polysaccharides led to coprecipitates that can act as vehicles for the sustained release of this drug after being displaced by the mediums ions. Technological parameters such as drug and polymer concentration, use of surfactant (kind and concentration), temperature and stirring of the solutions were evaluated in order to achieve coprecipitates with a particle size suitable for ophtalmic administration. In addition, mucoadhesion tests were performed on the leader formulations in order to understand if these systems are capable to be retained in the precornal region. Chondroitin sulphate coprecipitates exhibited the best properties in terms of particle size and mucoadhesivity, in particular with the use of surfactants during the process of preparation of these formulations.

INTRODUCTION

Biomaterials are considered biocompatible resources with the ability to interact with biological systems to evaluate, treat, augment or replace any function, tissue or organ of the body [1].

Polysaccharides are well-known carbohydrate polymers that constitute one of the most abundant supply of biomaterials for drug vehicles, controlled drug delivery, tissue engineering etc.

Polysaccharides have several natural resources from microbial, algal, plant and human origin [2].

The based-molecular structure is composed of one or more monosaccharide repeated units interconnected with o-glycosidic bonds. The backbone can be composed of only one kind of repeating monosaccharide, named homopolysaccharides or homoglycans (e.g. starch, cellulose), or formed by two or more different monomeric units, named heteropolysaccharides or heteroglycans (e.g. agar, alginate, carrageenan).

The general formula is $Cx(H2O)y$ where $200 \leq x \leq 2500$. Taking into account that the repeating units in the polymer backbone are usually monosaccharides with six carbons, the general formula can also be symbolized as $(C6H10O5)n$ where $40 \leq n \leq 3000$.

Polysaccharides possess linear or branched chains with the presence of reactive moieties such as hydroxyl, amino, and carboxylic acid groups. The presence of this reactive functional group indicates the prospect for chemical modifications [3]. Molecular weight range of this class of polymeric materials is from hundreds to thousands of Daltons [3].

Polysaccharides are widely applied in the drug delivery field due to their following merits:

1) they can be isolated in a well defined and reproducible way from natural sources including plants, animals, and microorganisms [4];

2) they are biocompatible and biodegradable due to their biochemical similarity with human extracellular matrix components. In particular, they can be immediately recognized and accepted by the human body with low immunogenic properties and they can go through enzymatic and/or hydrolytic degradation into non-toxic compounds [5]

3) they are capable of chemical and enzymatic modifications to give origin to different derivatives potentially suitable as drug delivery systems [6];

4) the ionic character and the presence of reactive functional group led them to be good candidates for the development of controlled release formulations;

5) ionic polysaccharides, which exhibit sensitiveness to environmental stimuli (chemical or physical), are an efficient alternative to synthetic polymers in the development of stimuli responsive drug delivery systems [7];

6) ionic polysaccharides have mucoadhesive properties [8];

7) they are capable to make conjugates and complexes with many macromolecules, such as proteins and peptides for achieving active targeting and controlled release systems [9];

8) large number of polysaccharides are capable to form interpenetrated hydrogel networks as matrices to encapsulate drugs and living cells, as biocompatible scaffolds for tissue engineering and for the controlled release of macromolecules like proteins. These hydrogels usually show physic-chemical characteristics more different from their macromolecular constituents [8,10,11].

The purpose of the present introduction is to describe five different polysaccharides that were used for the development of my thesis project.

Cellulose and derivatives

Cellulose is the most abundant compound of the cell walls of plants, bacteria, fungi and algae, which possesses a fundamental structural function. It is primary composed of glucose units interconnected with o-glycosidic bonds, organized in a fibrillary structure. This polymer shows high rigidity due to the various inter and intra-molecular hydrogen bonding between the hydroxyl groups of glucose units into elementary microfibrils which aggregate forming thick macrofibrils [12].

Cellulose presents different composition and morphology depending on the source from which it is obtained. No type of natural celluloses dissolves in common aqueous and organic solvents. The presence of hydroxyl groups in the glucose units of cellulose permits to synthesise many cellulose derivatives [13]. Among them, cellulose esters, cellulose ethers, microcrystalline cellulose, and cross-linked or graft copolymers are widely used in the pharmaceutical field as controlled drug delivery systems. Their applications include formulation of membrane controlled drug release systems or monolithic matrix systems [14]. The manufacture of membrane controlled release can be obtained by film coating with the aim to develop enteric coated dosage forms and osmotic pump delivery systems by using semi-permeable membranes [14].Monolithic matrix systems are amongst the most popular technologies for controlled drug delivery because of their simplicity of formulation, ease of manufacture, low cost, acceptance and applicability to drugs with a wide range of solubility [14].

Cellulose ethers and esters have been widely used for the development of oral sustained and controlled release dosage forms as coating agents that respond to variations in physiological environment, as matrices to enhance the bioavailability and solubility of drugs, to realise a pre-determined release profile from the final delivery system, and to increase the stability of the formulation [15].

Cellulose acetate phthalate and phthalated hydroxypropylmethyl cellulose are derivatives used as entering coating materials for the development of controlled intestinal targeting drug release formulations. Indeed, these polymers are stable in acidic conditions but soluble in a slightly alkaline environment [15].

Carboxymethyl cellulose and hydroxypropyl cellulose are considered mucoadhesive polymers applied for the delivery of drugs sublingually, orally, intravaginally, rectally, nasally and ophthalmically. Formulations made with this polymer prolongs the residence time of the drug at the site of absorption, allowing to high concentration gradient of the released compound, its protection from enzymatic degradation and enhanced absorption [16].

Typical cellulose esters used as hydrophobic matrices for sustained release of drugs (including highly water-soluble drugs) are cellulose acetate, cellulose acetate propionate, and cellulose acetate butyrate. The matrix of these polymers remain essentially intact in the GI tract while drug is released [17]. Cellulose esters are also used to construct the semi-permeable membrane of osmotic pump delivery systems. When the device is in contact with body fluids, water is able to permeate the cellulosic membrane and dissolves the osmotic agent resulting in a water activity gradient across the membrane [17].

Recently, Plackettet al. [18] have been developed nanocellulose which including cellulose nanocrystals, nanofibrilated cellulose, and bacterial cellulose as novel cellulose-based systems capable to entrap water soluble drugs and poorly water soluble drugs. These formulations exhibited long lasting drug release profile over weeks or even months.

Another important cellulose derivative is microcrystalline cellulose (MCC). MCC is a partially depolymerised cellulose obtained by treating high quality cellulose with hydrochloric acid at high temperature. MCC is one of the most important pharmaceutical excipients for pellet and tablet formulations. For example, it is used for the preparation of pellet formulations via extrusion–spheronisation process [19]. The rationale is its efficient binding properties that allow cohesiveness to a wetted mass containing MCC. In addition, its large surface area and high internal porosity permit to adsorb and retain a big amount of water, enhancing extrusion, wetted mass plasticity and

spheronisation [20]. Phase separation during extrusion or spheronisation is avoided because MCC is capable to control the movement of water through the plastic mass [21].
As a consequence of these advantages, MCC-pellets obtained via extrusion–spheronisation display good spherical shape, low friability, high density and smooth surface properties [20].
A possible explanation of the mechanism of action of MCC during extrusion–spheronisation process is reported by Dukic-Otta et al. [20]: "the MCC particles are able to retain water in a manner similar to a sponge. During extrusion these sponges are compressed, and water that is squeezed from the internal structures acts as a lubricant. After extrusion, the volume of the sponges expands and they appear dry and brittle, which facilitates the breaking of the extrudates during the initial phase of spheronisation. During the spheronisation phase, the sponges are densified due to collisions between particles and the spheronizer plate and wall, and water facilitates spheronisation of pellets".
MCC is used in the pharmaceutical industry as a diluent/binder in tablets for granulation and direct compression processes. MCC tablets display fast aqueous penetration even at low porosities, caused by breaking of the hydrogen bonds and subsequent widening of the pores [22].
MCC has also been studied as an absorption enhancer of the intranasal powder forms for peptides such as insulin [23], leuprolide and salmon calcitonin [24].
Cellulose and its derivatives have also been applied for bone tissue engineering because of their high mechanical and porous properties and osteoinductivity [5]. This polymer has structural and functional similarity with collagen, the major extra cellular matrix component of animal tissue. Several 3D porous systems of cellulose derivatives such as hydrogels, sponges, fiber matrices have been developed as scaffolds with high mechanical characteristics able to support large compressive loads.

Chitosan

Chitosan is a cationic polysaccharide composed of β-(1-4)-linked D-glucosamine and N-acetyl-D-glucosamine units obtained by partial N-deacetylation of chitin, a structural element in the exoskeleton of crustaceans and insects [25].
The cationic character of chitosan, based on its amino groups, rends it useful for the development of drug delivery systems [26]. In particular, these amino groups confer well defined properties on chitosan such as controlled drug release, mucoadhesion, in situ gelation, transfection, permeation enhancement, and efflux pump inhibitory properties [26]. Chitosans have been used to engineer

drug vehicles for various administration routes such as oral, buccal, nasal, transdermal, parenteral, vaginal, cervical, intrauterine and rectal [27]. These drug carriers include membranes, sponges, hydrogels, rods, nanoparticles and microspheres [27].

The controlled drug release properties of chitosan are mainly based on retardation mediated by ionic interactions [26]. At this point, chitosan is the best choice for sustained anionic drugs release. Anionic drugs such as naproxen [28], enoxaparin [29], indomethacin [30] etc., can interact with chitosan resulting in cross-linking between chitosan molecules and prolonged release profile.

In addition, polyanion polymers and/or multivalent inorganic anions were used to make polyelectrolyte complexes with chitosan as excipients in drug delivery systems [31]. Polyanions such as alginate, carrageenan, pectin, xantan gum, hyaluronic acid, gelatine, polymethacrylate copolymer, tripolyphosphate, exhibit favourable physicochemical properties with preservation of biocompatible characteristics of chitosan. Furthermore, drugs incorporated in these complexes are released in a sustained manner by diffusion and erosion processes [26,31].

Chitosan exhibits mucoadhesive characteristics due to the ionic interactions between the cationic amino groups of this polymer and the anionic substructures of the mucus gel layer. Better mucoadhesion was observed for chitosans with high-molecular weight (approximately 1400 kDa) [32]. These properties were used to improve the bioavailability of drugs such as amoxicillin, diclofenac sodium, nifedipine, buserelin as well as protein and peptides [32]. The muco-adhesion of chitosan is negatively influenced if it is used to formulate polyelectrolyte complexes because the ionic interactions between chitosan and mucus are in this way limited [33]. Several strategies have been proposed to improve the muco-adhesion properties of chitosan. For instance, Jintapattanakit et al. [34] developed trimethyl chitosan nanocomplexes exhibiting more cationic character compared to chitosan alone.

The major issue concerning the applicability of chitosan formulations is the impossibility of maintaining chitosan in solution up to physiological pH due to its pKa(~6.3). Above a pH of 6, chitosan has no charge and forms a gel-like precipitate [35]. Chenite and co-workers [35] developed a thermosensitive neutral aqueous solution based on chitosan/glycerophosphate which exhibit sol-gel transition around body temperature. They found that the addition of polyol salts, such as glycerophosphate, leads to the transformation of purely pH-dependent chitosan solutions into thermally sensitive pH-dependent solutions, without any chemical modification or crosslink. In the presence of glycerophosphate, chitosan solutions remain liquid below room temperature, even with pH values within a physiologically acceptable neutral range from 6.8 to 7.2 [35]. These nearly

neutral chitosan/glycerophosphate aqueous solutions gel when heated [36] (Chenite et al.2001). The neutralization behaviour of glycerophosphate is the main characteristic which determines chitosan/glycerophosphate solubility and phase transition phenomena. Glycerophosphate presents a mild alkalinity (pKa about 6.34) providing correct buffering without inducing immediate precipitation or gelation when the temperature provided is between 4 and 15ºC [36]. These properties indicate the ability of this liquid chitosan-based material of gelling within the desired tissue or body cavity in response to body temperature. Consequently a degradable gel implant in situ is formed [37]. Chitosan/glycerophosphate hydrogels are adapted to the delivery of drugs protecting them from hostile environments and controlling the release profile. In vitro release experiments revealed that these systems could deliver macromolecules and poor-water soluble drugs over a period of several hours to a few days [38]. Recently, it was also proposed to use these thermosensitive hydrogels for the local administration of paclitaxel at tumour resection sites to prevent local tumour recurrence [39].

Chitosan is also considered a polymer with transfection enhancing properties [26]. Non-viral vectors of chitosan have been engineered for the delivery of DNA and siRNA exploiting the ionic interaction between the cationic amino groups of chitosan and these polyanionic molecules that lead to the spontaneous formation of nanoparticles [40]. The variation of formulation parameters such as the molecular weight (Mw) of chitosan, degree of deacetylation (DD), stoichiometry of the chitosan/DNA complex (N/P ratio, charge ratio of amine (chitosan) to phosphate (DNA)), plasmid concentration, serum concentration, pH of the transfection medium, cell type affect the affinity between chitosan and DNA, size, cell uptake and release of the chitosan/DNA complex as well as their transfection efficiency [40]. The clinical application of these chitosan-based complexes was not recommended due to a low transfection efficiency of the conventional chitosan [26,40]. On the contrary, the use of thiolated chitosan and the trimethylation of amino groups led to plasmidic nanoparticles with a higher transfection rate [41].

The cationic amino groups of chitosan give permeation enhancing properties to this polymer. In particolar, thi polymer is able to improve absorption of hydrophilic and hydrophobic drugs through monostratified and pluristratified epithelia of intestine, nose, vagina and cornea mucosae that are rich in tight junctions [42]. The permeation enhancing result of chitosan is due to a transient widening of the junctions between cells [43]. The efficacy of chitosan as penetration enhancer is limited to its insolubility at pH > 6. The synthesis of partially quaternized derivative N-trimethyl chitosan chloride led to more efficient penetration enhancement properties opening the tight

junctions between cells and favouring the paracellular transport of hydrophilic and hydrophobic drugs [43].

Chitosan belongs to the family of polysaccharide with colon targeting properties thanks to its preservation in the stomach and small intestine and degradation in the colon by the bacterial flora. Thus, it was proposed as coating agent for tablets [26].

Taking into account all the above-mentioned properties chitosan-based drug vehicles for various administration routes were developed. Oral drug delivery formulations were prepared in the form of microspheres for the delivery of amoxicillin and diclofenac sodium to the gastric and intestinal region respectively [44,45]. Takeuchi et al. [46] developed insulin-loaded liposomes coated with chitosan to increase the enteral absorption of insulin exploiting the muco-adhesion properties of chitosan. Lueßen et al. [33] used a chitosan hydrochloride solution to improve the bioavailability of buserelin in the duodenum taking advantage of the intestinal transport-enhancing effect of chitosan. Chitosan glutamate was used as coating agent for pellets and tablets exhibiting swelling and permeability characteristics, which were dependent on pH and on the concentration of the crosslinking agent [43]. A vesicle system composed of palmitoyl glycol-chitosan was developed for gene delivery and as a system for oral delivery of proteins and peptides [47]. Colon-specific insulin delivery was obtained through capsules coated with chitosan that were stable in the stomach and in the small intestine but they exhibited degradation by the bacterial flora in the colon [48].

Chitosan is considered a good material for the development of ocular drug delivery systems thanks to its permeation enhancing properties. Chitosan-based in situ gelling systems were developed by Gupta et al. [49] with the aim to improve the retention and biodistribution of drugs applied topically onto the eye [26]. Chitosan-based nanoparticles loaded with cyclosporine A [50] and chitosan-based microparticles loaded with acyclovir [51] were prepared in order to improve the delivery of these drugs to the ocular mucosa.

The mucoadhesive and permeation enhancer properties of chitosan were considered for the development of nasal drug delivery carriers such as nanoparticles for the delivery of insulin [52], spray solutions loaded with fentanyl [53] and in situ gelling thermosensitive solutions [26].

Chitosan highly purified and with low molecular weight, was also used for the development of injectable preparations for the controller delivery of drugs. For instance, Kim et al. [54] prepared chitosan-based nanoparticles for the delivery of RGD peptide (Arg-Gly-Asp) to improve the antitumoral activity of this peptide intravenously. Ouchi et al. [55] developed a macromolecular system consisted of chitosan conjugated to 5-fluorouracil that was able to induce growth-inhibitory

effects on Met-A fibrosarcoma and MH-134Y hepatoma. Furthermore, the 5FU side effects were drastically reduced.

Alginates

Alginates or alginic acids, are polysaccharides isolated from brown seaweed and marine algae.
These compounds are linear unbranched copolymers consisted of homopolymeric blocks of (1,4)-linked β-D-mannuronic acid and α-L-guluronic acid, which are linked together, by covalent bonds, in different blocks [56]. This type of polymer is considered a biomaterial with excellent biocompatibility and non-immunogenicity. Alginates have been proposed as stabilizers in emulsions, suspending agents, binders and disintegrants in tablets [14]. A critical property is its gelling behaviour: the carboxylic groups of two guluronic blocks of adjacent polymer chains can be cross-linked with multivalent cations, such as Ca2+, allowing to the formation of a gel network [56]. The gelling ability of alginates depends on their selective cation binding. Hydrogels with high gel strength can be achieved from alginates with high content of guluronic acid residues [57].
The gelling properties of alginates were widely employed in the preparations of drug delivery systems such as beads, nanoparticles, microparticles, pellets, films and matrices able to encapsulate various substances [14].
Alginate has been applied in oral dosage forms. In particular, sodium alginate is a well known tablet binding agent, while alginic acid is considered a tablet disintegrant for immediate drug release tablets [57]. The suitability of alginates as oral dosage forms derives from the ability of this polymer to create a hydrocolloidal layer under hydration. This layer exhibits high viscosity making a diffusion barrier able to control the release of drugs. For this reason, alginate has been used for the preparation of gel capsules microspheres and tablets. Joseph et al. [58] developed capsules incorporating indomethacin. The release of the drug was controlled by the alginate-based encapsulating membrane following zero-order kinetics. In the case of microspheres and tablets, the drug is dispersed in the alginate-based matrix. The release of the drug depends on “diffusion through matrix swelling and dissolution/erosion at the matrix periphery” [57]. Drug release is more prolonged for high concentrations of alginate and when its guluronic content is predominant due to the formation of gels with high strength in which the swelling and erosion processes are less evident [59]. In the case of selective interactions between drug and alginate residues, higher content of the residue that interact with the drug lead to a more sustained release [60]. The drug release profile is also influenced by the type of cross-linker. For instance, Takka e al. [61] demonstrated that Ca2+

alginate beads exhibited more prolonged release compared to those prepared by using cross-link agents such as Ba2+ and Sr2+.

The release of drugs from alginate-based marices can be also modulated by using other cross-linking agents such as glutarladehyde or by using combination of alginates with other polymers [57]. Murata et al. [62] developed alginate beads coated with chitosan by strong ionic interaction between these polymers. The gel matrix erosion was markedly delayed due to the formation of the strong complex chitosan-alginate. Chitosan-alginate beads loaded with diclofenac were prepared by Fernandez-Hervas and co-workers [63]. It was demonstrated that a complex between both polymers subsisted in a gel form at low pH due to the protonation of chitosan in acid conditions. The release profile was dependent on the pH conditions and on the degree of cross-linking between chitosan and alginate. At neutral pH, the gel swells and a prolonged release of the drug is achieved by slow disintegration of this gel complex. Alginate-based matrices were also used for the preparation of compressed tablets. The release of both hydrophilic and hydrophobic drugs is influenced by the creation of a hydrated viscous layer surrounding the tablet. This layer is a sort of barrier avoiding the penetration of water into the matrix and the leakage of solutes [57].

An in situ forming hydrogel of sodium alginate for oral administration of theofilline was suggested by Miyazaki et al [64]. The in situ gelation was achieved by the sequential administration of two solutions, the first containing the polymer and the second containing Ca2+ions. The bioavailability of the drug was higher compare to conventional theofilline-based formulations.

In-situ-forming ophthalmic drug delivery systems prepared from alginates without the addition on ionic cross-linker were developed by Cohen et al. [65] An aqueous solution of sodium alginate loaded with pilocarpine nitrate was able to gel in the eye with a longer precorneal residence time compared to conventional liquid ophthalmic formulations. As a consequence, an increase of ocular bioavailability and duration of the pilocarpine action were achieved. The best results in terms of gelling time and sustained release were observed for alginates with high contents of guluronic residues.

Another important characteristic of alginate is the ability to incorporate biomacromolecules thanks to the following reasons:

- no use of organic solvents during the gelation process [57];
- controlled released due to the porous structure of alginate-based gels [66];
- stability of alginate-based gels in the temperature range from 0 to 100°C, allowing sterilization [67];

- biocompatibility and low immunogenicity [57].

For these reasons, many proteins have been encapsulated in beads consisted of alginate matrices. Promising results were also observed for oral and nasal administrations of antigens, DNA and cells[57].

Alginate-based gels are also able to incorporate other types of formulations. For istance, Josef et al [68] developed alginate hydrogels incorporating an o/w emulsion. The emulsion was suitable for the delivery of hydrophobic drugs, while the gel matrix was useful to achieve a sustained drug release profile.

Carrageenan

Carrageenan (CG) are sulphated polysaccharides isolated from red seaweeds and composed of D-galactose and 3,6-anhydro-D-galactose units linked together by glycosidic bonds [69.]. These residues are generally substituted with ester sulphates which are neutralized by cations, such as Na+, K+ and Ca2+. The major varieties of CGs are κ, λ- and τ-CG, which differs from the number and position of sulphate groups. The κ , λ-, and τ-CG dimers have one, two and three sulphate ester groups, respectively [70]. Furthermore, 3, 6-anhydro bridges are present only in κ- and τ-CG. These differences affects the properties of CGs, such as solubility temperature and gel strength [69]. Indeed, κ-CG can be dissolved in hot water, while λ-CG is soluble in hot and cold water [71]. The presence of 3, 6-anhydro bridges confers gelling properties on CGs.

As a consequence, κ- and τ-CG are able to form brittle gels and softer ones, respectively. On the contrary λ-CG cannot form gels due to the lack of 3, 6-anhydro bridges [72]. The gel formation of these CGs occurs in a two step process. At high temperatures, the CGs chains exist as random coils and upon cooling, a coil-to-helix transition takes place. Then, these helices start to aggregate in double helices in which sulphate groups are positioned outside of the helices. The gel network is composed of three dimensional double helices stabilised by hydrogen bonds between the two chains [73].

CGs are widely employed in the field of pharmaceutical technology with the aim to (1) improve drug formulation, (2) to develop prolonged drug release systems and (3) to create pH-/temperature-sensitive delivery systems, which respond to physiological environmental stimuli [72].

CG-based tablets were developed for the oral administration of drugs thanks to the appropriate properties of these polymers such as high molecular weight, high viscosity and gelling. Tablets can be prepared with a unique matrix composed of CG. When the water come in contact with this type

of matrix, its outer layer swells and become a gel layer or a viscous one, depending on the type of CG. The gel/viscous layer is able to control the release of the loaded drug with a marked resistance to erosion [74]. Furthermore, the type of CG influences the release rate. Ghanam et al. [75] demonstrated that κ-CG-based tablets had faster erosion compared to the same formulations prepared with the other two CG. In addition, the degree of water-uptake is affected by the number of sulphate groups on CGs: λ> τ> κ [76]. Prolonged drug release tablets were also obtained combining different types of CGs. Tripelennamine-HCL-loaded tablets made with equal amounts of λ-CG and τ-CG exhibited a near-zero-order release profile [77].

Tablets composed of a polymer mixture of CG and other types of polymers such as hydroxypropyl cellulose [78], hydroxypropyl methyl cellulose [79] were engineered in order to adjust drug release profiles.

CGs are able to form polyelectrolyte complexes with positively charged polymers such as chitosan. For instance, Li et al. [80] developed chitosan-CGs-based tablets that were capable to form an in situ polyelectrolyte film in the simulated intestinal fluid and this film could further control drug release.

Taking into consideration the above-mentioned capacity of CGs to interact with positive charged compounds, many researchers applied this property for the development of CGs-based formulations loaded with a positive charged drug. Among them, Bonferoni et al. [81] observed that λ-CG was able to prolong the release of salbutamol sulphate independently of the pH of the dissolution medium.

Polyelectrolyte complexes formed by CGs and chitosan were also used for the development of capsules, beads and nanoparticles in order to improve the controlled or prolonged release of drugs. The rationale of the preparation of beads with CGs is the thermo reversibility of the gel network and the adequate viscoelastic properties of these polymers [69]. For instance, Tomida et al. [82] prepared κ-CG-chitosan beads evaluating the release of theophylline as a model drug. It was observed that this drug displayed a zero-order release profile. Polyelectrolyte complex beads based on chitosan and CG have been also employed as a controlled release platform for colon-specific delivery of sodium diclofenac [83]. It was demonstrated that the release of this drug was slow in pH 1.2 and pH 6.8 fluids but much higher in pH 7.4.

Pinheiro et al.[84] engineered nanoparticles based on polyelectrolyte complex based on chitosan and CG as a potential platform either for the controlled release of drugs and for tissue engineering.

These nanoparticles displayed non cytotoxicity in L929 fibroblasts, and a controlled release for up to 3 weeks with ovalbumin, as a model protein,was observed.

CGs were also employed for the preparation of pellets by extrusion/spheronization process. It was observed that κ-CG could be used as an extrusion aid due to its elastic and brittle properties [69]. κ-CG-based pellets exhibited lower tensile strength, faster disintegration and drug release compared to pellets prepared with microcrystalline cellulose. Furthermore, the release profile of κ-CG-based pellets is less influenced by the drug's solubility [85]. Thus, κ-CG-based pellets could be considered a useful approach to surmount the bioavailability deficiency of poorly soluble drugs. Neverthless, considering the fast disintegration of these pellets, an adequate coating is necessary to obtain a sustained release [69].

Another important application of CGs is in the field of microspheres as delivery systems of drugs in a controlled and targeted manner. An important contribution in this field was performed by Bonferoni and coworkers [85], which developed λ-CG-gelatin-based microspheres loaded with timolol maleate for the ocular route, taking into consideration the adequate properties of CGs such as gelling, film forming and mucoadhesive ones. The results showed high timolol maleate concentration and bioavailability in the aqueous humour and a more efficient alternative to commercial formulations.

As previously reported, CGs such as κ-CG and τ-CG are able to gel. This property is widely used for the development of sustained delivery systems for various administration route. Miyazaki et al. [86] proposed a τ-CG gel for the oral delivery of drugs to dysphagic patients. CG-based hydrogel loaded with microbicides were developed by Li et al.[87] for vaginal administration.

Many researchers focus their attention on the utilization of gelling CGs added to other polymers in order to improve the controlled-release profiles of gels composed solely from conventional polymers. For instance, κ-CG-agarose-based hydrogels were able to decrease the release of drugs due to an increase of gel strength compared to agarose gels [88].

Starch-CG-based gels were prepared by Lefnaoui et al. [89] to improve the prolonged buccal delivery of miconazole. In addition, gels composed of methyl cellulose and CGs were able to prolong the retention of macromolecules for transscleral delivery [90].

Chondroitin sulphate

Chondroitin sulphate (CS) is a negatively charged linear polysaccharide composed of alternate sequences of β-glucuronic acid and N-acetylgalactosamine unites, linked by β bonds,
presenting sulfates, carboxylic acid and hydroxyl moieties. It is an important component of the extracellular matrix of articular cartilage linked to the core of proteins. This linkage makes proteoglycans, which are resistant to compression stress [91]. CS is synthesised by chondrocytes and its primary function is to preserve normal cartilage activities [5]. In particular, CS gives
cushioning properties to the cartilage by retaining water and acts like a lubricant at the
articulating surfaces [5]. Furthermore CS is indispensable for cartilage repair because it can synthesise the most important component of cartilage such as hyaluronan, collagen type II, and glucosamine and it is able to inhibit the enzymes involved in the degradation of extracellular matrix [5]. CS in an attractive biomaterial extracted from animal sources, which exhibit biodegradability, non-immunogenicity and non toxicity. Cs have been used for tissue engineering as well as for drug delivery or controlled drug release.

As it is reported by Doppaladupi et al. [91], "CS can bind with core protein to produce highly absorbent aggregan, which is a major structure inside cartilage and acts as a shock absorber; or, it can produce sydecan, a cell receptor that can interact with adhesion proteins, cells and the extracellular matrix".

From the delivery system's point of view, the negative charges of these polysaccharides are capable to make electrostatic interactions with positively charged polymers or drugs, allowing to the development of matrices-based hydrogels, nanoparticles and microparticles.

CS could be considered a potential carrier for colon-targeted delivery of bioactive agents. Since natural CS is water soluble, its persistence as a solid dosage form in the stomach and small intestine would not be successful. To overcome this limit, CS cross-linked with other polymers could be a better alternative decreasing CS hydrophilicity [92].

Wang et al. [93] developed hydrogels by crosslinking CS with poly(ethylene glycol) diglycidyl ether (CS-EX) or forming an interpenetrating polymer network (CS-EX-IPN). It was observed that CS-EX-IPN hydrogel exhibited better three-dimensional structures with smaller pore sizes than the CS-EX hydrogel. The release profiles of diclofenac sodium and bovine serum albumin displayed a diffusion from these platforms mechanism. Furthermore, the release for macromolecular drugs is more sustained than small molecular drugs. Jensen and co-workers [94] prepared CS-based hydrogels for the electro-controlled delivery of peptides and proteins. The negative charges of CS

allow loading efficiently proteins and peptides positively charged. Moreover, drug loading and the electrically-stimulated drug release were influenced by the size of the compound.
An interesting approach for targeting orally administered drugs to the colon was proposed by Amrutkar et al. [95]. Matrix tablets were obtained by forming a polyelectrolyte complex between chitosan and CS. Selective delivery of indomethacin to the colon was achieved and the release profile was influenced by time of cross-linking and concentration of the polymers used.
Chitosan-CS polyelectrolyte complex was also exploited for the development of microcapsules loaded with the anti-cancer drug 5-fluorouracil [96]. The drug release was affected by the degree of crosslinking. the release of 5-fluorouracil was lower for higher cross-link density due to a decrease of the swelling ability of the matrix.
Furthermore, Yeh et al. [97] prepared nanoparticles by using this chitosan-CS polyelectrolyte complex. This systems showed high degree of cross-linking and it was able to incorporate proteins and peptides. Cellular uptake studies performed on Caco-2 and HEK-293 cells showed edndocytose of these nanoparticles into the cells. As a consequence, the developed nanocarrier had the potential to deliver hydrophilic compounds such as vaccines.

On the basis of the multiple advantages and versatility of the above mentioned polysaccharides as materials for the preparation of pharmaceutical carriers, the aim of the present work was the development of polysaccharides-based platform formulations as novel and suitable delivery systems of specific drugs into determined anatomical districts.

References:

1. Nair LS, Laurencin CT. Polymers as Biomaterials for Tissue Engineering and Controlled Drug Delivery. Adv BiochemEngin Biotechnol. 2006;102:47–90.
2. Liu Z, Jiao Y, Wang Y, Zhou C, Zhang Z. Polysaccharides-based nanoparticles as drug delivery systems. Adv Drug Deliv Rev. 2008;60:1650–62.
3. Saravanakumar G, Jo DG, Park .H. Polysaccharide based nanoparticles: A versatile Platform for Drug Delivery and Biomedical Imaging. Curr Med Chem. 2012;19:3212–9
4. Pawar HA, Kamat SR, Choudhary PD. An Overview of Natural Polysaccharides as Biological Macromolecules: Their Chemical Modifications and Pharmaceutical Applications. Biol Med. 2015;7:1.
5. Shelke NB, James R, Laurencin CT, Kumbar SG. Polysaccharide biomaterials for drug deliveryand regenerative engineering. Polym Adv Technol. 2014;25:448–60.
6. Tian H, Tang Z, Zhuang X, Chen X, Jing X. Biodegradable synthetic polymers: Preparation, functionalization and biomedical application Prog Polym Sci. 2012;37:237–80.
7. Posocco B, Dreussi E, de Santa J, Toffoli G, Abrami M, Musiani F, Grassi M, Farra R, Tonon F, Grassi G, Dapas B. Materials. 2015;8:2569-615.
8. Kontogiorgos V, Smith AM, Morris GA. The parallel lives of polysaccharides in food and pharmaceutical formulations. Curr Opin Food Sci. 2015;4:13–8.
9. Reyes-Ortega F, Parra-Ruiz FJ, Averick SE, Rodríguez G, Aguilar MR, Matyjaszewski K, San Román J. Smart heparin-based bioconjugates synthesized by a combination of ATRP and click chemistry. Polym Chem. 2013;4:2800-14.
10. Coviello T, Matricardi P, Marianecci C, Alhaique F. Polysaccharide hydrogels for modified release formulations.J Control Release. 2007,119:5–24
11. Matricardia P, Di Meoa C, Covielloa T, Henninkb WE, Alhaique F. Interpenetrating Polymer Networks polysaccharide hydrogels for drug delivery and tissue engineering. Adv Drug Deliver Rev. 2013;65:1172–87.
12. Ding SY, Liu YS, Zeng Y, Himmel ME, Baker JO, Bayer EA. How does plant cell wall nanoscale architecture correlate with enzymatic digestibility? Science. 2012;338:1055–60.
13. Heinze,T, Petzold-Welcke K.(2012).Recent advances in cellulose chemistry. In Y.Habibi, & L. Lucia (Eds.), Polysaccharide building blocks: A sustainable approach to the development of renewable biomaterials (pp.1–50). John Wiley & SonsInc.

14. Beneke CE, Viljoen AM, Hamman JH. Polymeric Plant-derived Excipients in Drug Delivery. Molecules. 2009;14:2602-20.
15. Liu J, Willför S, Xu C. A review of bioactive plant polysaccharides: Biological activities, functionalization, and biomedical applications. Bioactive Carbohydrates and Dietary Fibre 2015;5:31–61.
16. Karolewicz B. A review of polymers as multifunctional excipients in drug dosage form technology. Saudi Pharm J. Available online 7 March 2015.
17. Edgar KJ, Buchanan CM, Debenham JS, Rundquist PA, Seiler BD, Shelton MC, Tindall D. Advances in cellulose ester performance and application. Prog. Polym. Sci. 2001;26:1605-85.
18. Plackett DV, Letchford K, Jackson JK, Burt HM. A review of nanocellulose as a novel vehicle for drug delivery. Nord Pulp Pap Res J. 2014; 29:105–18
19. Newton JM. Extrusion and extruders J. Swarbrick, J.C. Boylan (Eds.), Encyclopedia of Pharmaceutical Technology, Marcel Dekker Inc., New York and Basel (2002), pp. 1220–1236
20. Dukić-Otta A, Thommesb M, Remona JP, Kleinebuddeb P, Vervaeta C. Production of pellets via extrusion–spheronisation without the incorporation of microcrystalline cellulose: A critical review. Eur J Pharms Biopharm, 2009;71:38–46.
21. Fielden KE, Newton JM, Rowe RC. The influence of lactose particle size on spheronization of extrudate processed by a ram extruder. Int. J. Pharm. 1992;81:205–24
22. Lerk CF, Bolhuis GK, de Boer AH. Effect of Microcrystalline Cellulose on Liquid Penetration in and Disintegration of Directly Compressed Tablets. J Pharm Sci. 1979;68:205-11.
23. Nagai T, Nishimoto Y, Nambu N, Suzuki Y, Sekine K. Powder dosage form of insulin for nasal administration. J Control Release. 1984;1:15–22.
24. Suzuki Y, Makino Y. Mucosal drug delivery usingcellulose derivatives as a functional polymer. J Control Release 1999;62:101–7.
25. Bhattarai N, Gunn J, Zhang M. Chitosan-based hydrogels for controlled, localized drug delivery. Adv Drug Deliv Rev. 2010;62:83–99.
26. Bernkop-Schnürch A, Dünnhaupt S. Chitosan-based drug delivery systems. Eur J Pharm Biopharm. 2012;81:463–9.

27. Denkbas EB, Ottenbrite RM. Perspectives on: Chitosan Drug Delivery Systems Based on their Geometries J Bioact Compat Polym. 2006;21:351-68.
28. Bhise K, Dhumal R, Paradkar A, Kadam S. Effect of drying methods on swelling, erosion and drug release from chitosan–naproxen sodium complexes, AAPS Pharm Sci Tech. 2008;9:1–12.
29. Sun W, Mao S, Wang Y, Junyaprasert VB, Zhang T, Na L, Wang J. Bioadhesion and oral absorption of enoxaparin nanocomplexes, Int J Pharm. 2010;386:275–81.
30. Mi FL, Sung HW, Shyu SS. Release of indomethacin from a novel chitosan microsphere prepared by a naturally occurring crosslinker: Examination of crosslinking and polycation–anionic drug interaction. J Appl Polym Sci. 2001;81:1700–11.
31. Hamman JH. Chitosan Based Polyelectrolyte Complexes as Potential Carrier Materials in Drug Delivery Systems. Mar Drugs. 2010;8:1305-22.
32. Dodane V, Vilivalam VD. Pharmaceutical applications of chitosan. Pharm Sci Technol Today. 1998;1:246–53.
33. Lueßen HL, de Leeuw BJ, Langemeÿer MWE, de Boer AG, Verhoef JC, Junginger HE. Mucoadhesive polymers in peroral peptide drug delivery. VI. Carbomer and chitosan improve the intestinal absorption of the peptide drug buserelin in vivo. Pharm Res. 199613:1668–72.
34. Jintapattanakit A, Junyaprasert VB, Kissel T. The role of mucoadhesion of trimethyl chitosan and PEGylated trimethyl chitosan nanocomplexes in insulin uptake. J Pharm Sci. 2009;98:4818–30.
35. Chenite A, Chaput C, Wand D, Combes C, Bushmann MD, Hoemann CD, Leroux JC, Atkinson BL, Binette F, Selmani A, Novel injectable neutral solutions of biodegradable gels in situ. Biomaterials. 2000;1:155-61.
36. Chenite A, Buschmann M, Wang D, Chaput C, Kandani N. Rheological characterisation of thermogelling chitosan / glycerol-phosphate solutions. Carbohyd Polym. 2001;46:39–47
37. Chenite A, Chaput C, Combes C, Jalal C, Selmani A. Patent WO09907416A1 (1999).
38. Ruel-Garièpy E, Chenite A, Chaput C, Guirguis S, Leroux JC, Characterization of thermosensitive chitosan gels for the sustained delivery of drugs. Int J Pharm. 2000;203:89–98.
39. Ruel-Gariepy E, Shive M, Bichara A, Berrada M, Le Garrec D, Chenite A, Leroux JC. A thermosensitive chitosan-based hydrogel for the local delivery of paclitaxel. Eur J Pharms

Biopharm. 2004;57:53–63.

40. Mao S, Sun W, Kissel T. Chitosan-based formulations for delivery of DNA and siRNA. Adv Drug Deliv Rev. 2010;62:12–27.
41. Varkouhi AK, Verheul RJ, Schiffelers RM, Lammers T, Storm G, Hennink WE. Gene silencing activity of siRNA polyplexes based on thiolated N,N,N-trimethylated chitosan. Bioconjugate Chem. 2010;21:2339–46.
42. Sandri G, Rossi S, Bonferoni MC, Ferrari F, Zambito Y, Di Colo G., Caramella C. Buccal penetration enhancement properties of *N*-trimethyl chitosan: Influence of quaternization degree on absorption of a high molecular weight molecule. Int J Pharm. 2005;297: 146–55.
43. Dodane V, Amin Khan A, Mervin JR. Effect of chitosan on epithelial permeability and structure. Int J Pharm. 1999;182:21–32.
44. Roberts GAF, 1997. Chitosan production routes and their role in determining the structure and properties of the product. In Domard A, Roberts GAF, Varum KM (eds), Advances in Chitin Science. Volume II. Jacques André Publisher, Lyon: 22–31
45. Lorenzo-Lamosa ML, Remuñán-López C, Vila-Jato JL, Alonso MJ. Design of microencapsulated chitosan microspheres for colonic drug delivery. J Control Release 1997;52:109–18.
46. H. Takeuchi, Yamamoto H, Niwa T, Hino T, Kawashima Y. Enteral Absorption of Insulin in Rats from Mucoadhesive Chitosan-Coated Liposomes. Pharm Res. 1996;13:896–901.
47. Uchegbu IF, Schätzlein AG, Tetley L, Gray AI, Sludden J, Siddique S, Mosha E. J Pharm Pharmacol. 1998;50:453–8.
48. Tozaki H, Komoike J, Tada C, Maruyama T, Terabe A, Suzuki T, Yamamoto A, Muranishi S. Chitosan capsules for colon-specific drug delivery: improvement of insulin absorption from the rat colon. J Pharm Sci. 1997;86:1016–21.
49. Gupta H, Velpandian T, Jain S. Ion- and pH-activated novel in-situ gel system for sustained ocular drug delivery, J. Drug Targeting. 2010;18:499–505.
50. De Campos AM, Sánchez A, Alonso MJ. Chitosan nanoparticles: a new vehicle for the improvement of the delivery of drugs to the ocular surface. Application to cyclosporin A, Int J Pharm. 2001;224:159–68.
51. Genta I, Conti B, Perugini P, Pavanetto F, Spadaro A, Puglisi G. Bioadhesive microspheres for ophthalmic administration of acyclovir, J Pharm Pharmacol. 1997;49:737–42.

52. Zhang X, Zhang H, Wu Z, Wang Z, Niu H, Li C. Nasal absorption enhancement of insulin using PEG-grafted chitosan nanoparticles, Eur J Pharm Biopharm. 2008;68:526–34.
53. Fisher A, Watling M, Smith A, Knight A. Pharmacokinetic comparisons of three nasal fentanyl formulations; pectin, chitosan and chitosan–poloxamer 188. Int J Clin Pharmacol Ther. 2010;48:138–45.
54. Kim JH, Kim YS, Park K, Kang E, Lee S, Nam HY, Kim K, Park JH, Chi DY, Park RW, Kim IS, Choi K, Chan Kwon I. Self-assembled glycol chitosan nanoparticles for the sustained and prolonged delivery of antiangiogenic small peptide drugs in cancer therapy, Biomaterials 2008;29:1920–30.
55. T. Ouchi, T. Banba, H. Masuda J. Design of Chitosan-5Fu Conjugate Exhibiting Antitumor Activity. Macromol Sci-Chem A. 1991;28:959–75.
56. Augst AD, Kong HJ, Mooney DJ. Alginate Hydrogels as Biomaterials. Macromol Biosci. 2006;6:623-33.
57. Tønnesen HH, Karlsen J. Alginate in Drug Delivery Systems. Drug Dev Ind Pharm. 2002;28:621–30.
58. Joseph I; Venkataram S. Indomethacin sustained release from alginate-gelatin or pectin-gelatin coacervates. Int J Pharm. 1995;126:161–8.
59. Østberg T, Vesterhus L, Graffner C. Calcium alginate matrices for oral multiple unit administration: II. Effect of process and formulation factors on matrix properties. Int J Pharm. 93;1997:183–93.
60. Iannuccelli, V.; Coppi, G.; Cameroni, R. biodegradable intraoperative system for bone infection treatment .2. in-vivo evaluation. Int J Pharm. 1996;143:195–201.
61. Takka S, Acarturk F. Calcium alginate microparticles for oral administration : III. The effect of crosslink agents and various additive polymers on drug release and drug entrapment efficiency. Pharmazie. 1999;54:137–9.
62. Murata Y, Maeda T, Miyamoto E, Kawashima S. Preparation of chitosan-reinforced alginate gel beads — effects of chitosan on gel matrix erosion. Int J Pharm. 1993;96:139–45.
63. Fernandez-Hervas MJ, Holgado MA, Fini A, Fell JT. In vitro evaluation of alginate beads of a diclofenac salt. Int J Pharm. 1998;163:23–34.
64. Miyazaki S, Kubo W, Attwood D. Oral sustained delivery of theophylline using in-situ gelation of sodium alginate J Contr Rel. 2000;67:275–80.

65. Cohen S, Lobel E, Trevgoda A, Peled Y. A novel in situ-forming ophthalmic drug delivery system from alginates undergoing gelation in the eye J Control Release 1997;44:201–8.
66. Bhardwaj TR, Kanwar M, Lal R, Gupta A. Natural Gums and Modified Natural Gums as Sustained-Release Carriers. Drug Dev Ind Pharm. 2000;26:1025–38.
67. Daigle DJ, Cotty PJ. The Effect of Sterilization, pH, Filler and Spore Inoculum Concentration on the Preparation of Alginate Pellets. Biocontrol Sci Technol. 1997;7:3–10.
68. Joseph I; Venkataram S. Indomethacin sustained release from alginate-gelatin or pectin-gelatin coacervates. Int J Pharm. 1995;126:161–8.
69. Li L, Ni R, Shao Y, Mao S. Carrageenan and its applications in drug delivery. Carbohydr Polym. 2014;103:1–11.
70. Nanaki S, Karavas E, Kalantzi L, Bikiaris D. Miscibility study of car-rageenan blends and evaluation of their effectiveness as sustained releasecarriers. Carbohydr Polym. 2010;79:1157–67.
71. Bixler HJ. The carrageenan connection IV. Br Food J. 1994;96:12–7.
72. Liu J, Zhan X, Wan J, Wang Y, Wang C. Review for carrageenan-based pharmaceutical biomaterials: Favourable physical features versus adverse biological effects. Carbohydr Polym. 2015;121:27–36.
73. Stone AK, Nickerson MT.). Formation and functionality of whey proteinisolate-(kappa-, iota-, and lambda-type) carrageenan electrostatic complexes. Food Hydrocolloid. 2012;27:271–7.
74. Pavli M, Baumgartner S, Kos P, Kogej K. Doxazosin-carrageenan interac-tions: A novel approach for studying drug-polymer interactions and relation tocontrolled drug release. Int J Pharm. 2011;421:110–9.
75. Ghanam D, Kleinebudde P. Suitability of kappa-carrageenan pellets forthe formulation of multiparticulate tablets with modified release. Int J Pharm 2011;409:9–18.
76. Pavli M, Vrecer F, Baumgartner S. Matrix tablets based on carrageenanswith dual controlled release of doxazosin mesylate. Int J Pharm. 2010;400:15–23.
77. Hariharan M, Wheatley TA, Price JC. Controlled-release tablet matri-ces from carrageenans: Compression and dissolution studies. Pharm Dev Technol. 1997;2:383–93.
78. Nerurkar J, Jun HW, Price JC, Park MO. Controlled-release matrixtablets of ibuprofen using cellulose ethers and carrageenans: Effect of for-mulation factors on dissolution rates. Eur J Pharm Biopharm. 2005;61:56–68.

79. Bonferoni MC, Rossi S, Tamayo M, Pedraz JL, Dominguez-Gil A, Caramella C. On the employment of λ-carrageenan in a matrix system. II. Carrageenan and hydroxypropylmethylcellulose mixtures. J Control Release. 1994;30:175–82.
80. Li L, Wang L, Shao Y, Tian Y, Li C, Li Y, Mao S. Elucidation ofrelease characteristics of highly soluble drug trimetazidine hydrochloride fromchitosan-carrageenan matrix tablets. J. Pharm. Sci. 2013;102:2644–54.
81. Bonferoni MC, Rossi S, Tamayo M, Pedraz JL, Dominguez-Gil A, Caramella, C. On the employment of carrageenan in a matrix system. I. Sensitivityto dissolution medium and comparison with Na carboxymethylcellulose andxanthan gum. J Control Release. 1993;26: 119–27.
82. Tomida H, Nakamura C, Kiryu S. A novel method for the preparation of controlled-release theophylline capsules coated with a polyelectrolyte complex of κ-carrageenan and chitosan. Chem Pharm Bull (Tokyo).1994;42:979-81.
83. Piyakulawat P, Praphairaksit N, Chantarasiri N, Muangsin N. Prepa-ration and evaluation of chitosan/carrageenan beads for controlled release ofsodium diclofenac. AAPS Pharm Sci Tech. 2007;8:E1–E11.
84. Thommes M, Kleinebudde P. Use of kappa-carrageenan as alternativepelletisation aid to microcrystalline cellulose in extrusion/spheronisation. II.Influence of drug and filler type. Eur J Pharm Biopharm. 2006;63:68–75.
85. Bonferoni MC, Chetoni P, Giunchedi P, Rossi S, Ferrari F, Burgalassi S., Caramella C. Carrageenan–gelatin mucoadhesive systems for ion-exchange basedophthalmic delivery: In vitro and preliminary in vivo studies. Eur J Pharm Biopharm. 2004;57:465–72.
86. Miyazaki S, Ishitani M, Takahashi A, Shimoyama T, Itho K, Attwood D. Carrageenan gels for oral sustained delivery of acetaminophen to dysphagicpatients. Biol Pharm Bull. 2011;34:164–6.
87. Li B, Zaveri T, Ziegler GR, Hayes JE. User preferences in a carrageenan-based vaginal drug delivery system. PLoS One. 2013;8:e54975.
88. Caram-Lelham N, Sundelof LO. The effect of hydrophobic character ofdrugs and helix-coil transition of kappa-carrageenan on the polyelectrolyte-drug interaction. Pharm Res. 1996;13:920–5.

89. Lefnaoui S, Moulai-Mostefa N. Formulation and in vitro evaluation of kappa-carrageenan-pregelatinized starch-based mucoadhesive gels containingmiconazole. Starch-Starke. 2011;63:512–21.
90. Thrimawithana TR, Young SA, Bunt CR, Green CR, Alany RG. In-vitro and in-vivo evaluation of carrageenan/methylcellulose polymeric systemsfor transscleral delivery of macromolecules. Eur J Pharm Sci. 2011;44:399–409.
91. Doppalapudi S, Katiyar S, Domb AJ, Khan W. Chapter: Biodegradable Natural Polymers, Advanced Polymers in Medicine eds:Francesco Puoci 2014 pp 33-66.
92. Jain A, Gupta Y, Jain SK. Perspectives of Biodegradable Natural Polysaccharides for Site-Specific Drug Delivery to the Colon. J Pharm Pharmaceut Sci. 2007;10:86-128.
93. Wang SC, Chen BH, Wang LF, Chen JS. Characterization of chondroitin sulfate and its interpenetrating polymer network hydrogels for sustained-drug release. Int J Pharm. 2007;329:103–9.
94. Jensena M, Hansena PB, Murdanb S, Frokjaera S, Florence AT. Loading into and electro-stimulated release of peptides and proteins from chondroitin 4-sulphate hydrogels. Eur J Pharm Sci. 2002;15:139–48
95. Amrutkar JR, Gattani SG. Chitosan–Chondroitin Sulfate Based Matrix Tablets for Colon Specific Delivery of Indomethacin. AAPS Pharm Sci Tech. 2009;10:
96. Liangliang Huang a, Weiping Sui a,*, Yuanxiu Wang b, Qiang Jiao Preparation of chitosan/chondroitin sulfate complex microcapsules and application in controlled release of 5-fluorouracil. Carbohydrate Polymers 80 (2010) 168–173.

CHAPTER 1:

Relationships Between the Properties of Self-Emulsifying Pellets and of the Emulsions Used as Massing Liquids for Their Preparation

Adapted from:

Relationships Between the Properties of Self-Emulsifying Pellets and of the Emulsions Used as Massing Liquids for Their Preparation

Ioannis Nikolakakis, Athanasia Panagopoulou, **Andrea Salis**, Stavros Malamataris. AAPS PharmSciTech February 2015, Volume 16, Issue 1, pp 129-139

INTRODUCTION

Self-emulsifying pharmaceutical pellets combine the advantages of emulsions and multi-particulate solid dosage forms, namely improved absorption of lipophilic drugs with lower variability in gastric transit time (independently of nutrition state) and better stability in the gastric fluids and easier application of coatings for GI track targeting [1–7]. It has been reported that self-emulsifying pellets do release the drug in the dog GI tract, as if they were the emulsion liquid itself [8]. Furthermore, it has been found that bioavailability of poorly water soluble drugs is improved when they are administered as self-emulsifying pellets, although there are no such products yet on the market [9,10].

Self-emulsifying pellets can be prepared by incorporating self-emulsifying mixtures (oil/surfactant/drug) in the form of o/w emulsions in microcrystalline cellulose (MCC) during the process of wet massing, before extrusion–spheronization. It has been reported that with surfactants of higher hydrophilicity the massing liquid requirements for pelletization increase and faster disintegration of the self-emulsifying MCC pellets is achieved, while the reconstitution of emulsion is facilitated with higher oil/surfactant ratios [11,12].

Until now, the effect of the drug nature on the properties of self-emulsifying drug delivery systems has received relatively little attention and even fewer literature reports appear for self-emulsifying pellets [13,14]. From the available reports it appears that the presence of drug in the oily phase of o/w emulsions affects their droplet size and stability, with maximum destabilization occurring near drug saturation [15,16]. Furthermore, the presence of the drug may affect the viscosity of the emulsions through its effect on the droplet diameter and its presence on the oil/water interface [17] which in turn may affect agglomeration during wet massing of MCC with the emulsion, the rheological properties of the resulting wet mass, and the properties of the final pellets [18]. In addition, the presence of any free drug in the aqueous phase of the emulsion and its migration during drying, towards the surface of the pellets, may alter the distribution of the drug in the pellet [19–21]. So far, there is little bibliographic information on this point and no data at all for the distribution (migration) of drugs in self-emulsifying pellets, although previously published results on the kinetics of drug release and emulsion reconstitution, have indicated the operation of a bi-phasic release process, a fast initial and a slow terminal release attributed to migration of oil/surfactant/drug mixture during drying of pellets [22].

Therefore, the aim of the present work was to expand the already studied effects of formulation variables (drug lipophilicity, surfactant type, and oil/surfactant ratio) on the properties of the emulsions used for the preparation of MCC pellets (droplet size, ζ, and viscosity) and elucidate possible relationships between them and the properties of the produced self-emulsifying pellets (micromeritic, mechanical, and drug migration). Furosemide and propranolol that belong to BCS class IV and II, respectively, and of similar aqueous solubility (0.063 and 0.051 mg/ml at 25°C) but different lipophilicity (log P 2.0 and 3.5) were the drugs, medium chain triglycerides the oil and Cremophors ELP, RH40, and RH60, the surfactants, employed at oil/surfactant ratios of 1.5 and 2.3 previously found to give good reconstitution of emulsions from the self-emulsifying pellets [12,22].

MATERIALS AND METHODS

Materials

Microcrystalline cellulose (Avicel® PH-101, lot 6950C, FMC Ireland) was used as the pellet forming material. Furosemide (FS) and propranolol base (PR) were selected as the active pharmaceutical ingredients. Furosemide (Batch 9033HRII) from Ipca (Mumbai, India) was donated by Help Hellas (Athens, Greece) and propranolol base was prepared by reacting 20% w/w propranolol hydrochloride with 3% w/w sodium bicarbonate water solutions, followed by filtration and drying [23]. Medium chain triglycerides of caprylic/capric esters; C8: 59.6%, C10: 39.9%, C14 0.4% (Radia 7104, Oleon N.V., Oelegen, Belgium), and glyceryl polyethylene glycol ricinoleate (Cremophor ELP) or glyceryl polyethylene glycol oxystearate (Cremophors RH 40 and RH 60), donated by BASF (Ludwigshafen, Germany), were used as the oil and the surfactant components of the self-emulsifying liquid mixture. Distilled water was used as the external phase of the emulsions employed as massing liquids during pellet preparation.

Emulsion Preparation and Characterization

Appropriate amounts of oil and surfactant were mixed at ratios 1.5 and 2.3 and then drug (2% w/w) was added to them. The mixtures were heated at 50°C, until clear solutions were formed. Then, o/w emulsions used as massing liquids for the preparation of pellets were made by 1/4 dilution containing 25% (w/w) of oil/surfactant/drug mixture and 75% deionized water and their viscosity was measured. For the determination of droplet size and ζ of the emulsions, a higher dilution of oil/surfactant mixture in water (1/10) was applied to avoid multiple scattering effects.

Droplet Size

The droplet size was measured in triplicate using the Dynamic Light Scattering sizer (Zetasizer, ZEN3600, Malvern Instruments Ltd, Worcestershire, UK) and expressed as the average hydrodynamic diameter derived from the change of intensity of scattered light with time (laser 633 nm, detection angle 173°).

Zeta Potential (ζ)

Emulsions were placed in the electrophoretic cell of the above-mentioned Zetasizer and ζ, which represents the charge on the surface of the droplets, was obtained from the electrophoretic mobility using the M3-PALS technique which is a combination of Malvern's laser Doppler velocimetry method (M3 measurement technique) and the Phase Analysis Light Scattering technique (PALS).

Viscosity

Kinematic viscosity was measured with an Ubbelohde glass capillary viscometer (Schott Geräte, Mainz, Germany) of internal diameter 0.63 mm, taking as reference the viscosity of water at 25°C ($\eta = 0.89$ cST (centistokes, mm^2/s)) and the efflux time for water (81 ± 0.1 s). Measurement was applied to inert emulsions without drug, which were not used for pellet preparation, and, for the twelve emulsions containing drug. To convert the values to cP (centipoise, $g \cdot s/cm^2$), multiplication by the average density, calculated from the density of the oil (0.95 g/cm^3) and that of the surfactants (1.05 g/cc, Handbook of Pharmaceutical Excipients), was applied.

Pellet Preparation and Characterization

For the preparation of pellets by extrusion/spheronization, 30 g batches of MCC powder were mixed with 30 g emulsions (75% water and 25% w/w oil/surfactant/drug self-emulsifying mixture) for about 5 min in a 1-L cylindrical mixing vessel, fitted with a three-blade impeller [22]. The emulsions had milky appearance except for those containing FS and oil/surfactant ratio 1.5, which gave clear (RH40) or slightly turbid, translucent emulsions. Further addition of small amounts of 2 to 5 g of water was required to obtain most spherical pellets. The resulting wet mass was extruded in a radial extruder (Model 20, Caleva Process Solutions, Dorset, UK) operated at 25 rpm and fitted with a 1-mm circular orifice and 1.75 mm thickness screen. The extrudate was immediately processed for 10 min at 1,360 rpm corresponding to a linear perimeter speed of 8.55 m/s in a spheronizer (Model 120, Caleva Process Solutions, Dorset, UK) fitted with a cross-hatch friction

plate. The produced pellets were dried for 12 h in an air-circulation tray oven (UT6, Heraeus Instruments, Hanau, Germany) at 40°C. The final dry pellets contained 0.4% drug, 19.6% oil/surfactant mixture, and 80% MCC and their properties were evaluated as follows:

Size

Size distribution was determined by placing approximately 10 g of pellets on a stack of 10 cm diameter sieves of 300, 425, 600, 850, and 1,200 μm aperture (DIN/ISO3310-1, Retch, Haan, Germany) and vibrating for 10 min (Fritsch Analysette 3, Oberstein, Germany). Median pellet diameter was derived from cumulative weight plots of the weight of remaining pellets on each sieve.

Shape

Pellet shape was determined by using an image processing and analysis system comprised of stereomicroscope, top cold light source (Olympus SZX9, Japan and Highlight 3,100, Olympus Optical), video camera (VC-2512, Sanyo Electric, Japan), and software (Quantimet 500, Cambridge, England). About 100 pellets were examined, in 3–4 optical fields, at a total magnification of $6.5 \times 5 = 32.5$. The shape was expressed as fullness index [FI% = 100 × (actual surface area − convex surface area)/actual surface area] which represents the surface irregularity, as aspect ratio (AR = length/breadth) and as shape factor e_R which combines both geometrical and surface irregularity [24]. All shape parameters tend towards unity with increasing sphericity.

Friability

Friability was determined in a granule friabilator (Copley Scientific, type FRV 2000, Nottingham, UK) rotated at a speed of 25 rpm, for 10 min. Pellets (10 g) of the size fraction 600–1,200 μm were placed in the drum together with 20 g, 4 mm, glass beads. After rotation, the fines produced due to the shocks of the falling pellets were separated by sieving through a 600-μm sieve, for 5 min at 2 mm vibration amplitude (Fritsch Analysette, Oberstein, Germany). Friability, FR%, was calculated from the weight difference of the pellets remaining on the sieve (W_f) compared to initial pellet weight (W_o) expressed as percentage:

$$FR(\%) = 100 * (W_o - W_f)/W \quad (1)$$

Tensile Strength

Pellets from the 1,000–1,200 μm fraction were diametrically loaded by using a modified CT-5 testing machine (Engineering System, Nottingham, UK), at an upper platen speed of 1 mm/min. The tester was fitted with a 25 N load cell (model ELFM-T2M, Entran, USA) connected to a signal amplifier (RDP E308, UK). The signal was collected with a polymeter (Handyscope, Holland) and recorded in Microsoft Excel files. The tensile strength, σ_t, was calculated from the breaking force, F, and the pellet radius, R, by using the equation (25):

$$\sigma_t=0.4*F/\pi*R^2 \quad (2)$$

Disintegration

The disintegration time of pellets, 1,000–1,200 μm in diameter, was determined in a modified reciprocating cylinder USP Apparatus 3 (Bio-Dis RRT9, G.B. Caleva, UK) as described previously [12].

Drug Migration

Pellets (5 g) of the size fraction 850–1,200 μm were placed together with 20 g, 4 mm glass beads, in 250 mL specially modified cylindrical glass jars in order to separate surface layers from the pellets and estimate drug content. The interior surface of the jars was covered by glued sand paper type P800 (FEPA classification) corresponding to about 16 μm grain size, which was selected after preliminary trials on the basis of the yield of outer layer removal from pellets. The jars were mounted on a Turbula mixer (Type T2C, Willy Bachofen AG, Basel Switzerland) and tumbled at a speed of 90 rpm. At 3-min intervals, the fines (<212 μm) were removed by sieving the jar content and tumbling was continued until collecting more than 250 mg fine powder.

The drug content was determined in the two size fraction (<212 and >212 μm) applying a validated UV spectrophotometric method in five samples as follows. Samples (50 mg) corresponding to 200 μg drug (nominal amount) were mixed for 5 min with 40 mL methanol, centrifuged for 3 min at 4,500 rpm (Heraeus Labofouge 400R, Thermo Electron Corporation, Osterode, Germany), and the concentration of extracted drug in the supernatant was determined at 272 and 290 nm for FS and PR, respectively. The extraction process and UV determination was repeated once with 20 and then with 10 mL methanol until absorbance lower than 0.003 was obtained.

Validation of the method was based on linearity between absorbance, A, and concentration, C, ($R^2 > 0.999$, in the range 0.5–20.0 μg/mL and 1.0–50.0 μg/mL for FS and PR, respectively). The relationships between concentration and absorbance were: $C = 16.8067 \times A + 0.4403$ and $C = 42.9185 \times A + 0.4206$. Considering the sensitivity of the spectrophotometer as $A = 0.001$, the lower limit of detection (LLOD) was 0.45 and 0.55 μg/mL and the lower limit of quantification LLOQ was 1.0 and 1.5 μg/mL for FS ($A = 0.034$) and PR ($A = 0.026$), respectively, which corresponds to coefficient of variation <2% (for five samples).

From the drug content in the two fractions (Douter and Dinner) the drug migration (M%) was expressed as:

$$M\% = 100 * (Douter - Dinner)/200 \quad (3)$$

On the basis of LLOQ (1.0 μg/mL for FS and 1.5 μg/mL for PR), any difference ($Douter - Dinner$) greater than 0.5% for FS and 0.75% for PR will be valid.

Reconstituted Emulsions

The evaluation of reconstituted emulsions was based on the determination of droplet size and zeta potential as already described for the emulsions used as wet massing liquids in the preparation of pellets. The reconstitution was evaluated using a USP II dissolution apparatus (Pharma-Test, Hainburg, Germany) by adding 3 g pellets corresponding to 0.6 g of oil/surfactant/drug mixture in 200 mL distilled water, at 37 ± 0.5°C, and stirring for 3 h at 100 rpm. These conditions ensured complete reconstitution for most pellet batches [22].

Experimental Design and Statistical Analysis

A mixed level full factorial, completely randomized design (12 runs) with two factors at two levels (drug lipophilicity and oil/surfactant ratio) and one factor at three (type of surfactant), was employed to study their effects on the properties of emulsions and pellets. The prepared batches according to the experimental design are shown in Table 1.

Table 1. Mixed Level Full Factorial Experimental Design

Formulation	Drug	Surfactant	Oil/surfactant ratio
1	FS	ELP	1.5
2	FS	ELP	2.3
3	FS	RH40	1.5
4	FS	RH40	2.3
5	FS	RH60	1.5
6	FS	RH60	2.3
7	PR	ELP	1.5
8	PR	ELP	2.3
9	PR	RH40	1.5
10	PR	RH40	2.3
11	PR	RH60	1.5
12	PR	RH60	2.3

For the statistical analysis, a 3-way analysis of variance (ANOVA) was applied and the statistical index adjusted coefficient of determination (R_a^2) was used, representing the proportion of the variability in the data explained by the ANOVA, after adjusting for the number of experiments and the number of variables [26]. Furthermore, pairwise comparison of means (2-tailed t test) was applied for the estimation of the significance of the differences in the properties of emulsions due to the addition of drugs. For the analysis of the data, the SPSS 20.0 statistical software was used (IBM SPSS Statistics, Inc., Chicago, IL USA). Effects were considered significant at p value <0.05, less significant at p between 0.05 and 0.10, and without significance at $p > 0.10$.

RESULTS AND DISCUSSION

The physicochemical properties of drugs, surfactants and oil are summarized in Table 2. From the physicochemical properties, it can be seen that the aqueous solutions of FS and PR have high surface tensions (64 and 66 mN/m) indicating minor surface activity compared to the surface tensions of surfactants (41.3–44.8 mN/m). The molecular size of drugs is similar (330.8 and 259.3), but they have different lipophilicities (log P 2.0 and 3.5, respectively) and different solubilities in the oil/surfactant mixtures (24.7–63.2 mg/mL; ref. 22). Therefore, the drugs are expected to be

distributed differently between the droplets and the external aqueous phase [15]. Similarly, the surfactants employed are expected to be distributed differently in the oil/water interface, due to their different hydrophilicity (HLB 13.9–15.7), and also to present different excess surface concentration in the water/air interface at the pellet surface during drying (Figure 1). Consequently, the combinations of different drug and surfactant types in altered proportions are expected to influence the formation of emulsions and the properties of the self-emulsifying pellets [12,13].

Table 2. Physicochemical properties of drugs, surfactants and oil

Material	Molecular weight	Log*P*	HLB[e]	m.p. (°C)	Surface tension (mN/m)
Drugs					
Furosemide	330.8 [a]	2.0 [d]	n/a	219 [a]	64.0 (1.0) [g]
Propranolol	259.3 [a]	3.5 [e]	n/a	95 [a]	66.0 (1.0) [g]
Surfactants					
Cremophor ELP	2,500 [b]	n/a	13.9	20 [c]	41.3 (0.3) [g]
Cremophor RH40	2,500 [b]	n/a	14.3	30 [c]	44.0 (0.1) [g]
Cremophor RH60	2,800 [b]	n/a	15.7	30[c]	44.8 (0.3) [g]
Oil					
Medium chain triglyceride	498 [c]	n/a	n/a	−20 [c]	31.1 [c]

[a]Merck index

[b]BASF Technical Information May 2010

[c]Handbook of Pharmaceutical Excipients

[d]Alvarez-Nunez and Yalkowsky [31]

[e]Avdeef *et al*. [29]

[f]Matsaridou*et al*. [12]

[g]Saturated drug and 0.1% *w*/*v* surfactant solutions in distilled water measured after filtration (0.1 μm) with a du Nuoy balance (Krüss 8600, Germany)

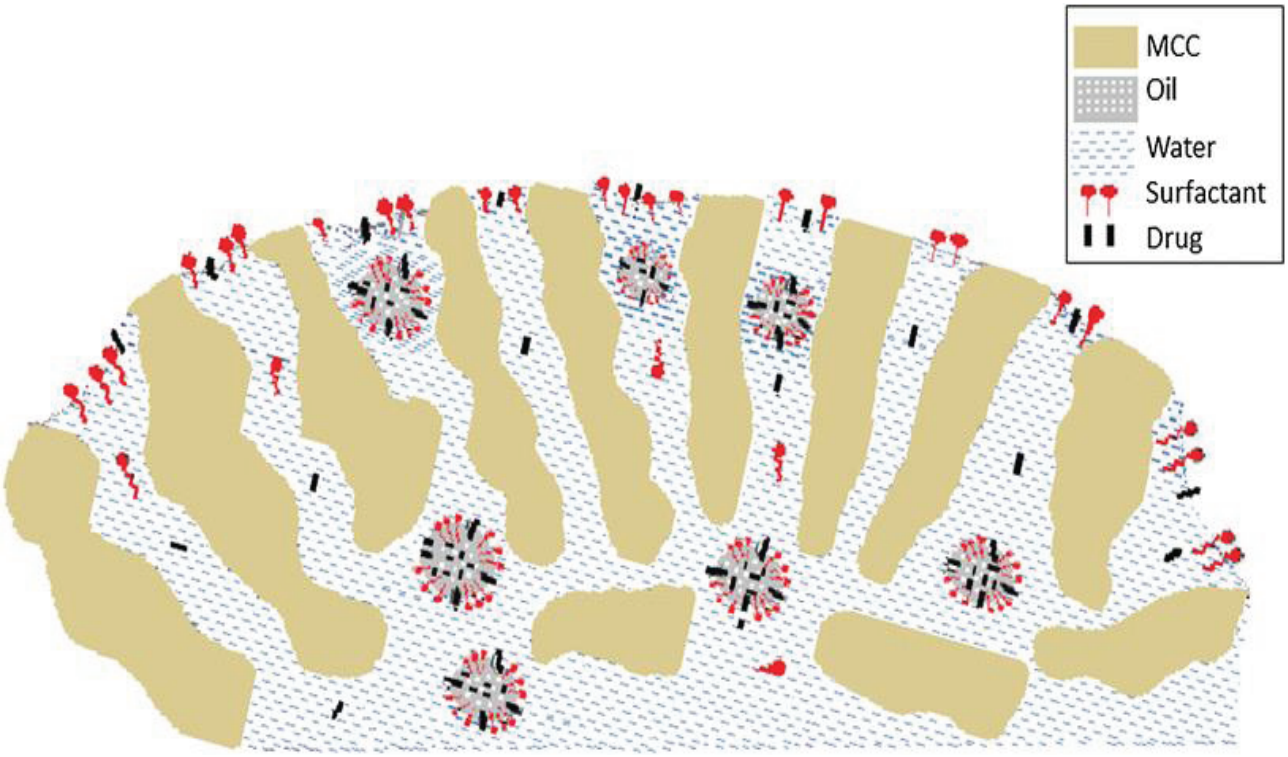

Figure 1. Schematic representation of drug, surfactant and oil in the MCC pellets

Effect of Drug Incorporation on Emulsion Properties

In Figure 2a–c, the properties of emulsions without (inert) and with drug are compared. It can be seen (Figure 2a) that the presence of FS decreases the droplet diameter in all cases (pairwise comparison of means, t test, $p = 0.009$), whereas that of PR decreases the diameter of emulsions with ELP and RH40 but not with RH60. Since the surface activity of the drugs is minor compared to the surfactants, the decrease in droplet diameter caused by the presence of drug implies a co-surfactant drug effect.

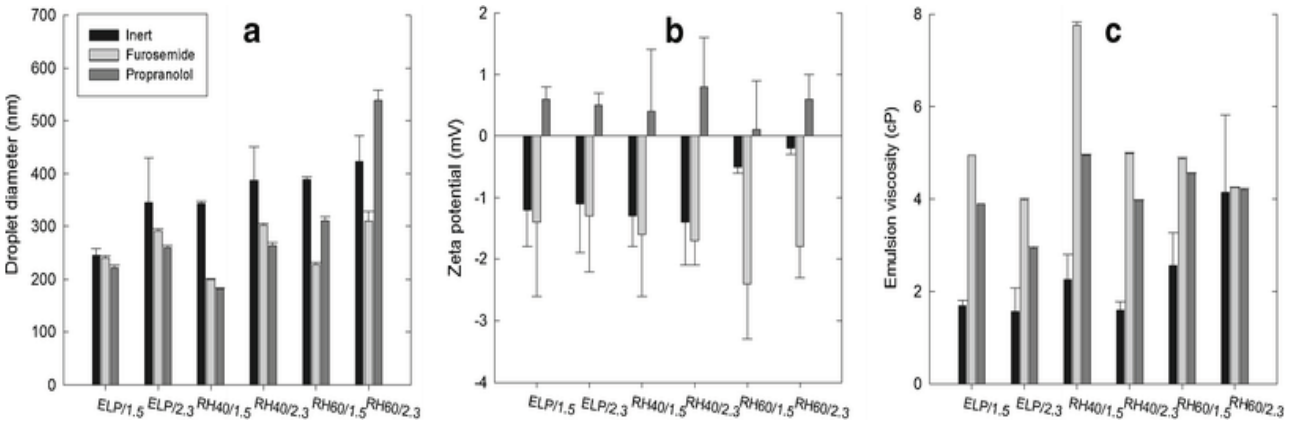

Figure 2. Comparison of a droplet diameter, b zeta potential, and c viscosity for inert and drug-loaded emulsions used for the preparation of pellets

Regarding the zeta potential (ζ), it can be seen in Figure 2b that for inert emulsions it is negative due to the free fatty acids present in the oil which confirms previously reported data for self-emulsifying systems with nonionic surfactants [13,27]. In the case of inert emulsions with RH60, the zeta potential is less negative compared to the other surfactants probably due to their generally greater droplet diameter and its influence on droplet mobility (Figure 1a and ref. 12). Interestingly, in Figure 2b, it can be seen that ζ changes significantly due to the presence of drug, negatively for furosemide and positively for propranolol. These ζ changes should be related to the presence of drug in the oil/water interface affected by both, the surfactant type and the oil/surfactant ratio.

More specifically, for furosemide which is a weak acid (pKa = 4.25), its carboxylic acid ionizes in the aqueous solution giving negatively charged carboxylate and negative overall droplet surface charge, which explains the decrease of zeta potential. Conversely, the characteristic turning to positive values by propranolol should arise from its basic character due to the presence of amino group (−NH, pKa = 9.53) which neutralize the free fatty acids present in the oil of the self-emulsifying mixture [28].

Regarding the emulsion viscosity, it can be seen from Figure 2c that in all cases, incorporation of drugs causes an increase. This can be attributed to the presence of drugs in the oil/water interface and the consequent alteration in the surrounding the droplet hydrated layer and hence in the shearing resistance [29]. In general, FS addition gave greater viscosity than PR, which is in agreement with its higher hydrophilicity and therefore increased presence in the oil/water interface [15]. Pairwise comparison of means, t test, gave $p = 0.012$ for FS and $p = 0.006$ for PR. The higher viscosity seen in Figure 2c for formulation with Cremophor RH40 with oil/surfactant ratio 1.5 and

furosemide in comparison with the formulation with ratio 2.3 is associated with the transparent appearance of the emulsion and its lower average droplet diameter (part of Pellet preparation in Materials and Methods and Table 3). Formation of transparent dispersions of RH40 with medium chain triglycerides was also previously observed for emulsions without drug [12].

Table 3. Droplet diameter, polydispersity index, and zeta potential of added and reconstituted emulsions together with the viscosity of added emulsions [mean, (SD), n = 3]

Cremophor/ratio	Added emulsions			Reconstituted emulsions			Viscosity (cP)
	dv (nm)	PDI	ζ (mV)	dv (nm)	PDI	ζ (mV)	
Furosemide							
ELP/1.5	240 (4)	0.264	−1.4 (2.7)	494 (43)	0.406	−25.7 (0.9)	4.94 (0.00)
ELP/2.3	291 (4)	0.285	−1.3 (0.9)	562 (40)	0.468	−27.9 (1.8)	3.98 (0.03)
RH40/1.5	182 (1)	0.283	−1.6 (3.3)	303 (16)	0.488	−24.3 (0.6)	7.75 (0.08)
RH40/2.3	302 (4)	0.411	−1.7 (0.4)	632 (74)	0.498	−27.8 (0.4)	4.98 (0.02)
RH60/1.5	227 (4)	0.262	−2.4 (1.4)	533 (30)	0.447	−28.5 (1.1)	4.86 (0.03)
RH60/2.3	310 (18)	0.290	−1.8 (0.5)	643 (69)	0.487	−28.2 (0.8)	4.25 (0.01)
Propranolol							
ELP/1.5	222 (4)	0.236	0.6 (0.2)	467 (52)	0.381	−19.2 (0.4)	3.89 (0.00)
ELP/2.3	259 (4)	0.205	0.5 (0.2)	596 (119)	0.447	−22.6 (0.2)	2.93 (0.03)
RH40/1.5	200 (2)	0.236	0.4 (1.0)	552 (8)	0.407	−11.6 (0.3)	4.94 (0.02)
RH40/2.3	263 (6)	0.212	1.2 (1.4)	349 (10)	0.452	−13.4 (0.4)	3.97 (0.01)
RH60/1.5	311 (7)	0.371	0.0 (3.2)	401 (39)	0.418	−15.2 (0.3)	4.56 (0.01)
RH60/2.3	499 (20)	0.406	0.6 (0.4)	405 (96)	0.411	−14.7 (0.7)	4.20 (0.03)

dv average hydrodynamic droplet diameter, PDI polydispersity index, ζ zeta potential

Effect of Surfactant Type and Ratio on Droplet Size, Zeta Potential, and Viscosity

In Table 3 are presented the results of droplet diameter and polydispersity index (PDI) and of ζ for the added to the MCC during pellet preparation and for the reconstituted emulsions, together with the viscosity of the added emulsions. Viscosity of the added emulsions was evaluated in order to be

compared with the pellet properties. In Table 4 are given the results of ANOVA for the main effects and interactions of the studied factors on the properties of added emulsions and self-emulsifying pellets.

Table 4. ANOVA of the main effects and interactions of the type of drug (A), the type of surfactant (B), and the oil/surfactant ratio (C) on the properties of added emulsions and self-emulsifying pellets

Property	Main and effects			Interactions			R_a^2
	A	B	C	A × B	B × C	A × C	
Added emulsions							
Droplet diam. (dv)	0.333	0.135	0.070	0.164	0.413	0.568	0.742
ζ-potential (ζ)	**0.006**	0.213	0.202	0.481	0.486	0.562	0.943
Viscosity (η)	0.066	0.096	0.059	0.240	0.324	0.349	0.822
Pellets							
Median diameter	**0.025**	**0.016**	0.614	**0.049**	0.104	0.191	0.951
Fullness index (FI%)	0.329	0.491	0.213	0.320	0.287	0.185	0.503
Aspect ratio (AR)	0.121	0.254	0.201	0.250	0.535	0.405	0.594
Shape factor (e_R)	0.059	0.096	0.054	0.110	0.317	0.148	0.861
Friability (%)	**0.021**	**0.028**	**0.012**	**0.046**	0.169	**0.044**	0.959
Tensile strength	0.244	0.688	0.123	0.081	0.126	0.142	0.797
Migration%	0.132	0.473	0.204	0.822	0.972	0.620	0.248
Disintegration time	0.649	0.624	0.633	0.389	0.586	0.236	0.048
Reconstituted emulsions							
Droplet diameter (dv)	**0.025**	0.259	0.095	0.084	0.777	0.641	0.858
ζ-potential (ζ)	**0.013**	0.112	0.177	0.212	0.373	0.511	0.901

Numbers in bold correspond to statistical significance $p < 0.05$ and numbers in italics to statistical significance p between 0.05 and 0.100

Droplet Size

Comparing the droplet diameters of added to the MCC emulsions with those of the corresponding reconstituted, it can be seen that they are significantly smaller, except in the case of propranolol with RH60 at oil/surfactant ratio 2.3. The range of PDI values increase from 0.205–0.406 for the added emulsions (the majority between 0.205 and 0.290) to 0.381–0.498 for the reconstituted, which is still under 0.500, thus, allowing comparison of the droplet diameters of the different formulations [30]. The increase in reconstituted emulsions is by about a factor of 2, although still in the nano-size range (303–643 nm) which is desirable for absorption. The increase in the droplet size and the higher PDI values of the reconstituted emulsions, are attributed to the expected reduction in excess surface concentration of surfactant and drug in the oil/water interface due to the incomplete reconstitution of emulsions from pellets, as reported previously [12,22].

Regarding the effect of drug type on the droplet diameter of reconstituted emulsions, the more lipophilic PR appears giving emulsions with lower overall diameter (ANOVA $p = 0.025$, Table 4), implying better stability of the reformed emulsion due to the easier incorporation and more firmly bound lipophilic drug to the oil/surfactant and to the greater surfactant availability. Regarding the effect of oil/surfactant ratio on droplet diameter, from Table 3 appears that for the added emulsions and for the same drug and surfactant, the diameters for the high oil/surfactant ratio are greater than those of the low ratio ($p = 0.070$, Table 4) which should be attributed to decreased interfacial film formation due to the lower surfactant content.

Zeta Potential (ζ)

The effects of formulation variables on the ζ of the added emulsions have been already presented and discussed during the comparison of inert and pharmaceutical emulsions. Now, comparing the ζ of the reconstituted emulsions with that of the added, it can be seen from Table 3 that ζ in the reconstituted emulsions changes considerably towards negative values, which can be ascribed to the effect of dilution on the composition of oil/water interface, and consequently, in the diffuse electrical layer around the droplets. In particular, this change shows the predominance of the free acids in the oil of the self-emulsifying mixture. ANOVA (Table 4) shows significant effect of the type of drug on ζ values for both added and reconstituted emulsions ($p = 0.006$ and $p = 0.013$, respectively) which means that drug charges still exist after reconstitution, resulting in significant differences in the droplet charges of the reconstituted emulsions of the two drugs. In fact, bivariate

correlation analysis between the ζ values of added (1/10 dilution of oil/surfactant in water) and reconstituted emulsions gave linear relationship:

$$\zeta_{reconstituted} = 4.5626 * \zeta_{added} - 18.9680 (R^2 = 0.7626) \quad (4)$$

The higher dilution of droplets in the reconstituted emulsions is due to the volume of the reconstitution medium used in the test (200 mL in which 3 g pellets were suspended, corresponding to 0.6 g self-emulsifying mixture and 1/333 dilution instead of 1/10 in the prepared emulsions) and also due to the contact and adherence of the hydrophilic surfactants on the MCC fibrils of the dry pellets, resulting in incomplete reconstitution [12].

Viscosity

Viscosity of the added emulsions was determined as a quantitative measure of the difficulty to flow, which is expected to vary, since their appearance varied from clear to translucent or milky liquid, due to the different composition and relatively high content (25% w/w) of the drug/oil/surfactant mixture. More importantly, emulsion viscosity may affect the micromeritic and particularly the drug migration during pellet drying [19]. The effect of drug addition on viscosity has already been discussed and now the surfactant type and oil/surfactant ratio will be considered.

From Table 3, it appears that although the effect of surfactant on viscosity is of low statistical significance ($p = 0.096$, Table 4) RH40 contributes highest in viscosity, followed by RH60 and ELP. Taking into account the surfactant properties, Table 2, we can see that their effect on emulsion viscosity should be a combination of molecular weight and HLB value, both of which (together with the surfactant content) affect their concentration in the oil/water interface. The increase of viscosity at lower oil/surfactant ratio is clear for all the emulsions studied and ANOVA confirmed this effect at significance $p = 0.059$ (Table 4) which can be attributed to the increased surfactant content at the oil/water interface and hence greater hydration and shearing resistance.

Pellet Properties

In Table 5 are summarized the micromeritic together with the mechanical properties and in Table 6 the pharmaco-technological properties of the pellets respectively. From Table 5 it can be seen that the extra amount of water required, additionally to the emulsion (30 g) for the formation of pellets with narrowest size distribution and most spherical shape, increases slightly with oil/surfactant ratio for half of the batches of both drugs. Also, for a fixed ratio it increases in the order ELP < RH40 < RH60, which is the same as the order of their HLB value or hydrophilicity. Therefore, the effects of

the surfactant content and type on the pellet properties should be ascribed to the hydration of MCC [12].

Table 5. Extra water required during MCC wet massing, micromeritic (size, shape) and mechanical (friability and tensile strength) properties of self-emulsifying pellets [mean, (SD), n = 3 and for tensile strength n = 10]

Cremophor/ratio	Extra water (g)	Modal[a] fraction%	Median diameter (μm)	Shape parameters[b]			Friability[b] (%)	Tensile[b] strength (MPa)
				FI(%)	AR	e_R		
Furosemide								
ELP/1.5	2	79	1,071	3.34	1.09	0.53	3.6	0.81
ELP/2.3	3	69	1,096	3.49	1.09	0.54	2.2	0.67
RH40/1.5	2	70	1,083	3.45	1.11	0.47	3.6	0.88
RH40/2.3	3	80	1,062	3.84	1.10	0.50	2.5	0.67
RH60/1.5	5	87	1,000	3.47	1.09	0.52	2.3	1.10
RH60/2.3	5	87	1,012	3.11	1.08	0.55	1.7	0.78
Propranolol								
ELP/1.5	3	79	1,043	3.47	1.10	0.51	2.8	0.99
ELP/2.3	3	84	1,037	3.34	1.08	0.54	2.4	0.72
RH40/1.5	3	78	1,048	3.90	1.12	0.44	2.1	0.98
RH40/2.3	4	86	1,018	3.18	1.11	0.50	1.6	0.65
RH60/1.5	5	90	1,013	6.11	1.18	0.37	2.0	0.60
RH60/2.3	5	89	1,019	3.22	1.10	0.49	1.9	0.52

FI% fullness index, *AR* aspect ratio, e_R shape factor
[a]Modal size fraction: 850–1,200 μm
[b]Standard deviation for FI% 0.37–0.94, for AR 0.020–0.058, for e_R 0.051–0.090, for friability 0.0–0.2, and for tensile strength 0.05–0.10

Table 6. Pharmaco-technological properties of pellets (disintegration time, drug content in outer and inner part of pellets, migration %) and drug solubility in oil/surfactant mixtures [mean, (SD), n = 3]

Cremophor/ratio	Disin/tion time (min)	Drug (μg) in		Migration (%)	Drug solubility[a] in oil/surfactant (mg/mL)
		Outer part	Inner part		
Furosemide					
ELP/1.5	6.2 (0.4)	210 (6)	193 (4)	9.0	26.0 (0.5)
ELP/2.3	4.5 (0.7)	235 (8)	215 (2)	9.8	24.7 (0.9)
RH40/1.5	4.5 (0.2)	214 (9)	209 (2)	2.5	40.7 (0.9)
RH40/2.3	4.4 (0.4)	241 (5)	212 (3)	14.5	28.0 (2.0)
RH60/1.5	4.8 (0.3)	206 (1)	197 (2)	4.3	29.9 (0.7)
RH60/2.3	4.5 (0.1)	233 (1)	195 (1)	18.5	29.8 (2.5)
Propranolol					
ELP/1.5	4.2 (0.1)	194 (2)	192 (1)	0.8	63.2 (2.7)
ELP/2.3	3.7 (0.1)	210 (4)	189 (6)	11.0	47.6 (2.3)
RH40/1.5	5.7 (0.1)	218 (1)	214 (2)	1.8	61.5 (1.3)
RH40/2.3	4.9 (0.1)	220 (5)	211 (1)	4.3	49.6 (2.8)
RH60/1.5	10.8 (0.3)	202 (1)	199 (1)	1.3	57.0 (2.5)
RH60/2.3	4.3 (0.1)	220 (1)	217 (2)	1.8	49.9 (2.6)

[a]Data from Nikolakakis and Malamataris 2014 [22]

Pellet Size

The results in Table 5 show that most pellet batches have a high percentage (69–89%) in the modal size fraction 850–1,200 μm and median diameters in a narrow size range (1,000–1,096 μm). ANOVA (Table 4) showed interaction of the effects of drug type and surfactant type on the median diameter ($p = 0.049$). This is depicted in Figure 3a by comparing the mean values of pellet diameters for the two drugs and the three surfactants. It can be seen that the difference between drugs are pronounced for pellets with ELP and RH40 but small for those with RH60. Also, for FS, the difference between ELP and RH60 or between RH40 and RH60 is large; whereas for PR, it is small, indicating that the effect of drug depends on the surfactant. The decreasing size of the pellets with

increasing surfactant hydrophilicity (Figure 3a) can be explained due to the greater extra water required for their preparation (Table 5) and hence greater water loss and decrease in diameter during drying. As can be seen in Table 5 the range of required extra water is smaller for propranolol compared to furosemide (2 to 5 compared with 3 to 5) which accounts for the different effect of surfactant type for the two drugs.

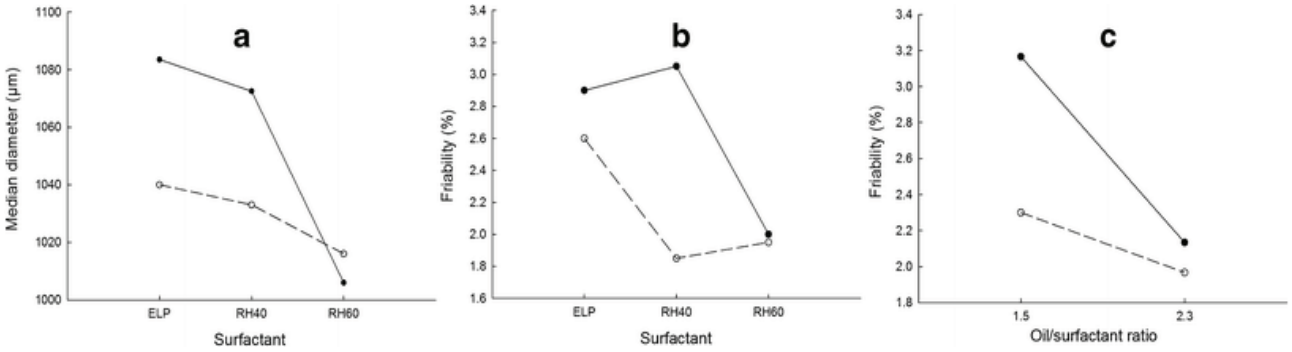

Figure 3. Interaction plots of the effects of drug and surfactant on **a** pellet diameter and **b** friability, and **c** interaction plots of the effects of drug and oil/surfactant ratio on friability (solid symbols with solid lines for furosemide and open symbols with dotted lines for propranolol)

Pellet Shape

From Table 5, it can be seen that, except for formulation of PR with RH60 at oil/surfactant ratio 1.5, the values of the fullness index (FI% <3.90), aspect ratio (AR <1.12) and shape factor (e_R>0.44) indicate production of spherical pellets. However, the values of e_R for the different formulations vary considerably (0.37–0.55), meaning that e_R is more discriminative. Comparing pellet batches of the two drugs, it can be seen that e_R is lower for PR batches (drug effect significant at $p = 0.059$, Table 5). For the different surfactants, the results in Table 5 do not show a certain trend, whereas for different oil/surfactant ratios e_R increases clearly with the increase of oil/surfactant ratio or lower surfactant content ($p = 0.054$, Table 5). Comparing the effects of the three studied factors on pellet shape and emulsion properties, we can see that viscosity and e_R are both affected at similar significant level by the type of drug and the oil/surfactant ratio. Therefore, the differences in e_R values should be related to the viscosity of emulsions used for the preparation of the pellets.

More specifically, considering the data in Tables 3 and 5, it can be seen that emulsions of furosemide with RH40 at oil/surfactant ratio 1.5 and 2.3 (denoted as FS/RH40/1.5 and FS/RH40/2.3) and emulsions of propranolol with RH40 and RH60 at ratio 1.5 (denoted as PR/RH40/1.5 and PR/RH60/1.5) with higher viscosity, correspond to more irregular pellets with higher FI% and AR and lower e_R. Accordingly, the relationship between pellet shape and emulsion viscosity was examined by plotting data of the more established shape parameters aspect ratio (AR) and shape factor (e_R) against emulsion viscosity. The plots in Figure 4a, b show that except for formulation PR/RH60/1.5, AR increases linearly with viscosity ($R^2 = 0.711$ and 0.893 for FS and PR, respectively, Figure 4a), whereas e_R decreases ($R^2 = 0.740$ and 0.977, Figure 4b).

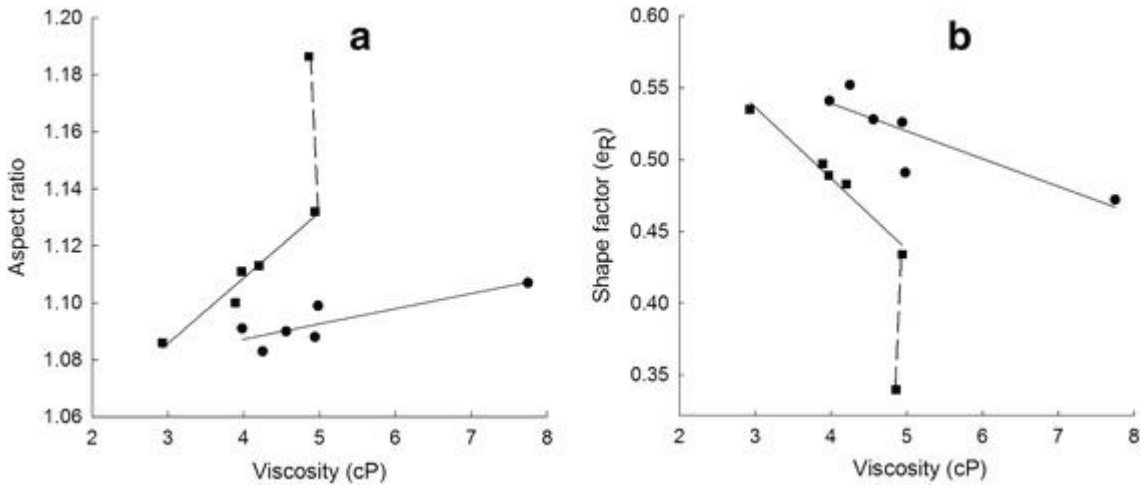

Figure 4. Plots of **a** aspect ratio and **b** shape factor (e_R) with the viscosity of emulsions used for the preparation of pellets (round symbols for furosemide and square for propranolol)

The increased sphericity with decreasing viscosity should be due to even spreading of emulsions in MCC powder resulting in more homogeneous wet mass and improved distribution of the self-emulsifying oil/surfactant/drug mixture in the pellets. The deviation of formulation PR/RH60/1.5 representing high drug lipophilicity, high surfactant hydrophilicity and content, may be ascribed to the difficulty of spreading of the respective emulsion in MCC, resulting in high FI% and low e_R values (Table 5).

Pellet Friability and Tensile Strength

From the results in Table 5, it appears that all batches of self-emulsifying pellets exhibit friability >1.6%. This is expected considering the relatively high proportion of self-emulsifying mixture (20% w/w), resulting in weaker MCC interparticle bonding and less coherent pellets. More specifically, from Table 5, it appears that overall, furosemide pellets show higher friability than propranolol and that for the same drug and surfactant, the friability of pellets with higher oil/surfactant ratio is always lower. This should be related to the greater deformability of pellets due to the higher oil content and hence their greater ability to absorb shocks during tumbling in the friabilator and also to lubricating action of the oil. From the results of ANOVA (Table 4), it is seen that all studied formulation factors affect friability and there are significant interactions between the effect of drug and surfactant type ($p = 0.046$) as well as between the effect of drug type and oil/surfactant ratio ($p = 0.044$).

The former of the two interactions is depicted in Figure 3b, where the differences in friability for the two drugs are seen to be greater for Cremophor RH40, with FS showing highest and PR lowest friability, whereas there are no differences for Cremophor RH60. The latter of the two interactions is depicted in the plots of Figure 3b, where the decrease in friability with oil/surfactant ratio is seen to be steeper for FS. The greater friability of FS pellets compared to PR and, in particular, those made with Cremophor RH 40 (Figure 3b) can be ascribed to the higher viscosity of the added FS/RH40 emulsions (7.75 and 4.98 cP at oil/surfactant ratios 1.5 and 2.3 for FS compared with 4.94 and 3.97 cP for PR, Table 3). The higher viscosity impairs the movement of emulsions and distribution into MCC powder, as manifested by high extrusion forces [18], and consequently the efficiency of incorporation of oil/surfactant in the dry pellet, which adversely affects pellet deformability or the ability to absorb stresses during friability testing. The low and similar friability of the pellets of both drugs made with RH60 could be ascribed to the increased presence of the highly hydrophilic surfactant (HLB = 15.7) on the pellet surface, migrating along with the water during drying and also, to its high molecular weight and solid nature (Table 2), resulting in harder pellet surface. The different effect of oil/surfactant ratio for the two drugs on friability (interaction shown in Figure 3c) can be ascribed to the greater difference in the viscosities of the emulsions of the two drugs at ratio 1.5 (1.39 cP, Table 3) compared with ratio 2.3 (1.33 cP) and consequently greater difference in pellet deformability as explained above.

From the data in Table 5, it appears that the type of drug and the surfactant do not have an effect on tensile strength. However, for the same drug and surfactant type, tensile strength clearly decreases

with the increase in oil/surfactant ratio which should be attributed to the weakening of the interparticle MCC bonds due to the masking action of the oil [12].

Pellet Disintegration

From Table 3, the disintegration time does not seem to be influenced by the type of drug or surfactant. However, for the same drug and surfactant type, there is a general decrease with the increase in oil/surfactant ratio. This is in agreement with the weaker MCC interparticle bonding which is responsible for the tensile strength reduction due to the increased oil content and, additionally, it can be ascribed to lesser gel formation due to the lower surfactant content [11,12]. The nearly double disintegration time of formulation PR/RH60/1.5 can be ascribed to the inefficient spreading and uneven distribution of oil/surfactant in the pellets which probably limits the presence of surfactant and wetting at certain parts of the pellet surface only, resulting in less efficient liquid penetration and longer disintegration time. This is also indicated by the lowest sphericity of PR/RH60/1.5 pellets (highest FI% and AR and lowest e_R, Table 5).

Drug Migration in Pellets

The results of drug content in outer and inner part of pellets together with the calculated migration (%) and solubility of drug in the corresponding oil/surfactant mixture are given in Table 6. Migration appears greater for the less lipophilic furosemide and particularly for higher oil/surfactant ratio.

The drug lipophilicity and oil/surfactant ratio should affect migration due to their combined influences on the solubilization of drug in the oil of droplets and on capillary flow (viscosity) of the emulsion used. In pellets, before drying, drug may exist as solubilized in the oil droplets and as dissolved or suspended in the continuous aqueous emulsion phase, Figure 1. Since the solubilities of the two studied drugs in water at the ambient temperature of pellet preparation, are similar (0.063 mg/mL for FS and 0.051 mg/mL for PR) and remarkably lower (about 3 orders of magnitude) than those in oil/surfactant mixtures (24.7–63.2 mg/mL), the drug lipophilicity should determine partitioning in the two emulsion phases and the concentration in the droplets [13,15]. During drying, instability of the emulsion and deposition of drug dissolved in the aqueous phase may occur. Therefore, in dried pellets the drug exists as solubilized in the oil/surfactant mixture dispersed in the MCC particles, and/or as solid particles, mainly in the outer part of the pellets, carried there by the migrating aqueous phase of the emulsion during drying.

In addition, viscosity affects capillary flow of liquid phase towards the pellet surface and drug deposition due to water evaporation during drying together with surface tension as has been already reported for wet granulations dried in conventional oven [19]. The contribution of surface tension on migration is not expected to be significant for the examined formulations, since it is similar for the aqueous solutions of the two drugs (64.0 and 66.0 mN/m) and the three surfactants (41.3–44.8 mN/m, Table 2).

Comparing the effects of drug lipophilicity and oil/surfactant ratio on emulsion viscosity and drug migration (%) (Tables III and VI), there is apparently some controversy. As expected, decreased emulsion viscosity due to increase of oil/surfactant ratio (for the same drug) corresponds to increased migration (%) but decreased viscosity due to increased drug lipophilicity corresponds to decreased migration (%). This controversy reveals predominance of drug lipophilicity and solubility in oil droplets on migration (%) over that of capillary flow.

From the above discussion, it is clear that both the viscosity of the emulsion (η) and drug solubility in oil/surfactant mixture (S) should control drug migration towards pellet surface. Accordingly, from the drug migration (M%) plots against the product [η•S], Figure 5, it can be seen that M% decreases exponentially with the product [η•S], following the simple equation ($R^2 = 0.856$):

$$M\% = 98.1e^{-0.016[\eta \cdot S]} \quad (5)$$

that could be useful during formulation work.

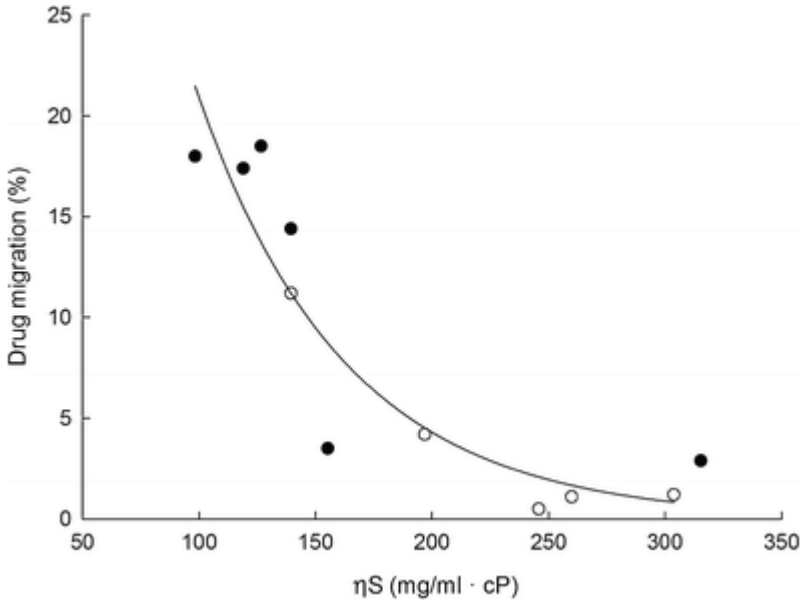

Figure 5. Plot of drug migration with the product of viscosity (η) and solubility of drug (S) in oil/surfactant mixtures

CONCLUSIONS

Regarding the emulsion properties, viscosity is affected by the type of drug and oil/surfactant ratio, the droplet size by the oil/surfactant ratio, while zeta potential is affected by the drug.

For the micromeritic properties and mechanical strength of pellets, pellet shape is affected by the studied formulation variables and there was significant interaction between the effects of the drug and surfactant type on pellet diameter. There were also significant interactions between the effects of drug and surfactant type and between the effects of drug and oil/surfactant ratio on pellet friability.

Regarding the pharmaco-technological properties of pellets, drug migration is higher for furosemide of lower lipophilicity and for higher oil/surfactant ratio. The droplet size of the reconstituted emulsions and the zeta potential of both added to the MCC (for the preparation of pellets) and reconstituted emulsions are affected by the type of drug. Linear relationships between the emulsion viscosity and shape parameters of pellets (aspect ratio and shape factor) and exponential relationship between drug migration (%) and the product of viscosity and solubility of drug in oil/surfactant were established, which may be useful during formulation work of self-emulsifying pellets.

References

1. Bechgaard H, Hegermann NG. Controlled-release multiple-units and single-unit doses. Drug Dev Ind Pharm. 1978;4:53–67.
2. Schulz P, Kleinebudde P. A new multiparticulate delayed release system. Part I: dissolution properties and release mechanism. J Control Release. 1997;47:181–9.
3. Constantinides PP. Lipid microemulsions for improving drug dissolution and oral absorption: physical and biopharmaceutical aspects. Pharm Res. 1995;12(11):1561–72.
4. Pouton CW. Formulation of self-emulsifying drug delivery systems. Adv Drug Deliv Rev. 1997;25:47–58.
5. Newton M, Petersson J, Podczeck F, Clarke A, Booth S. The influence of formulation variables on the properties of pellets containing a self-emulsifying mixture. J Pharm Sci. 2001;90(8):987–95.
6. Serratoni M, Newton JM, Booth S, Clarke A. Controlled drug release from pellets containing water-insoluble drugs dissolved in a self-emulsifying system. Eur J Pharm Biopharm. 2007;65:94–8.
7. Newton JM. Gastric emptying of multi-particulate dosage forms. Int J Pharm. 2010;395:2–8.
8. Tuleu K, Newton M, Rose J, Euler D, Saklatvala R, Clarke A, et al. Comparative bioavailability study in dogs of a self-emulsifying formulation of progesterone presented in a pellet and liquid form compared with an aqueous suspension of progesterone. J Pharm Sci. 2004;93(6):1495–502.
9. Iosio T, Voinovich D, Grassi M, Pinto JF, Perissutti B, Zacchina M, et al. Bi-layered self-emulsifying pellets prepared by co-extrusion and spheronization: Influence of formulation variables and preliminary study on the in vivo absorption. Eur J Pharm Biopharm. 2008;69:686–97.
10. Wang Z, Sun J, Wang Y, Liu X, Liu Y, Fu Q, et al. Solid self-emulsifying nitrendipine pellets: Preparation and in vitro/in vivo evaluation. Int J Pharm. 2010;383:1–6.
11. Nazzal S, Smalyukh II, Lavrentovich OD, Khan MA. Preparation and in vitro characterization of a eutectic based semisolid self-nanoemulsified drug delivery system (SNEDDS) of ubiquinone: mechanism and progress of emulsion formation. Int J Pharm. 2002;235:247–65.
12. Matsaridou I, Barmpalexis P, Salis A, Nikolakakis I. The Influence of Surfactant HLB and Oil/Surfactant Ratio on the Formation and Properties of Self-emulsifying Pellets and Microemulsion Reconstitution. AAPS PharmSciTech. 2012;13(4):1319–30.

13. Shah NH, Carvajal MT, Patel CI, Infeld MH, Malick AW. Self-emulsifying drug delivery systems (SEDDS) with polyglycolyzed glycerides for improving in vitro dissolution and oral absorption of lipophilic drugs. Int J Pharm. 1994;106(1):15–23.

14. Nielsen FS, Gibault E, Ljusberg-Wahren H, Arleth L, Pedersen JS, Mullertz A. Characterization of prototype self-nanoemulsifying formulations of lipophilic compounds. J Pharm Sci. 2007;96(4):876–92.

15. Chidambaram N, Burgess DJ. Effect of nonionic surfactant on transport of surface-active and non-surface-active model drugs and emulsion stability in triphasic systems. AAPS Pharm Sci. 2000;2(3):1–11.

16. Sznitowska M, Janicki S, Dabrowska E, Zurowska-Pryczkowska K. Submicron emulsions as drug carriers. Studies on destabilization potential of various drugs. Eur J Pharm Sci. 2001;12(3):175–9.

17. 17.Ktistis G. A viscosity study on oil-in-water microemulsions. Int J Pharm. 1990;61:213–8.

18. Podczeck F, Maghetti A, Newton JM. The influence of non-ionic surfactants on the rheological properties of drug/microcrystalline cellulose/water mixtures and their use in the preparation and drug release performance of pellets prepared by extrusion/spheronization. Eur J Pharm Sci. 2009;37:334–40.

19. Kapsidou T, Nikolakakis I, Malamataris S. Agglomeration state and migration of drugs in wet granulations during drying. Int J Pharm. 2001;227:97–112.

20. Poutiainen S, Honkanen M, Becker J, Nachtweide D, Järvinen K, Ketolainen J. X-ray microtomography analysis of intragranular drug migration during fluidized bed and oven tray drying. J Pharm Sci. 2012. doi:10.1002/jps.23051.

21. Schrank S, Hodzic A, Zimmer A, Glasser JB, Khinast J, Roblegg E. Ibuprofen-loaded calcium stearate pellets: drying-induced variations in dosage form properties. AAPS PharmSciTech. 2012;13(2):686–98.

22. Nikolakakis I, Malamataris S. Self-emulsifying pellets: relations between kinetic parameters of drug release and emulsion reconstitution, influence of formulation variables. J Pharm Sci. 2014;103(5):1453–65.

23. Ktistis G, Niopas I. A study on the in-vitro percutaneous absorption of propranolol from disperse systems. J Pharm Pharmacol. 1998;50(4):413–8.

24. Podczeck F, Newton JM. A shape factor to characterize the quality of spheroids. J Pharm Pharmacol. 1994;46:82–5.

25. Shipway PH, Hutchings IM. Attrition of brittle spheres by fracture under compression and impact loading. Powder Technol. 1993;76:23–30.

26. Montgomery DC. Design and analysis of experiments. 4th ed. New York: Wiley; 1987. p. 108–10.

27. Thi TD, Van Speybroeck M, Barillaro V, Martens J, Annaert P, Augustijns P, et al. Formulate-ability of ten compounds with different physicochemical profiles in SMEDDS. Eur J Pharm Sci. 2009;38:479–88.

28. Avdeef A, Box KJ, Comer JEA, Hibbert C, Tam KY. pH-Metric logP 10. Determination of Liposomal membrane-water partition coefficients of ionizable drugs. Pharm Res. 1998;15(2):209–15.

29. Florence AT, Attwood D. Physicochemical principles of pharmacy. 2nd ed. New York: The Macmillan Press; 1988. p. 239–40.

30. Zetasizer Nanoseries User Mannual MANO 317 Issue 1.1 Feb. 2004 page 5.6. Malvern Instruments Ltd, Worcestershire.

31. Alvarez-Nunez FA, Yalkowsky SH. Relationship between polysorbate 80 solubilization descriptors and octanol-water partition coefficients of drugs. Int J Pharm. 2000;200:217–22.

CHAPTER 2:

Development of thermosensitive chitosan/glicerophospate injectable in situ gelling solutions for potential application in intraoperative fluorescence imaging and local therapy of hepatocellular carcinoma: a preliminary study

Adapted from:

Development of thermosensitive chitosan/glicerophospate injectable in situ gelling solutions forpotential application in intraoperative fluorescence imaging and local therapy of hepatocellular carcinoma: a preliminary study

Andrea Salis, Giovanna Rassu, Maria Budai-Szűcs, Ilaria Benzoni, Erzsébet Csányi, Szilvia Berkó, Marcello Maestri, Paolo Dionigi, Elena Piera Porcu, Elisabetta Gavini, Paolo Giunchedi. Expert Opinion on Drug Delivery. May 2015Volume 12, Issue 10, pages 1583-1596.

INTRODUCTION

Hepatocellular carcinoma (HCC) is an important cause of cancer deaths: each year > 600,000 people die from HCC in the world [1]. The hepatic resection represents the initial treatment for localized HCCs in patients without vascular invasion and with preserved hepatic functions [2]: the precise imaging of HCC nodules is clearly important for the success of the surgical procedure.

HCC is classified as a highly chemoresistant disease and conventional systemic chemotherapy plays almost no role in the treatment of advanced HCCs. For these reasons, localized anticancer therapies must be taken into account [3]. Among several locoregional ablative methods, transarterial embolization (TAE) consists of embolization of the artery feeding the tumor, which results in ischemia and subsequent tumor necrosis, whereas transarterial chemoembolization (TACE) implies the localized delivery of chemotherapeutic drugs combined with the use of embolic materials. The rationale is based on the fact that normal liver tissue receives its blood supply from the portal vein, whereas liver tumors mostly from the hepatic artery [4,5]: a combination of concentrated chemotherapy and local ischemia within the tumor can be synergistic in achieving tumor necrosis [6].

Nowadays, microparticles are used both as embolic agents (TAE), and as embolic drug carriers (TACE). In humans microparticles of size larger than 10 μm are used considering that the capillary diameter is ∼ 6 – 8 μm. Diameters from 40 to almost 1000 μm are suitable. Particles greater than 1000 μm can determine catheter clogging during the intra-arterial administration [3].

The microparticles can be classified as non-biodegradable (e.g., polyvinyl-alcohol [PVA] microspheres) or biodegradable (e.g., microspheres based on natural polymers such as starch, gelatin, chitosan or on synthetic polymers such as polylactic-co-glycolic acid. Commercial products are available constituted by calibrated microspheres (drug empty particles to be loaded before use) that have changed the conditions of embolization: radiologists can adapt the size of microspheres to the size of the vessels to be occluded, in such a way to obtain an accurate targeting [7]. Several agents can be used for hepatic embolization; they have been recently reviewed [8]. Briefly, there are microspheres available on the market for so-called bland embolization or TAE. These include Bead Block®, Embospheres®, Embozene® and Contour SE®. DC Bead® was designed to load therapeutic agents to enable one-step TACE and consists of PVA hydrogel modified with sulfonate groups that were first to demonstrate the ability to load and release chemotherapeutics in a controlled manner – a concept known as a drug-eluting bead (DEB). Other DEB systems are also now commercially available but based on microspheres with carboxylic acid functionality instead

(HepaSphere® and Tandem®) [9]. All these commercial products are quite successful in the clinic, even if the intra-arterial local administration of microparticles can present some difficulties (such as catheter clogging). There is therefore the need of new embolizing systems, possibly not based on the intra-arterial administration of particles.

Indocyanine green (ICG) is a water-soluble, amphiphilic tricarbocyanine dye that has a broad range of clinical applications due to its low toxicity and capacity to absorb and emit in the near-infrared (NIR) spectral range [10]. Human tissue has the lowest absorption coefficient in the NIR part of the spectrum; therefore this dye is utilized for diagnostic and therapeutic applications.

Recent studies report the usefulness of ICG-based intraoperative fluorescence imaging for the detection of HCC nodules. HCC tumors show very strong fluorescent signals in patients who had been given an ICG bolus several days before surgery as a routine preoperative liver function test [11-14]. The real mechanisms that mediate the preferential accumulation of ICG in HCC nodules instead of the normal liver tissue are still unknown. A hypothesis could be that ICG accumulates in regions of tissue possessing leaky capillaries of vessels [15] or disturbance of bile secretion [11].

As reported in the literature [11,12,16], fluorescent nodules can be examined by an NIR camera system named PDE (photo dynamic eye, Hamamatsu Photonics K.K. Hamamatsu, Japan), that activates ICG with emitted light at a wavelength of 760 nm and filters out light with a wavelength < 820 nm [17]. The light source is a light emitting diode, and the detector is a charge-coupled device camera. The camera unit of the device is directly handled and real-time fluorescence images can be observed on the monitor in the operating room. Thus, either nodules detection or hepatic resection could be performed under the guide of the PDE.

'Smart' hydrogels are constituted by polymer solutions, which exhibit sol–gel phase transition in response to environmental stimuli such as pH, temperature, ionic strength, electric field, magnetic fields [18].

In situ thermo-sensitive hydrogels use temperature as the trigger of the gelation. Hence, it is possible to obtain hydrogels that are solutions at room temperature, but under physiological conditions (i.e., the body temperature) they form gels [19]. They can be designed as fluids that can be introduced into the desired tissue, organ or body cavity by simple syringe injection.

The viscosity of solutions can be low enough to allow direct blood administration. Thus after intra-arterial injection the solutions quickly form a gelled structure able to embolize the tumor [8,20] and to deliver imaging agents and/or drugs (if loaded in the precursor solution) [21]. Chitosan (C) is a cationic polysaccharide obtained by partial N-deacetylation of chitin. This polymer is widely used

in the field of controlled drug release for its gelling properties, biodegradability and high biocompatibility [22-24].

The major issue concerning the applicability of C formulations is the impossibility of maintaining C in solution up to physiological pH due to its pKa (~ 6.3). Above pH 6, C has no charge and it forms a gel-like precipitate [25].

Chenite et al.[25] developed a thermosensitive neutral aqueous solution based on C and glycerophosphate (GP), which exhibit sol–gel transition around body temperature. The addition of polyol salts, such as GP, leads to the transformation of pH-dependent C solutions into thermally sensitive pH-dependent solutions. In the presence of GP, C solutions remain liquid below room temperature, even with pH values within a physiologically acceptable neutral range from 6.8 to 7.2 [25]. These nearly neutral C/GP aqueous solutions gel when heated [26]. The neutralization behavior of GP determines C/GP solubility and phase transition phenomena. GP presents a mild alkalinity (pKa ~ 6.34) providing correct buffering without inducing immediate precipitation or gelation when the temperature provided is between 4 and 15°C [26].

Taking into account these considerations, the aim of this work was the design and preparation of polymeric platforms based on C/GP and loaded with ICG that might be used in the field of TAE and following intraoperative fluorescence imaging of HCC.

MATHERIALS AND METHODS

Materials

C was obtained from Primex ehf (Oslo, Norway). The deacetylation degree was 94% and the molecular weight was 103 kDa. GP, hydrated disodic salt, was purchased from Sigma Aldrich (St. Louis, USA). ICG Pulsion was obtained from SEDA (Trezzano, Italy). The molecular weight was 774.96 Da. All other chemicals were of analytical grade.

Preparation of C/GP blank solutions

C/GP blank solutions at different concentrations (Table 1) were prepared according to the method of Kashyap et al. [27]. C was dissolved in 18 ml HCl 0.1 N and GP was solubilized in 2 ml of bidistilled water, at room temperature. The two solutions were put into an ice bath until the temperature of 4°C was reached. Thereafter, the GP solution was dropwise added, under vigorous magnetic stirring, into the C solution. The final solution was then left under stirring into the ice bath for 15 min, at 4°C. As reported in the literature, in order to obtain liquid C/GP systems below room

temperature a pH range of 6.8 – 7.2 is required [25]. For this reason the pH of all solutions was measured (pH meter 510, XS instruments) (Table 1).

Table 1. Composition and pH of C/GP blank solutions prepared for the evaluation of gel formation.

C (%w/v)	GP (%w/v)	pH
2.0	12.0	7.31
2.0	10.0	7.25
2.0	7.0	7.21
2.0	6.0	7.17
2.0	5.0	6.98
2.0	4.0	6.98
2.0	3.5	6.95
2.0	3.0	6.95
1.6	18.0	7.42
1.6	15.0	7.34
1.5	7.0	7.29
1.5	6.0	6.98
1.5	5.0	6.96
1.5	4.0	6.96
1.5	3.5	6.85
1.5	3.0	6.81
1.0	7.0	6.89
1.0	6.0	6.88
1.0	5.0	6.86
1.0	4.0	6.84
1.0	3.5	6.80
1.0	3.0	6.80

Gel formation

In order to assess their thermo-sensitivity at 37°C, the C/GP blank solutions obtained (Table 1) were placed inside a plastic syringe, conveniently cut and isolated with a rubber cap and Parafilm®. The syringe was then emerged in a temperature-controlled water bath at 37°C (±1°C). The solutions were left there for 20 min in order to make a preliminary assessment of their gelation behavior.

Gelation time of C/GP blank solutions

Gelation time of C/GP blank solutions was studied using the inverted tube test method, according to the methodology described by Gupta et al. [28]. The inverted tube test was performed with the solutions that exhibited gel formation in 20 min with the previous method (Table 2). Two ml chromatographic glass tubes were thermo-stabilized in a temperature-controlled bath at 37°C (±1°C). Five hundred µl of the sample solution were placed into the tubes and incubated in the bath. At predetermined time intervals of 30 s, the tubes were taken out of the water bath and horizontally inverted in order to verify the solution flowability. If the solution did not flow within 15 s, the time is recorded as gelation time. Inverted tube tests were carried out immediately after the preparation of the solutions, which were then stored at 4°C. New measurements were taken the day after the preparation and every week through 3 weeks, in order to evaluate the solution stability and the possible changes of the gelation time over that period.

Table 2.Composition and gelation time of C/GP blank solutions (S) and formulations (F) performed with inverted tube test.

composition		**Gelation time(min:s)**									
C (%w/v)	**GP (%w/v)**	**after prep.**		**1 day**		**1 week**		**2 weeks**		**3 weeks**	
		S	**F**	**S**	**F**	**S**	**F**	**S**	**F**	**S**	**F**
2.0	12.0	06:00	06:00	06:00	06:30	06:00	06:00	05:30	05:30	05:00	05:30
2.0	10.0	07:00	07:00	07:00	07:00	07:00	07:30	04:30	04:30	04:00	04:00
2.0	7.0	14:00	14:30	03:00	03:00	02:00	02:30	01:30	01:30	01:00	01:00
2.0	6.0	16:30	16:00	04:30	05:00	01:00	01:00	00:30	00:30	00:30	00:30
2.0	5.0	18:00	18:00	07:30	07:30	00:30	01:00	00:30	00:30	00:30	01:00
1.6	18.0	02:00	02:00	02:00	02:00	02:00	02:00	02:00	02:00	01:30	01:30
1.6	15.0	03:00	03:00	03:00	03:00	03:00	02:30	03:00	03:00	02:30	02:30

Preparation of formulations and determination of their gelation time

ICG was incorporated in the C/GP solutions; composition is reported in Table 2. About 5 mg of ICG were dissolved in each C/GP solution (20 ml) under stirring condition at 4°C. Gelation time of formulations was determined following the inverted tube test method previously reported. The rationale was the assessment of the dye influence in the gelling properties of these thermosensitive fluids. Inverted tube tests were performed considering the same time intervals carried out for C/GP blank solutions.

Biodegradability

The leader solutions and formulations that exhibited the best gelation time were selected for further studies and named as reported in Table 3.

Biodegradability studies were conducted following the method of Zang et al. [29]. Hydrogels formed from blank solutions and formulations were prepared at 0.6 cm3 volume and 1 cm diameter and immersed in 2 ml of DMEM medium with 0.1% sodium azide containing 1.91 μg/ml chicken egg white lysozyme. Samples were placed in incubator thermostabilized at 37°C for 14 days. The medium was replenished every week of storage. Dried weights of the samples were measured on the 1st, 4th, 7th and 14th days of incubation. Degradation was determined by percentage of weight loss [29].

Table 3. Composition of leader solutions and formulations.

Code	C (% w/v)	GP (% w/v)	ICG (% w/v)
C2/GP12	2.0	12.0	-
C2/GP12d	2.0	12.0	25
C2/GP10	2.0	10.0	-
C2/GP10d	2.0	10.0	25
C2/GP7	2.0	7.0	-
C2/GP7d	2.0	7.0	25
C1.6/GP18	1.6	18.0	-
C1.6/GP18d	1.6	18.0	25
C1.6/GP15	1.6	15.0	-
C1.6/GP15d	1.6	15.0	25

Rheological characterization

Leader solutions (Table 3) and their corresponding hydrogels were analyzed by rheological methods. The gelling and rheological properties were performed with a Physica MCR101 rheometer (Anton Paar, Austria). The measuring system was parallel-plate type (diameter 50 mm, gap 0.2 mm). Each type of rheological measurement was performed immediately after the preparation of solutions and after 1 week of storage at 4 and 20°C. Data were expressed as mean ± standard deviation (n = 3).

Viscosity measurements

Viscosity measurements of solutions were carried out at 4°C applying a shear rate from 0 to 100 1/s. For all curves the slope (n) was determined in order to evaluate the changes of the viscosity increasing the shear rate.

Frequency sweep measurements

Dynamic frequency sweep tests were performed at constant temperature (37°C) and strain (1%) in the limit of the linear viscoelastic region. The storage (G′), and loss moduli (G″) damping factors

were determined for angular frequencies (ω) between 0.1 and 100 1/s. The viscoelastic behavior on the hydrogels was analyzed via their corresponding damping factors (tan(δ)) at ω = 10 1/s.

Gelation time performed with rheometer

Gelation time was determined at 37°C at a constant angular frequency (ω) of 1.0 1/s at a constant strain of 1 % measuring the G′ and G″ as a function of time. Gelation time of the samples was established at the time of the intersection of G′ and G″, where tanδ = 1. The differences between gelation time values gained by the rheometer and the inverted tube test were assessed.

In vitro dye release studies

Each formulation (Table 3) was filled in a dialysis bag previously activated with ethylene diamine tetra-acetic acid. The molecular weight cut off of the dialysis bag was 12,000 – 14,000 and higher than the molecular weight of the dye. The dye release was studied by using the USP dissolution apparatus (DT70, Erweka GmbH, Germany). Each dialysis bag was fixed to the rotating bar of the dissolution tester and lowered into the dissolution vessel containing 900 ml of phosphate buffer (PBS) at pH = 6.5, 37°C (±1°C). The rotation speed of the dialysis bag was 100 rpm. The dissolution test was performed up to 16 h. At each prefixed time point, the medium (1 ml) was removed for analysis and it was replaced with the corresponding volume of fresh PBS. The samples removed from the medium were immediately analyzed spectrophotometrically (λ = 779 nm) (ThermoSpectronic, Helios, UK). The dissolution studies were conducted in triplicate (mean values are reported). The dye contents of the samples were measured from the reference absorption–concentration curve of the dye that was constructed by using standard solutions of known ICG concentration in PBS. The same test was performed filling 10 mg of ICG in the aqueous solution in another dialysis bag in order to make a comparison with the release behavior of C/GP systems loaded with ICG.

Dye uptake from a preformed hydrogel

The eventual ability of blank hydrogels to up-take ICG dispersed in the liver was investigated filling a preformed blank hydrogel (C1.6/GP15) into a solution of known ICG concentration (0.01 mg/ml) in PBS pH = 6.5, 37°C (±1°C). The variation of ICG concentration in the medium was analyzed via the UV spectrophotometer (λ = 779 nm) (ThermoSpectronic, Helios, UK) removing

samples (1 ml) from the medium at 15, 30, 45, 60 and 90 min. The medium removed for analysis was always replaced with the corresponding volume of fresh PBS.

Ex vivo embolization procedure

Ex vivo studies were carried out on a bovine liver (weight of ~ 8 kg), thermostabilized at 37°C in a saline bath. The experiments were carried out in standard conditions, with the organ preserved outside of the body. It was flushed at a low pressure saline solution (NaCl 0.9%) and immersed into ~ 10 – 15 cm of H2O.

The leader formulations were selected for these studies (Table 3).

The hepatic artery was surgically exposed and then catheterized with a catheter (CVC 14 Gauge). Successively, 5 ml of formulation was slowly injected till a predetermined area of the organ through the distal branches of the hepatic artery (in the right lateral lobe) to selectively embolize an area of 3 – 4 cm2. Selective visualization of the injection site with an NIR fluorescence imaging system (PDE; Hamamatsu Photonics K.K. Hamamatsu, Japan) and intraoperative ultrasound (Flexfocus 800, BK medical) were performed in order to assess the localization and gelation of the solutions and the occlusion of the artery. Our group has previously described the combined use of ICG fluorescence and ultrasounds as a useful combine technique to detect small nodules into a liver [16]. In this experiment the probe could allow us to confirm the site of gelation shown by fluorescence detection. The site visualized by PDE was then cut open in order to evaluate the hydrogel formation.

RESULTS

Preparation of C/GP blank solutions and gel formation

Twenty-two C/GP blank solutions, characterized by different C/GP weight ratios, were prepared (Table 1). Solutions with the highest concentrations of GP (12 – 18% w/v) were clear solutions at 4°C when polyol salt was dropwise added. On the contrary, solutions with the lowest concentration of GP (3.0 – 7.0% w/v) showed a different behavior at 4°C: the formation under stirring of a milky suspension was observed, whereas a gel-like milky precipitate formed without stirring. However, by shaking or intense stirring, the milky suspension was again obtained.

Gelation of the solutions was assessed through their incubation in a plastic syringe inside a thermo-stabilized bath (37 ± 1°C) and left there for 20 min. Solutions which displayed gelation within that time interval are showed in Table 2. An increase in the hydrogel compactness was found by rising

the concentration of C and GP. For the same amount of C, hydrogels with higher amounts of GP were more opaque and they presented a stronger milk coloration, which was in conformity with the observations reported by Ahmadi and De Bruijn [30].

Gelation time of C/GP blank solutions and formulations

Figure 1 shows gel set in the inverted tube of a formulation chosen as an example Gelation time results following the inverted tube test method are presented in Table 2. After the preparation, solutions with 2% of C showed the increase of gelation time as the GP concentration decreases from 6 min (12% w/v) to 18 min (5% w/v). When C concentration is lowered to 1.6%, higher GP concentrations are necessary to obtain more rapid gelation time: 2 min (18% w/v) and 3 min (15% w/v) were gained.

A decrease in the gelation time values taken 1 day after the preparation was observed for 2% C solutions with the lowest amount of GP (5.0 – 7.0%) till 7 – 3 min, respectively; this behavior was observed also along the time as a further remarkable decrease in the gelation time from the first to the third week was observed.

The incorporation of ICG into C/GP blank solutions did not display any significant change in the gelation rates of these systems (Table 2). Even after 3 weeks of storage at 4°C, all of the C/GP solutions analyzed remained temperature-sensitive.

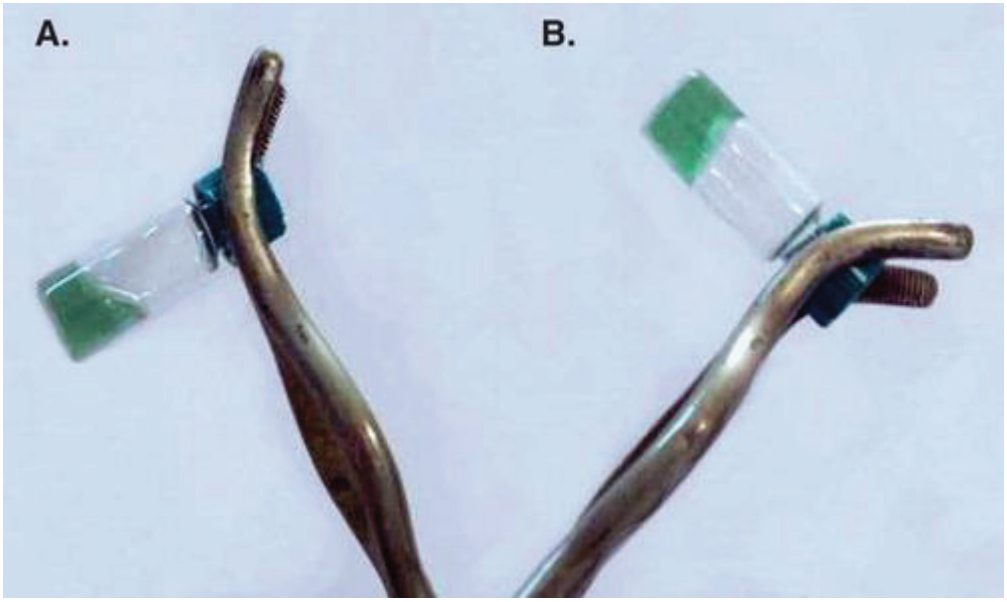

Figure 1. Photographs of the gelation process observed by the inverted tube test. Formulation is a flowable liquid at room temperature (A) and it is transformed to a rigid hydrogel at 37°C (B).

Biodegradability

Figure 2 shows the degradation rate of blank hydrogels or containing ICG. The degradation rate was independent of dye loading and decreased as the C concentration in the solution increased. Over the 14 days of degradation, formulations with 2% C concentration were degraded no more than 54%, whereas formulations with 1.6% C concentration exhibited a degradation rate > 60% (Figure 2B). Nevertheless, the cross-link density between C and GP did not affect the degradation rate in the case of formulations with 2% C concentration. The only exception was formulation C2/GP7d that exhibited the lowest degradation rate despite the lowest concentration of GP (lowest cross-link density between C and GP). As concerning 1.6% C concentration, the formulation degradation rate increased as the cross-link density decreased.

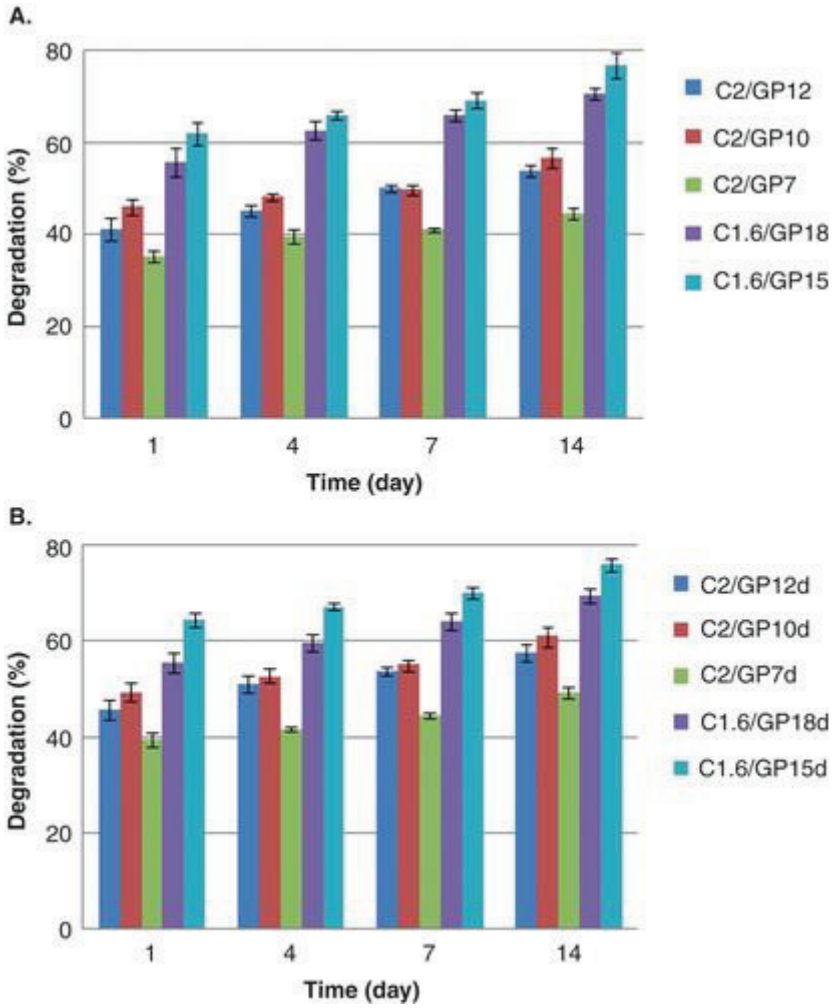

Figure 2. Degradation of hydrogel obtained from blank solutions (A) and formulations (B) > 14 days. Data are depicted as mean ± SD (n = 3).

Rheological characterization:

Viscosity measurements

For all solutions, the viscosity curve was determined at 4°C. In this type of diagram, viscosity is plotted versus shear rate in order to get information about the flow behavior of polymer solutions. Figure 3 shows viscosity of C1.6/GP18, chosen as example. This formulation exhibited a shear-thinning behavior showing viscosity decreases when the shear rate has increased. Furthermore, the storage time and temperature had also an effect on the viscosity. Other solutions displayed similar viscosity performance.

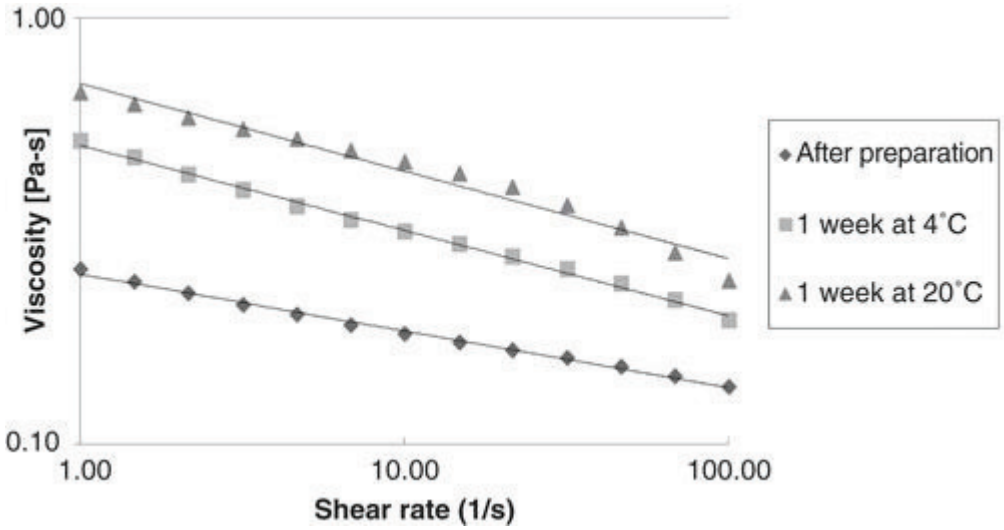

Figure 3. Viscosity curves of C1.6/GP18, chosen as example, after preparation and after 1 week of storage at 4 and 20°C.

Data in Table 4 show the viscosity values at the shear rate of 100 1/s. Solutions with high cross-link density between C and GP (formulation C1.6/GP18 and C1.6/GP 15) exhibited an increase of the viscosity during the storage, as already reported in the literature [31].

For all viscosity curves, the slope (n) was determined. Table 4 shows that the solution with the lowest cross-link density between C and GP (C2/GP7) exhibited the highest value of n. Solutions with the highest cross-link density (formulation C1.6/GP18 and C1.6/GP15) displayed the lowest values of n as it was expected. The slopes were quite independent from storage temperature (data not shown).

Table 4. Viscosity, η, at shear rate of 100 1/s of solutions stored at 4°C and 20°C.

Solution	η (Pa × s)			Slopes (n) after preparation
	Storage at 4°C		Storage at 20°C	
	after preparation	1 week	1 week	
C2/GP12	0.476 ± 0.06	0.412 ± 0.05	1.040 ± 0.07	0.379 ± 0.09
C2/GP10	0.358 ± 0.03	0.302 ± 0.08	0.710 ± 0.10	0.333 ± 0.08
C2/GP7	0.205 ± 0.02	0.370 ± 0.03	0.152 ± 0.03	1.163 ± 0.10
C1.6/GP18	0.157 ± 0.02	0.244 ± 0.03	0.317 ± 0.05	0.125 ± 0.01
C1.6/GP15	0.160 ± 0.01	0.274 ± 0.03	0.270 ± 0.07	0.129 ± 0.01

Frequency sweep measurements

Figure 4 displays the frequency dependency of G′ of hydrogels. High gel strengths (high G′) were obtained increasing the cross-link density between C and GP. The only exception was solution C2/GP7 that exhibited a good gel structure despite the lowest cross-link density. Data in Table 5 show the damping factor of hydrogels at ω of 10 1/s. The lowest values of tan (δ) are related to solutions with the highest molar ratio GP/C. This tendency was general at 4 and 20°C. The tan (δ) slightly changed during the storage time (at 4 and 20°C) except for C2/GP7 whose tan (δ) was similar and even lower than tan (δ) plotted for C2/GP10 and C2/GP12, made with the same concentration of C but with higher concentration of GP.

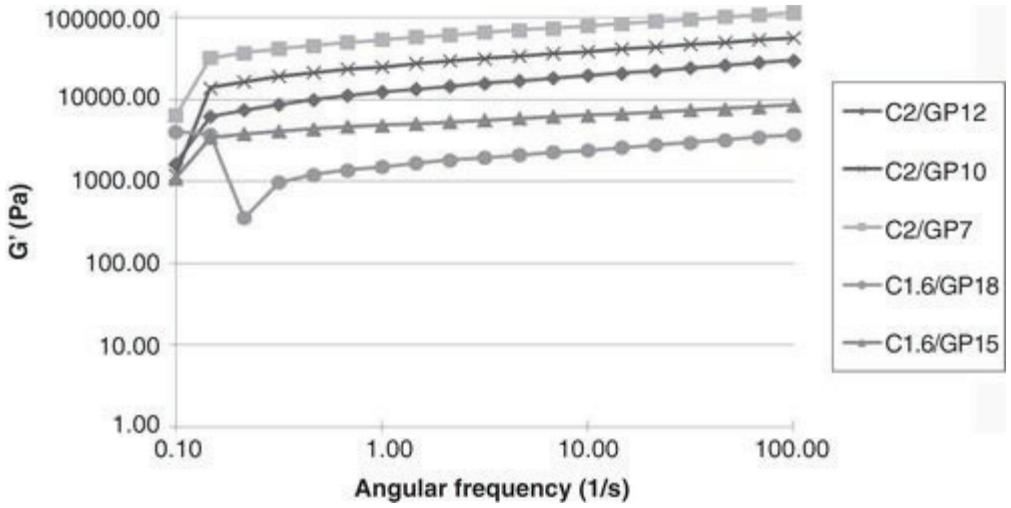

Figure 4. Frequency dependence of hydrogels after preparation.

Table 5. Damping factors (tan (δ)) at 10 1/s of hydrogels, obtained from solutions stored at 4 and 20°C.

Solution	tan (δ)		
	Storage at 4°C		Storage at 20°C
	after preparation	1 week	1 week
C2/GP12	0.28 ± 0.01	0.29 ± 0.02	0.26 ± 0.01
C2/GP10	0.29 ± 0.03	0.30 ± 0.01	0.28 ± 0.01
C2/GP7	0.30 ± 0.03	0.27 ± 0.02	0.24 ± 0.01
C1.6/GP18	0.19 ± 0.02	0.17 ± 0.03	0.16 ± 0.04
C1.6/GP15	0.22 ± 0.03	0.24 ± 0.03	0.22 ± 0.03

Gelation time performed with rheometer

The dynamic viscoelastic functions G′ and G″ were measured as a function of time at 37°C. Gelation time (tg) is defined as the crossing point between G′ and G″. Figure 5 shows the changes of the storage and the loss modulus as a function of time at 37°C of C1.6/GP18, chosen as an example. The gelation point of the samples was established at the intersection of G′ and G″.

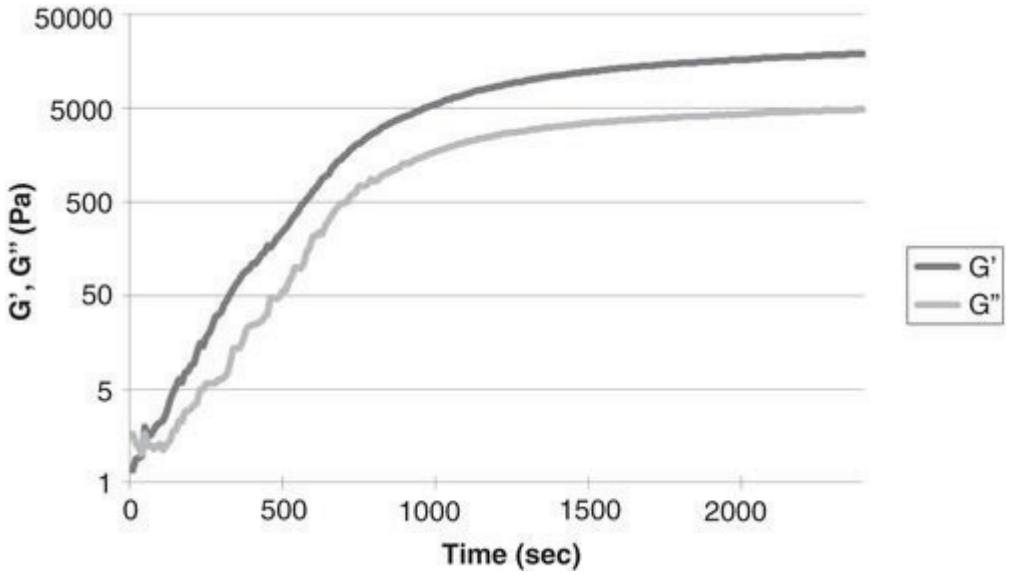

Figure 5. Sol–gel transitions versus time of C1.6/GP18 at 37°C after preparation, chosen as example.

Values of tg of all samples extrapolated from sol–gel transitions versus time curves (data not shown) are quite similar to gelation time values carried out with inverted tube test. Thus, there was a good correspondence between the two methodologies.

For C2/GP7, it was not possible to identify the crossing point, and consequently the tg because G′ was always higher than G″ during the time.

From G′ versus time curves (Figure 6), the gelation speed of the samples necessary to reach an adequate gel structure can be evaluated, through the slopes of those curves (Table 6). The slopes were dependent on the cross-link density between C and GP and on C and GP concentrations. The only exception was C2/GP7 that exhibited a rapid gelling despite the lowest cross-link density between C and GP.

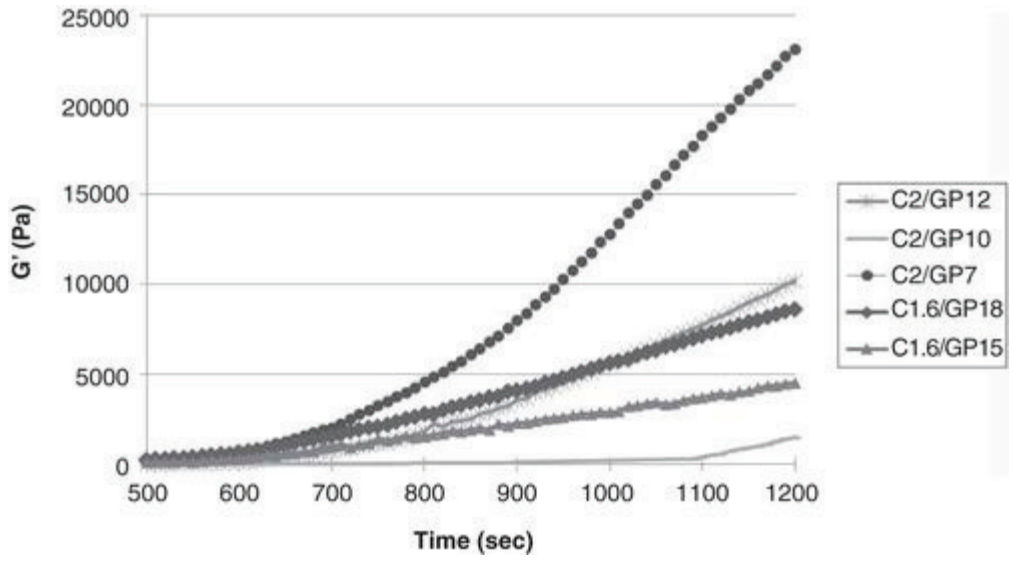

Figure 6. Comparison of the slopes of solutions after preparation.

Table 6. Slopes (n) of G′ versus time curves of solutions after preparation.

Solution	Slope (n)
C2/GP12	21.75 ± 6.53
C2/GP10	13.80 ± 4.00
C2/GP7	47.70 ± 4.31
C1.6/GP18	16.80 ± 2.11
C1.6/GP15	6.84 ± 1.05

In vitrodye release studies

Release of ICG from hydrogels into PBS at 37°C over the course of 16 h was measured spectrophotometrically. The results are displayed in Figure 7. The dye in the aqueous solution was able to diffuse across the membrane. On the contrary, no significant release of ICG from C1.6/GP15d hydrogel occurred. Indeed, ICG cross through the cutoff of the dialysis bag neither in the first minutes when formulation was still in solution, nor when it gelled. No difference in the release profile was found in the case of other formulations.

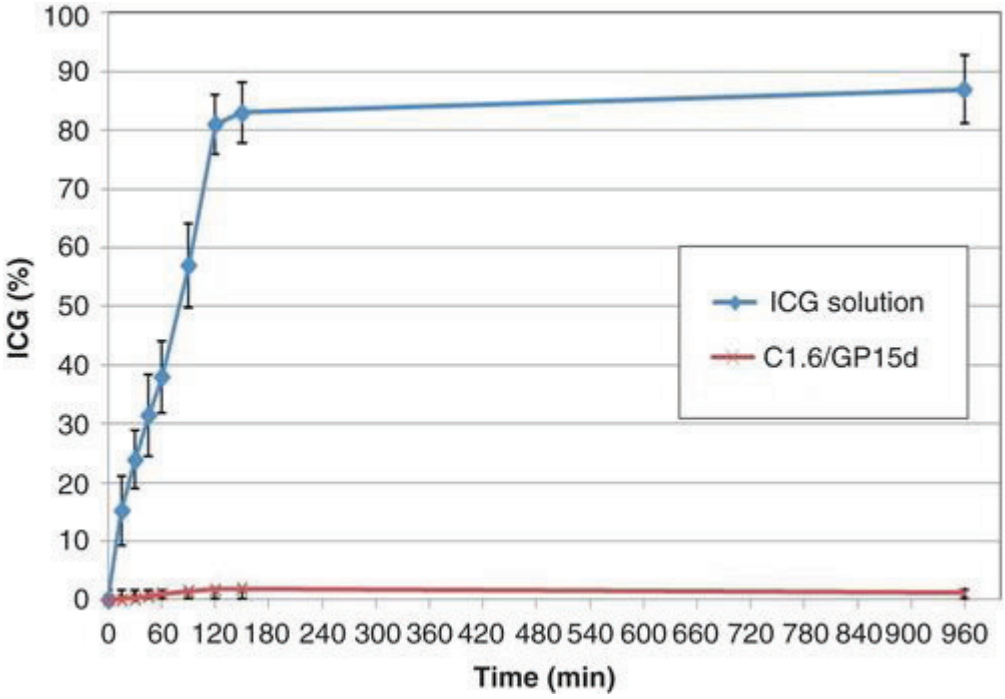

Figure 7. In vitro release profile of ICG from C1.6/GP15d, chosen as example, compared with that of diffusion from the ICG water solution. Data were expressed as mean ± SD (n = 3).

Dye uptake from preformed hydrogel

Considering the results from in vitro release studies, which showed the ability of hydrogels to retain ICG, the present test was done to confirm the strong affinity between ICG and hydrogels. A preformed hydrogel (C1.6/GP15) was immersed into the PBS solution of known ICG concentration (Figure 8A); the variation of ICG concentration was measured spectrophotometrically at different time intervals. It was observed a loss of dye absorbance in the PBS solution just only after 15 min from 0.952 to 0.294 and decreased till 0.092 after 60 min (Figure 8B). The observed loss of dye absorbance could be correlated with the strong interaction between C and ICG [32]. As the hydration of C1.6/GP15 hydrogel occurs, an interaction between chitosan and the dye could be hypotized: in fact, green gelled clots were observed suspended into the PBS solution, which appeared decolored (Figure 8C).

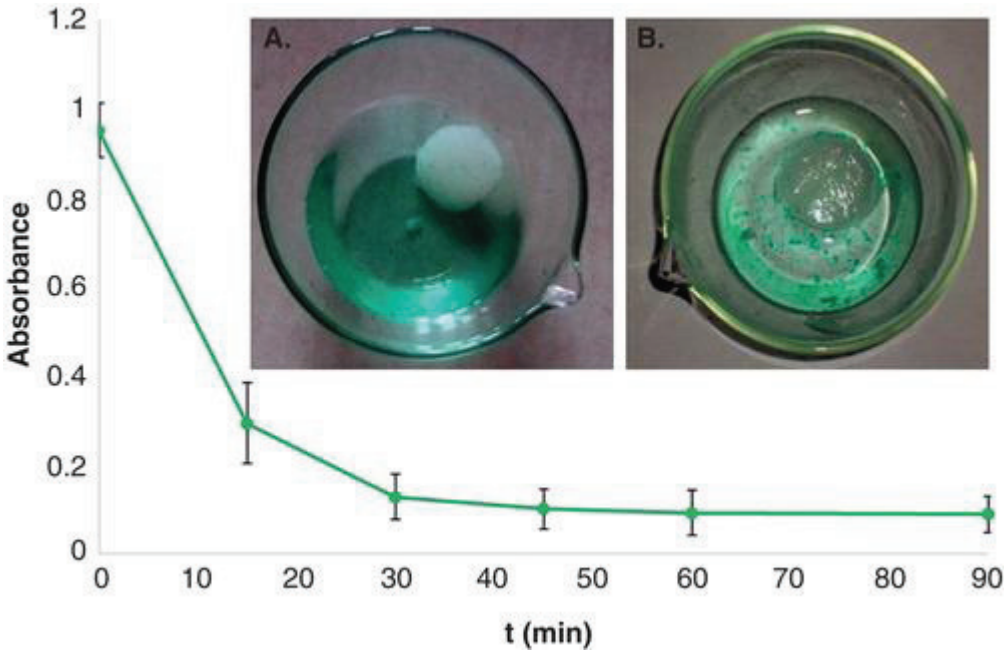

Figure 8. Absorbance curve of ICG solution versus time during dye uptake from preformed hydrogel; picture of ICG solution immediately after the immersion of C1.6/GP15 hydrogel. (A) and after 90 min (B).

Ex vivo embolization procedure

The injection of the leader formulations (Table 3) through the hepatic artery was performed as previously described. Considering the results gained from the inverted tube test, C2/GP7d was injected the day after the preparation in order to achieve a faster gelation inside the artery.

In all cases the formation of a stable gelled clot was macroscopically observed at the site of embolization in the hepatic parenchyma, due to the rapid gelation of the injected solution, containing the thermosensitive polymer. In this set of experiments, the hydrogel was apparently completely stabilized after 1 – 5 min at 37°C. The same clot was evident at PDE examination (Figure 9). Furthermore, sections of the liver in correspondence of the injected site confirmed the presence of the gelled clot (Figure 10).

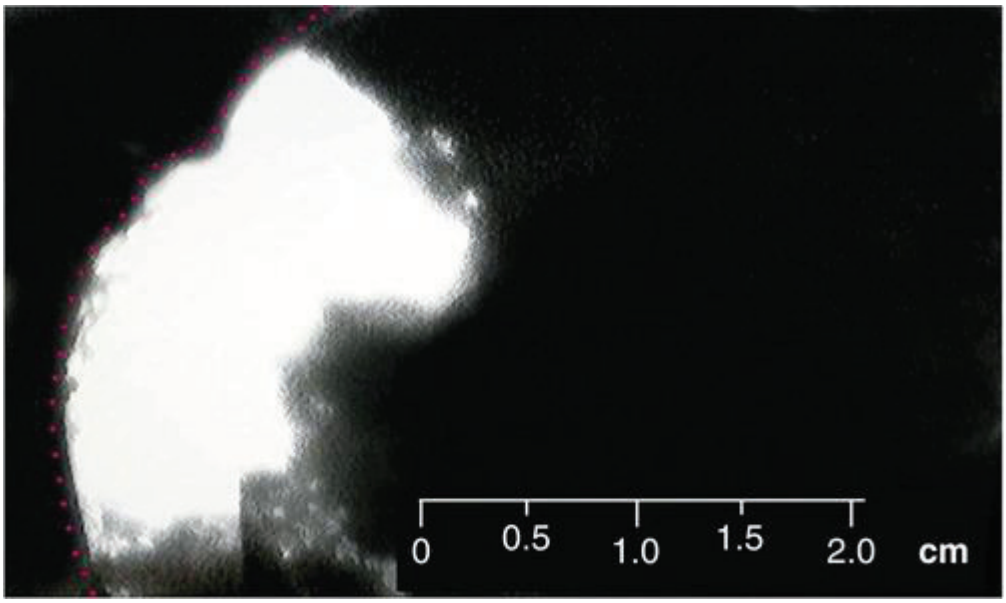

Figure 9. Selective visualization of the injection site with a near-infrared fluorescence imaging system PDE. The embolizing formulation was injected through the hepatic artery in the right lateral lobe. The figure shows the bright fluorescence of ICG under the infrared PDE camera and its neat localization into the injection site. The dotted line indicates the limit of the organ.

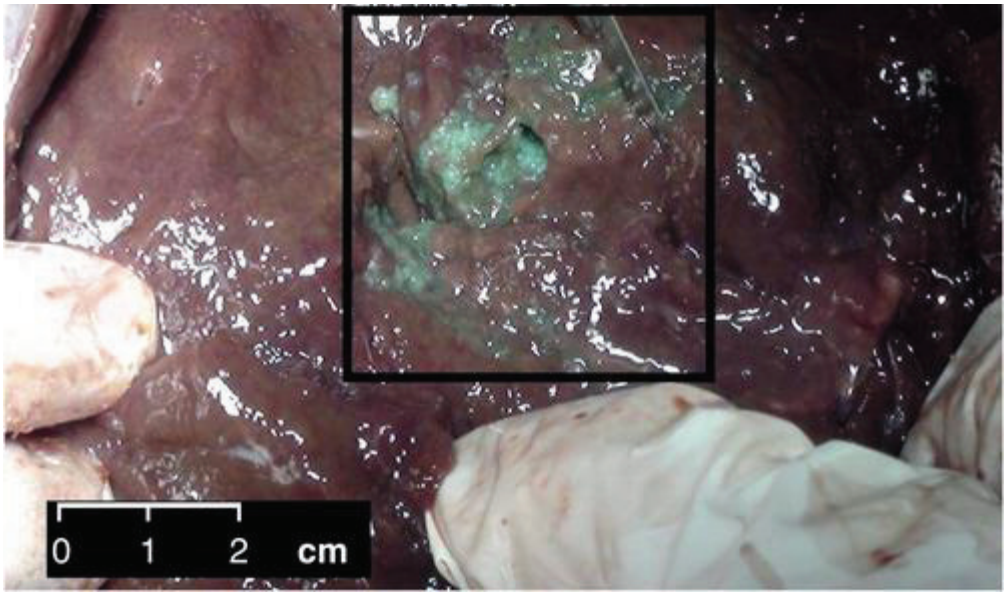

Figure 10. Section of the liver after the in situ gelation of C1.6/GP15d. The picture demonstrates gelled clots at the site of injection after cutting open the area previously localized by PDE and showed in Figure 9.

DISCUSSION

C/GP solutions were prepared to develop a class of ICG-loaded injectable hydrogels, whose potential application is the loco-regional detection and treatment of HCC nodules. Particularly, the solution should be injected down a catheter, which is selectively placed into the arterial branches of a predetermined liver area, similarly to the technique used for superselective TACE. The polymeric compound should be delivered close to the tumor and saturate its vessels. The sol–gel transition should be fast enough to allow a saturation of the microcirculation. These solutions should be able to exhibit an adequate viscosity to be injected and gelation behavior at physiological temperature (about 37°C). The formed gel should have suitable viscosity to embolize and avoid that hydrogel fragments can flow in the blood circulation. Any peripheral escape of the dye should not be observed.

Most of the solutions prepared are characterized by low concentrations of GP, ranging from 3 to 7% w/v (Table 1); in spite of its endovenous use being approved by the Food and Drug Administration, certain GP toxicity issues have been arisen: after gelation GP starts diffusing out of the physically cross-linked network, resulting in a linear increase of the extraction medium osmolality, which results in possible local cytotoxic effects [33]. Therefore the rationale was the preparation of in situ gelling solutions containing the minimum GP amount. In C/GP systems three types of interactions may be involved in the gelation process: i) hydrogen bonding between C chains, as a consequence of reduced electrostatic repulsion after neutralization with GP; ii) electrostatic attraction between C ammonium groups and GP phosphate groups; iii) C–C hydrophobic interactions [25,34]. Although sol–gel phase transition is driven by hydrophobic interactions, gelation would not occur without mechanisms i) and ii). This explains the role of pH in the temperature-controlled gelation of C/GP aqueous systems [25]. At low temperatures, C/GP solutions with a pH around 7 do not immediately turn into a gel suggesting that repulsive forces between the C chains are stabilized at low temperatures and destabilized at high temperatures. Ruel-Gariépy et al.[35] hypothesized that GP prevents or slows down gelation at low temperature. In fact, polyols are known to stabilize several compounds in aqueous solutions, promoting the formation of a shield of water around some macromolecules in polyol-water mixtures [36]. Accordingly, the presence of GP into the C solution promotes the protective hydration of C chains, preventing at low temperatures their association and consequently gelation. C chain hydration is then dependent on the amount of GP added to the C solution. If GP concentration is too low, as in the solutions prepared, the formation of a water shield around C chains and their neutralization is only partial, preventing just part of their association and

leading to a gel-like precipitate at low temperatures. The gel-like precipitate formation at 4°C is reversible. At 4°C hydrogen bonding between C–C and C–water are predominant and there is not enough energy for hydrophobic bonds to be established, resulting in a reversible gelation process. Gelation time values obtained immediately after the preparation of the final solutions (Table 2) are in accordance with the results reported by Chenite [25]. In order to achieve a physiologically acceptable pH range and fast gelation at 37°C, high concentrations of C and GP are required. As a consequence, gelation time increased with the decreasing of GP and C amounts. The increase of the gelation rate observed for solutions with the lowest amount of GP (5.0 – 7.0%) during the storage, at 4°C, could be explained in the following way: as we previously reported, low proportions of GP lead to a reversible gelation of C solutions at low temperature even if the pH of the formulations is neutral. Although the hydrogels turned back into a solution under stirring, the presence of small gel nucleus dispersed into the C/GP solutions was observed. As a result, shear stress allows the breaking of the gel network and the formation of small gel nucleus of C/GP, which are suspended in the aqueous solution. Gel nucleus can aid and accelerate the final gelation induced by temperature through a mechanism of nucleation and growth. The small increase in the gelation rate for the formulations with the highest GP concentrations after 3 weeks of storage was also dependent on the high deacetylation degree of C used for the preparation of these formulations. The combination of high deacetylation degree with high GP concentration leads to high cross-link density between the phosphate groups of GP and the ammonium groups of C [34].

Although all solutions and formulations (Table 2) gel at body temperature, the solutions that exhibited slow gelation cannot be considered suitable for local treatment of HCC as embolic agents. The C/GP solution should form a gel quickly in order to provide good occlusion of blood flow [37]. The viscosity and compactness of the corresponding hydrogels that strictly depend on C and GP concentrations could be further critical parameters [36]. High viscosity may help to control injection, to avoid dilution of the solution and to limit the possibility of migration into collateral arteries [31]. In the latter case, if the arterial blood flow disperses the embolic agent, cardiopulmonary embolism may occur [38-42]. However, too fast gelation may be problematic because it could determine catheter occlusion. Accordingly, five leader solutions and formulations were selected for further in vitro and ex vivo studies (Table 3). By virtue of the high viscosity, high compactness and adequate gelation rate, these formulations are supposed to remain in the injection site, filling and gelling in vessel cavities. In all cases, formulations remained easily injectable through (CVC 14 Gauge) catheters. Data in Table 4 show the viscosity values at the shear rate of

100 1/s in order to make a comparison with the high shear rate evolving during a hypothetical injection of our solutions. Thus, it is possible to evaluate the injectability of these systems immediately after the preparation and after 1 week of storage. These systems could be considered still injectable, nevertheless an increase of the viscosity during the storage was observed for solutions with high cross-link density between C and GP. The determination of the slope (n) of viscosity curves is a useful approach to understand the resistance to flow of our solutions and consequently the injectability of such systems. The high slope determines low resistance to flow, which indicates a good injectability for these pseudoplastic liquids and, in terms of applicability, a good fit to the desired blood vessel or body cavity. As shown in Table 4 the solution with the lowest cross-link density between C and GP (C2/GP7) exhibits the best injectability despite the formation of a gel-like precipitate at 4°C. This because the gel-like precipitate structure is quite easy to be destroyed during the injection procedure.

Frequency sweep tests were used to characterize the final gel-structure of the five solutions at body temperature. The gels can be described as systems in which the G′ are higher than the G″ and/or they are relatively independent from frequency. Lapasin and Pricl [43] classified gels into two classes: strong gels, where the moduli are relatively independent from frequency and weak gels, where the moduli are slightly dependent from frequency. Frequency sweep measurements were carried out in the limit of the linear viscoelastic range, in order to evaluate the frequency dependency of the G′ and G″. The high gel strengths (high G′) showed by solutions with high cross-link density between C and GP were in conformity with the results previously reported in the literature [35]. The unexpected result of C2/GP7, which exhibited a good gel structure despite the lowest cross-link density, could be explained with the presence of the gel-like precipitation at 4°C. The gel-like precipitate can aid the reaching of a strong gel structure thanks to a nucleation mechanism.

The damping factor reveals the ratio of the viscous and the elastic portion of the viscoelastic deformation behavior. In the hydrogel field, the determination of this value is an important criterion to assess gel formation and the hardening process. Therefore, tan (δ) > 1 defines the liquid state and tan (δ) < 1 defines the gel state. Furthermore, tan (δ) indicates the elasticity property of the hydrogels: the low tan (δ) determines strong gel structure and, as a consequence, good gel resistance and stability inside the desired tissue, organ, or body cavity.

Data in Table 5 show that the lowest values of tan (δ) are related with solutions with the highest molar ratio GP/C, due to a better neutralization of C chains that leads to an improvement of the

interactions involved in the gelation process (hydrogen bonding and hydrophobic interactions). The unexpected tan (δ) of C2/GP7 displayed during the storage time (at 4 and 20°C) could be explained by the nucleation growth mechanism previously supposed. As previously reported, it was not possible to extrapolate the tg from sol–gel transitions versus time curves for C2/GP7: G′ was always higher than G″ during the time. This comportment is probably due to the presence of the gel-like precipitation at 4°C that leads to an elastic response of the material and that is stronger than the viscous response. As described before, low proportions of GP lead to a reversible gelation of C solutions at low temperature.

The unexpected result for formulation C2/GP7 is found and it is in contrast with the theories reported in the literature [25,35]. C2/GP7 exhibited a rapid gelling despite the lowest cross-link density between C and GP. This performance could be explained by the gel-like precipitation at 4°C. For the other solutions, the slopes are dependent on the cross-link density between C and GP and on C and GP concentrations as we expected.

The degradation rate of C/GP hydrogels with lower concentration of C was faster than those with higher concentrations of this polymer. This behavior was in accordance with previous studies [29,44]. As concerning as the cross-link density, the literature reports that hydrogels with high cross-link density have strong gel intensity prohibiting enzyme permeation and causing less degradation [44,45]. However, our results demonstrated that C concentration mainly affects the degradation rate as C1.6/GP15d and C1.6/GP18d (although they have high cross-link density) showed higher weight loss compared to 2% C formulations. It can be attributed to the susceptibility of C toward lysozyme [46]. The lowest degradation rate observed for formulation with the lowest cross-link density (C2/GP7d) was also supported by our frequency sweep experiments. This hydrogel exhibited a good gel structure that can be attributed to the nucleation growth mechanism previously mentioned.

The release of ICG from formulations analyzed was not significant. This behavior could be due to an electrostatic interaction between C and ICG [32]. In the aqueous solution, the dye is negatively charged thanks to its sulphonic groups, whereas C is cationic. Therefore, the molecular weight of the ionic complex is bigger than cutoff of dialysis membrane used in our release study and ICG is not quantified in the dissolution medium.

A final consideration must be done about the sterilization of these systems: the formulations described in this preliminary work are not sterile because the kind of experiments performed (in vitro and ex vivo) does not require sterile systems. The literature shows that steam sterilization of

chitosan may have different effects depending on whether sterilization was performed during its dry state or after it was in solution. Results show that autoclaving the dry chitosan power had no effect on viscosity and thus chitosan dry after sterilization does not undergo any structural changing. Thus, sterile hydrogel can be obtained by treating the dry material and working in aseptic environment [29].

At the current point of this research, we have demonstrated that a polymeric platform can be loaded with a dye to mark a liver area. Considering the results gained from the ex vivo procedure, these in situ gelled C/GP formulations have the potential to remain in correspondence of the injected site for a long period of time. As we reported before, the time of gelation of these hydrogels was a matter of second, and the process starts immediately at contact with the warmth of blood resulting in an embolization effect of the tumor. Such an approach could stop the growth and shrink the tumor burden, while leaving on site a marker, to help the following intraoperative detection of the cancer. At the same time, the removal of the fluorescent tissue would be guided throughout the operation by a real time observation of the parenchymal margins. The final result could be a better outcome for the patients, with an advantage offered by the pre-treatment of the tumor and a resulting aid during the resection. However, this preliminary study is a 'proof of concept' and its clinical use still requires further experiments.

CONCLUSIONS

Thermosensitive C/GP platforms were prepared and loaded with ICG, which did not interfere with their gelation process. C2/GP7d thanks to a gel-like precipitation, rapidly forms in situ compact gels and represents a good candidate for filling vessels. Taking into consideration the obtained results, formulations could be injected through a catheter into tumor nodules; as the solution gels in these areas, a prolonged visualization of these nodules can be achieved in 'real time imaging' during the embolization and the following hepatic resection of HCC.

References:

1. Ferenci P, Fried M, Labrecque D, Hepatocellular carcinoma (HCC): a global perspective. J Clin Gastroenterol. 2010;44:239–45
2. Tam KY, Leung KC, Wang YX. Chemoembolization agents for cancer treatment. Eur J Pharm Sci. 2011;44:1–10
3. Giunchedi P, Maestri M, Gavini E, Transarterial chemoembolization of hepatocellular carcinoma. Agents and drugs: an overview. Part 1. Expert Opin Drug Deliv. 2013;10:679–90
4. Breedos C, Young G. The blood supply of neoplasms in the liver. Am J Pathol. 1954;30:969–77
5. Kemeny NE, Niedzwiecki D, Hollis DR, Hepatic arterial infusion versus systemic therapy for hepatic metastases from colorectal cancer: a randomized trial of efficacy, quality of life, and molecular markers (CALGB 9481). J Clin Oncol. 2006;24:1395–403
6. Raoul JL, Heresbach D, Bretagne JF, Chemoembolization of hepatocellular carcinomas. A study of the biodistribution and pharmacokinetics of doxorubicin. Cancer. 1992;70:585–90
7. Laurent A. Microspheres and nonspherical particles for embolization. Tech Vasc Interv Radiol. 2007;10:248–56
8. Giunchedi P, Maestri M, Gavini E, Transarterial chemoembolization of hepatocellular carcinoma. Agents and drugs: an overview. Part 2. Expert Opin Drug Deliv. 2013;10:799–810
9. Lewis AL, Gonzalez MV, Lloyd AW, DC Bead: in vitro characterization of a drug-delivery device for transarterial chemoembolization. J Vasc Interv Radiol. 2006;17:335–42
10. Landsman ML, Kwant G, Mook G. A, Light-absorbing properties, stability, and spectral stabilization of indocyanine green. J Appl Physiol. 1976;40:575–83
11. Gotoh H, Yamada T, Ishikawa O, A Novel Image-Guided Surgery of Hepatocellular Carcinoma by Indocyanine Green Fluorescence Imaging Navigation. J Surg Oncol. 2009;100:75–9
12. Ishizawa T, Fukushima N, Shibahara J, Real-time identification of liver cancers by using indocyanine green fluorescent imaging. Cancer. 2009;115:2491–504
13. Kokudo N, Ishizawa T. Clinical application of fluorescence imaging of liver cancer using indocyanine green. Liver Cancer. 2012;1:15–21
14. Ishizawa T, Masuda K, Urano Y, Mechanistic background and clinical applications of indocyanine green fluorescence imaging of hepatocellular carcinoma. Ann Surg Oncol. 2014;21:440–8

15. Alacam B, Yazici B, Intes X, Extended Kalman filtering for the modeling and analysis of ICG pharmacokinetics in cancerous tumors using NIR optical methods. IEEE Trans Biomed Eng. 2006;53:1861–71

16. Peloso A, Franchi E, Canepa MC, Combined use of intraoperative ultrasound and indocyanine green fluorescence imaging to detect liver metastases from colorectal cancer. HPB (Oxford). 2013;15:928–34

17. Unno N, Inuzuka K, Suzuki M, Preliminary experience with a novel fluorescence lymphography using indocyanine green in patients with secondary lymphedema. J Vasc Surg. 2007;45:1016–21

18. Qiu Y, Park K. Environment-sensitive hydrogels for drug delivery. Adv Drug Deliv Rev. 2001;53:321–39

19. Klouda L, Mikos AG. Thermoresponsive hydrogels in biomedical applications. Eur J Pharm Biopharm. 2008;68:34–45

20. Wang J, Pang Q, Liu Z, A new liquid agent for endovascular embolization: initial clinical experience. ASAIO J. 2009;55:494–7

21. Weng LN, Zantek ND, Rostamzadeh P, An in situ forming biodegradable hydrogel-based embolic agent for interventional therapies. Acta Biomater. 2013;9:8182–91

22. Muzzarelli RAA. Human enzymatic activities related to the therapeutic administration of chitin derivatives. Cell Mol Life Sci. 1997;53:131–40

23. Hirano S, Seino H, Akiyama Y, Chitosan: a biocompatible material for oral and intravenous administrations. In: Progress in biomedical polymers. Springer; USA: 1990. p. 283–90

24. Rassu G, Gavini E, Mattana A, Improvement of antiamoebic activity of rokitamycin loaded in chitosan microspheres. Open Drug Deliv. J 2008;2:38–43

25. Chenite A, Chaput C, Wand D, Novel injectable neutral solutions of biodegradable gels in situ. Biomaterials. 2000;1:2155–61

26. Chenite A, Buschmann MD, Wang D, Rheological characterisation of thermogelling chitosan/glycerol-phosphate solutions. Carbohydr Polym. 2001;46:39–47

27. Kashyap A, Viswanad B, Sharma G, Design and evaluation of biodegradable, biosensitive in-situ gelling system for pulsatile delivery of insulin. Biomaterials. 2007;28:2051–60

28. Gupta D, Tator CH, Shoichet MS. Fast-gelling injectable blend of hyaluronan and methylcellulose for intrathecal, localized delivery to the injured spinal cord. Biomaterials. 2006;27:2370–9

29. Zang S, Dong G, Peng B, A comparison of physicochemical properties of sterilized chitosan hydrogel and its applicability in a canine model of periodontal regeneration. Carbohydr Polym. 2014;113:240–8

30. Ahmadi R, De Bruijn JD. Biocompatibility and gelation of chitosan-glycerol phosphate hydrogels. J Biomed Mater Res A. 2007;86A:824–32

31. Ruel-Gariépy E, Leclair G, Hildgen P, Thermosensitive chitosan-based hydrogel containing liposomes for the delivery of hydrophilic molecules. J Control Release. 2002;82:373–83

32. Wu H, Zhao H, Song X, Self-assembly-induced near-infrared fluorescence nanoprobes for effective tumor molecular imaging. J Mater Chem B. 2014;2:5302–8

33. Jauhari S, Dash AK. A mucoadhesive in situ gel delivery system for paclitaxel. AAPS PharmSciTech. 2006;7:154–9

34. Zhou HY, Chen XG, Kong M, Preparation of chitosan-based thermosensitive hydrogels for drug delivery. J Appl Polym Sci. 2009;112:1509–15

35. Ruel-Gariépy E, Chenite A, Chaput C, Characterization of thermosensitive chitosan gels for the sustained delivery of drugs. Int J Pharm. 2000;203:89–98

36. Back JF, Oakenfull D, Smith MB. Increased thermal stability of proteins in the presence of sugars and polyols. Biochemistry. 1979;18:5191–6

37. Coutu JM, Fatimi A, Berrahmoune S, A new radiopaque embolizing agent for the treatment of endoleaks after endovascular repair: influence of contrast agent on chitosan thermogel properties. J Biomed Mater Res B Appl Biomater. 2013;101B:153–61

38. Khan I, Vasudevan V, Nallagatla S, Acute lung injury following transcatheter hepatic arterial chemoembolization of doxorubicin-loaded LC beads in a patient with hepatocellular carcinoma. Lung India. 2012;29:169–72

39. Wu JJ, Chao M, Zhang GQ, Pulmonary and cerebral lipiodol embolism after transcatheter arterial chemoembolization in hepatocellular carcinoma. World J Gastroenterol. 2009;15:633–5

40. Shiah HS, Liu TW, Chen LT, Pulmonary embolism after transcatheterarterial chemoembolization. Eur J Cancer Care (Engl). 2005;14:440–2

41. Naorungroj T, Naksanguan T, Chinthammitr Y. Pulmonary lipiodol embolism after transcatheter arterial chemoembolization for hepatocellular carcinoma: a case report and literature review. J Med Assoc Thai. 2013;96:270–5

42. Zhao H, Wang HQ, Fan QQ, Rare pulmonary and cerebral complications after transarterial chemoembolisation for hepatocellular carcinoma: a case report. World J Gastroenterol. 2008;14:6425–7

43. Lapasin R, Pricl S. Rheology of industrial polysaccharides: theory and applications. Springer, London: 1995

44. Ganji F, Abdekhodaie MJ, Ramazani ASA. Gelation time and degradation rate of chitosan-based injectable hydrogel. J Sol-Gel Sci Techn. 2007;42:47–53

45. Dang QF, Yan JQ, Li JJ, Controlled gelation temperature, pore diameter and degradation of a highly porous chitosan-based hydrogel. Carbohydr Polym. 2011;63:171–8

46. Drury JL, Mooney DJ. Hydrogels for tissue engineering: scaffold design variables and applications. Biomaterials. 2003;24:4337–51

CHAPTER 3

Nasal Chitosan Microparticles Target A Zidovudine Prodrug To Brain Hiv Sanctuaries

Adapted from:

Nasal Chitosan Microparticles Target A Zidovudine Prodrug To Brain Hiv Sanctuaries.

Alessandro Dalpiaz, Marco Fogagnolo, Luca Ferraro, Antonio Capuzzo, Barbara Pavan, Giovanna Rassu, **Andrea Salis**, Paolo Giunchedi, Elisabetta Gavini. Antiviral Research, November 2015, Volume 123, Pages 146–157

INTRODUCTION

Combination antiretroviral therapy (cART) has made a significant impact against HIV infection. However, the efficacy of this therapy is limited by the poor bioavailability of anti-HIV drugs at viral reservoir sites, such as the central nervous system (CNS) [1,2], particularly in cerebrospinal fluid (CSF) subarachnoid spaces that contain macrophages, which constitute the only site of HIV replication in the brain [3,4]. The lack of drug penetration into these "HIV sanctuaries" occurs primarily due to the expression of active efflux transporters (AETs) on the blood–brain (BBB) and blood−cerebrospinal fluid (BCSFB) barriers [5,6]. In vivo, these transporters induce the asymmetric transport of anti-HIV drugs across these barriers, where the rate of drug efflux from the CNS to the blood is greater than the influx rate [7].

We recently proved that the conjugation of zidovudine (AZT), which is an antiretroviral drug used in cART protocols [8], with the bile acid ursodeoxycholic acid (UDCA) generates a prodrug (UDCA−AZT) that can elude the AET systems [9]. We have therefore proposed that when this prodrug is taken up in the CNS, it should not be extruded into the bloodstream because it is able to elude the AET systems. Accordingly, we demonstrated that the nasal administration of solid lipid microparticles loaded with the UDCA–AZT prodrug facilitates its uptake into the CSF of rats [10]. Nasal administration constitutes a potentially efficacious way of achieving the brain uptake of neuroactive agents [11-14]. Indeed, drugs deposited on the olfactory epithelium of the nose can gain direct access to the CNS, particularly the CSF, via transcellular transport through olfactory epithelial cells. The drugs absorbed in the CSF can then diffuse into the interstitial fluid (ISF) and subsequently penetrate the brain parenchyma [13,15,16]. Moreover, drugs deposited on the olfactory epithelium can be transported into the brain parenchyma by olfactory neurons or trigeminal nerves that reach the nasal cavity [16-18]. Finally, nasally administered drugs can be absorbed into the systemic circulation from the respiratory epithelium [19] and can then reach the CNS if they are able to cross the BBB [13].

In general, appropriate strategies are required to improve the brain delivery of drugs, such as the addition of penetration enhancers and mucoadhesive materials to formulations or the preparation of micro- and nano-particulate delivery systems [20-24]. In this regard, chitosan is a polysaccharide derived from the alkaline deacetylation of chitin that is used in different formulations for the nose-to-brain delivery of drugs [20] due to its biocompatibility, nontoxicity and high charge density, which confers mucoadhesive properties [25,26]. Chitosan is poorly soluble in water at physiologic pH values, but it forms salts with inorganic or organic acids, such as hydrochloride and glutamic

acid, that are soluble in water and possess better characteristics than chitosan itself, such as mucoadhesiveness and the ability to enhance the penetration of neuroactive agents into the CNS [21,27,28]. Chitosan is also characterized by the ability to reversibly open tight junctions, which is associated with a potential increase in the transcellular transport of drugs across the olfactory mucosa [29]. Nasal formulations obtained in the presence of water have drawbacks, such as the risk of chemical and physical instability and microbiological growth. In addition, the residence time of the liquid formulation in the nasal cavity is short, as the liquid is often rinsed into the gastrointestinal tract (GIT) or out of the nose [30]. These disadvantages can be overcome by using powder-based formulations [31,32].

The purpose of the present work was first to demonstrate that UDCA–AZT can permeate and remain in macrophages more efficiently than its parent drug AZT and then to prepare microspheres based on chitosan chloride in order to increase the nose-to-brain delivery of UDCA–AZT by using a particulate formulation that is suitable for nasal administration. The characterization of microparticles was performed in vitro and in vivo. All in vitro and in vivo measurements performed for the loaded microparticles were also performed for a parent physical mixture of chitosan chloride and UDCA–AZT in order to verify the efficacy of the microparticulate system for the brain delivery of the prodrug.

MATERIALS AND METHODS

Materials

The prodrug UDCA−AZT was synthesized as described previously [9]. Chitosan chloride (Protasan UP CL 113, molecular weight and degree of deacetylation of 160,000 g/mol and 83%, respectively) was purchased from FMC BioPolymer AS (Drammen, Norway). Dow Corning 345, which is a blend of polydimethylcyclosiloxane, was obtained from Dow Corning (Brussels, Belgium). AZT, 7-n-propylxanthine (7n-PX), and bovine serum albumin (BSA) were obtained from Sigma Aldrich Italy (Milan, Italy). Methanol, acetonitrile, ethyl acetate and water were high performance liquid chromatography (HPLC) grade and obtained from Sigma Aldrich Italy. Monopowder P® insufflators were furnished by Valois Dispray (Mezzovico, Switzerland). Male Wistar rats were purchased from Harlan SRC (Milan, Italy). All other reagents and solvents were of analytical grade (Sigma–Aldrich).

Uptake of AZT and UDCA–AZT in macrophages

The J774A.1 murine macrophage cell line was obtained from the American Tissue Type Culture Collection (LGC Standards, Milan, Italy). J774A.1 macrophages were grown as adherently cultured cells in Dulbecco's modified Eagle's medium + Glutamax supplemented with 10% fetal bovine serum (FBS), 100 U/mL penicillin, and 100 μg/mL streptomycin at 37°C. All cell culture reagents were provided by Invitrogen (Life Technologies, Milan, Italy). Briefly, a total of 5 × 105 cells J774A.1 cells were seeded in 12-well culture plates, and when semi-confluent, the cells were exposed to 100 μM AZT and 10 or 100 μM UDCA–AZT in growth medium for 30 min. At the end of the treatment, the cells were washed and lysed. The cell lysates were dried under a nitrogen stream, resuspended in methanol and centrifuged to remove cell debris. The supernatant (10 μl) was used to measure the levels of AZT and UDCA–AZT via HPLC analysis. All of the values obtained from experiments with J774A.1 cells are the mean of three independent experiments.

Toxicity texts (MTT assay)

J774A.1 cells were seeded in 96-well plates at a density of 8000 cells per well and reached an optimal population density within 48–72 h. The cells were then incubated for 15, 30 and 60 min in 200 μL of culture medium in the presence and absence of 100 μM UDCA–AZT. At the end of the time-course, the incubation medium was removed and replaced with 200 μL of fresh culture medium, and 20 μL of 3-(4,5-dimethylthiazol-2-yl)-2,5-diphenyltetrazolium bromide (MTT) stock solution (5 mg/mL) were added to each well and incubated at 37°C for 4 h. A negative control of 20 μL of the MTT stock solution added to 200 μL of medium alone was included. Then, 100 μL of DMSO were added to each well and incubated at 37°C for 2 h in an orbital shaker incubator. Finally, the absorbance of each well was measured at 570 nm using a microtiter plate reader.

Preparation of loaded and unloaded chitosan microspheres

Chitosan microspheres containing UDCA−AZT (named CP) were prepared using the spray-drying method. Chitosan chloride (400 mg) was dissolved in water (15 mL), whereas UDCA−AZT (100 mg) was dissolved in methanol (35 ml). The drug solution was dispersed into chitosan one (solid concentration: 1% w/v of UDCA−AZT and chitosan). Due to the very low solubility of the drug, a fine suspension was obtained and spray-dried using a mini spray-dryer equipped with a high performance cyclone (Büchi B-191, Büchi Labortechnik AG, Flawil, Switzerland) and with a 0.7 mm two-fluid nozzle. The following standard operating conditions were utilized: inlet and outlet

temperature, 100°C and 73°C, respectively; spray flow rate, 500 L/h; pump setting, 8% (2.00 mL/min); and aspirator setting, 90%. Aqueous solutions of chitosan chloride (0.8% w/v) were sprayed under the same conditions to obtain drug-free microspheres (CH). The microparticles were stored in a desiccator at room temperature.

HPLC analysis

The prodrug UDCA−AZT and its hydrolysis product AZT were quantified using HPLC. The chromatographic apparatus consisted of a modular system (model LC-10 AD VD pump and model SPD-10A VP variable wavelength UV–vis detector; Shimadzu, Kyoto, Japan) and an injection valve with a 20 μL sample loop (model 7725; Rheodyne, IDEX, Torrance, CA, USA). Separations were performed at room temperature on a 5 μm Hypersil BDS C-18 column (150 mm × 4.6 mm i.d.; Alltech Italia Srl, Milan, Italy) equipped with a guard column. Data acquisition and processing were accomplished with a personal computer using CLASS-VP Software, version 7.2.1 (Shimadzu Italia, Milan, Italy). The detector was set to 260 nm. The mobile phase consisted of a mixture of water and methanol that was regulated by a gradient profile programmed as follows: isocratic elution with 20% (v/v) MeOH in H2O for 10 min; a 1-min linear gradient to 75% (v/v) MeOH in H2O; and the mobile phase composition was then maintained at 75% MeOH for 10 min. After each cycle, the column was conditioned with 20% (v/v) MeOH in H2O for 10 min. The flow rate was 1 mL/min. The xanthine derivative 7n-PX was employed as an internal standard for the analysis of rat blood (see below). The retention times for 7n-PX, AZT and the prodrug UDCA−AZT were 6.5, 8.4, and 19.6 min, respectively. The HPLC assay of UDCA–AZT alone was performed isocratically with 80% (v/v) MeOH in H2O. In this case, the retention time of UDCA–AZT was 4.8 min. The chromatographic precision was evaluated.

Characterization of microspheres

The prepared microspheres were characterized in terms of production yield, drug content and encapsulation efficiency, particle size and particle size distribution, particle morphology, true density and water uptake capacity.

Production yields

The production yields (YP) were calculated as a percent weight of microspheres obtained with respect to the initial amounts of UDCA−AZT and chitosan that were employed for the preparation of the feed suspension.

UDCA−AZT content in CP

The UDCA–AZT content in the microparticulate powders was determined. The microparticles (approximately 0.95 mg) were accurately weighed and dissolved in 3 ml of water to which 300 µl of 0.2% H_3PO_4 was added; the final volume of the solution was adjusted to 10 mL with methanol. Then, 10 µL of the filtered solutions (0.45 µm) were injected into the HPLC system for the UDCA–AZT assay. The drug loading and entrapment efficiency were calculated according to Eqs. (1) and (2) [33].

$$\text{Drug loading}\left(\%\frac{\text{W}}{\text{W}}\right) = \frac{\text{Mass of drug in microparticles}}{\text{Mass of microparticles}} \times 100 \quad (1)$$

$$\text{Entrapment efficiency}\ (\%) = \frac{\text{Mass of drug in microparticles}}{\text{Starting mass of drug}} \times 100 \quad (2)$$

All of the obtained values are the mean of four independent experiments.

Particle size measurement

The size and size distribution of the microspheres were analyzed via the light diffraction method using a Coulter LS 100Q (Beckman Coulter Particle Characterization, Miami, FL, USA). A sample (2 mg) of unloaded and drug-loaded microspheres was suspended in silicon oil, sonicated for approximately 3 s and analyzed. The reported results are the averages of triplicate averages. For comparison, a test was also performed on the physical mixture containing UDCA−AZT and chitosan chloride (87:13 w/w) (MIX) that was prepared by geometric dilution using an agate mortar pestle, as well as on chitosan chloride and UDCA–AZT alone, before and after grinding.

Particle morphology

The shape and surface characteristics of the powders were studied using scanning electron microscopy (VP-SEM; Zeiss EVO40XVP, Arese, Milan, Italy). The samples were placed on

double-sided tape that had previously been secured to aluminum stubs and then analysed under an argon atmosphere at an 18 kV acceleration voltage after gold sputtering.

True density

The true density of the microspheres was measured via helium pycnometry (Micromeritics Accupyc II 1340 Analysis system, Peschiera Borromeo, Italy) at 21 C [34]. The density (ρ) of the powder was determined in triplicate for each batch.

Determination of water uptake capacity

Investigations of the water uptake capability of CP and CH were carried out using a modified Enslin apparatus, as described previously by Rassu et al. [35]. Briefly, the dried microspheres were spread uniformly on the filter paper, which was previously soaked with phosphate buffer, pH 6.5. The volume of fluid absorbed from the microspheres during the time of the experiment (0–60 min) was recorded. The values (mean of at least 3 experiments) were expressed as µl of fluid absorbed per gram of microspheres during the time of the experiment. For comparison, the test was also performed using MIX.

***In vitro* release and dissolution studies**

The release tests were performed using the flow-through dissolution method (European Pharmacopoeia, Apparatus 4), with a modified glass cell that is useful for organic solvents. The CP formulation (20 mg) was placed into the glass cell. The dissolution medium was warmed to 37 ± 0.1 C and introduced through the bottom of the cell to obtain a suitable continuous flow. A methanol–water blend (70–30 v/v) was used as the dissolution medium. The test solution (10 µL) was analyzed via HPLC to evaluate the amount of UDCA–AZT released from the microspheres, which was calculated as a percentage of the initial amount of UDCA−AZT incorporated into the microspheres prior to the dissolution test. For comparison, the test was also performed using MIX. All experiments were performed with at least three replicates.

***In vivo* UDCA–AZT administration and quantification**

Male Wistar rats (200–250 g) were anesthetized during the experimental period and received a femoral intravenous infusion of 0.1 mg/mL of UDCA–AZT dissolved in a medium constituted by

20% (v/v) DMSO and 80% (v/v) physiologic solution, at a rate of 0.2 mL/min for 10 min. At the end of the infusion and at fixed time points, blood samples (100 μL) were collected and CSF samples (50 μL) were withdrawn using the cysternal puncture method described by van den Berg et al. [36], which requires a single needle stick and allows the collection of serial (40–50 μL) CSF samples that are virtually blood-free [10]. A total volume of approximately 150 μL of CSF was collected during the experimental session. Four rats were employed for femoral intravenous infusions. The CSF samples (10 μL) were immediately injected into the HPLC system for AZT and UDCA–AZT detection. The blood samples were hemolysed immediately after their collection with 500 μL of ice cold water, and 50 μL of 10% sulfosalicylic acid and 100 μL of internal standard (30 μM 7n-PX) were then added. The samples were extracted twice with 1 mL of water-saturated ethyl acetate, and after centrifugation, the organic layer was reduced to dryness under a nitrogen stream. Two hundred microliters of a water–methanol mixture (70:30 v/v) were added, and after centrifugation, 10 μL were injected into the HPLC system for AZT and UDCA–AZT detection.

The precision of the analytical method was determined. The *in vivo* half-life of AZT in the blood was calculated by nonlinear regression (exponential decay) of concentration values in the time range within 3h after infusion and confirmed by linear regression of the log concentration values versus time.

Nasal administration of UDCA–AZT was performed on anesthetized rats laid on their backs, following two main procedures. The first procedure consisted of the introduction of 50 μL of an aqueous suspension of UDCA–AZT (2 mg/mL) into each nostril, as described previously [10]. After administration, blood (100 μL) and CSF samples (50 μL) were collected at fixed time points and analysed using the same procedures described above. Four rats were employed for nasal administration of the UDCA–AZT suspension.

The second procedure was based on the insufflation of CP microparticles into each nostril of anesthetized rats using single dose Monopowder P® insufflators (Valois Dispray SA, Mezzovico, Switzerland). These devices were constituted by a pump, a nasal adapter and a solid formulation reservoir [37]. The insufflators were loaded with approximately 0.8 mg of UDCA–AZT-loaded microparticles (corresponding to approximately 100 μg of UDCA–AZT), or with approximately 0.8 mg of the corresponding physical mixture (MIX). The rats received this amount in each nostril. The amount of powder emitted during administration was determined based on the difference between the insufflator weights before and after each insufflation. After administration, blood (100 μL) and

CSF samples (50 μL) were collected at fixed time points and analysed using the same procedures described above. Four rats were employed for nasal administration of the microparticulate powder.
All *in vivo* experiments were performed in accordance with the guidelines issued by the Italian Ministry of Health (D.L. 116/92 and D.L. 111/94-B), the Declaration of Helsinki, and the Guide for the Care and Use of Laboratory Animals as adopted and promulgated by the National Institute of Health (Bethesda, Maryland, USA). The protocols for all *in vivo* experiments were approved by the Local Ethics Committee (University of Ferrara, Ferrara, Italy). All efforts were made to reduce the number of animals and their suffering.
The areas under the concentration curves of UDCA–AZT in the CSF (AUC, μg mL^{-1} min) were calculated using the trapezoidal method. The *in vivo* half-life of UDCA–AZT in the CSF was calculated by linear regression of the log concentration values versus time between 1 and 3 h after nasal administration of the loaded microparticles. All calculations were performed using the computer program Graph Pad Prism (GraphPad Software, Incorporated, La Jolla, CA, USA).

Statistical analysis

Statistical comparisons of the amounts of water uptake of the powder samples and the UDCA–AZT C_{max} and AUC values obtained in the CSF of rats were made using the Student's *t* test or one-way ANOVA (GraphPad Prism). *P* values <0.05 were considered to be statistically significant.

RESULTS

Uptake of AZT and UDCA–AZT in macrophages

The incubation of 100 μM zidovudine or its prodrug with the macrophages for 30 min allowed us to detect 0.054 ± 0.007 nmoles of AZT and 1.12 ± 0.16 nmoles of UDCA–AZT in 10^6 cells, as reported in Figure 1. The amount of AZT detected in the cells after incubation with UDCA–AZT for 30 min was 0.081 ± 0.009 nmoles/10^6 cells (Figure 1). The cell counter measured the volume of macrophages as 1.7 ± 0.1 pL; as a consequence, the amount of AZT released by the macrophages after incubation with 100 μM UDCA–AZT incubation corresponds to a concentration of 47 ± 5 μM. No toxicity was observed for cells incubated with 100 μM UDCA–AZT. These data indicate not only that the prodrug is able to permeate and remain in the macrophages with an efficiency twenty times higher than that of its parent drug (*P*<0.001) but also that the macrophages hydrolyze the prodrug, facilitating intracellular AZT release (Figure 1). Moreover, the incubation of macrophages

with 10 μM UDCA–AZT allowed us to detect 0.21 ± 0.03 nmoles of the prodrug in 10^6 cells (Figure 1). In this case, the AZT amounts were lower than the limit of detection of the analytical system. Therefore, the ability of UDCA–AZT to elude the AET systems [9] appears to be useful for inducing uptake into macrophages. According to the data reported in Figure 1, the presence of the prodrug in the CSF should allow its permeation and permanence in the macrophages, therefore making the prodrug an efficient carrier for AZT.

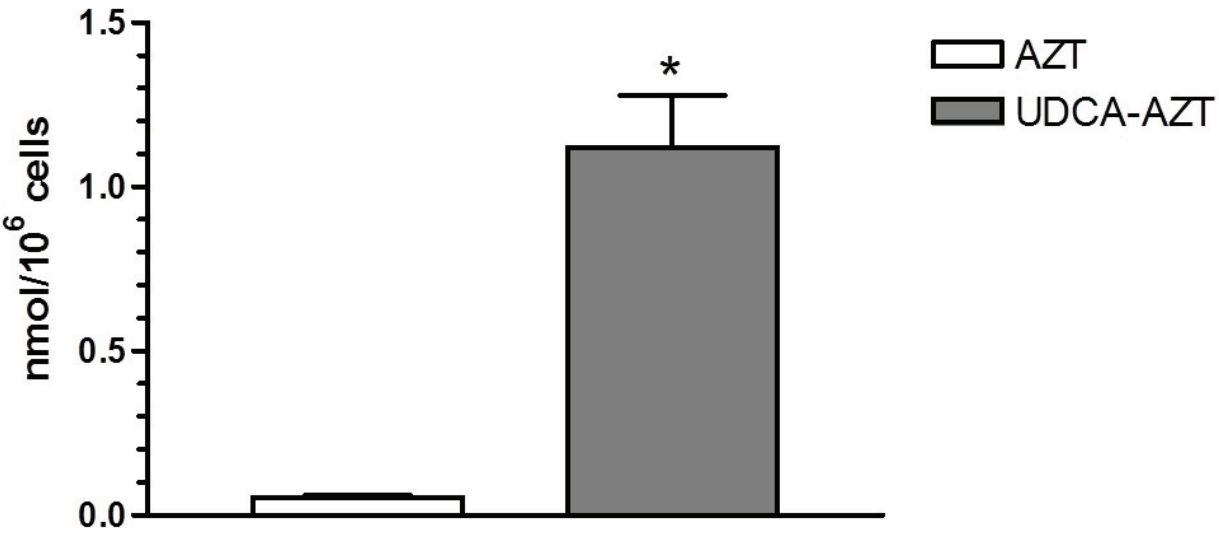

Figure 1. Intracellular levels of AZT and its prodrug UDCA–AZT after incubation (30 min) with J774A.1 murine macrophages. The incubation concentrations were 100 μM for AZT and 10 and 100 μM for UDCA–AZT. The graph also reports the intracellular levels of AZT after the incubation of the macrophages with 100 μM UDCA–AZT. The data are reported as the mean ± S.D. of three independent experiments. *: $P < 0.001$ versus 100 μM AZT.

Characterization of microspheres

Production yields

The spray-drying technique proved to be suitable for preparing loaded and unloaded chitosan microparticles; in fact, these microparticles were obtained with good production yields of between 61.7% (CP) and 64.7% (CH). Generally, the yields obtained with the spray-drying at laboratory scale with conventional spray-dryers are in the range of 20–70% due to the loss of product on the

walls of the drying chamber and the low capacity of the cyclone to separate fine particles [38,39]. However, the yield strongly depends on the work scale; the yield is high in larger scale setups because large batch sizes and separators (e.g., filter systems) are used.

UDCA−AZT content in CP

The amount of encapsulated UDCA−AZT in the CP sample was found to be 13 ± 0.3% (w/w), showing that chitosan, which is characterized by hydrophilic properties, was able to encapsulate the lipophilic prodrug with a good encapsulation efficiency (64.9 ± 1.5%).

Particle size measurement

Table 1 reports the volume-surface diameters (d_{vs}) obtained for the loaded (CP) and unloaded microparticles (CH), for MIX and for chitosan chloride and UDCA–AZT before and after grinding using an agate mortar and pestle. The loading of UDCA−AZT into chitosan microparticles caused an increase in the particle size: CP microspheres had a d_{vs} of 3.59 ± 0.1 μm in comparison to a d_{vs} of 2.32 ± 0.01 μm for CH (P<0.0001). Furthermore, the presence of the drug resulted in a change in the particle size distribution: loaded microparticles showed a larger curve than drug-free microspheres (Figure 2 up). In particular, CH showed a Gaussian curve while the CP curve appeared to be leptokurtic, right skewed and wide, with the presence of small shoulders.

Table 1. Volume-surface diameters (d_{vs}, μm) of unloaded (CH) and loaded (CP) microparticles together with d_{vs} values of the parent mixture (MIX) of chitosan chloride and UDCA-AZT and its single components before and after grinding by agate mortar and pestle. Data are reported as the mean ± SD of three independent experiments.

Sample	**d_{vs} (μm)**
CP	3.59 ± 0.14
CH	2.32 ± 0.11
MIX	6.11 ± 0.02
Grinded Chitosan HCl	12.67 ± 0.82
Grinded UDCA–AZT	5.12 ± 0.02
Chitosan chloride before grinding	19.98 ± 0.06
UDCA–AZT before grinding	23.33 ± 0.06

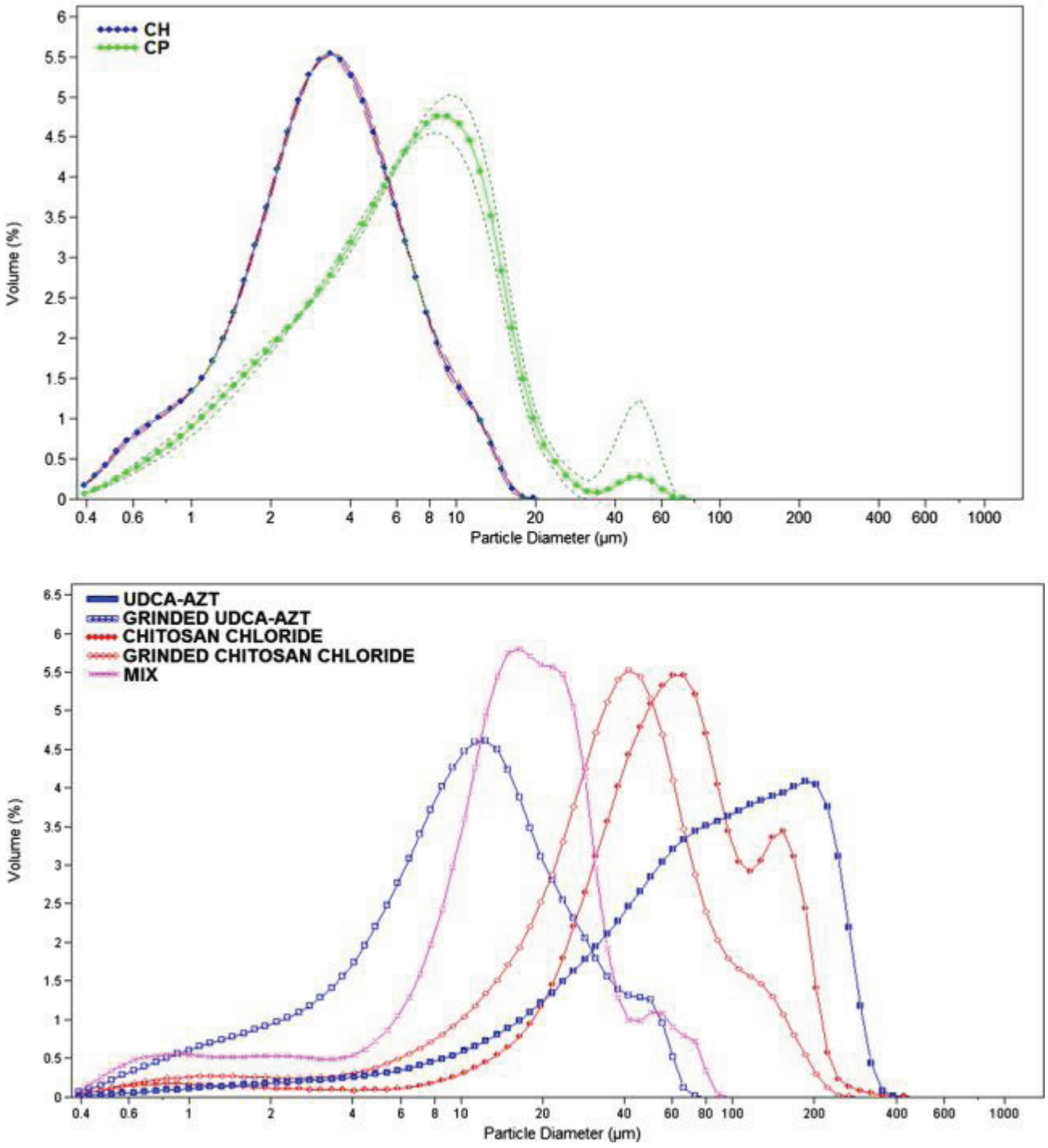

Figure 2. Size distribution of loaded (CP) and unloaded (CH) chitosan microspheres (up), MIX and chitosan chloride and UDCA–AZT alone, before and after grinding (down). The particle size distribution was graphically expressed as curves obtained by plotting the volume of the particles as a percentage versus size (µm), shown on a logarithmic scale.

MIX had a d_{vs} of 6.11 ± 0.022 μm, which was significantly higher than the values obtained for microspheres (P<0.001) and UDCA–AZT alone but significantly lower than the value obtained for chitosan chloride alone, which were both analyzed after grinding. The grinding of the drug and the polymer in an agate mortar reduced the particle size and shifted the size distributions to lower values (Figure 2, lower panel). In fact, the d_{vs} of chitosan chloride changed from 19.98 ± 0.24 μm to 12.67 ± 0.819 μm due to aggregate breaking. The size reduction of UDCA–AZT crystals was even more pronounced: the d_{vs} decreased from 23.33 ± 0.06 μm to 5.12 ± 0.018 μm after grinding.

Particle morphology

Figure 3A presents an SEM image of MIX obtained by geometric dilution using an agate mortar and pestle. This picture reveals not only particles characterized by a round morphology and a relatively smooth surface but also the presence of fragments characterized by an irregular shape. For comparison, Figure 3B and C present SEM images of chitosan chloride and UDCA–AZT, respectively, which were ground using an agate mortar and pestle. Figure 3B shows particles characterized by a round morphology and a smooth surface. These morphologic characteristics did not appear to be significantly different from those of chitosan chloride before grinding, as evidenced by the SEM image presented in Figure 3E. The SEM picture of ground UDCA–AZT, Figure 3C, showed fragments characterized by an irregular shape (details are evident in the SEM image reported in Figure 3D) and a high aptitude to aggregate. These morphologic characteristics appeared to be significantly different from those of the prodrug UDCA–AZT before grinding, as evidenced in Figure 3F, where fragments of an irregular shape are shown to be characterized by diameters at least one order of magnitude higher than those of the ground UDCA–AZT particles. Taking into account these aspects, we can conclude that the SEM image of the physical mixture of chitosan chloride and UDCA–AZT (Figure 3A) allows us to discriminate its two components; in particular, the particles with a round morphology can be attributed to chitosan chloride, whereas the fragments of irregular shape can be attributed to UDCA–AZT.

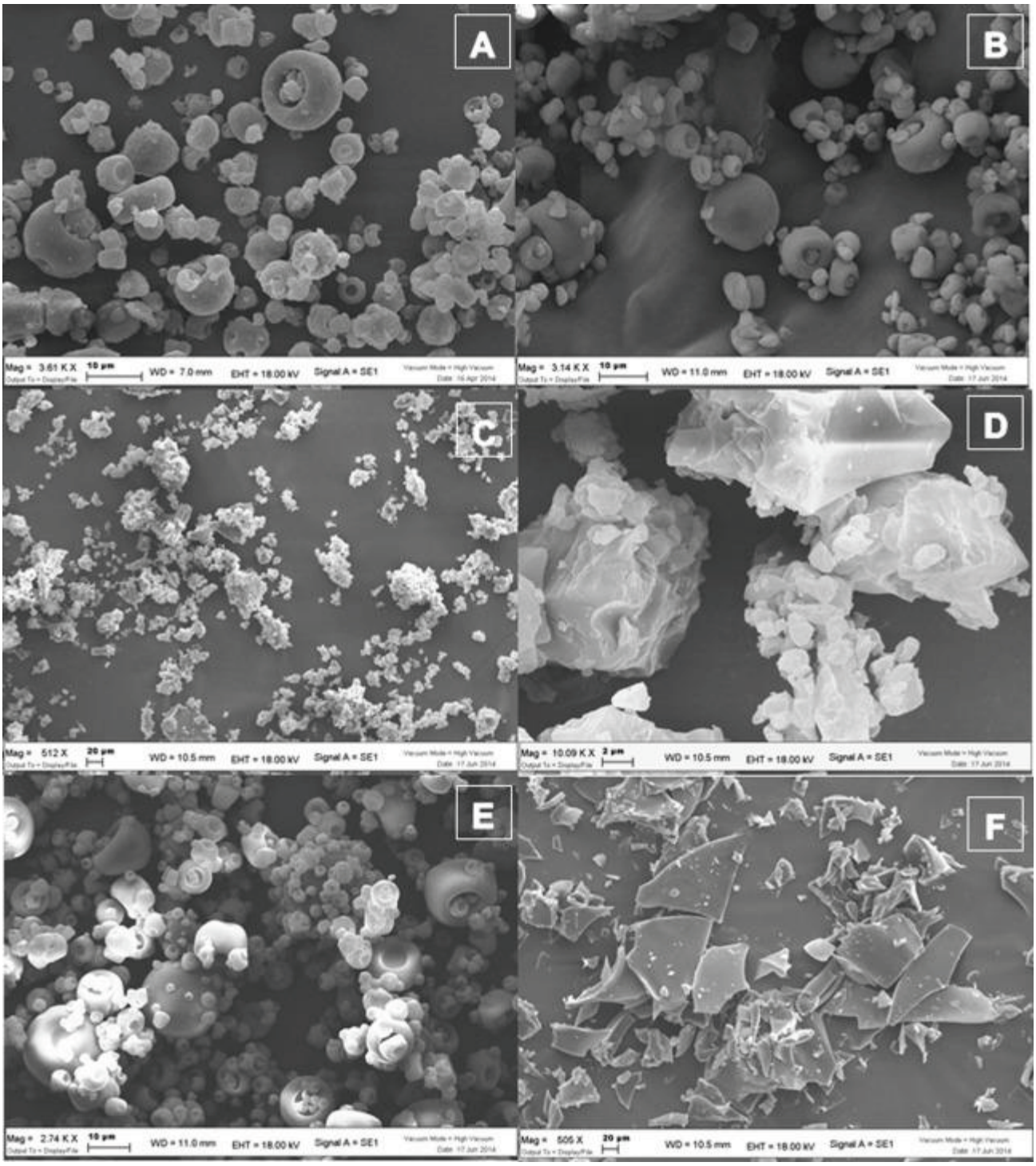

Figure 3. Scanning electron microscopy (SEM) micrographs of the mixture of chitosan chloride and UDCA–AZT (87:13 w/w, magnification of 3610 times) [A]; ground chitosan chloride (magnification of 3140 times) [B]; ground UDCA–AZT with magnifications of 512 times [C] and 10,000 times [D]; chitosan chloride before grinding (magnification of 2740 times) [E]; and UDCA–AZT before grinding (magnification of 505 times) [F].

Figure 4A and B present SEM images of CP, which is constituted by the loaded UDCA–AZT microparticles based on chitosan chloride. The pictures reveal the presence of spherical particles characterized by a smooth surface and several fragments characterized by an irregular shape and high porosity, similar to spongy balls, with some degree of aggregation. For comparison, a SEM image of the unloaded microparticles (CH) [21] reveals their round shape and smooth surfaces. Taking into account these aspects, we can hypothesize that the spherical particles presented in images 3A and 3B are constituted by unloaded chitosan chloride, whereas the spongy balls were obtained from the interaction between chitosan chloride and UDCA–AZT, which gave rise to the highly porous structures.

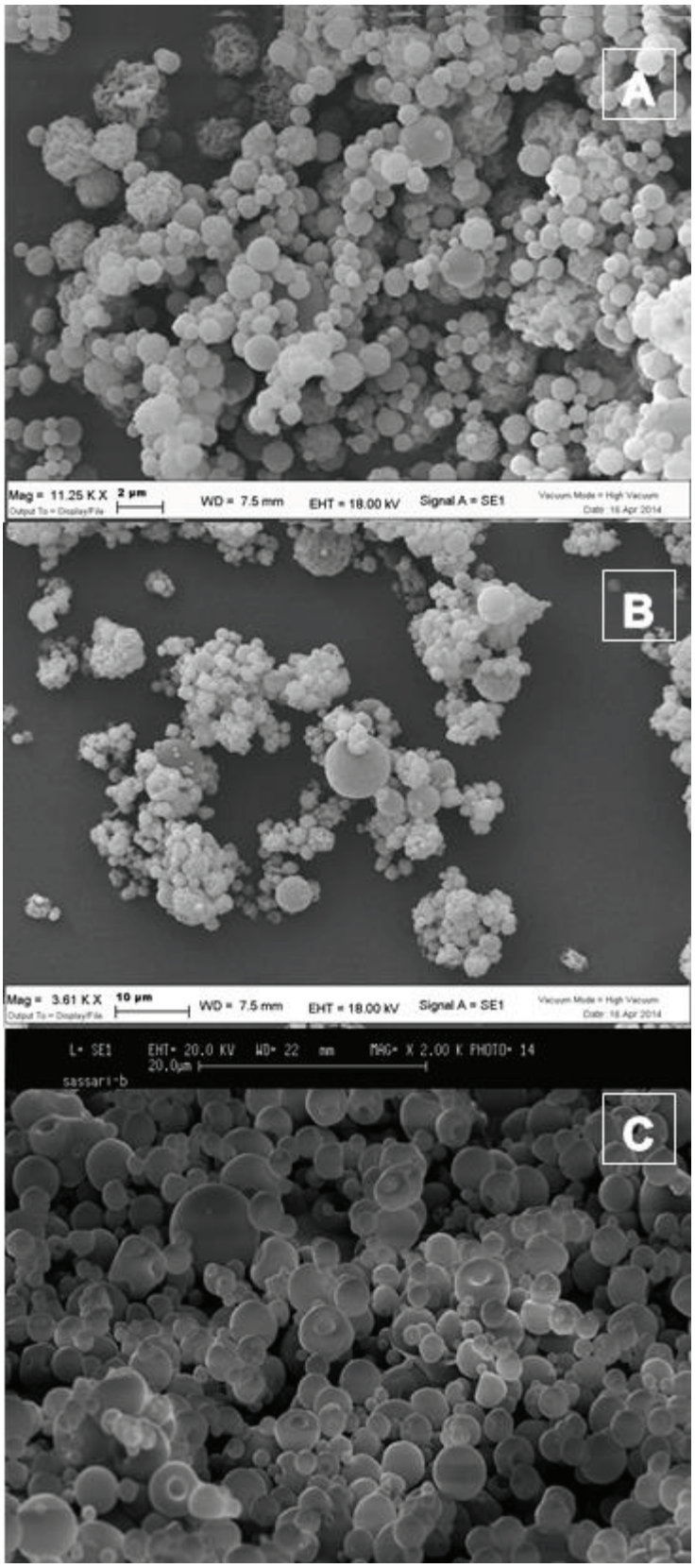

Figure 4. Scanning electron microscopy (SEM) micrographs of the loaded microparticles (sample CP) with magnifications of 11,250 times [A] and 3620 times [B].

True density

The true density of the microspheres was 1.48 ± 0.02 g/cm^3, which is comparable to the ρ of nasal microspheres [34].

Determination of water uptake capacity

Figure 5 shows the water uptake of both loaded and unloaded formulations. The drug-free formulations absorbed a greater amount of water than the loaded microparticles. Drug loading decreased the water absorption capability of chitosan microspheres (P<0.05). UDCA−AZT and the chitosan chloride physical mixture also exhibited water uptake capabilities stronger than that of CP but weaker than that of CH after 15–60 min (P<0.05).

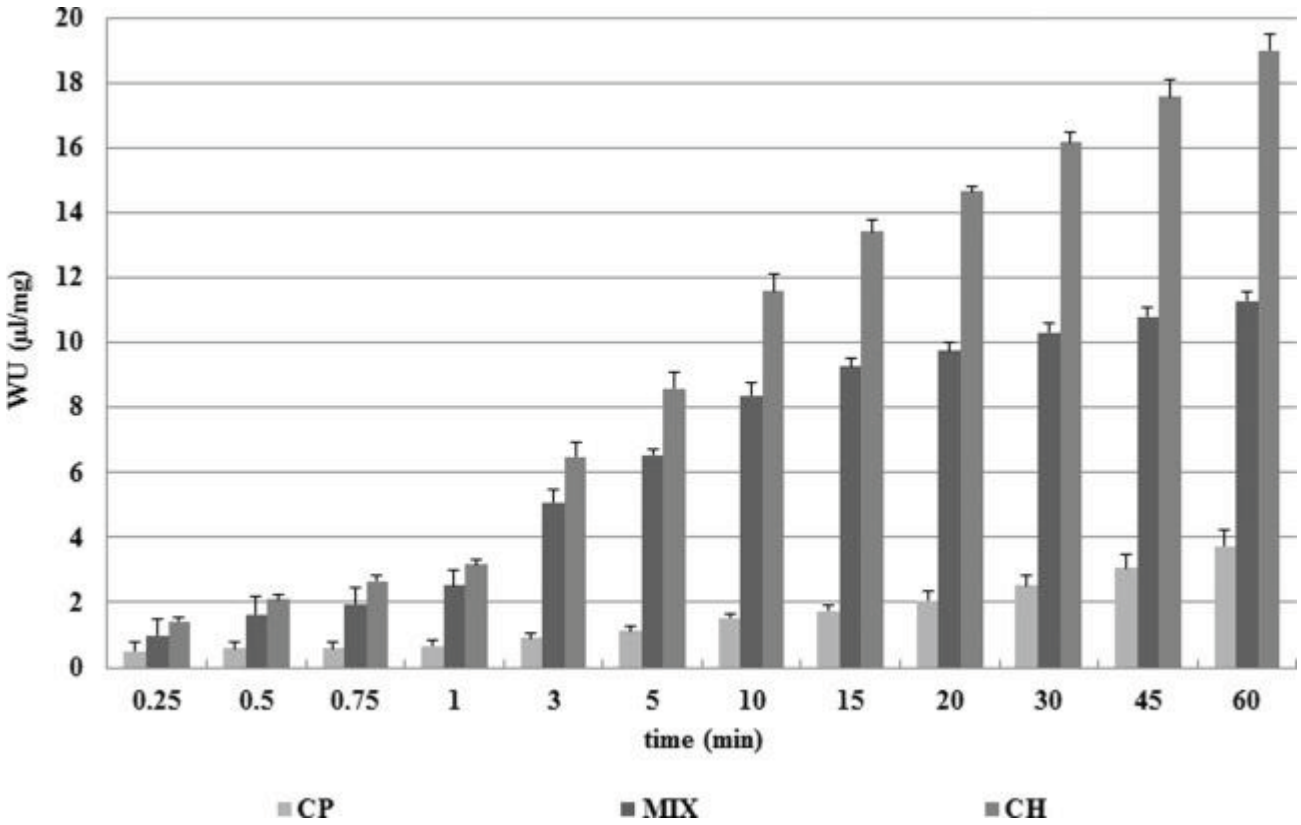

Figure 5. Water uptake profiles of loaded (CP) and unloaded (CH) microspheres over 60 min in comparison to that of the physical mixture (MIX, chitosan chloride and UDCA−AZT (87:13 w/w). The data are reported as the mean ± SD of three independent experiments.

In vitro release and dissolution studies

The dissolution and release studies of UDCA−AZT were performed in a MeOH/H_2O (70:30, v/v) mixture. The employment of methanol as a cosolvent was necessary to increase the low solubility of the prodrug in water (0.0030 ± 0.0001 mg/ml; [9]), thus ensuring sink conditions.

Figure 6 reports the release profile of UDCA−AZT from the loaded CP sample. The release pattern is compared with that of UDCA–AZT dissolution from its physical mixture with chitosan chloride. The dissolution rate of the prodrug included in MIX appeared to be significantly lower than that of UDCA–AZT loaded in the CP sample. Indeed, after 2 h of incubation, 38.4 ± 1.6% of the prodrug loaded in the dissolution apparatus appeared to have dissolved, whereas in the case of CP loaded microparticles, the amount of dissolved UDCA–AZT was 86.2 ± 3.4%. As a consequence, the dissolution half-life of UDCA–AZT loaded in CP sample appeared to be approximately 15 min, whereas for the prodrug in the physical mixture (MIX), the dissolution half-life was greater than 2 h. These profiles suggest that the employment of the CP sample as a nasal formulation should be appropriate, as this formulation is able to release the prodrug UDCA–AZT in a relatively short time, allowing potentially rapid absorption of the prodrug after the administration of the microparticles.

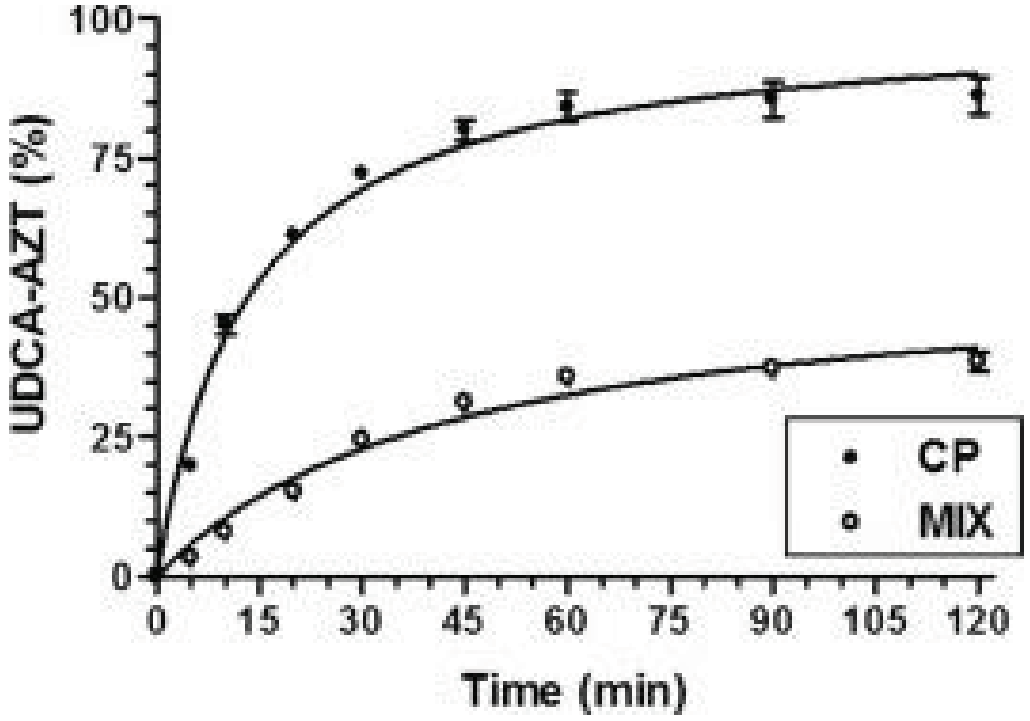

Figure 6. *In vitro* release of UDCA−AZT from CP microparticles based on chitosan chloride. The release profile is compared with the dissolution profile obtained for the parent physical mixture of chitosan chloride and UDCA–AZT (87:13 w/w) (MIX). The data are reported as the mean ± SD of three independent experiments.

***In vivo* UDCA–AZT administration**

Taking into account the fact that the CP microparticles were characterized not only by a satisfactory encapsulation efficiency but also by the ability to induce relatively rapid dissolution of UDCA−AZT, we tested these microparticles for nasal administration of the prodrug in order to verify potential uptake in the CNS. The nasal administration of UDCA−AZT was performed using three different formulations: (I) a suspension of the raw UDCA–AZT powder in water, (II) the powder constituted by loaded CP microparticles and (III) for comparison, the parent physical mixture of chitosan chloride and UDCA–AZT (87:13 w/w). The results were compared with those obtained after the intravenous infusion of UDCA−AZT into rats.

Intravenous administration of UDCA−AZT

The prodrug was undetectable in rat blood samples following intravenous infusion. This result is in agreement with the very fast hydrolysis of UDCA−AZT in rat blood at 37°C [9]. Significant

amounts of AZT were therefore detected following the intravenous administration of the prodrug, as evidenced in Figure 7. In particular, after the infusion of 0.200 mg of UDCA−AZT into the rats, the AZT concentration in the bloodstream was 4.50 ± 0.31 μg/mL. This concentration decreased over time with apparent first order kinetics, as confirmed by the linearity of the semilogarithmic plot reported in the inset of Figure 7 (n = 9, r = 0.990, P<0.0001), and a half-life of 60.4 ± 3.8min. These data are in good agreement with those obtained from previous studies of *in vivo* UDCA–AZT pharmacokinetics [10]. No AZT or UDCA−AZT was detected in the CSF within 180 min after the intravenous administration of UDCA−AZT.

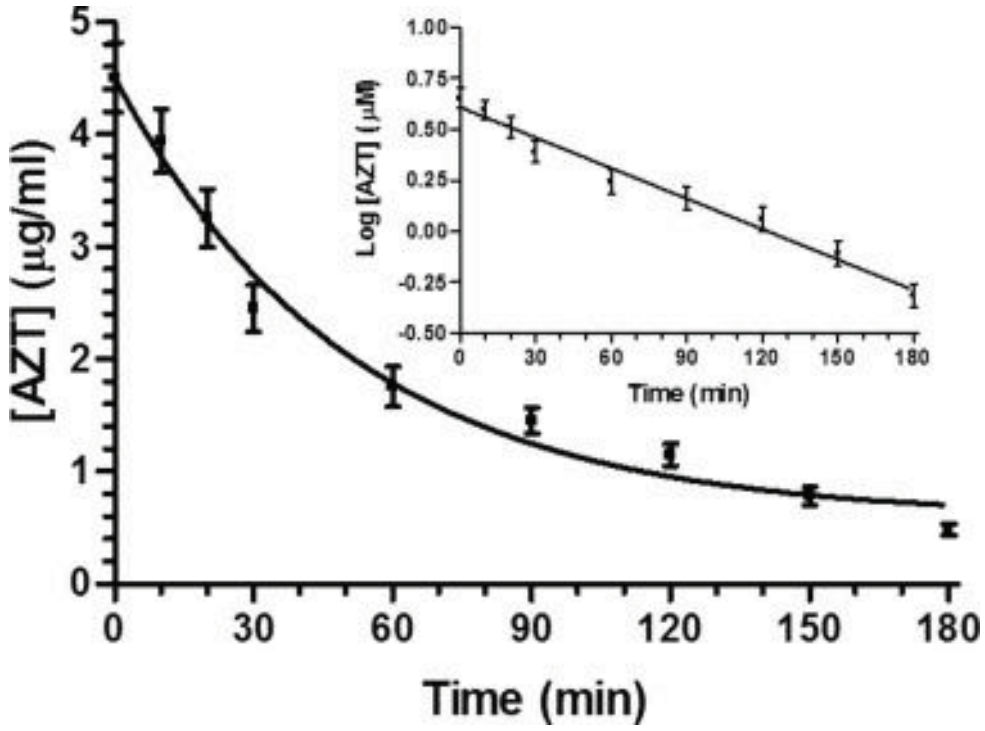

Figure 7. Elimination profile of AZT after the infusion 0.200 mg of UDCA−AZT into rats. The data are expressed as the mean ± SD of four independent experiments. The elimination followed apparent first order kinetics, as confirmed by the semilogarithmic plot reported in the inset (n = 9, r = 0.990, P<0.0001). The half-life of AZT was calculated to be 60.4 ± 3.8 min.

Nasal administration of UDCA−AZT

The nasal administration of pure UDCA–AZT as a water suspension did not allow us to obtain detectable amounts of AZT or the prodrug in the blood or in the CSF, respectively, within 180 min of administration, as reported previously [10]. In contrast, the nasal administration of the powders constituted by MIX or by the CP microparticles (0.8 mg, approximately 100 μg of UDCA−AZT in each nostril) produced detectable amounts of UDCA−AZT in the CSF of the rats, as reported in Figure 8. In particular, the UDCA−AZT C_{max} was obtained after 60 min, with a value of 1.96 ± 0.29 μg/mL (3.1 ± 0.4 μM), after nasal administration of the mixture.

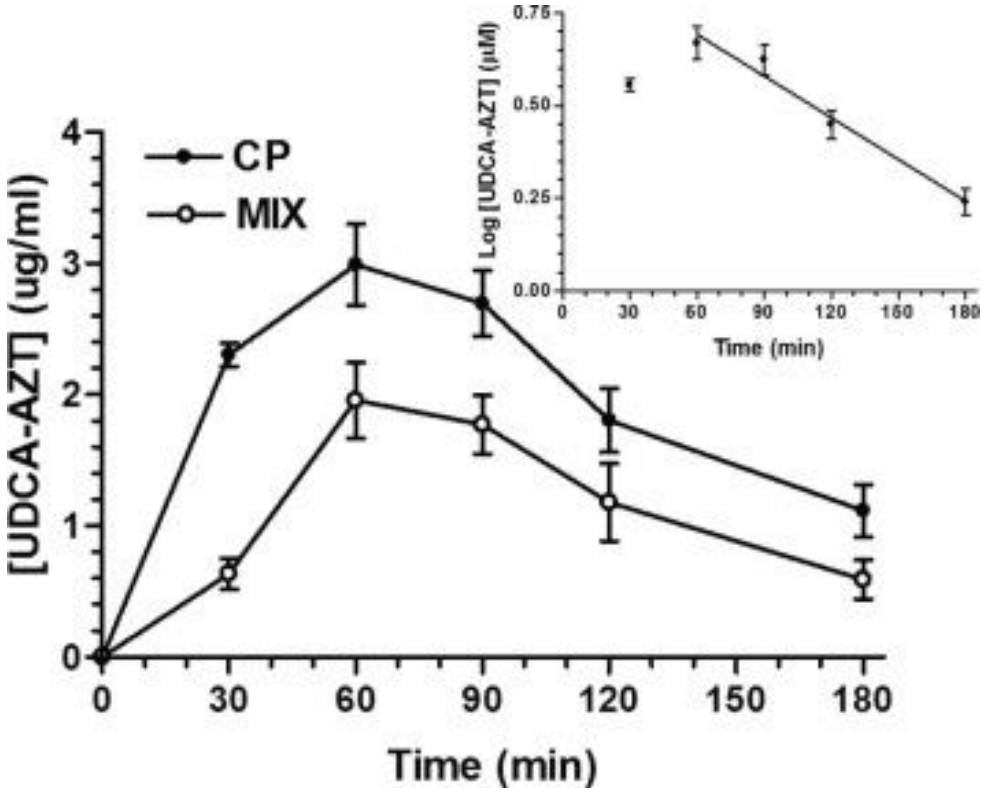

Figure 8. UDCA−AZT concentrations (μg/mL) detected in the CSF after the nasal administration of dry powders constituted by loaded CP microparticles and its parent mixture (MIX) of chitosan chloride and UDCA–AZT. Each dose contained 200 μg of the prodrug. The inset reports the semilogarithmic plot of the UDCA–AZT concentrations (μM) in the CSF after the nasal administration of the CP sample. The elimination of UDCA–AZT from the CSF followed apparent first order kinetics, as confirmed by the linear regression of the points ranging from 60 to 180 min (n = 4, r = 0.988, p<0.05). The data are expressed as the mean ± SD of four independent experiments.

The nasal administration of the same amount of CP microparticles increased the rate of uptake of the prodrug into the CSF of rats. Indeed, the UDCA−AZT C_{max} was obtained at 60 min, with a value of 2.99 ± 0.31 μg/mL (4.7 ± 0.5 μM), which was significantly higher than the C_{max} value obtained for the MIX sample (P<0.001).

No AZT was detected in the bloodstream or in the CSF within 180 min after nasal administration of the powders constituted by MIX or the CP microparticles.

The areas under the concentration (AUC) curve values obtained for UDCA−AZT in the CSF after the nasal administration of MIX and CP microparticles (Figure 8) were 201.39 ± 13.51 μg mL^{-1} min and 354.4 ± 13.3 μg mL^{-1}min, respectively. The ratio between the AUC of the CP sample and the AUC of the mixture was 1.76, indicating that the nasal formulation constituted by the CP microparticles allowed an uptake of UDCA−AZT into the CSF that was 76% higher than that obtained after the administration of the parent mixture (P<0.001).

The UDCA–AZT concentration in the CSF after nasal administration of CP microparticles decreased over time with apparent first order kinetics, as confirmed by the linearity of the semilogarithmic plot reported in the inset of Figure 8 (n = 4, r = 0.998, P< 0.05), and a half-life of 80.4 ± 9.2 min.

DISCUSSION

Although antiretroviral nucleoside derivatives are largely used against HIV infection for their efficacy at the peripheral level, the total eradication of this virus from the body is currently difficult to achieve. Indeed, antiretroviral drugs are unable to reach the CNS [40,41]; in contrast, the CNS is easily reached by HIV through infected monocytes [42,43] that differentiate into macrophages and microglia in the brain [44]. Therefore, the CNS and those macrophages constitute sanctuaries for HIV, where drug resistance is induced and from which the periphery can be re-infected [1,2]. These phenomena are attributed primarily to the expression of AETs on the membranes of macrophages [45,46] and blood brain barrier (BBB) cells [5,6], whose activity prevents the penetration of antiretroviral drugs into HIV sanctuaries.

Among numerous nucleoside antivirals, AZT was the first to be approved and remains the most widely used for the treatment and prophylaxis of HIV/AIDS [47]. Unfortunately, long-term clinical use of AZT is associated with significant side effects, but despite these drawbacks, AZT is considered to be one of the more potent inhibitors of the HIV DNA polymerase (reverse

transcriptase) [48,49]. Currently, tenofovir (TDF) is known to be a more potent and less toxic antiretroviral (ARV) drug than AZT; however, a higher virological failure rate was observed after a clinical TDF-containing ARV regimen in comparison to AZT-containing ARV therapy [50].

AZT activity in the CNS appears to be necessary not only in the brain tissue but also in the CSF subarachnoid spaces that contain macrophages and constitute the only site of HIV replication in the brain [3,4]. It is therefore important to obtain formulations that are able to target AZT to the CSF, but it is equally important to induce the ability of AZT to elude the AET systems in order to avoid its extrusion from the CNS and the associated macrophages. In this regard, we know that the prodrug UDCA–AZT, which was obtained by the conjugation of AZT to ursodeoxycholic acid (UDCA), is able to elude the AET systems [9]. Moreover, the results reported in this paper demonstrate for the first time that the prodrug UDCA–AZT is more efficient than AZT in permeating and remaining inside the murine macrophage-like J774A.1 cell line, which is commonly used as model system for studying the internalization process of macrophages [51]. Human cells can be used for *in vitro* studies of inflammation and infection, and many similarities between immortalized human monocytic cell lines (e.g., U937 and THP-1) and primary human blood monocytes have been reported [52]. However, these immature cells often require the addition of stimulant factors to promote their differentiation to a mature, adherent phenotype [53]. This requirement complicates the study of inflammatory outcomes related to these cell types, as stimulant factors exert specific effects on cellular behaviour. Additionally, maturation protocols vary across studies. In contrast, murine cell lines offer the advantage of an immortalized, relatively stable, mature, adherent macrophage phenotype. The murine cell lines J774A.1, RAW 264.7 and IC-21 exhibit the maturity markers F4/80 and Mac-1, indicating their macrophage-like phenotypes, and have been used as models of macrophage activation in numerous studies [54]. As an example, J774 mouse macrophages have been successfully used to demonstrate the uptake of azidothymidine triphosphate (AZT-TP)-loaded nanoparticles and the related efficient delivery of AZT-TP into the cell cytoplasm [55].

Moreover, our results demonstrate that the prodrug UDCA–AZT is hydrolysed in macrophages, facilitating intracellular AZT release. Interestingly, no toxicity was observed in the macrophages during their incubation with UDCA–AZT. We demonstrated previously that this prodrug is not a substrate of human AETs [9]. This result suggests that UDCA–AZT should not be subject to efflux from human macrophages. Furthermore, AZT is known to induce anti-HIV activity in the HTLV-1-

transformed cell line MT-4, which is highly susceptible to and permissive for HIV infection [56], thus suggesting that AZT is able to induce anti-HIV activity in human macrophages.

It is important to note that the prodrug UDCA–AZT is quickly hydrolysed in whole blood, so intravenous administration is not suitable for its permeation across the BBB. Indeed, following this type of administration, we detected only AZT, which exhibited concentration values that decreased over time with a half-life of approximately 1 h. No AZT or UDCA−AZT were detected in the CSF of rats after intravenous administration. In contrast, the nasal administration of this prodrug appears promising for achieving uptake into the CNS and particularly the CSF. We demonstrated that the nasal administration of chitosan-based microparticles can induce the selective uptake of neuroactive agents into the CSF of rats, probably by promoting drug permeation across the olfactory nasal mucosa [21,24,27]. Very recently, the poor water solubility of UDCA–AZT encouraged us to encapsulate this prodrug in solid lipid microparticles [10]. In particular, the nasal administration of UDCA–AZT loaded in stearic acid-based microparticles induced the selective uptake of the prodrug into the CSF of rats, with amounts of up to approximately 0.4 μg/ml within 60 min after administration [10]. These amounts increased (up to approximately 1.50 μg/mL within 120 min after administration) when the same quantity of microparticles were administered nasally as a water suspension in the presence of chitosan chloride [10]. This result was attributed to the good mucoadhesive properties of chitosan [21] and to its ability to transiently open the tight junctions in the epithelial membranes [57,15].

Nasal formulations obtained in the presence of water can be associated with the risk of chemical and physical instability and microbiological growth. Moreover, in the nasal cavity, liquid formulations are often rinsed into the GIT or out of the nose, so their residence time is generally short [58]. These disadvantages can be overcome by using powder-based formulations [32,59]. For this reason, we prepared microspheres based on chitosan chloride in order to increase the nose-to-brain delivery of UDCA–AZT. The efficacy of the microparticulate system for the brain delivery of the prodrug was verified by comparing the properties of the microparticles with those of their parent physical mixture, which was obtained by geometrical dilution of the components using an agate mortar and pestle. The grinding process induced a reduction of the d_{vs} diameters of chitosan chloride and the UDCA–AZT particles. The chitosan chloride particles were characterized by a round morphology and a relatively smooth surface before and after grinding, whereas UDCA–AZT appeared as fragments with an irregular shape. These two different morphological characteristics were distinctly apparent in the SEM picture of the physical mixture, where small irregular

fragments of UDCA–AZT appeared on the surface of larger and rounder chitosan chloride microspheres.

The spray-drying process allowed us to obtain unloaded microparticles of chitosan chloride (CH) with the "classical" round morphology and a small d_{vs} diameter. The loaded microparticles (CP) evidenced a slight increase in size and a morphology characterized by spherical particles mixed with fragments of irregular shape and high porosity, similar to spongy balls, with some degree of aggregation. We can conclude that the spherical particles are attributable to pure chitosan chloride that has not interacted with UDCA–AZT during the spray-drying process, whereas the "spongy balls" were obtained by a combination of the prodrug with polymer, inducing the formation of the highly porous structures. The different degrees of water solubility between UDCA–AZT and chitosan can justify these characteristics of the CP formulation. The description of the CP formulation's morphology appears to be consistent with the observed dissolution and water uptake profiles. Indeed, we observed that the dissolution rate of UDCA–AZT from the CP sample was significantly higher than that of the parent physical mixture. This phenomenon can be attributed to the highly porous structures observed in the CP sample, which allows a faster dissolution of UDCA–AZT with respect to its fragments included in MIX. Moreover, as demonstrated previously by Gavini et al. [27], water soluble chitosans, such as salts, are more able to completely amorphize poorly soluble drugs into the polymer matrix compared to the chitosan base; as a consequence, the dissolution rate and bioavailability of poorly soluble drugs improve.

Moreover, we observed that the water uptake rate of the CH sample was significantly reduced if chitosan chloride was mixed with UDCA–AZT, but a drastic decrease was observed in the case of the CP sample. The presence of UDCA–AZT, which is a very poorly water soluble molecule, in the physical mixture can explain its reduction of water uptake with respect to the CH sample, but the drastic reduction observed for the CP microparticles can be attributed to their porous structures, in which the presence of the prodrug and chitosan chloride together contributed to dramatically reducing the water uptake aptitude of the polymer.

Therefore, the CP sample appeared to be a valuable formulation for the nasal administration of UDCA–AZT. In particular, we hypothesized that the size and density of the microparticles should induce their deposition on the nasal mucosa, which should not be dehydrated by their presence, given the poor the water uptake of this sample. Moreover, the ability of the loaded microparticles to increase the dissolution rate of UDCA–AZT suggested their potential aptitude for inducing prodrug

permeation across the nasal mucosa, a phenomenon that is probably potentiated by the ability of chitosan to transiently open tight junctions [20].

The nasal administration of raw UDCA−AZT to rats did not produce any detectable levels of UDCA−AZT or AZT in the bloodstream or the CSF, whereas the nasal administration of the CP sample and its parent physical mixture allowed us to obtain relatively high levels of UDCA–AZT in the CSF of rats 60 min after administration. The relative bioavailability of the CP sample was 176% of that of its parent physical mixture (P<0.001). No AZT was detected in the bloodstream of rats after nasal administration of the CP sample and its parent physical mixture, confirming the existence of a direct nose−CNS pathway for this prodrug [10]. Our results demonstrate that the role of chitosan in inducing selective UDCA–AZT uptake into the CSF is potentiated when the prodrug is formulated as a microparticulate system by spray-drying. This phenomenon is illustrated in Figure 9, which presents a comparison of the AUC values obtained in the CSF after nasal administration of the same dose of UDCA–AZT (200 μg) to rats using different formulations (i.e., the solid lipid microparticles (SLMs), their water dispersion in the presence of chitosan (SLMs + Ch), which was obtained previously by Dalpiaz et al. [10], MIX and CP, which was described here). In particular, CP was able to induce an uptake of UDCA–AZT into the CSF of rats that was 1.8, 3.2 and 18.6 times greater than that of its parent physical mixture (MIX), the dispersion of solid lipid particles in the presence of chitosan (SLMs + Ch) and the SLMs in solid form, respectively.

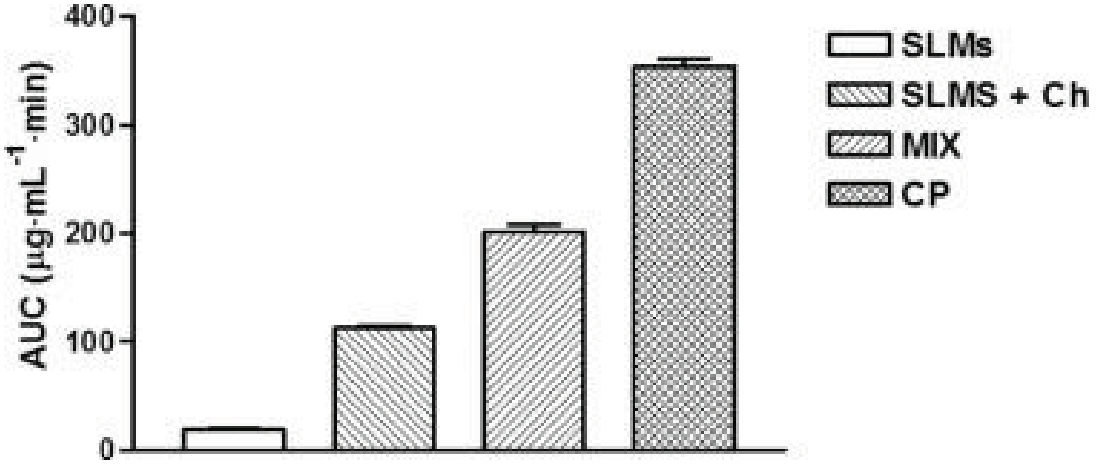

Figure 9. A comparison among the AUC values obtained in the CSF of rats after the nasal administration of 200μg of UDCA–AZT using different formulations (i.e., loaded solid lipid microparticles (SLMs), their water dispersion in the presence of chitosan (SLMs + Ch), the physical mixture of chitosan and prodrug (MIX) and the loaded microparticles based on chitosan chloride

(CP)). The data pertaining to SLMs and the SLM + Ch formulations were reported previously [10]. The data are expressed as the mean ± SD of four independent experiments.

To summarize, after nasal administration, chitosan microspheres induce the efficient uptake of UDCA–AZT into the CSF. We demonstrated previously that this prodrug is able to elude the AETs and avoid their inactivation [9]; as a consequence, the ability of the prodrug to elude the AET systems can prevent its extrusion into the bloodstream and induce AZT transport in the macrophages located in the subarachnoid spaces of the CSF. Consistent with these findings, it was demonstrated previously that the nasal co-administration of AZT and probenecid (an inhibitor of AETs) increased AZT uptake into the CSF of rats [60].

Taking into account the observations that the UDCA–AZT C_{max} obtained in the CSF after the nasal administration of the sample CP was approximately 5 μM and that the half-life of the prodrug in the CSF was approximately 90 min, we can hypothesize that multiple nasal administrations every 90 min will allow rats to obtain UDCA–AZT concentrations ranging between approximately 5 and 10 μM in their CSF [61]. We demonstrated that the incubation of macrophages with 10 and 100 μM UDCA–AZT allowed us to detect prodrug amounts ranging from approximately 0.2–1 nmoles in 10^6 cells. We also demonstrated that the AZT concentration in macrophages after incubation with UDCA–AZT was 47 μM. AZT exhibits anti-HIV activity in the HTLV-1-transformed cell line MT4, with an IC_{50} value of approximately 30 nM [56], which is more than three orders of magnitude lower than the concentration of AZT that we detected in the macrophages after incubation with 100 μM UDCA–AZT. Therefore, it seems reasonable to deduce that incubation with 5 or 10 μM UDCA–AZT can allow the macrophages to attain AZT concentrations sufficient to induce anti-HIV activity. As a consequence, taking into account the aspects we described above, we predict that the amount of UDCA–AZT taken up in the CSF following the nasal administration of the loaded microparticles might be sufficient to achieve anti-HIV activity in the CNS.

REFERENCES

1. Cunningham PH, Smith DG, Satchell C, Cooper DA, Brew B,. Evidence for independent development of resistance to HIV-1 reverse transcriptase inhibitors in the cerebrospinal fluid. AIDS. 2000;14:1949−54.
2. Kolson DL, Gonzalez-Scarano F. HIV and HIV dementia. J Clin Invest. 2000;106:11−3.
3. Cunningham AL, Naif H, Saksena N, Lynch G, Chang J, Li S, Jozwiak R, Alali M, Wang B, Fear W, Sloane A, Pemberton L, Brew B. HIV infection of macrophages and pathogenesis of AIDS dementia complex: interaction of the host cell and viral genotype. J Leukocyte Biol. 1997;62: 117−25
4. Ghersi-Egea JF, Finnegan W, Chen JL, Fenstermacher JD. Rapid distribution of intraventricularly administered sucrose into cerebrospinal fluid cisterns via subarachnoid velae in rat. Neuroscience. 1996;75:1271−88
5. Namanja HA; Emmert D, Davis DA, Campos C. Miller DS, Hrycyna CA, Chmielewski J. Toward eradicating HIV reservoirs in the brain: inhibiting Pglycoprotein at the blood-brain barrier with prodrug abacavir dimers. J Am Chem Soc. 2012.
6. Pavan B, Dalpiaz A. Prodrugs and endogenous transporters: are they suitable tools for drug targeting into the central nervous system? Curr Pharm Des. 2011;17: 3535−60.
7. Wang Y, Sawchuk RJ. Zidovudine transport in the rabbit during intravenous and intracerebroventricular infusion. J Pharm Sci. 1995;7:871−6.
8. De Clercq E. Anti-HIV Drugs: 25 compounds approved within 25 years after the discovery of HIV. Int J Antimicrob Agents. 2009;33:307−20.
9. Dalpiaz A, Paganetto G, Pavan B, Fogagnolo M, Medici A, Beggiato S, Perrone D. Zidovudine and ursodeoxycholic acid conjugation: design of a new prodrug potentially able to bypass the active efflux transport systems of the central nervous system. Mol Pharm. 2012;9:957−68.
10. Dalpiaz A, Ferraro L, Perrone D, Leo E, Iannuccelli V, Pavan B, Paganetto G, Beggiato S, Scalia S. Brain uptake of a zidovudine prodrug after nasal administration of solid lipid microparticles. Mol Pharm. 2014;11:1550-61.
11. Fine JM, Forsberg AC, Renner DB, Faltesek KA, Mohan KG, Wong JC, Arneson LC, Crow JM, Frey WH. 2nd, Hanson LR. Intranasally-administered deferoxamine mitigates toxicity of 6-OHDA in a rat model of Parkinson's disease. Brain Res. 2014;1574:96-104.

12. Fine J.M, Renner DB, Forsberg AC, Cameron RA, Galick BT, Le C, Conway PM, Stroebel, BM, Frey WH 2nd, Hanson LR. Intranasal deferoxamine engages multiple pathways to decrease memory loss in the APP/PS1 model of amyloid accumulation. Neurosci Lett. 2015;584:362-7.
13. Illum L. Transport of drugs from the nasal cavity to the central nervous system. Eur J Pharm Sci. 2000;11:1−18.
14. Vyas TK, Shahiwala A, Marathe S, Misra A.. Intranasal drug delivery for brain targeting. Curr Drug Del. 2005;2:165−75.
15. Illum L. Is nose-to-brain transport of drugs in man a reality? J Pharm Pharmacol. 2004;56:3−17.
16. Thorne RG, Frey WH. Delivery of neurotropic factors to the central nervous system. Clin Pharmacokinet. 2001;40:907−946.
17. Finger TE, Jeor St. VL, Kinnamon JC, Silver WL. Ultrastructure of substance P- and CGRP-immunoreactive nerve fibers in the nasal epithelium of rodents. J Comp Neurol. 1990;294:293-305.
18. Johnson NJ, Hanson LR, Frey WH. Trigeminal pathways deliver a low molecular weight drug from the nose to the brain and orofacial structures. Mol Pharm. 2010;7:884−93.
19. Cho W, Kim MS, Jung MS, Park J, Cha KH, Kim JS, Park HJ, Alhalaweh A, Velaga SP, Hwang SJ. Design of salmon calcitonin particles for nasal delivery using spray-drying and novel supercritical fluid-assisted spray-drying processes. Int J Pharm. 2014;478:288-96.
20. Casettari L, Illum L. Chitosan in nasal delivery systems for therapeutic drugs. J Control Release. 2014;190:189-200.
21. Dalpiaz A, Gavini E, Colombo G, Russo P, Bortolotti F, Ferraro L, Tanganelli S, Scatturin A, Menegatti E, Giunchedi P. Brain uptake of an antiischemic agent by nasal administration of microparticles. J Pharm Sci. 2008;97:4889−903.
22. Horvát S, Fehér A, Wolburg H, Sipos P, Veszelka S, Tóth A, Kis L, Kurunczi A, Balogh G, Kürti L, Eros I, Szabó-Révész P, Deli MA. Sodium hyaluronate as a mucoadhesive component in nasal formulation enhances delivery of molecules to brain tissue. Eur J Pharm Biopharm 2009;72:252−9.
23. Mistry A, Stolnik S, Illum L. Nanoparticles for Direct nose to-brain delivery of drugs. Int J Pharm. 2009;379:146−157.

24. Rassu G, Soddu E, Cossu M, Brundu A, Cerri G, Marchetti N, Ferraro L, Regan RF, Giunchedi P, Gavini E, Dalpiaz A. Solid microparticles based on chitosan or methyl-β-cyclodextrin: a first formulative approach to increase the nose-to-brain transport of deferoxamine mesylate. J Control Release. 2015a;201:68–77
25. Bernkop-Schnürch A, Dünnhaupt S. Chitosan-based drug delivery systems. Eur J Pharm Biopharm. 2012;81:463-9.
26. Sinha VR, Singla AK, Wadhawan S, Kaushik R, Kumria R, Bansal K, Dhawan S. Chitosan microspheres as a potential carrier for drugs. Int J Pharm. 2004;274:1-33.
27. Gavini E, Rassu G, Ferraro L, Generosi A, Rau JV, Brunetti A, Giunchedi P, Dalpiaz A. Influence of chitosan glutamate on the ± intranasal absorption of rokitamycin from microspheres. J Pharm Sci. 2011;100:1488-502.
28. Maestrelli F, Zerrouk N, Chemtob C, Mura P. Influence of chitosan and its glutamate and hydrochloride salts on naproxen dissolution rate and permeation across Caco-2 cells. Int J Pharm. 200;271:257-267.
29. Dhuria SV, Hanson LR, Frey II WH. Intranasal delivery to the central nervous system: Mechanisms and experimental considerations. J Pharm Sci. 2010;99:1654–73.
30. Kublik H, Vidgren MT. Nasal delivery systems and their effect on deposition and absorption, Adv Drug Del Rev. 1998;29:157–77.
31. Marttin E, Romeijn SG, Verhoef JC, Merkus FWHM. Nasal absorption of dihydroergotamine from liquid and powder formulations in rabbits. J Pharm Sci 1997;86:802–7.
32. Rassu G, Soddu E, Cossu M, Gavini E, Giunchedi P, Dalpiaz A. Powder formulations based on chitosan for nose-to-brain delivery of drugs. JDDST. 2015b, in press, doi:10.1016/j.jddst.2015.05.002.
33. Rassu G, Nieddu M, Bosi P, Trevisi P, Colombo M, Priori D, Manconi P, Giunchedi P, Gavini E, Boatto G. Encapsulation and modified-release of thymol from oral microparticles as adjuvant or substitute to current medications. Phytomedicine. 2014;21:1627–32.
34. Gavini E, Rassu G, Ciarnelli V, Spada G, Cossu M, Giunchedi P. Mucoadhesive drug delivery systems for nose-to-brain targeting of dopamine. J Nanoneurosci 2012;2:47-55.
35. Rassu G, Gavini E, Jonassen H, Zambito Y, Fogli S, Breschi MC, Giunchedi P. New chitosan derivatives for the preparation of rokitamycin loaded microspheres designed for ocular or nasal administration. J Pharm Sci. 2009;98:4852-65.

36. Van den Berg MP, Romeijn SG, Verhoef JC, Merkus FW. Serial cerebrospinal fluid sampling in a rat model to study drug uptake from the nasal cavity. J Neurosci Method 2002;116:99–107.
37. Sacchetti C, Artusi M, Santi P, Colombo P. Caffeine microparticles for nasal administration obtained by spray drying. Int J Pharm. 2002;242:335–9.
38. Giunchedi P, Gavini E, Bonacucina G, Palmieri GF. Tabletted polylactide microspheres prepared by a w/o emulsion-spray drying method. J Microencapsul. 2000;17:711–20.
39. Sosnik A, Seremeta KP. Advantages and challenges of the spray-drying technology for the production of pure drug particles and drug-loaded polymeric carriers. Advances in Colloid and Interface Science. 2015;223:40–54
40. Kaufmann GR, Cooper DA. Antiretroviral therapy of HIV-1 infection: established treatment strategies and new therapeutic options. Curr Opin Microbiol. 2000;3:508−14.
41. Strazielle N, Belin MF, Ghersi-Egea JF. Choroid plexus controls brain availability of anti-HIV nucleoside analogues via pharmacologically inhibitable organic anion transporters. AIDS. 2003;17:1473−85.
42. Davis LE, Hjelle BL, Miller VE, Palmer DL, Llewellyn AL, Merlin TL, Young SA, Mills RG, Wachsman W, Wiley CA. Early viral brain invasion in iatrogenic human immunodeficiency virus infection. Neurology. 1992;42:1736−9.
43. Gray F, Scaravilli F, Everall I, Chretien F, An S, Boche D, Adle-Biassette H, Wingertsmann L, Durigon M, Hurtrel B, Chiodi F, Bell J, Lantos P. Neuropathology of aarly HIV-1 infection. Brain Pathol. 1996;6:1−15.
44. Rausch DM, Stover ES. Neuroscience research in AIDS. Prog Neuropsychopharmacol Biol Psychiatry. 2001;25:231−57.
45. Chaudhary PM, Mechetner EB, Roninson IB. Expression and activity of the multidrug resistance p-glycoprotein in human peripheral blood lymphocytes. Blood 1992;80:2735−2739.
46. Neyfakh AA, Serpinskaya AS, Chervonsky AV, Apasov SG, Kazarov AR. Multidrug-resistance phenotype of a subpopulation of T-lymphocytes without drug selection. Exp Cell Res. 1989;185:496−505.
47. Hughes SH. Reverse transcription of retroviruses and LTR Retrotransposons. Microbiol Spectr. 2015;3:0027.

48. Arts EJ, Hazuda DJ. HIV-1 antiretroviral drug therapy. Cold Spring Harb Perspect Med 2012;2: a007161.
49. Golan DE, Tashjian AH, Armstrong EJ. Principles of Pharmacology: The Pathophysiologic Basis of Drug Therapy, third ed. Lippincott Williams & Wilkins, Philadelphia 2011.
50. Tang MW, Kanki PJ, Shafer RW. A review of the virological efficacy of the 4 World Health Organization-recommended tenofovir-containing regimens for initial HIV therapy. Clin Infect Dis. 2012;54:862-75.
51. Wang H, Wu L, Reinhard BM. Scavenger receptor mediated endocytosis of silver nanoparticles into J774A.1 macrophages is heterogeneous. ACS Nano. 2012;6:7122-32.
52. Yagil-Kelmer E, Kazmier P, Rahaman MN, Bal BS, Tessman RK, Estes DM. Comparison of the response of primary human blood monocytes and the U937 human monocytic cell line to two different sizes of alumina ceramic particles. J Orthop Res. 2004;22:832–8.
53. Shelley CS, Teodoridis JM, Park H, Farokhzad OC, Bottinger EP, Arnaout MA.. During differentiation of the monocytic cell line U937, Pur alpha mediates induction of the CD11c beta 2 integrin gene promoter. J Immunol. 2002;168:3887–93.
54. Chamberlain LM, Godek ML, Gonzalez-Juarrero M, Grainger DW. Phenotypic non-equivalence of murine (monocyte-) macrophage cells in biomaterial and inflammatory models. J Biomed Mater Res A. 2009,88:858-71.
55. Giacalone G, Bochot A, Fattal E, Hillaireau H. Drug-induced nanocarrier assembly as a strategy for the cellular delivery of nucleotides and nucleotide analogues. Biomacromolecules. 2013;14:737-42.
56. Magnani M, Casabianca A, Fraternale A, Brandi G, Gessani S, Williams R, Giovine M, Damonte G, De Flora A, Benatti U. Synthesis and targeted delivery of an azidothymidine homodinucleotide conferring protection to macrophages against retroviral infection. Proc Natl Acad Sci USA 1996;93:4403-8.
57. Dodane V, Khan MA, Merwin JR. Effect of chitosan on epithelial permeability and structure. Int J Pharm. 1999;182:21−32.
58. Kublik H, Vidgren MT. Nasal delivery systems and their effect on deposition and absorption. Adv Drug Del Rev. 1998;29:157–77.
59. Marttin E, Romeijn SG, Verhoef JC, Merkus FWHM. Nasal absorption of dihydroergotamine from liquid and powder formulations in rabbits. J Pharm Sci. 1997;86: 802–7.

60. Seki T, Sato N, Hasegawa T, Kawaguchi T, Juni K. Nasal adsorption of zidovudine and its transport to cerebrospinal fluid in rats. Biol. Pharm. Bull. 1994;17:1135−7.
61. Bourne DW, Dittert LW.. Pharmacokinetics, in: Banker, G,S, Rhodes, C.T. (Eds), Modern Pharmaceutics , Marcel Dekker INC, New York, pp. 91-142 1990.

CHAPTER 4

Composite Chitosan/Alginate Hydrogel For Controlled Release Of Deferoxamine: A System To Potentially Treat Iron Dysregulation Diseases

Adapted from:

Composite Chitosan/Alginate Hydrogel For Controlled Release Of Deferoxamine: A System To Potentially Treat Iron Dysregulation Diseases.

Giovanna Rassu, **Andrea Salis**, Elena Piera Porcu, Paolo Giunchedi, Marta Roldo, Elisabetta Gavini. Carbohydrate Polymers. October 2015, http://dx.doi.org/10.1016/j.carbpol.2015.10.048

INTRODUCTION

Iron is a redox active metal, essential for life and indispensable for several biological reactions [1]. Nevertheless, its excess is toxic due to the release of reactive oxygen species (ROS) [1-3]. The hydroxyl radical is very reactive and can cause oxidative damage to various cell components, including lipid membranes, DNA, and proteins, thereby causing cell damage [2,4].Disruption of iron regulation plays a key role in the etiology of neurological disorders, cancer, stroke, muscle diseases such as Duchenne's muscular dystrophy, and aging [3,5]. Iron overload in the cytoplasm of hepatocytes contributes to hepatocellular damage and hepatocarcinogenesis [4]. In the skin, excess iron combined with UV radiation exerts pro-oxidant effects [3]. Furthermore, it is hypothesized that iron may contribute to the pathogenesis of ocular diseases [2].

Iron chelators are currently being investigated for their benefit in limiting iron-induced oxidative damage. The best known iron chelator in clinical use is deferoxamine (DFO, Desferal™) [2]. DFO as mesylate salt is the treatment of choice for acute iron intoxication and chronic iron overload due to transfusion-dependent anemia [6]. Data to support DFO use in other disorders associated with iron overload are growing. Several studies have shown the beneficial effects of DFO in reducing skin necrosis [7-11]. DFO appears to mitigate radiation-induced hypovascularity and improve tissue elasticity in a rat model [12]. DFO can prevent liver injury and development of preneoplastic lesions in rats [13,14], and it was proposed as an anticancer agent for the therapy of advanced hepatocellular carcinoma (HCC) [4,15]. Over the past few years, a variety of studies have been conducted on DFO demonstrating some positive effects on fracture healing [16-21]. Unfortunately, DFO has properties that significantly limit its usefulness in a clinical setting. Administration of this drug is limited to the parenteral route due to its poor absorption in the gut. Furthermore, DFO has a very short plasma half-life because of rapid renal excretion; thus, repetitive or continuous subcutaneous infusions are necessary to maintain its effective therapeutic levels [1,22]. These are associated with toxic effects [23]. Furthermore, repeated injection of DFO at the bony injury may not be practical or effective clinically [19]. In most studies DFO was administered in solution [4,12,15,16], and to date, very few formulation strategies have been developed in order to improve DFO biopharmaceutical properties: (i) conjugation to hydroxyethyl starch (Hespan) [24] or to hyperbranched polyglycerol (HPG) [25] for increasing plasma half-life; (ii) formulation in nasal microparticulate delivery systems to improve the nose to brain transport [26]; (iii) loading in morselized beads of calcium sulfate [27] or in true bone ceramic scaffolds [21] for the treatment of bone defects.

Hydrogels are widely used as debriding agents, moist dressings, components of pastes for wound care, as well as ocular drug delivery carriers, and subcutaneous inserts. Furthermore, hydrogels are able to both locally embolize the hepatic tumor and deliver drugs in a controlled manner [28,29]. Tissue engineering is one of the most recent applications of hydrogels as space filling agents, delivery vehicles for bioactive substances or as three-dimensional structures that organize cells and ensure the development of a required tissue [30]. Composite hydrogels are a co-formulation of particulate systems incorporated into the hydrogel matrix forming "plum pudding" hydrogel networks [31]. Incorporating degradable micro- or nanoparticles loaded with a drug in the hydrogel can further extend the possibilities for controlling drug delivery [32]. This can have the added benefits of reducing burst release commonly displayed in microsphere formulations and can prevent microsphere displacement away from the site of action [31].

In order for DFO therapy to progress to clinical treatment, methods of delivery, timing, and dosage need to be considered and optimized [14,18,20]. In this study, the feasibility of hydrogel as prolonged delivery systems of DFO, useful for solving the criticalities common to several iron dysregulation diseases, was investigated. Physical chitosan/alginate hydrogel was selected in order to obtain a carrier able to control the delivery of this drug to the target site, and at the same time, depending on the disease, to serve as structural support (e.g. on fracture healing) or embolic agent (e.g. in the therapy of advanced hepatocellular carcinoma). Finally, it should be reabsorbed after it has served its function. This system should be entirely biocompatible and biodegradable, no toxic, injectable or implantable. The materials used well correspond to the characteristic quality of the required drug delivery systems making alginate and chitosan more suitable carriers than others. The advantages of chitosan/alginate hydrogel alone or co-formulated with PLGA microparticles were evaluated in vitro.

MATERIALS AND METHODS

Materials

Sodium alginate (Protanal LF 120 L, batch: 907788; MW: 221 kDa; viscosity (1% sol): 93 cP; Seaweed species: *Lessonia nigrescens;* F_G: 0.41; F_M: 0.59; F_{GG}: 0.22; F_{GM}: 0.19; F_{MM}: 0.40; F_{GGM}: 0.05; F_{MGM}: 0.14; F_{GGG}: 0.17; $N_{G>1}$: 5.6 [33] was purchased from FMC BioPolymer, now FMC Health and Nutrition (Philadelphia, USA). Chitosan (ChitoClear TM 1358, deacetylation degree: 95%; viscosity (1% sol): 63 cP; MW: 103 kDa; ash residue: 0.9% (according to the manufacturer's specifications)) was acquired from PRIMEX EHF, Siglufjordur, Island. Poly(d,l-lactide-co-

glycolide) (PLGA) RG502 (viscosity: 0.16–0.24 dl/g (50:50), MW: 7000–17,000), RG504 (viscosity: 0.45–0.60 dl/g, MW: 38,000–54,000), and deferoxamine mesylate salt (DFO) were purchased from Sigma–Aldrich, St. Louis, USA. All other solvents and chemicals were of analytical grade.

Hydrogel preparation

Unloaded hydrogel characterized by a molar ratio 1/1 between alginate and chitosan and 2.5% (w/v) concentration of polymers, in the final volume, were prepared. Sodium alginate solution (2.44% w/v) was made dissolving alginate powder in water with the aid of a magnetic stirrer at room temperature. Separately, chitosan (2.75% w/v) was dissolved in hydrochloric acid solution pH 0.7, under magnetic stirring. Then, 1.25 mL of chitosan solution was added to 3.75 mL alginate solution (pH 7.0) and stirred vigorously in order to obtain the final pH of 3.0. Loaded hydrogels were prepared by dissolving DFO (3 mg) in chitosan solution before mixing polymer solutions.

Microsphere preparation

Microspheres, composed by PLGA, hydrophobic polymer, and DFO, hydrophilic drug, were prepared by using the emulsification/spray drying method previously described [34]. After preliminary studies, the total solid (drug + polymer) concentrations of 4% w/v was selected; drug to polymer ratios of 1:4 and 1:10 were considered. Table 1 lists the formulations prepared. Briefly, w/o emulsion was prepared by dissolving DFO in water and PLGA in 25 mL of dichloromethane. The aqueous solution was added dropwise to the organic one within 5 min, under homogenization at 10,000 rpm (Ultra-Turrax T25 basic, IKA, Germany). The w/o emulsion was then sprayed through the nozzle (0.7 mm) of a spray-dryer, co-current flow type (Buchi Mini Spray Dryer B-191, Milano, Italy). The process conditions are shown in Table 1. The temperature of emulsion was maintained at about 5°C throughout the process. No phase separation during the spray-drying process was observed in the emulsion, thus rendering unnecessary the use of surfactants (Figure S1). Microspheres were collected and kept under vacuum for 48 h at room temperature.
Blank microspheres were produced as control by dissolving PLGA in dichloromethane.

Table 1. Microsphere formulations: composition and spray-dryer manufacturing parameters. Mean diameter and d90/d10 ratio were also reported.

	Microspheres composition[a]		Spray dryer parameters		Particle size and distribution	
Formulation	**DFO (g)**	**water (mL)**	**Air In (°C)**	**Air Out (°C)**	**dm (µm)**	**d90/d10**
502	-	-	50	41	5.63±0.31	8.33
504	-	-	50	41	8.19±2.09	15.95
D502 4	0.250	5	80	55	33.13±23.75	10.37
D504 4	0.250	5	80	51	66.38±11.86	9.10
D502 10	0.100	1.5	50	39	18.21±3.2	8.62
D504 10	0.100	1.5	50	42	21.93±17.76	13.08

[a]Drug to polymer ratio of 1:4 and 1:10 were used; The following conditions were also used during spray-drying: drying airflow, 31.3 m^3/h; spraying airflow, 500 l/h; solution feed rate,4.09± 0.05 ml/min.

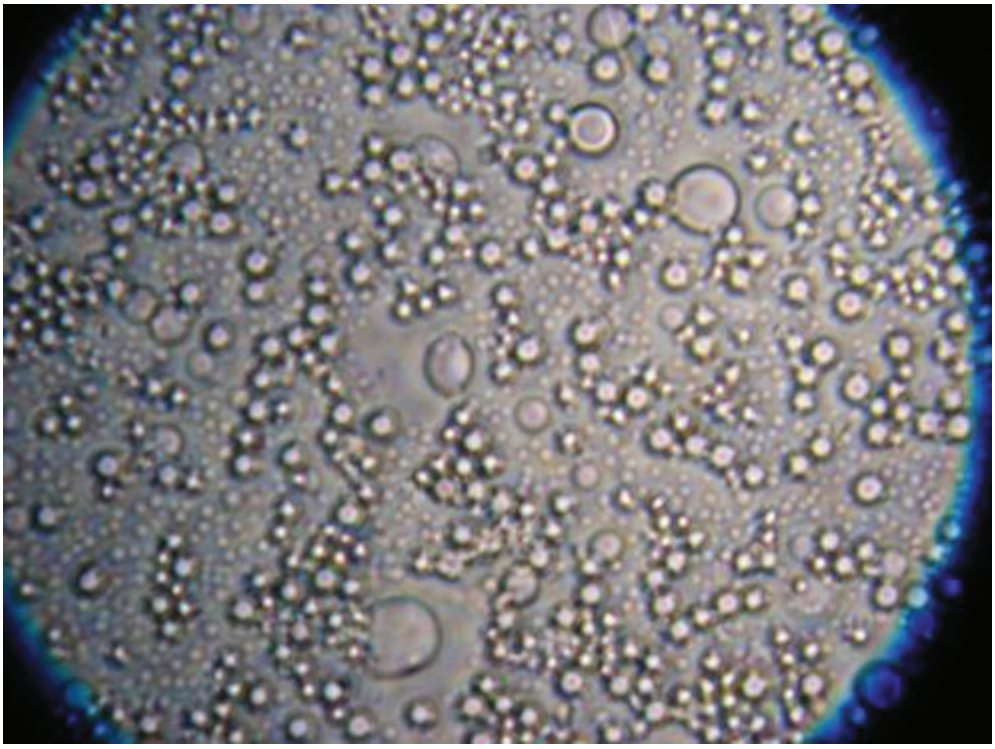

Figure S1. Photomicrograph of emulsion almost at the end of spray-drying process. Magnification 80x.

Composite hydrogel preparation

Composite hydrogels were prepared by combining the microspheres and the hydrogel. Two methods were tested: (1) PLGA microspheres (30mg) were added into the chitosan solution; which was then loaded onto the alginate solution and stirred vigorously; and (2) the addition of microspheres was performed after the formation of chitosan/alginate hydrogel.

Microsphere characterization

Yield of production

The yield of production was calculated as percentage of the weight of the final product with respect to the total solid (drug and polymer) solubilised in the feed solutions.

Particle size analysis using a suspension method

The particle size and particle size distribution of the microspheres were determined with a Coulter LS 100Q Laser diffractometric equipment (Beckman Coulter Particle Characterization, Miami, FL, USA). For particle size analysis using a suspension method, microspheres (2 mg) were suspended in 1 mL of Tween 80 solution (0.1% w/v); the suspension was further diluted and dispersed by vortexing for 10min in case of formulation based on RG502 and vortexing for 10 min and sonication for 2 min in case of RG504. Values reported are the averages of three determinations for five samples of each formulation (standard deviation, SD, $n = 15$).

Powder particle size analysis

The particle size in the dry powder was measured by an HELOS Particle Size Analyser from Sympatec GMbH, fitted with an Aspiros doser (pressure, 2.00 bar; vacuum, 36.00 mbar; feed velocity; 25.00 mm/s). A lens able to detect particles in the size range 0.9–175 μm was fitted.

Drug content

DFO loaded microspheres (15 mg) were dissolved in 2–4 mL dichloromethane with the aid of magnetic stirring. The solution was then diluted with 40 mL of water and the organic phase was evaporated using a rotavapor at 35°C before transferring the remaining aqueous solution into a volumetric flask (50 mL) and analyzed by HPLC as described below. One extraction was enough for complete DFO recovery.

Loading efficiency (LE), as percentage, was calculated by using the following equation:

$$LE = \frac{DC_A}{DC_T} \times 100 \quad (1)$$

where DC_A and DC_T are the amount of drug loaded into the polymer matrix and the expected theoretical value, respectively. DC_A was calculated as previously reported [35].

Drug burst test

Microspheres (15 mg) were suspended in 50 mL of water, at either 37 °C or at room temperature. The samples were then vortexed for 10 s before centrifugation (3000 rpm for 5 min) and then analyzed by HPLC.

HPLC analysis of deferoxamine mesylate

For the quantification of DFO in buffer samples, a Varian ProStar 210 with AutoSampler 410 and a PDA photodiode array detector (Varian Inc Scientific Instruments, Walnut Creek, CA, USA) was employed. The chromatographic separation was performed as previously reported [26]. Briefly, separation was performed at room temperature on a C18 column with polar endcapping (Phenomenex Synergi Hydro-RP 80A, 150 × 4.6 mm I.D. and 4 μm of particle size). Twenty microliters of samples were directly injected into the column and eluted with a binary mixture consisting of acetonitrile (pH 4.6 with 0.5 M H_3PO_4) and a 0.1 M KH_2PO_4 (3.4 g/250 mL), 120 mg/L (30 mg/250 mL) 1-eptane sulfonic acid sodium salt solution ratio 17:83 (v/v) adjusted to pH 4.6 by 0.5 M phosphoric acid. DFO was detected by UV at 210 nm wavelength. Concentrations of analyte were calculated by interpolation of DFO standard curves.

Hydrogel characterization

Viscosity measurement

Viscosity of unloaded hydrogel as well as polymer solutions was measured, at room temperature, by rotational viscometer (Alpha-L, Fungilab, Barcelona, Spain) at a constant rotation speed of 60 rpm or 100 rpm, respectively.

Porosity measurement

The solvent replacement method was used to determine the porosity of the hydrogel samples [36]. Freeze-dried hydrogels (unloaded, loaded and composite) were immersed in absolute ethanol overnight and weighed after blotting excess ethanol on the surface. The porosity was calculated from the following equation:

$$\text{Porosity} = \frac{(M_2 - M_1)}{\rho V} \times 100 \quad (2)$$

whereM_1 and M_2 are the masses of the hydrogel before and after immersion in ethanol, respectively, ρ is the density of absolute ethanol and V is the volume of the hydrogel.

Water uptake and swelling

Hydrated and freeze-dried hydrogels (unloaded, loaded and composite) were weighed and fully immersed in a sealed container with phosphate buffered saline (PBS; pH 7.4) for 24 h at 37°C [37] to study the water uptake (WU%) and swelling characteristics. Then, samples were taken out, wiped with paper and weighed. The water uptake percentage was determined gravimetrically using following equation:

$$\text{WU} = \frac{(M_2 - M_1)}{M_1} \times 100 \quad (3)$$

whereM_1 is the dry weight and M_2 is the saturated weight.
Similarly, the swelling ratio was calculated from the volume of dry and saturated hydrogel.

Dynamic vapor absorption (DVS) studies

Dynamic vapor sorption (DVS) analysis of the freeze-dried hydrogels (unloaded, loaded and composite) was carried out with a Surface Measurement Systems DVS Advantage instrument. Using nitrogen as the carrier gas; the mass change of samples subjected to a changing water vapor partial pressure at 25°C was recorded. The partial pressure was increased from 0 to 90% in 10% increments; the partial pressure was increased to the next step either after equilibrium or after a maximum time of 360 min. A full adsorption/desorption cycle was performed; the data collected were used to calculate the adsorption and desorption isotherms as well as the hysteresis. The data were further analyzed according to the following equation:

$W_p=K_p t^{np}$ (4)

where W_p is the weight gain; K_p is the kinetic constant of water penetration into the composite material; n_p is the exponent describing the mechanism of water penetration.

Biodegradability

The weight loss of the composite hydrogels was monitored as a function of incubation time in PBS (pH 7.4) at 37°C for 24 days [37]. Weights of the samples were measured at 10, 17 and 24 days of incubation, after freeze-drying. Degradation was determined by percentage of weight loss (W_L) using following equation:

$$W_L(\%) = \frac{W_L - W_0}{W_0} \times 100 \quad (5)$$

where W_0 was the initial weight and W_L was the weight after degradation. Each experiment was repeated three times, and the value is reported as mean ± SD (n = 3). No significant change in pH was found during the test.

Drug release studies

Release studies of DFO from microspheres, loaded and composite hydrogels were carried out. Microspheres or hydrogels were put in 50 mL of PBS containing 0.01% Tween 80 and shaken at 80 rpm, 37°C for 10 days.

At predetermined time points, 1 mL of medium was withdrawn and centrifuged at 13,000 rpm for 10 min, the supernatant was removed and stored at −20°C until HPLC analysis. Pellets eventually obtained after centrifugation were resuspended in 1 mL PBS and poured back into the release medium to restore the initial volume. Standard DFO solutions (60 mg/L) were stored in the same conditions in order to check the possible degradation of DFO during the time.

Release profiles were corrected to remove the degradation aspect and analyzed with regards to release kinetics and mechanism of release. The following equation describes the method used for the corrections. Ftn is the corrected percentage release, Ft is the cumulative percentage release, t is the time at which Ft level was taken.

$$\mathrm{Ftn} = \mathrm{Ft} \times \left(\frac{100}{-0.2428 \times t + 107.31} \right) \quad (6)$$

The corrected data were then investigated for fit into various release models. Zero order is demonstrated by plotting the corrected cumulative release fraction versus time. Zero order describes the concentration-independent drug release rate from a formulation:

$$C=k_0t \quad (7)$$

First order release is described by plotting log cumulative drug fraction versus time and describes concentration-dependent drug release from the system:

$$\log C = \log C_0 - \frac{kt}{2.303} \quad (8)$$

The Hixson–Crowell cube root law describes the release from systems where there is a change in surface area and diameter of particles (therefore applies to microsphere only formulations). As described by Eq. (9), a straight line will confirm this type of release.

$$Q_0^{1/3} - Q_t^{1/3} = K_{HC}\, t \quad (9)$$

The Korsmeyer–Peppas equation as shown in Eq. (10), describes the mechanism of drug release. The release exponent can be used to characterize different release mechanisms[38].

$$\frac{M_t}{m_\infty} = K_{kp}\, t^n \quad (10)$$

whereM_t/M_∞ is the fraction of drug released at time t, K_{kp} is the rate constant and n is the release exponent.

At the end of test, the microspheres, loaded and composite hydrogel were recovered, frozen at −80°C and freeze-dried for morphological examination.

Scanning electron microscope (SEM) studies

The morphology of microspheres and freeze-dried hydrogels was analyzed by SEM. A Jeol JSM-6060LV Scanning Electron Microscope was used and samples were coated with gold using a Quorum Q 150RES spatter coater.

Statistical analysis

Data were analyzed using the nonparametric Kruskal–Wallis test; individual differences were evaluated using a post hoc Dunn's multiple comparison test (GraphPad Prism, version 6.02;

GraphPad Software Incorporated). When suitable, analysis of variance (ANOVA) followed by a Tukey test was done.

RESULTS

Microsphere preparation and characterization

Yield of production

Microspheres were produced by spray-drying technique using RG502 and RG504 as polymers. Spray-drying appears to be a suitable method for the preparation of unloaded and DFO loaded microspheres, but with yield of production ranging from 34% to 67%. Loss of yield was due to deposition in the spray-drying apparatus. This is a common problem with small drying chambers and does not normally occur in industrial scale spray-drying due to the large cyclone area [39].

Particle size analysis

The particle size and particle size distribution of the microspheres were determined by analyzing the powder in the dry state or in suspension. When measured in suspension (Table 1) there was no significant difference in particle size between the two unloaded formulations (502 versus 504, p = 0.423), that differed only in molecular weight of the polymers used. The skewness in 502 is slightly more to the right with almost double the leptokurtic value compared to 504. 502 also had smaller d90/d10 showing reduced distribution (Table 1). The loading of DFO in the polymer matrix determined an increase of particles size regardless of the PLGA used mainly when the highest drug amount was employed. In fact, the loaded D502 4 and D504 4 compared to the unloaded samples, 502 and 504, were significantly larger in size (p<0.05). Significant difference between particle sizes of 502 versus D502 10 and 504 versus D504 10 were also observed (p> 0.05) (Table 1). Both unloaded and loaded samples were skewed to the right with leptokurtic properties.

The increase in particle size of all 504 formulations can be attributed to the increase in water/DCM ratio (p = 0.0029) (Figure S2). The distribution also narrows with increasing water content (d90/d10 = 15.95, 14.00 and 8.74). Less evident but significant is the change of size of 502 formulations according to the ratio drug polymer used (Table 1, p<0.05).

In order to observe whether an improvement in particle size distribution with reduced aggregation was observed using a dry method, samples were analyzed using this method as a qualitative assessment. The mean particle size was mostly larger using the dry method (Figure S3), which

could indicate that sample preparation for the suspension method for 502, 504, D502 4 and D502 10 broke aggregates and reduced the average particle size.

In comparison of the two particle size analysis methods, it is evident that suspending the microspheres in solution containing surfactant as well as vortexing and sonicating is beneficial in reducing aggregation which is advantageous to creating a true distribution curve of particle sizes.

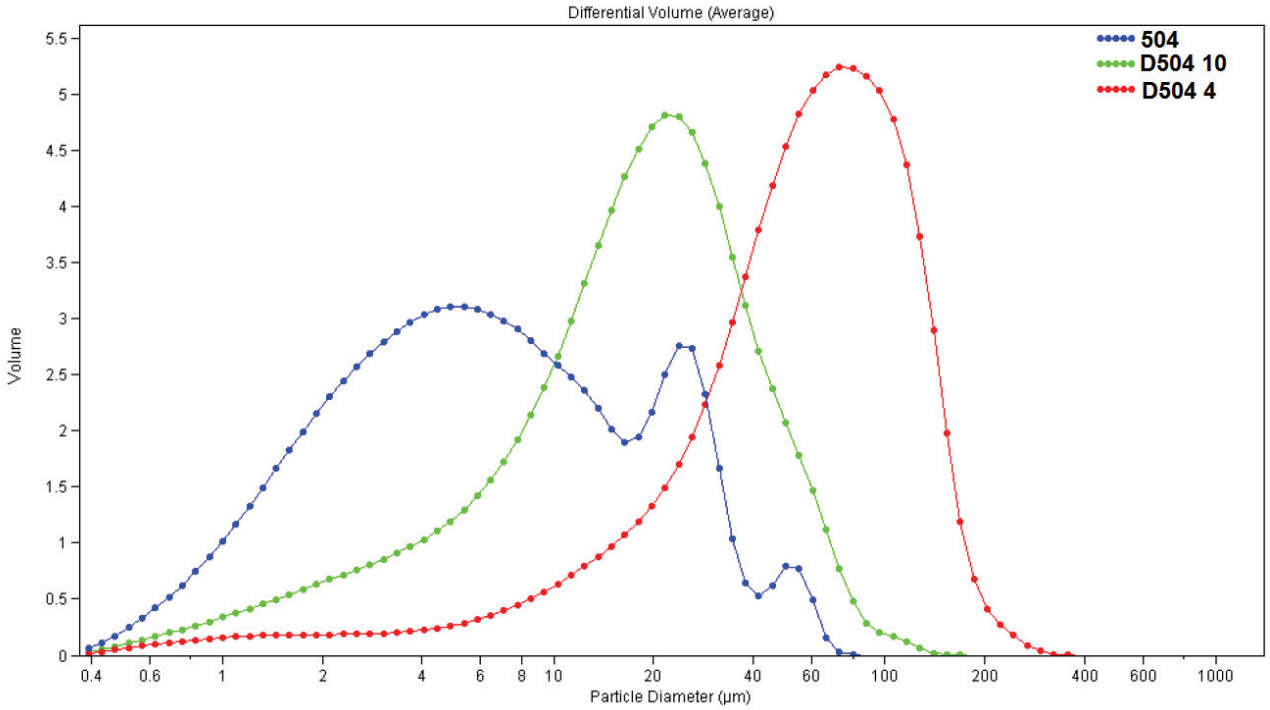

Figure S2. Comparative overlay of 504 (blue), D504 10 (green) and D504 4 (red) in order of increasing water content.

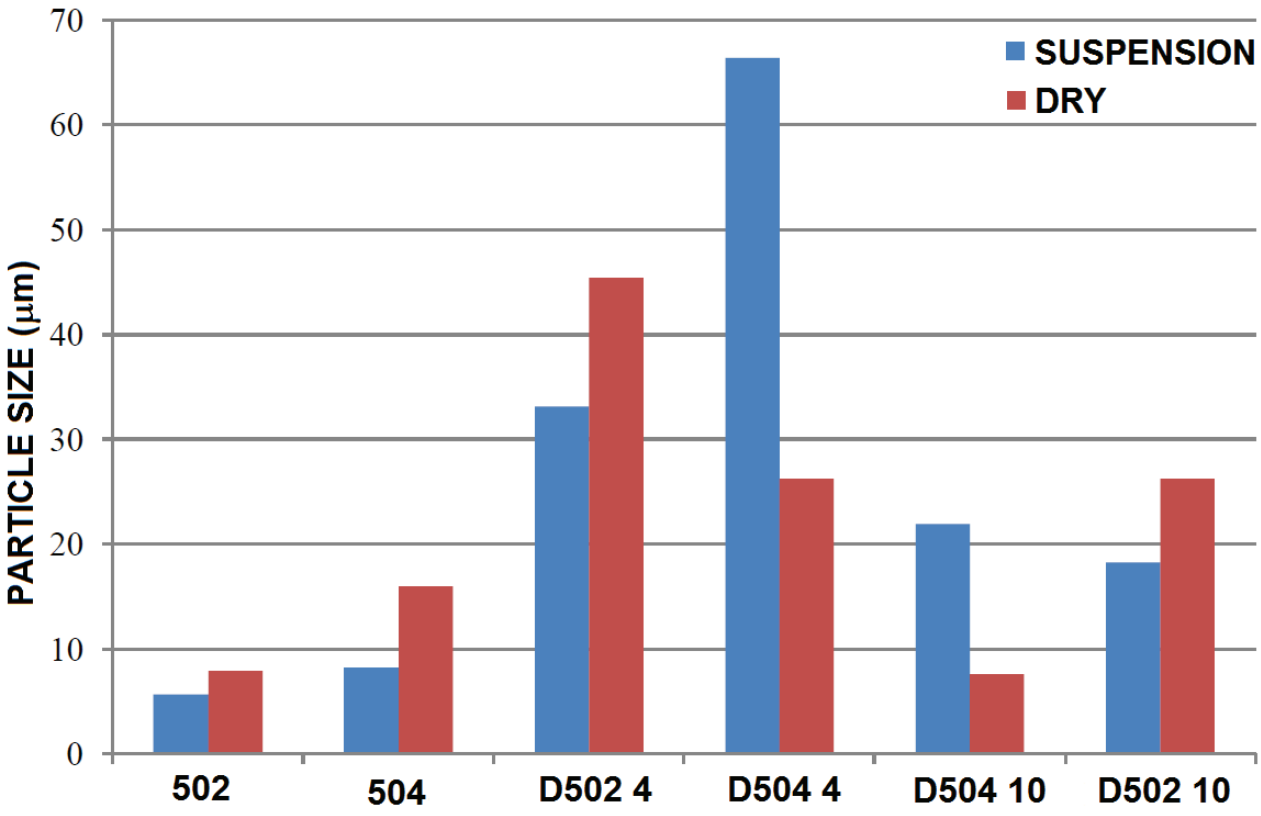

Figure S3. Comparison of mean particle size diameter of microsphere formulations using the suspension and the dry methods.

Drug content and drug burst release

In order to accurately determine drug loading efficiency and drug release of PLGA particles, the actual drug content of the microspheres was investigated as well as the burst release. Burst release as a proportion of actual drug content will help to determine which formulation manages to sustain drug release. All loading efficiency (LE) were above 83% of theoretical values (Figure 1). LE depends on factors such as kind of PLGA and drug to polymer ratio. When 1:4 drug to polymer ratio was used, LE increased if PLGA with high molecular weight was used (D502 4 versus D504 4 $p = 0.0068$); no significant differences were observed when high concentration of polymer was used (D502 10 versus D504 10 $p>0.05$). The drug to polymer ratio affected the LE only in the case of 502 formulations (D502 4 versus D502 10 $p = 0.0310$). Higher molecular weight formulations tended to have a significant reduction in burst release (D504 4 versus D504 10, $p>0.05$). Figure 1 shows a significant difference between D502 4 and D504 4, D502 10 and D504 10 and between D502 4 versus D502 10. Temperature did not significantly affect the burst test.

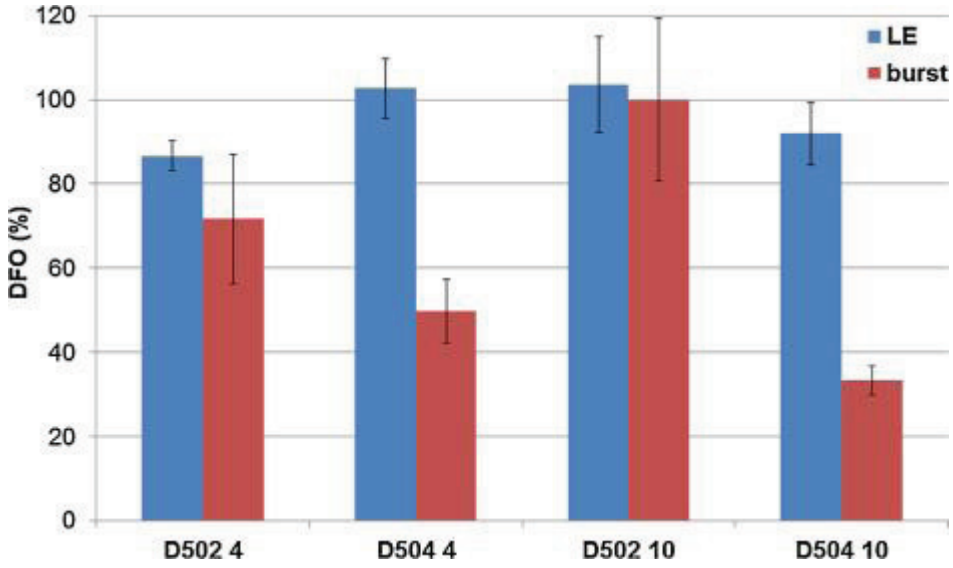

Figure 1. Loading efficiency (LE) of formulations and the percentage of DFO released during the burst test.

Microspheres morphology by (SEM)

The image of unloaded 502 microspheres in Figure 2A and C concurs with the particle size distribution profiles discussed above. Figure 2 shows not only the wide range of particle size present in the formulations but it also provides evidence that agglomeration is the cause for anomalous spikes that occur in the distribution graphs (Figure S2). In contrast, 504 presented less visible aggregation between the microspheres which is likely due to the higher glass transition temperature of the polymer. Figure 2 also shows the presence of fibrous polymer between microspheres; this could be due to the difficulty in separating the longer strands of polymer for incorporation in individual spheres during the preparation process. Studies found that increasing the drying gas flow rate will reduce this fibrous formation and therefore increase efficiency due to better separation in the cyclone [40].

504 microspheres also had a comparatively more textured surface than 502. As all other manufacture and formulation parameters, apart from the molecular weight of the polymer, were kept constant, it is hypothesized that the more amorphous nature of the RG502 allowed the formation of a smoother surface.

Regardless of the polymer used, unloaded microspheres appeared to have a better spherical appearance compared to loaded microspheres (Figure 2A–D). The difference could be due to the

use of water in the formulation of loaded microspheres, this could cause disruption during structural formation [41]. On examination of the manufacturing parameters, the increase in outlet temperature from unloaded batches to loaded batches could also contribute to the large morphological change.
The surface of loaded microspheres appeared to be smooth with pores and did not show presence of crystallized drug on the surface. This opposes theories that indicate drug deposited on the surface as the reason for the burst release observed. The filamentous appearance of 504 is still present in the loaded microspheres D504 10 (Figure 2D).
Morphology of D504 10 was observed also after drug release studies. Samples analyzed after release tended to show more agglomerated and fused particles (Figure 2E). This occurrence is explained by the reduction in glass transition temperature and therefore the increase in rubbery nature of the PLGA in the presence of water. The filamentous structures disappeared after dissolution, possibly due to degradation. Pores are present in this formulation which alongside microsphere collapsing is the primary cause for burst release. There is some evidence of the presence of drug after dissolution, indicating there is good internalization of the drug in the dry microspheres (Figure 2F).

Drug release studies

Release studies of DFO from microspheres were carried out. Standard deferoxamine solutions (60 mg/L) were stored in the same conditions in order to check the degradation of DFO in solution during the time.
Degradation of DFO over time was observed in DFO solution. Whereas D502 4 and D504 4 curves displayed concomitant release and degradation and had no significant difference in gradient (1–250 h) when compared to the standard (Figure S4). The high initial release of the microspheres (86% and 90%) indicated a burst release, followed by a negative correlation to the same degree as the DFO standard indicative of drug degradation with time.
In an attempt to reduce the burst release of the microspheres, an increase in the ratio of polymer to drug was used as well as a reduction in water content in the preparation process. D504 10 shows a high initial release followed by non-significant difference in degradation gradient (time 1–240 h, $p = 0.11629$) when compared to the DFO solution.
D502 10 was not tested because of the very high percentage of DFO released during the burst test.
Even though the release profile was similar, they could be the result of a different ratio of drug being released and being degraded. In order to examine the release profile, data points were

corrected to remove the degradation aspect. Most microsphere batches on their own exhibited very little correlation with any of the kinetic or mechanistic equations (R^2<0.9). It was found that D502 4 had strong correlation with first order (concentration dependent), Hixson–Crowell and Korsmeyer–Peppas at 1–6 h. The application of the Hixson–Crowell equation shows that there is a change in surface area and diameter of particles in the time frame 1–6 h and from the close fit to the Korsmeyer–Peppas equation, it can be deduced that D502 4 releases the drug with diffusion as the rate controlling factor (n<0.45).

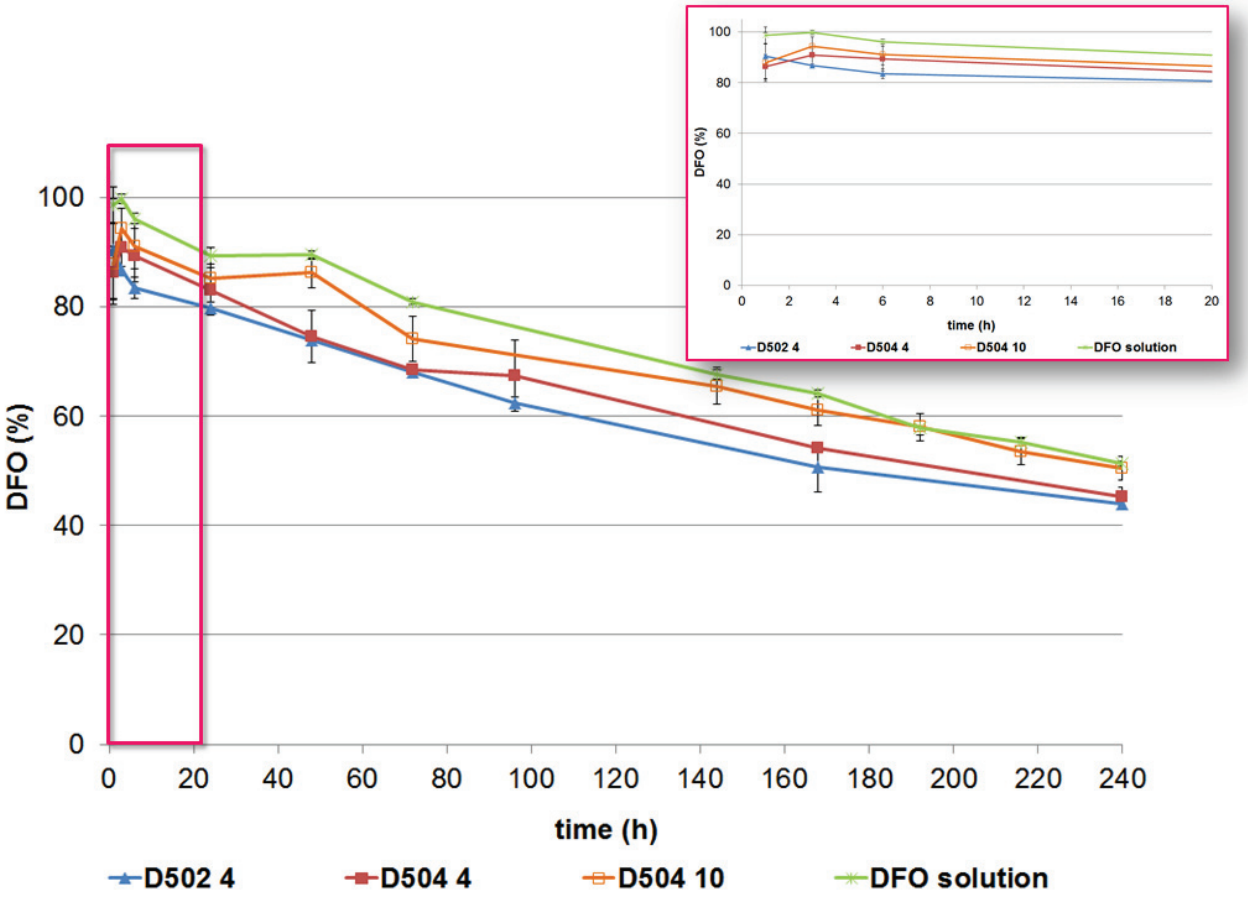

Figure S4. DFO release from microspheres and concomitant degradation of DFO solution, without corrected data of degradation.

Preparation of hydrogels and characterization

Unloaded and DFO loaded hydrogels as well as composite hydrogel were prepared. The molar ratio 1/1 and pH of 3.0 were found to be critical to formation of alginate and chitosan hydrogel. The gelation was immediate after vigorously stirring the chitosan and alginate solutions at room temperature (Figure S5).

Figure S5. Photographs of chitosan solution added to alginate solution (left) and gel instantaneously formed after stirring (right).

Viscosity measurement

The viscosity of alginate and chitosan solutions employed for hydrogel formation was 460.3 ± 8.7 cP and 658.1 ± 59.1 cP, respectively. The viscosity of hydrogel was 10-fold higher (4470.1 ± 458.9 cP).

Porosity measurement

Porosity of unloaded, loaded and composite hydrogels was measured by the solvent replacement method. Results demonstrate that the porosity of the system remains unchanged regardless the presence of DFO and microspheres and the preparation method of composite hydrogel (p>0.05). The porosity of unloaded and loaded hydrogels was 84.86 ± 4.23%, and 82.11 ± 7.32% respectively. D502 hydrogel produced by 2nd method, showed a porosity of 78.68 ± 2.00%. No significant differences in porosity were found in case of other composite hydrogels.

Water uptake and swelling

In order to study the water uptake (WU, %) and swelling characteristics, the weight and volume variations of hydrated and freeze-dried hydrogels were measured (Table 2). Freeze-dried hydrogels absorbed a considerable amount of water and the unloaded ones showed the highest WU percentage. The presence of microspheres reduces the WU value compared with the unloaded hydrogel (p<0.05). After water absorption, the hydrogels obtained have a bigger volume than freeze-dried forms. In particular the hydrogels containing DFO showed a 54% volume increase, a much higher value compared to any other (p<0.05).

Table 2. Water uptake (WU, %) and swelling ratio (SW, %)of unloaded, loaded and composite hydrogels both hydrated and freeze-dried.

Hydrogel	freeze-dried		hydrated	
	WU (%) ± SD	SW (%)	WU (%)	SW (%)
unloaded	2759.9 ± 246.9$^{\$}$	3.6 ± 0.7*	-16.9 ± 2.2$^{\$}$*	-8.3 ± 2.8*
loaded	2379.2 ± 151.4	54.2 ± 6.7*§	-1.04 ± 1.5*§	-32.3 ± 3.0*§
D502(2ndmethod)	1954.1 ± 139.8$^{\$}$	16.1 ± 1.5§	7.9 ± 0.2$^{\$\S}$	-0.3 ± 3.7§

$^{\$\,\S}$ *P< 0.05

When the test was performed with the hydrated hydrogel, no water absorption was observed. On the contrary, weight loss was observed as well as volume contraction. As a consequence, negative WU and SW values were obtained. As concerning the preparation method, the composite hydrogel obtained by 1st method did not differ from loaded hydrogel. On the contrary, the composite hydrogel from the 2nd method absorbed smaller amount of water but did not change in volume.

No significant differences in water uptake and swelling were observed when different microspheres were incorporated.

Dynamic vapor absorption (DVS) studies

Dynamic vapor sorption (DVS) studies describe the mechanism of water sorption by the gels. The unloaded hydrogel (Figure 3A) showed a profile typical of bulk water absorption; the hysteresis is due to the reversible and elastic swelling deformations caused by the introduction of water molecules within the polymeric network. This hydrogel fits the type II model according to the BDDT classification, indicative of a multilayer mechanism of absorption. Loaded and composite hydrogels (Figure 3B and C), presented a type III isotherm: this profile is generally observed when the interaction between vapor/surface and vapor/vapor are similar so only a few molecules of vapor adsorb on the surface at low partial pressure followed by condensation when higher humidity is reached. For all hydrogels, hysteresis was greatly reduced for RH values greater than 60%, indicating this value as a critical RH after which no further structure deformation is occurring.

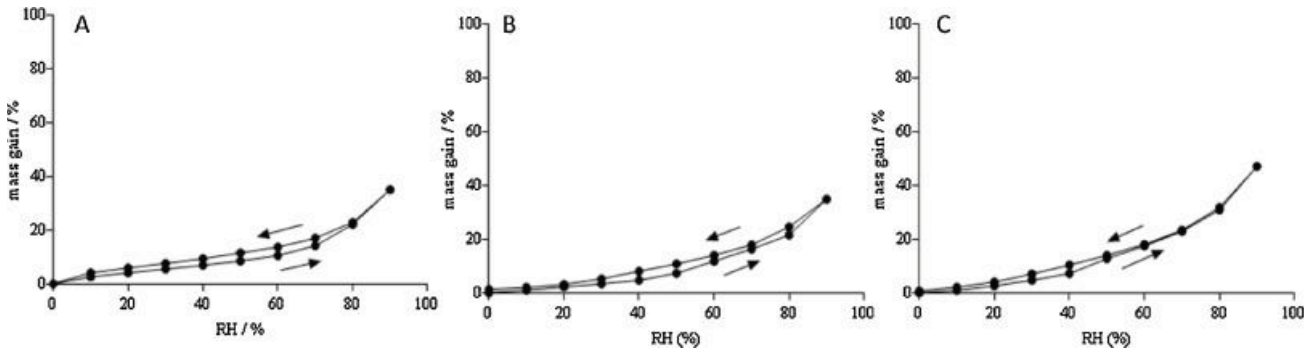

Figure 3. Isotherm curves for unloaded (A), loaded (B) and composite (C) hydrogels.

By applying the Korsmeyer–Peppas equation to the plots of percentage water sorbed versus time, the mechanism of hydration can be further understood. By comparing the diffusion exponent, it is

evident that the unloaded hydrogel (n_p = 1.018) presents a Case-II transport mechanism where the rate limiting factor is relaxation and chain disentanglement. For all loaded hydrogels (0.45 <n_p<0.89) diffusion is controlled by a combination of Fickian diffusion and gel deformation.

Hydrogels morphology by SEM

The morphology of the hydrogels was evaluated in order to observe their overall structural characteristics, the presence of microspheres, the presence of the drug and also the changes after drug release.

The unloaded hydrogel (Figure 4A) presented a layered structure, whereas porous appearance was observed for the loaded hydrogel. Furthermore, crystals of DFO were evident on the structure of the loaded hydrogel (Figure 4B).

Observing the composite hydrogel prepared with the two methods, the included microspheres were clearly visible. Figure 4C shows the composite hydrogel produced by the 1st method, chosen as example; it can be seen that particles included in the gel showed integral spherical shape without collapse phenomena. After dissolution, crystals were found in the hydrogel indicating that the composite hydrogel is able to entrap the drug released from the microspheres further delaying its release (Figure 4D). Greater drug crystallization on composite hydrogel obtained with the 2nd method occurred. Microspheres are visible after dissolution too (Figure 4D).

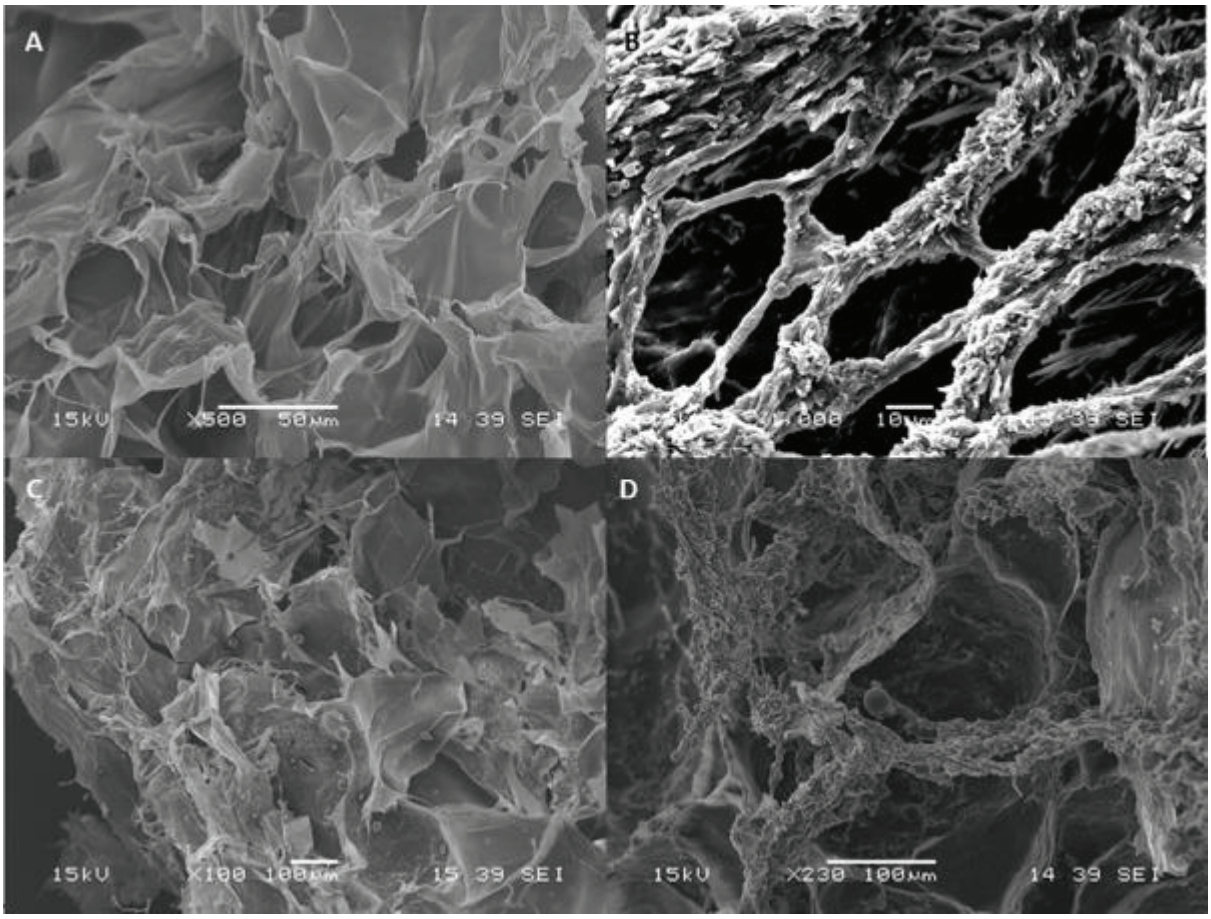

Figure 4. SEM pictures showing morphology of unloaded (A) and loaded (B) hydrogel (magnification 500× and 1000×). SEM pictures showing morphology of D502 10 composite hydrogel, produced by 1st method, before (C) and after (D) drug release studies (magnification 100× and 230×), chosen as examples.

Drug release studies

Figure 5 shows the release of DFO from loaded and composite hydrogels. Loaded chitosan/alginate hydrogel was able to control the release of DFO incorporated: 46% of the drug was quickly released within 1 h, the release continued gradually till reaching a plateau at 72% after 48 h. After 144 h, no statistical differences are observed between profiles of loaded hydrogel and standard DFO solution. Data obtained are affected by the degradation process of DFO and therefore Figure 5 shows release profiles corrected and not corrected to account for the degradation. The release of DFO from the composite hydrogels was affected by the method of incorporation of the microspheres. If microspheres were added into the chitosan solution before hydrogel formation, the resulting

hydrogel showed a DFO release profile superimposable to the loaded hydrogel (p>0.05) during the first 48 h. Afterwards, the concentration of released DFO from the composite hydrogel declined indicating degradation exceeding release.

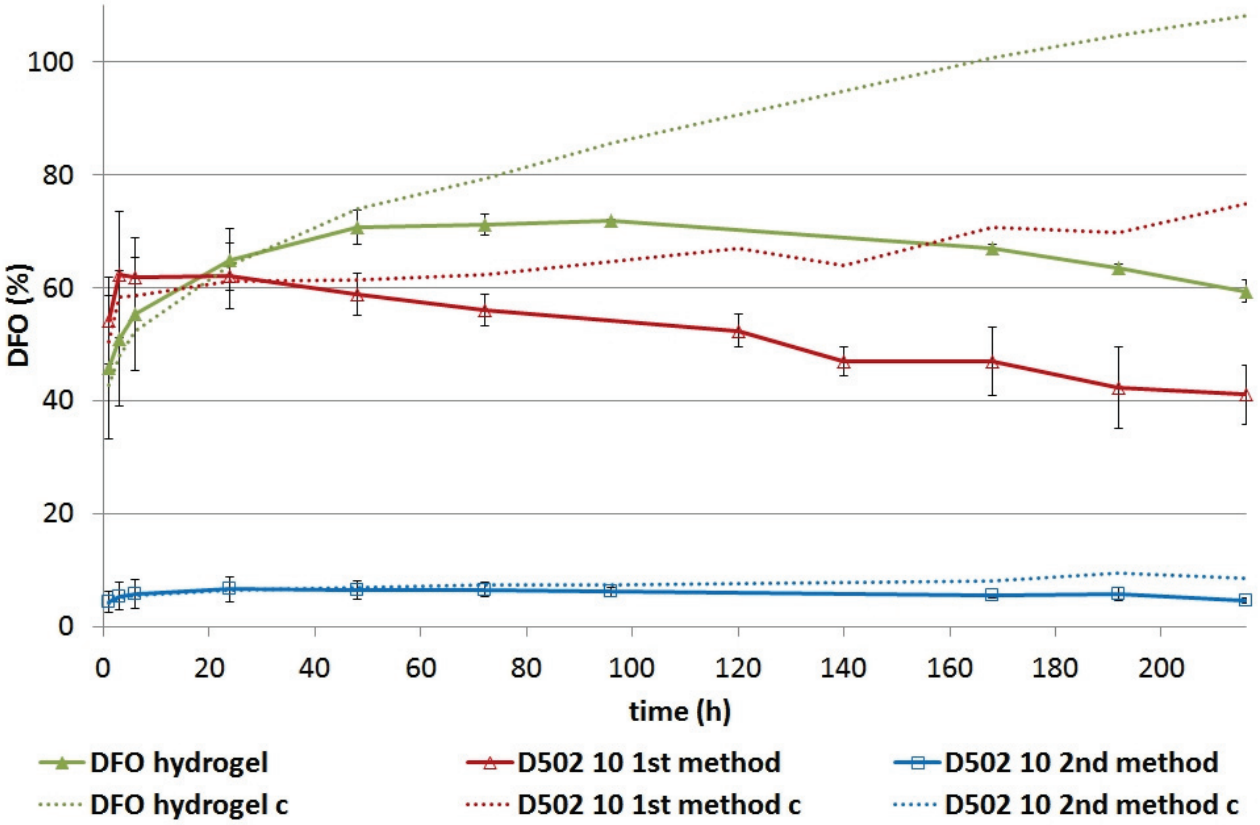

Figure 5. DFO release from composite hydrogel with incorporated D502 10 prepared adding microspheres into the chitosan solution before hydrogel formation (1st method) or at preformed hydrogel (2nd method). Data corrected (dotted lines) and not corrected (continuous lines).

When microspheres were incorporated into the preformed hydrogel, a much more sustained release profile was observed (Figure 5): 4% of drug incorporated in the microspheres was released within 1 h and no further release was observed until 216 h. The ability of this composite hydrogel to provide a more sustained release was attested also by the higher amount of DFO observed by SEM after dissolution test, as above described.

It must be kept in mind that the release profile of all systems is the result of two different phenomena occurring at the same time: release and degradation.

In order to examine the release profile, data points were corrected to remove the degradation aspect using Eq. (6). The D502 10 composite hydrogel formulation prepared with the 1st method did not show a strong relationship with either zero or first order overall, however, there was indication of a first order release (concentration dependent) after 48 h. This hydrogel also fits with Korsmeyer–Peppas to show Fickian diffusion as the mechanism of drug release (n< 0.45) (Table 3).

Table 3. Table showing significant R^2 values for the release kinetics and mechanism of release models for microspheres and composite hydrogels. R^2 was taken for the whole experimental time frame, from points at the beginning and toward the end of the dissolution duration.

	t (h)	Zero Order	First Order	Hixson-Crowell	Korsmeyer-Peppas
D502 4	1≤ t <240	0.0857	0.0727	0.1345	0.0465
	1≤ t <6	0.969	0.9724	0.9581	0.9940
	1≤ t <24	0.4785	0.483	0.4651	0.8401
	48≤ t <240	0.6221	0.6165	0.6359	0.4182
D502 10 1st method	1≤ t <216	0.8658	0.8474	-	0.9437
	1≤ t <24	0.7934	0.78	-	0.9918
	48≤ t <216	0.947	0.9477	-	0.9568
D502 10 2nd method	1≤ t <216	0.7562	0.6873	-	0.9612
	1≤ t <24	0.8017	0.7368	-	0.978
	48≤ t <216	0.6816	0.7115	-	0.7183

D502 10 composite hydrogel obtained with the 2nd method did not fit strongly to either zero or first order overall or at selected time intervals. Korsmeyer–Peppas in this composite hydrogel shows overall Fickian diffusion as the mechanism of drug release (n< 0.45) (Table 3).

No statistical differences were observed regardless the microspheres formulation employed.

The different behavior of the composite hydrogel, can be attributed to the diverse water uptake and swelling capability. The hydrated hydrogel from 2nd method, indeed, absorbed water but did not reduce in volume whereas the other formulations significantly decreased in volume loosing water

entrapped into the hydrogel network. As a consequence the drug dissolved in water is released from the hydrogel.

Biodegradability

Since ionically crosslinked alginate hydrogels do not specifically degrade but undergo slow, uncontrolled dissolution [42], biodegradability in PBS (pH 7.4) at 37°C was studied. Figure S6 shows the percentage of degradation measured for the composite hydrogel obtained with the 1st method, containing microspheres characterized by 1:10 drug–polymer ratio. At the end of the drug release studies, the hydrogel biodegraded by approximately 32–34% on the first day. No significant difference was observed regardless the kind of microspheres included in the hydrogel (p>0.05) at each time point. Concerning D502 10 and D504 10 composite hydrogels, a significant increase of degradability was observed between 10 and 24 days (p<0.05), reaching 53% and 49% respectively. The biodegradability of chitosan/alginate hydrogel studied was independent of the preparation method employed.

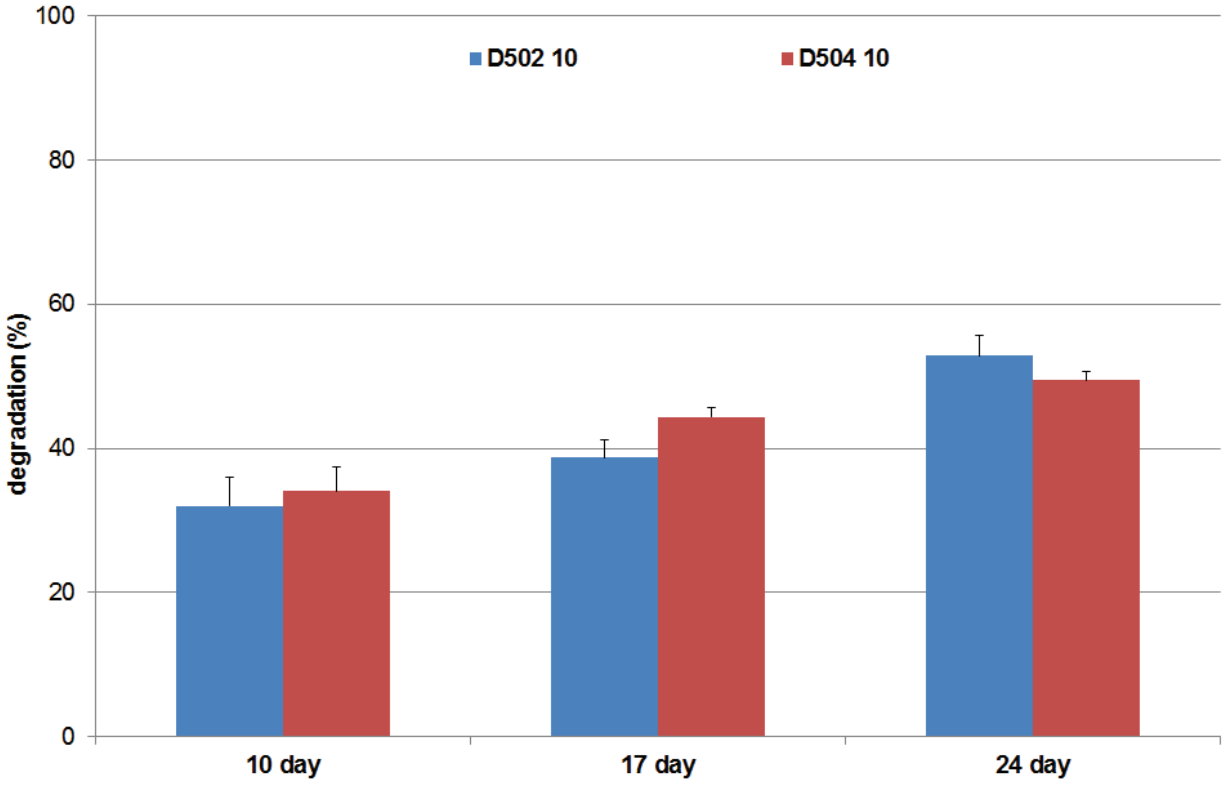

Figure S6. Degradation degree of composite hydrogels obtained with the 1st method

Conclusion

In this work, we proposed a new application of physical chitosan/alginate hydrogel and PLGA microspheres for the modified release of DFO, for which there is a therapeutic demand. These formulations produced can represent one of the few formulative approaches of DFO exploited. DFO, highly water soluble drug, can be encapsulated in biodegradable microspheres of PLGA; nevertheless, formulation into a composite hydrogel is necessary in order to obtain sustained drug release: hydrogel is better capable to control the DFO release compared to PLGA microspheres and thus absolutely necessary for achieving the prearranged aim; the composite chitosan/alginate hydrogel gave the most efficient delivery system. Furthermore, the preparation method affected the performance of the obtained systems, the DFO release from them and consequently the kind of therapeutic application. As example, hydrogel prepared by the first method can be formed in situ after injection of both solutions/suspension; on the other hand, the second method gives an implantable hydrogel.

In conclusion, disruption of iron regulation plays a key role in the etiology of several diseases (neurological disorders, cancer, stroke, skin, muscle and bone diseases), which require different approaches, methods and time of treatment. The prepared systems not only could solve the criticalities common to several iron dysregulation diseases, but show versatility and usefulness with regard to the disease and/or administration route.

REFERENCES

1. Camaschella C, Strati P. Recent advances in iron metabolism and related disorders. Internal and Emergency Medicine. 2010;5:393–400.
2. Loh A, Hadziahmetovic M, Dunaief JL. Iron homeostasis and eye disease. Biochim Biophys Acta. 2009;1790:637–49.
3. Pouillot A, Polla A, Polla BS. Iron and iron chelators: a review on potential effects on skin aging. Curr Aging Sci. 2013;6:225–31.
4. Yamasaki T, Sakaida I. Hepatic arterial infusion chemotherapy for advanced hepatocellular carcinoma and future treatments for the poor responders. Hepatol Res 2012;42:340–48.
5. Jomova K, Valko M. Importance of iron chelation in free radical-induced oxidative stress and human disease. Curr Pharm Design. 2011;17:3460–73
6. Hua Y, Keep RF, Hoff JT, Xi G. Deferoxamine therapy for intracerebral haemorrhage. Act Neur S. 2008;105:3–6.
7. Angel M, Narayanan K, Swartz W, Ramasastry SS, Kuhns DB, Basford RE, Futrell JW. Deferoxamine increases skin flap survival: additional evidence of free radical involvement in ischemic flap survival. Brit J Plast Surg.1986;9:469–72.
8. Diaz DD, Freeman SB, Wilson JF, Parker GS. Hematomainduced flap necrosis and free radical scavengers. Archiv Otolaryngol. 1992;118:516–8.
9. Hom DB., Goding GS. Jr, Price JA, Pernell KJ, Maisel RH. The effects of conjugated deferoxamine in porcine skin flaps. Head Neck. 2000;22:579–84.
10. Morris SF, Pang CY, Lofchy NM, Davidson G, Lindsay WK, Zuker RM, Boyd B. Deferoxamine attenuates ischemia- induced reperfusion injury in the skin and muscle of myocutaneous flaps in the pig. Plast Reconstr Surg. 1993;92:120–32.
11. Weinstein G, Maves M, McCormack M. Deferoxamine decreases necrosis in dorsally based pig skin flaps. Otolaryngol. Head Neck Surg. 1989;10:559–61.
12. Mericli AF, Das A, Best R, Rodeheaver P, Rodeheaver G, Lin KY. Deferoxamine mitigates radiation-induced tissue injury in a rat irradiated tram flap model. Plast Reconstr Surg. 2015;135:124e–134e.
13. Jin H, Terai S, Sakaida I. The iron chelator deferoxamine causes activated hepatic stellate cells to become quiescent and to undergo apoptosis. J Gastroenterol. 2007;42:475–484.

14. Sakaida I, Hironaka K, Uchida K, Okita K. Iron chelator deferoxamine reduces preneoplastic lesions in liver induced by choline-deficient L-amino acid-defined diet in rats. Digest Dis Sci. 1999;44:560–9

15. Yamasaki T, Terai S, Sakaida I. Deferoxamine for advanced hepatocellular carcinoma. The New Engl J Med. 2011;365:576–8.

16. Farberg AS, Sarhaddi D, Donneys A, Deshpande SS, Buchman SR. Deferoxamine enhances bone regeneration in mandibular distraction osteogenesis. Plas Reconstr Surg. 2014;133:666–71.

17. Felice PA, Ahsan S, Donneys A, Deshpande SS, Nelson NS, Buchman SR. Deferoxamine administration delivers translational optimization of distraction osteogenesis in the irradiated mandible. Plast Reconstr Surg. 2013;132:542e–48e

18. Grewal BS, Keller B, Weinhold P, Dahners LE. Evaluating effects of deferoxamine in a rat tibia critical bone defect model. J. Orthop. 2014;11:5–9.

19. Hertzberg BP, Holt JB, Graff RD, Gilbert SR, Dahners LE. An evaluation of carrier agents for deferoxamine, an upregulator of vascular endothelial growth factor. J Biomate Appl. 2013;27:1046–54.

20. Stewart R, Goldstein J, Eberhardt A, Chu GT, Gilbert S. Increasing vascularity to improve healing of a segmental defect of the rat femur. J Orthop Trauma 2011;25:472–6.

21. Zhang W, Li G, Deng R, Deng L, Qiu S. New bone formation in a true bone ceramic scaffold loaded with desferrioxamine in the treatment of segmental bone defect: a preliminary study. J Orthop Sci. 2012;17:289–98.

22. Allain P, Mauras Y, Chaleil D, Simon P, Ang KS, Cam G, Le Mignon L, Simon M. Pharmacokinetics and renal elimination of desferrioxamine and ferrioxamine in healthy subjects and patients with haemochromatosis. Brit J Clin Pharm. 1987;24:207–12.

23. Cappellini MD, Pattoneri P. Oral iron chelators. Annu Revi Med. 2009;60:25–38.

24. Hallaway PE, Eaton JW, Panter SS, Hedlund BE. Modulation of deferoxamine toxicity and clearance by covalent attachment to biocompatible polymers. P Natl Acad Sci USA. 1989; 86:10108–12.

25. Imran ul-haq M, Hamilton JL, Lai BF, Shenoi RA, Horte S, Constantinescu I, Leitch HA, Kizhakkedathu JN. Design of long circulating nontoxic dendritic polymers for the removal of iron in vivo. ACS Nano. 2013;7:10704-16.

26. Rassu G, Soddu E, Cossu M, Brundu A, Cerri G, Marchetti N, Ferraro L, Regan RF, Giunchedi P, Gavini E, Dalpiaz A. Solid microparticles based on chitosan or methyl-β-cyclodextrin:

A first formulative approach to increase the nose-to-brain transport of deferoxamine mesylate. J Control Release. 2015;68–77.

27. Grewal BS, Keller B, Weinhold P, Dahners LE. Evaluating effects of deferoxamine in a rat tibia critical bone defect model. J. Orthop. 2014;11:5–9

28. Giunchedi P, Maestri M, Gavini E, Dionigi P, Rassu G. Transarterial chemoembolization of hepatocellular carcinoma – Agents and drugs: An overview. Part 2. Expert Opin Drug Del. 2013;10:799–810

29. Salis A, Rassu G, Budai-Szűcs M, Benzoni I, Csányi E, Berkó S, Maestri M, Dionigi P, Porcu EP, Gavini E, Giunchedi P. Development of thermosensitive chitosan/glicerophospate injectable in situ gelling solutions for potential application in intraoperative fluorescence imaging and local therapy of hepatocellular carcinoma: a preliminary study. Expert Opin Drug Del. 2015;In Press doi:10.1517/17425247.2015.1042452 .

30. Caló E, Khutoryanskiy VV. Biomedical applications of hydrogels: A review of patents and commercial products. Eur Polym J. 2015;65:252–67.

31. Hoare TR, Kohane DS. Hydrogels in drug delivery: Progress and challenges. Polym. 2008;49:1993–2007.

32. Buwalda SJ, Boere KW, Dijkstra PJ, Feijen J, Vermonden T, Hennink WE. Hydrogels in a historical perspective: From simple networks to smart materials. J Control Release. 2014;190:254–73

33. Hartmann M, Dentini M, Draget KI, Skjåk-Bræk G. Enzymatic modification of alginates with the mannuronan C-5 epimerase AlgE4 enhances their solubility at low pH. Carbohyd Polym. 2006;63.257–62.

34. Gavini E, Chetoni P, Cossu M, Alvarez MG, Saettone MF, Giunchedi P. PLGA microspheres for the ocular delivery of a peptide drug, vancomycin using emulsification/spray-drying as the preparation method: in vitro/in vivo studies. Eur J Pharm Biopharm. 2004;57:207–12.

35. Rassu G, Nieddu M, Bosi P, Trevisi P, Colombo M, Priori D, Manconi P, Giunchedi P, Gavini E, Boatto G. Encapsulation and modified-release of thymol from oral microparticles as adjuvant or substitute to current medications. Phytomedicine. 2014;21:1627–32.

36. Ranjha NM, Qureshi UF. Preparation and characterization of crosslinked acrylic acid/hydroxypropyl methyl cellulose hydrogels for drug delivery. Int J Pharmacy Pharm Sci. 2014;6:400–10.

37. Zang S, Dong G, Peng B, Xu J, Ma Z, Wang X, Liu L, Wang Q. A comparison of physicochemical properties of sterilized chitosan hydrogel and its applicability in a canine model of periodontal regeneration. Carbohyd Polym. 2014;113:240–8.

38. Arora G, Malik K, Singh I, Arora S, Rana V. Formulation and evaluation of controlled release matrix mucoadhesive tablets of domperidone using Salvia plebeian gum. J Adv Pharm Technol Res. 2011;2:163–9

39. Sosnik A, Seremeta KP. Advantages and challenges of the spray-drying technology for the production of pure drug particles and drug-loaded polymeric carriers. Adv Colloid Interfac. Science, 2015;223:40–54.

40. Sollohub K. Spray Drying Technique. I: Hardware and Process Parameters. J Pharm Sci. 2009;99:575–87.

41. Freiberg S, Zhu XX. Polymer microspheres for controlled drug release. Int J Pharm. 2004;282:1–18.

42. Drury JL, Mooney DJ. Hydrogels for tissue engineering: scaffold design variables and applications. Biomaterials. 2003;24:4337–51.

CHAPTER 5

Engineered microparticles based on drug–polymer coprecipitates for ocular-controlled delivery of Ciprofloxacin: influence of technological parameters

Adapted from:

Engineered microparticles based on drug–polymer coprecipitates for ocular-controlled delivery of Ciprofloxacin: influence of technological parameters.

Elisabetta Gavini, Maria Cristina Bonferoni, Giovanna Rassu, Giuseppina Sandri, Silvia Rossi, **Andrea Salis**, Elena Piera Porcu, and Paolo Giunchedi. Drug Development and Industrial Pharmacy. September 2015, DOI: 10.3109/03639045.2015.1100201

INTRODUCTION

Topical eye drops represent a remarkable part of ophthalmic medications present in the market for treating diseases of the anterior segment of the eye. The rapid ocular clearance is however a remarkable limit of this kind of formulations. The bioavailability of the drug administered topically is consequently very low because once the drops are placed onto the eye surface, they are rapidly diluted and washed out by tearing and blinking. Most of the liquid ocular formulations are consequently drained away from the precorneal area in few minutes. The preparation of ocular solutions containing a drug overdose can be a method to compensate these effects, but this is not the optimal choice because greater doses can also determine increased side effects and toxicity [1].The therapeutic effect of an ocular drug formulation can be improved by prolonging its contact with the corneal surface.

Fluoroquinolones are characterized by a remarkable activity against the most frequent Gram-positive and Gram-negative ocular pathogens. They are broad spectrum bactericidal agents with activity against many important corneal pathogens including staphylococci, Neisseria gonorrhea, Haemophilus influenzae, Enterobacteriaceae and Pseudomonas aeruginosa [2,3]. Bacterial keratitis is an important infective pathology because it may arise secondary to corneal epithelial breakdown associated with dry eye, use of contact lens and trauma. The optimal therapeutic approach should firstly require the identification of the causative microorganism; however, the etiological agent could be rarely identified in time for the selection of the correct antibiotic therapy. For a rapid and successful therapeutic treatment, the empirical choice of a wide broad-spectrum agent can therefore be very important3. Recently, an interesting paper has been published regarding the surveillance of the activity of fluoroquinolones against ophthalmic pathogens in Europe in the 2010–2011 period [4]. Ciprofloxacin, a fluoroquinolone antibiotic, is active against a broad spectrum of aerobic Gram-positive and Gram-negative bacteria. Its partition coefficient (log P, octanol-Tris model) is –1.31 [5]. The resistance to this drug is developed slowly, with aminimal toxicity associated with its use. For all these reasons, this drug can be currently considered the anti-bacterial agent of choice for the eye [6,7] and it is often utilized for the treatment of ocular pathologies, such as bacterial infections and/or corneal ulcers. However, the ocular treatment with this antibiotic is characterized by low compliance because it requires frequent drug administrations. It is reported that ciprofloxacin eye drops need to be administered every 15–30 min in acute infections and at least 6–7 times daily in severe pathologies [8]. Furthermore, ciprofloxacin presents a pH-dependent solubility, which

becomes very low at the pH of tears [9,10] with consequent possible problems of low bioavailability.

The development of topical controlled release formulations of ophthalmic drugs can be a way to improve their low ocular bioavailability with respect to the traditional eye drops, in particular by decreasing the clearance rate of the formulation from the precorneal area [11] and by controlling as much as possible drug release in this more prolonged time of contact. Therefore, ciprofloxacin is a good candidate for the preparation of ocular controlled release formulations to be administered in the precorneal site. The preparation of drug delivery systems for the sustained release of actives to the precorneal regions of the eye is a field of general and remarkable interest for the design of an ocular therapy. The main challenge of such treatments is to sustain sufficiently high concentrations of the drug in the corneal region.

In order to enhance the bioavailability of the drugs administered by the ocular route and to improve their compliance, the design and preparation of different delivery systems and/or new strategies are possible. Early examples of improvement of the ocular bioavailability concerned the use of hydrogels or solutions that change to a gel after instillation, such as those based on Gelrite [12,13] or poly(vinylalcohol) and polymethacrylic acid

Derivatives [14]. Vesicular systems, such as liposomes [14–19], chitosan coated liposomes [20] and niosomes [11] have also been prepared. Recently, gel-forming ocular films based on xyloglucan for the ocular delivery of ciprofloxacin have been proposed [21]. Moreover, the preparation of microparticles with suitable size can be a way to achieve a precorneal prolonged residence time. These microparticles are polymeric microspheres, constituted by biodegradable and/or mucoadhesive polymers [22–30]. Microspheres based on ion-exchange resins for ocular drug administration have been used, even if until now there are very few examples of this kind of controlled release formulations designed for the ophthalmic route [31–33]. The ionic interaction between polymers (polyelectrolytes) and oppositely-charged drugs has been previously proposed by our group as a way to develop ocular controlled release drug formulations. The drug–polymer interaction results in insoluble coprecipitates that dissociate only in the presence of the medium's counterions, thus slowly releasing the drug. Once the drug is released, the polymer dissolves, leaving no residues in the site of administration [34–37]: this is particularly important in the case the route is constituted by the eye.

The aim of this work was the study of the influence of the technological parameters on the particle size of drug/polymer

coprecipitates obtained by a procedure of ionic interaction and engineered for ocular administrations. Ciprofloxacin was chosen as a model alkaline drug. The polyelectrolytes used are two anionic polymers able to interact with alkaline drugs: lambdacarrageenan and chondroitin sulfate. Lambda carrageenan is anatural hydrocolloid, already proposed as viscolyser in eye-drop formulations [38]. Chondroitin sulfate is a polysaccharide similar to hyaluronic acid in its properties [36,37], already used as lubricant for the treatment of dry eye [39]. The final goal was to obtain aqueous suspensions containing microparticulate coprecipitates engineered with a size suitable for ocular controlled drug administrations. This size should be lower than 25 mm40 limit that fulfills requirements of American Pharmacopeia for ophthalmic formulations.

In some suspensions, Carbomer (Carbopol 934P) was added to improve the mucoadhesive behavior of the microparticles. This polymer has good and well-known mucoadhesive properties and it has been already used for the preparation of ocular formulations [41,42].

Different technological parameters were taken into account for the preparation of the suspensions: concentration of the solutions of drug and polymer, temperature, kind and concentration of surfactant(s), stirring. A light scattering technique was used for the studies of particle size of the coprecipitates. Mucoadhesion tests were carried out using the ‘‘inclined plane’’ method [43,44], in order to characterize the capability of these systems to be retained in the precorneal region.

MATHERIALS AND METHODS

Materials

Ciprofloxacin HCl (CPX) was a generous gift from Bayer, Milan, Italy. Chondroitin 6 sulfate (CS) was purchased from Fluka Chemie (Buchs, AG CH). Lambda-carrageenan (CR) Viscarin GP Q1 109 NF (FMC Corporation) was donated by Prodotti Gianni, Q1 Milan, Italy. Carbomer (CB) (Carbopol 934P, BF Goodrich, Brecksville, OH).Polyoxyethylene 20 sorbitan monooleate (Tween 80), Aldrich Chemie Gmbh, Steinheim, Germany. Sorbitan monooleate (Span 80) Aldrich Chemie Gmbh, Steinheim, Germany. Mucin type II crude from porcine stomach was purchased from Sigma Chemical Co., St Louis, MO. All of the other solvents and chemicals used were of reagent grade.

Preparation of the CPX/CS and CPX/CR microparticle systems

Solutions of the two polyelectrolytes, CS and CR, were prepared separately in distilled water at the concentration of 0.5% w/v. These solutions were then slowly added dropwise into an equal volume of 1% w/v CPX solution in distilled water, under magnetic stirring and at room temperature. This

slow addition determined the formation of microparticles represented by coprecipitates, due to the ionic interaction that happens between drug and polyelectrolytes.

The resulting formulations (constituted by suspensions) are named hereafter as COP 1 and COP 2, respectively. An aqueous solution of CB at the concentration of 0.25% w/v (pH 7.5, adjusted with triethanolamine) was then added at room temperature to samples of the two suspensions, achieving two other suspensions named COP 3 and COP 4, respectively. Table 1 summarizes the compositions (expressed as percentage w/v) of all the suspensions prepared.

On the basis of the experimental results obtained in the particle size characterization (carried out as below described), the suspension more suitable in terms of size of particles for ocular administration (COP 1, based on CS), was used as reference formulation for the further studies of formulation parameters.

Table 1 Compositions (% w/v) of CPX suspensions prepared

Suspensions	CPX (% w/v)	CS (% w/v)	CR (% w/v)	CB (% w/v)
1	0.50			
2	0.50		0.25	
3	0.25			0.125
4	0.25		0.125	0.125

The influence of the following parameters on the particle size of the coprecipitates in suspension was studied: (a) concentrations of drug (CPX) and polymer (CS) solutions; (b) possible use of surfactants (kind and concentration); (c) temperature; (d) stirring. Concentrations of the solutions: aqueous solutions of CPX and CS at different concentrations (w/v) were prepared and mixed together with the method previously described, in such a way to obtain suspensions (named A1–4) of drug/polymer (CPX/CS) coprecipitates of different final concentrations. The concentrations of the solutions are reported in Table 2, while the concentrations of the corresponding suspensions obtained from these solutions are reported in Table 3. In all these preparations, the drug/polymer weight ratio was always maintained 2/1.

Use of surfactants: the kind and amount of surfactant(s) were evaluated as a possible formulation parameter. Tween 80 was used alone or in combination with Span 80 in two different weight ratios,

named Mix 1 (72:28 w/w) and Mix 2 (53:47 w/w), respectively. The surfactants were dissolved in the CPX and CS solutions, to obtain the suspensions T1–T3, whose final composition is reported in Table 4. Temperature: an aqueous solution of CS (0.5% w/v) was added dropwise, as previously described, to a solution of CPX (1% w/v) maintained under magnetic stirring, at a temperature of 40 °C. The obtained suspension is named as B1 (final concentration 0.5%w/v). Stirring: CS solution (0.5% w/v) was dropwise added to CPX solution (1% w/v), sonicated and stirred by paddle. The obtained suspension was named C1 (final concentration 0.5% w/v).

Table 2. Compositions (% w/v) of the solutions of CPX and CS used for the preparation of the suspensions A1–4.

Components	Solution A1	Solution A2	Solution A3	Solution A4
CPX	0.250	0.50	1.00	1.50
CS	0.125	0.25	0.50	0.75

Table 3. Compositions (% w/v) of the CPX/CS suspensions A1–4.

Components	A1	A2	A3	A4
CPX	0.125	0.250	0.50	0.750
CS	0.075	0.125	0.25	0.375
Final total concentrarion	0.200	0.370	0.75	1.130

Table 4. Compositions (% w/v) of the suspensions T1–3 containing surfactants.

Components	T1	T2	T3
CPX	0.500	0.500	0.500
CS	0.250	0.250	0.250
Tween 80	0.100		
Mix 1		0.100	
Mix 2			0.020

Resuspension test

To determine the resuspendability of the formulations, a test was carried out as follows: a sample of A3 suspension was centrifuged, the supernatant was then eliminated, and the coprecipitate resuspended in distilled water to obtain the original concentration (0.50% w/v CPX and 0.25 w/v CS) giving the suspension named C2.

Particle-size analysis

Particle size and particle-size distributions were determined and studied by the method of laser diffractometry, using the Colter Laser Diffraction apparatus (Colter LS 100Q Laser Sizer, Beckman Colter, Miami, FL). Particle size analyses were performed, at room temperature, on different samples of the prepared suspensions constituted by the drug/polymer coprecipitates. The samples of the suspensions were always manually stirred (for about 5 s) before analysis. The average particle sizes were expressed as volume-surface diameters (dvs, mm)45. The results were calculated as a mean of six determinations (SD50.30). Particle size distributions were expressed as percentage distribution by volume. The results of the particle size distributions were also expressed in terms of SPAN factor (mm), which was calculated as follows:

$$SPAN = (d_{90} - d_{10}) / d_{50} \quad (1)$$

where d_{10}, d_{50} and d_{90} are the diameter sizes and the given percentage value (by volume) is the percentage of particles smaller than that size. A high SPAN value indicates a wide particle size distribution [46,47].

Morphological analysis

SEM microphotographs (Zeiss DSM 962, Zeiss, Germany) of the coprecipitate were taken as follows: after freeze-drying, the samples were placed on double-sided tape, which had been previously secured to aluminum stubs, and then analyzed at 20 kV acceleration voltage after gold spattering in an argon atmosphere.

Evaluation of mucoadhesion by means of the ‘‘inclined plane’’

Mucoadhesion was measured using the method of the ‘‘inclined plane’’, as previously described [43,44]. Briefly, the ‘‘inclined plane’’ apparatus basically consisted of an inclined plane (angle of inclination = 60°, surface area = 28 cm^2) thermostated at 37 °C and of an electronic microbalance

(Sartorius L420P, Germany) Q1 connected with a personal computer. Porcine gastric mucin (Sigma, Italy) was used as a biological substrate. Mucin films Q1 were prepared directly on the plane: 2.5 ml of an aqueous 8% w/w mucin dispersion were placed on the plane, which was kept horizontal at 45 °C for 45 min to dry, and 250 mg of formulation (suspension) was placed on the plane previously coated with the biological substrate and kept horizontal. The plane was then inclined and the amount of formulation dropped on the microbalance was recorded: the mucoadhesivity was expressed as percentage of formulation remained on the surface of the plane. As a comparison, measurements without mucin were also carried out using the inclined plane as such, at the same experimental conditions employed in presence of the biological substrates. The results are expression of three measurements (SD <4%). The ‘‘inclined plane’’ method aimed to evaluate the contribution of rheology of formulation to the mucoadhesive potential.

Statistical analysis

Statistical analysis of data was performed using analysis of variance (ANOVA) followed by a post-hoc Tukey's All Pairs Comparison (Graph-Pad Prism, version 2.01; GraphPad Software Incorporated). Significance was taken as $p < 0.05$.

Stability test

The stability of the leader formulation (A3) was carried out as follows: the aqueous suspension of methylparaoxybenzoate (0.08% w/v) and propylparaoxybenzoate (0.02% w/v) was added and stored at 4–8 °C and 25 °C for 6 months. The morphology of the microparticles was checked by an optical microscope.

RESULTS AND DISCUSSION

The results of particle size analyses of COP 1–4 suspensions, expressed as percentage distribution by volume are reported in Table 5. Among all the suspensions, COP 1 (prepared using CS as polyelectrolyte) presents the best results in terms of particle size suitable for ocular administration. In fact 97% of the population of particles has a size <25 mm and 100% of particles have a size <<50 mm. The polyelectrolyte CR leads to particles of larger size: COP 2 presents in fact only 13.6% of particles with a size <25 mm and about 44% with a size<50 mm. This result is probably due to the formation of aggregates among the microparticles, whose size becomes lower after

prolonged sonication (data not reported). SEM pictures confirmed that the process of coprecipitation creates almost spherical particles with rough surface, as previously reported [36]. The roughness of the microparticles depends on the technique of preparation, which involves the precipitation of self-assembled polymer chains, more hydrophobic owing to the interaction with the drug [36]. In order to keep the ocular formulation in the conjunctive area as long as possible, a mucoadhesive polymer was added. However, the addition of the mucoadhesive polymer CB determines different consequences on the particle size of the suspensions, depending on the polyelectrolyte used for the formation of the coprecipitates. The suspension based on CS (COP 3) is characterized by particles with a larger size with respect to the corresponding suspension without CB (COP 1) (about 49% <25 mm versus 97%, respectively). The suspension based on CR (COP 4) has particles with lower size with respect to the corresponding suspension without CB (COP 2) (47% <25 mm versus about 13%,respectively). As a consequence of this different effect of CB on the size of the suspensions based on the two polymers (CS and CR), COP 3 and COP 4 present a similar particle size distribution. The modification of the particle size of the suspensions that is found after the addition of the mucoadhesive polymer CB could be due to the adsorption of this polymer onto the surface of the microparticles made by the preformed coprecipitates. However, also a possible chemical interaction between the drug and the polyelectrolyte (CB) should be taken into account. Sahoo et al. [48] in fact recently prepared an oral controlled release gastro-retentive dosage form constituted by mucoadhesive suspensions of CPX with Carbopol 934, using a method of ultrasonication. Results from FTIR and Raman spectroscopic analyses carried out by the authors, suggested that in these formulations the carboxylic groups of CPX and hydroxyl groups of Carbopol undergo a chemical interaction, probably leading to esterification and hydrogen bonding, even if they do not report any influence of this chemical interaction on the particle size of the suspensions [48].

Table 5Percentage distribution by volume (d_{vs}, µm).

	% by volume		
Suspensions	**< 25 µm**	**< 50 µm**	**< 90 µm**
COP 1	97.0	100.0	100.0
COP 2	13.6	43.8	81.0
COP 3	49.0	81.1	99.1
COP 4	47.3	80.2	99.6

Starting from the results of particle size analyses and from the consideration that the suspension containing CS has a good mucoadhesive behavior itself, even without the addition of Carbopol, it was decided to use CS as polyelectrolyte for the further preparation of the ocular suspensions, without any addition of CB to the formulations. The parameter evaluated was then the concentration of CPX and CS solutions used for the preparation of the microparticulate coprecipitates. Four different suspensions (A1–4) were prepared and characterized in terms of particle size, starting from four different combinations of CPX and CS concentrations (solutions A1–4, Table 2). The results were expressed as mean volume-surface diameter (d_{vs}) [45] and SPAN values, calculated using Equation (1). The concentrations of the CPX and CS solutions used for the preparation of the suspensions have a remarkable influence in determining the particle size and particle size distributions. As shown in Figure 2 (where mean diameters dvs are reported), the solutions A2 and A3 lead to the suspensions A2 and A3, which are characterized by the lowest mean diameters (d_{vs} about 3 μm). The solutions A4, characterized by higher CPX and CS concentrations with respect to A2 and A3, lead to the formation of A4 suspension, which has particles with a bigger size (d_{vs} 4.25 μm; $p < 0.0001$). The use of more diluted concentrations (A1 solutions), leads to the highest mean diameter (d_{vs}8.5 mm; $p < 0.0001$).

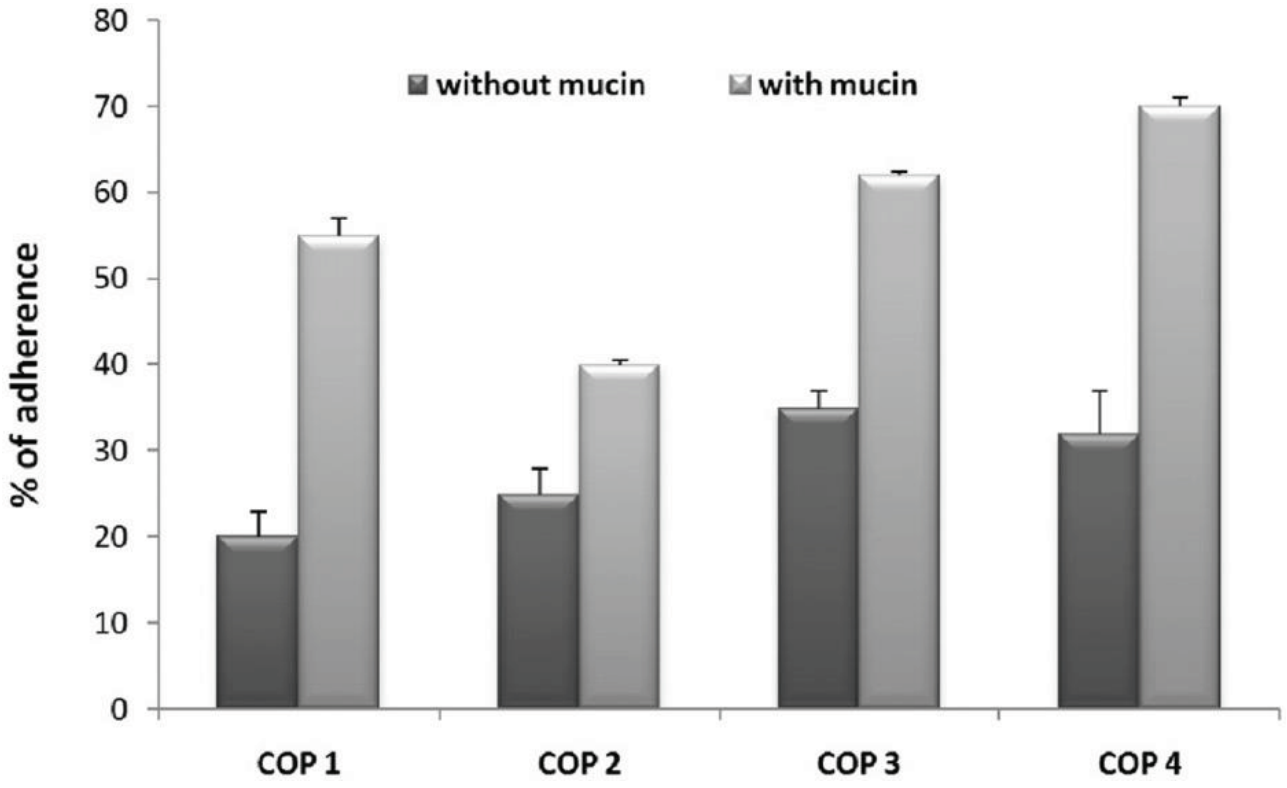

Figure 1. Mucoadhesive properties of COP 1–4 suspensions.

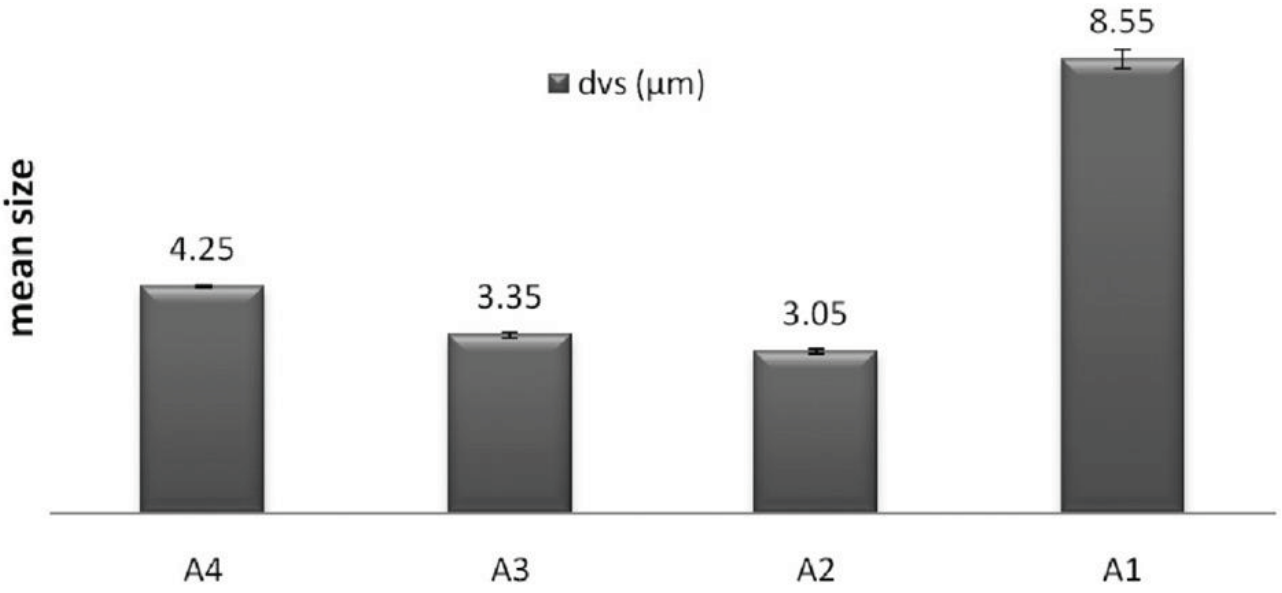

Figure 2. Mean diameters (d_{vs}, µm) of A1–4suspensions.

This latter result is probably due to the formation of aggregates among the microparticles, as suggested by the comparison between the particle size distributions of A3 (d90 = about 13 µm) and A1 (d90 = about 40 µm) suspensions, reported in Figure 3. A1 suspension in fact presents a typical bimodal profile, with a second peak located at higher d_{vs} values, probably due to the presence of the aggregates, while A3 has a substantially monomodal profile.

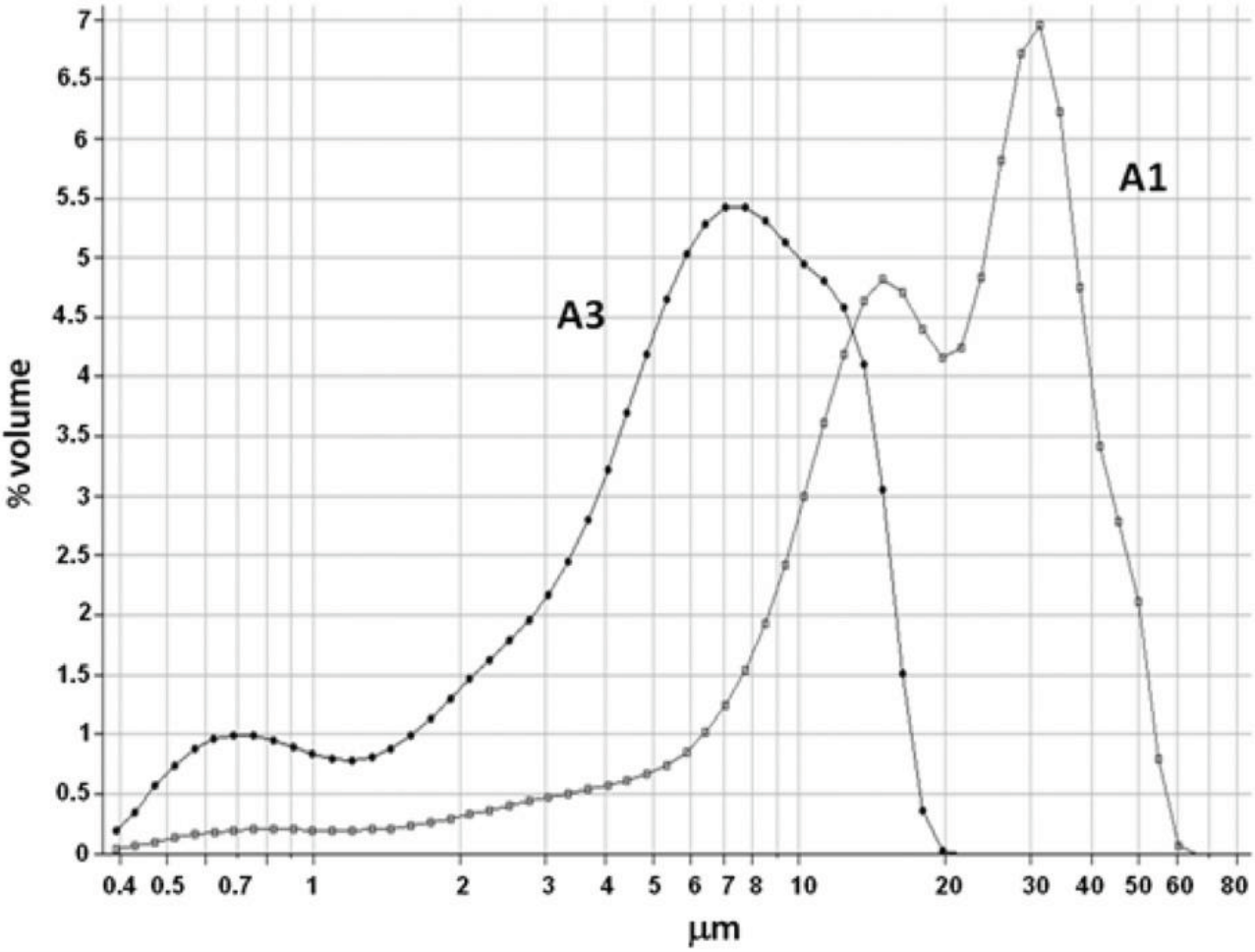

Figure 3. Particle size distributions of A1 and A3 suspensions.

The comparison among SPAN values of A1–4 suspensions (Figure 4) shows that A3 suspension has the lowest SPAN value (1.94), thus corresponding to the narrowest particle size distribution, while A1 suspension (prepared from the more diluted CPX and CS solutions) has the highest SPAN value. A possible explanation of this behavior could be that drug and polymer concentrations influence the rate of the interaction process that leads to the formation of the microparticles, consequently the interaction rate is responsible of the final size of the microparticles formed. As a matter of fact, the more dilute solution determines the formation of microparticles with a larger particle size distribution.

Therefore, A3 suspension presents the lower dvs and the lower SPAN value at the same time with respect to the other suspensions and for these reasons, it can be considered the formulation with the best characteristics for a potential ocular administration of CPX. It has a final concentration of drug–polymer product of interaction of 0.75% w/v (corresponding to 0.50% w/v of drug and 0.25% w/v of polymer).

Therefore, this suspension was chosen as reference formulation for the further study concerning the influence of the addition of surfactants on the size of the coprecipitates. Surfactants are in fact important additional excipients, which may be included in ophthalmic suspensions to disperse the microparticles during the product use and for this reason their addition can be an additional parameter to be evaluated in the preparation of an ocular formulation. Non-ionic surfactants are used in this study. Three different samples of A3 suspension were added of 0.100% w/v of Tween 80 (obtaining T1 suspension), of 0.100% w/v or0.020% w/v of different weight ratios of Tween 80 and Span 80(Mix1 and Mix2, as previously reported) leading to T2 and T3suspensions, respectively.

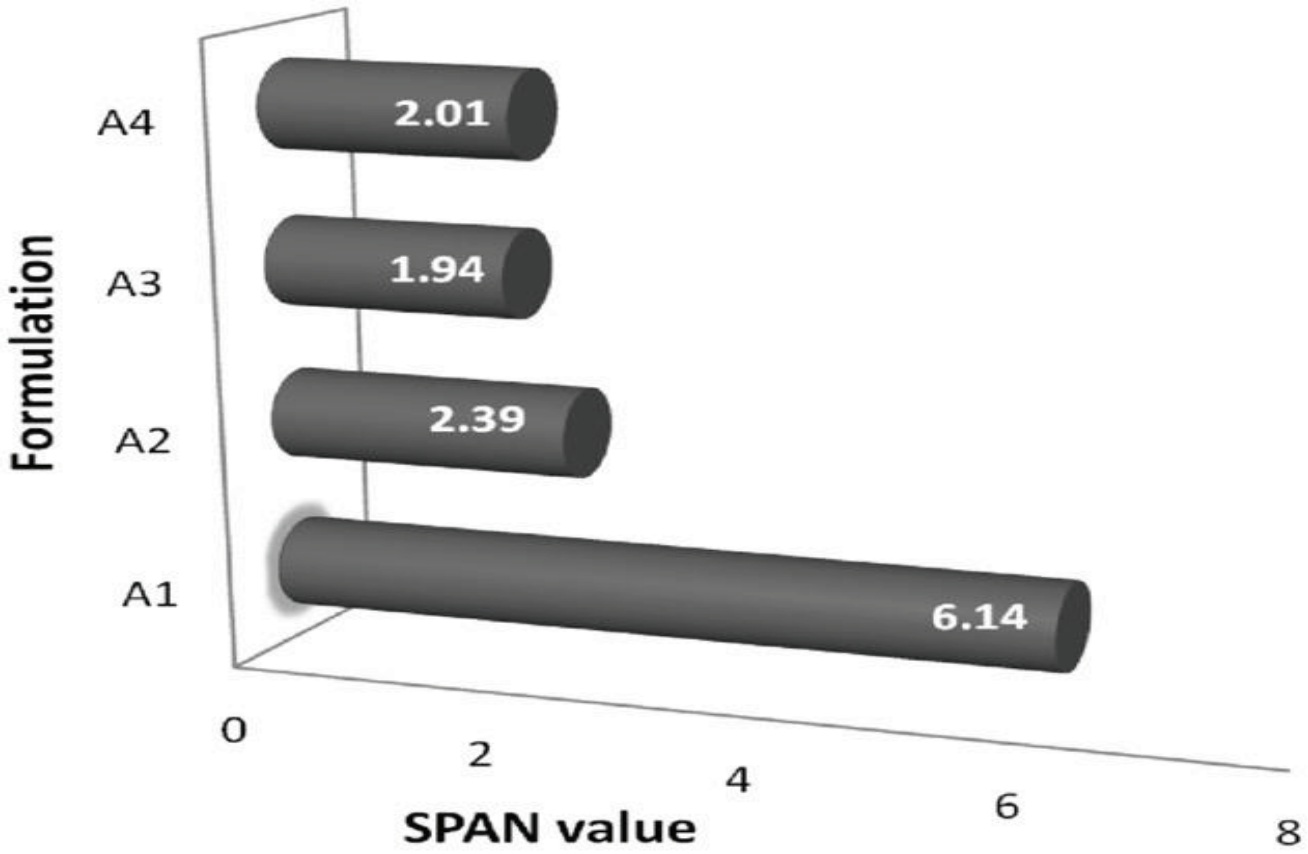

Figure 4. SPAN values of A1–4 suspensions

Figure 5 reports the mean diameters (d_{vs}, μm) of T1–3 compared to the mean diameter of reference A3. As shown by this comparison, T1 (0.1% w/v concentration of Tween 80) has the lowest mean diameter (d_{vs} 2.67 μm), even lower with respect to the reference formulation A3 (d_{vs} 3.35 μm) ($p < 0.0001$). T2 suspension (0.1% w/v of a mixture of Tween 80 and Span 80) has a d_{vs} of 3.20 μm, while T3 suspension (0.02% w/v of surfactant mixture) presents the highest dvs value (5.13 mm) ($p < 0.0001$). The comparison among SPAN values (Figure 6) shows that this parameter is low for T1 and T3 (1.75 and 1.78 μm, respectively) and very close to that of A3 (1.94 μm), meaning that a narrow particle size distribution is maintained. On thecontrary, T2 suspension has a SPAN value quite increased (6.96 μm), meaning that its particle size distribution is quite larger with respect to A3 and T1, despite mean diameters are similar (dvs of about 3 μm).

These data show that Tween 80 alone (present in T1 formulation) gives the best results in terms of particle size suitable for ocular administration, preventing the formation of aggregates. The characteristics of A3 formulation are therefore even improved in T1 formulation, characterized by lower values of d_{vs} and SPAN with respect to this reference formulation. The lower concentration of Tween 80, despite the presence of Span 80, always determines worse particle size characteristics, in terms of dvs and/or particle size distributions. Both surfactants are non-ionic; however, Tween 80 is characterized by a higher hydrophilicity with respect to Span 80 and for this reason it is more suitable for the prevention of formation of aggregates in an aqueous suspension. This probably occurs by a process of interfacial adsorption of the surfactant onto the surface of drug/polymer coprecipitates.

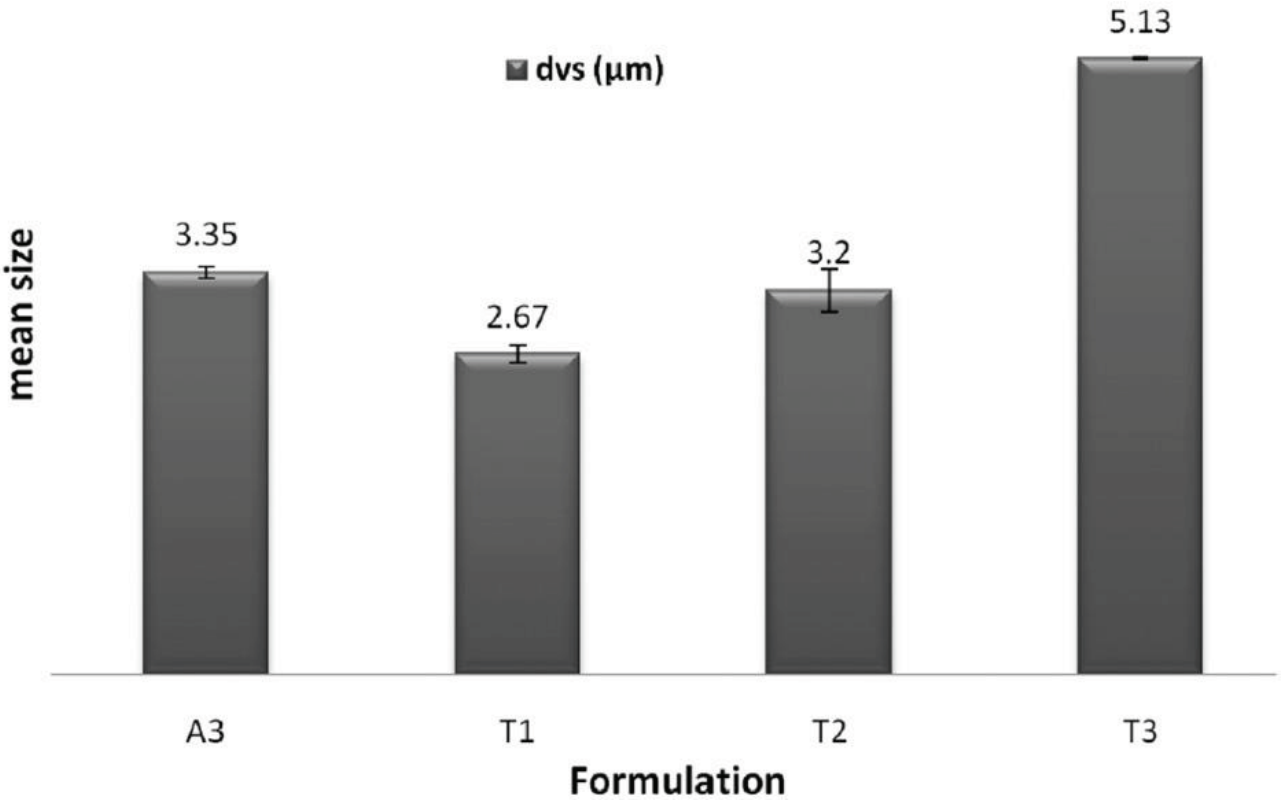

Figure 5. Mean diameters (d_{vs}, µm) of T1–3 suspensions, compared to the suspension A3.

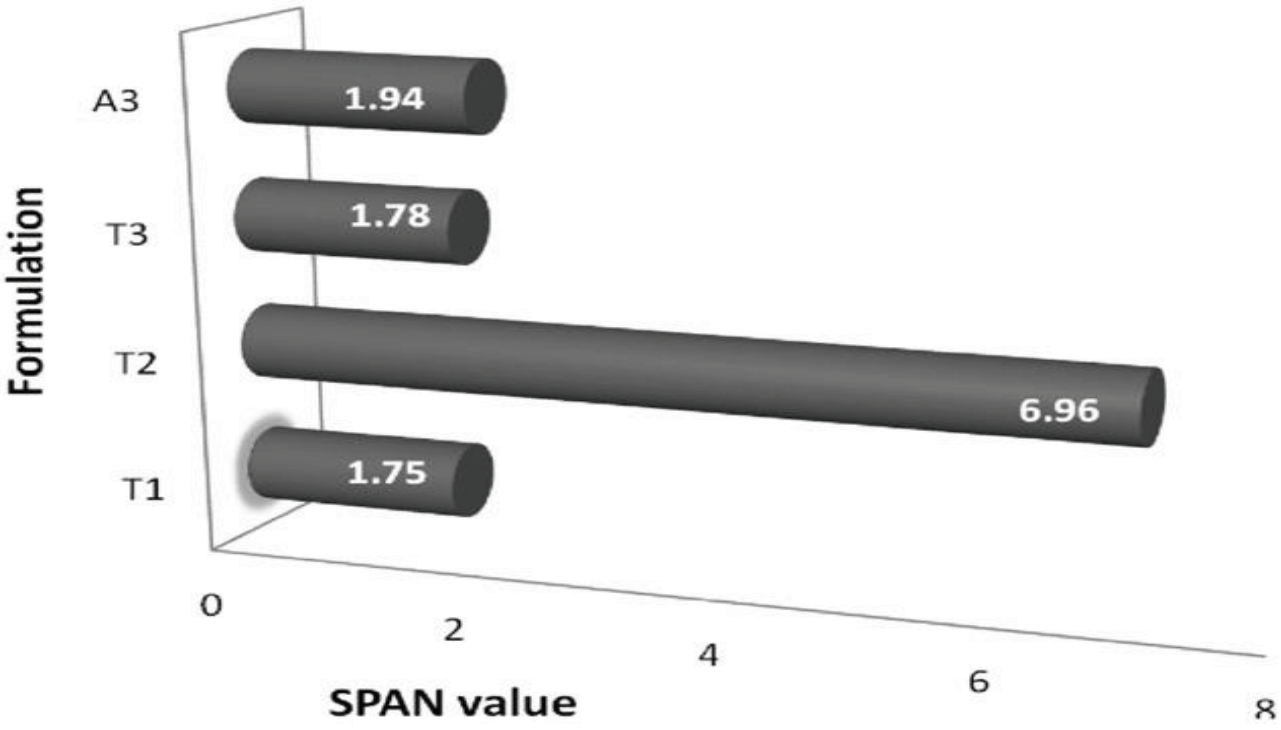

Figure 6. SPAN values of T1–3 suspensions, compared to the suspension A3.

The fact that Tween 80 gives the best results in terms of particle size and stabilization of the suspension is particularly important for an ocular formulation because this non-ionic surfactant is widely utilized in ophthalmic formulations, due to its safety [49,50]. It is listed in the US Pharmacopeia-NationalFormulary, in the European Pharmacopeia and in the Japanese Pharmacopeia [49,50]. Furthermore, Tween 80 has been classified as practically non-irritant as shown by an interesting test of evaluation of ocular irritation, set up and described by Alany et al. [51].

Other suspensions were prepared using different conditions of preparation, in terms of temperature (B1) and stirring (C1). Moreover, the sedimentation of A3, followed by its resuspension led to the formation of the suspension named C2. Figure 7 showsthe corresponding mean diameters (dvs) compared to reference formulation A3.

B1 and C1 present mean diameters (dvs 4.88 and 3.65 mm, respectively), which are higher than the mean diameter of A3 (d_{vs}3.35 μm) ($p < 0.0001$ and <0.006, respectively), while C2 has a mean diameter lower (d_{vs} 2.03 μm) ($p < 0.0001$). B1 and C2 are characterized by SPAN values higher with respect to A3, while C1 has a lower parameter (Figure 8). In the case of B1, an improvement of both mean particle size (d_{vs}) and SPAN value with respect to A3 can be therefore found, meaning that in the preparation of the suspension the use of a higher temperature (40 °C), with respect to the room temperature, leads to worse characteristics of the suspensions.

The sonication of the drug solution during the addition of polymer solution does not lead to any further improvement ofparticle size characteristics of the suspension (C1). The results obtained from the analyses carried out on C2 show that the sedimentation of the coprecipitates, followed by their resuspension with fresh medium leads to a new homogeneous suspension that maintains the good particle size characteristics, suitable for an ocular administration.

Owing to its good characteristics, A3 formulations were chosen for preliminary stability tests. The morphology of the microparticles was not changed before and after the storage period: as shown by microscope pictures (not reported), no aggregation was found and no formation of drug crystals. This is particularly important because, as previously reported [36], CPX instability results in the precipitation of the drug in large acicular crystals (length of a few hundred microns) than can cause discomfort and/or damage.

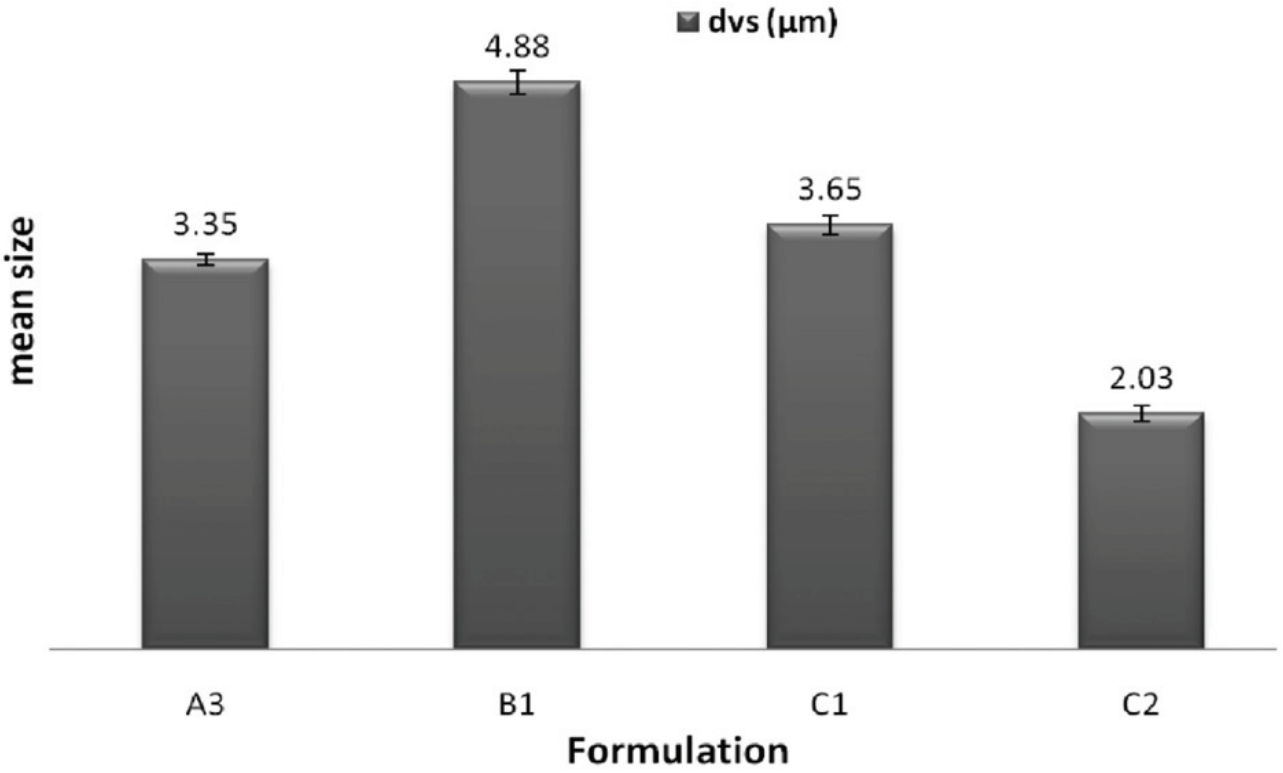

Figure 7. Mean diameters (d_{vs}, µm) of B1 and C1–2 suspensions, compared to the suspensionA3.

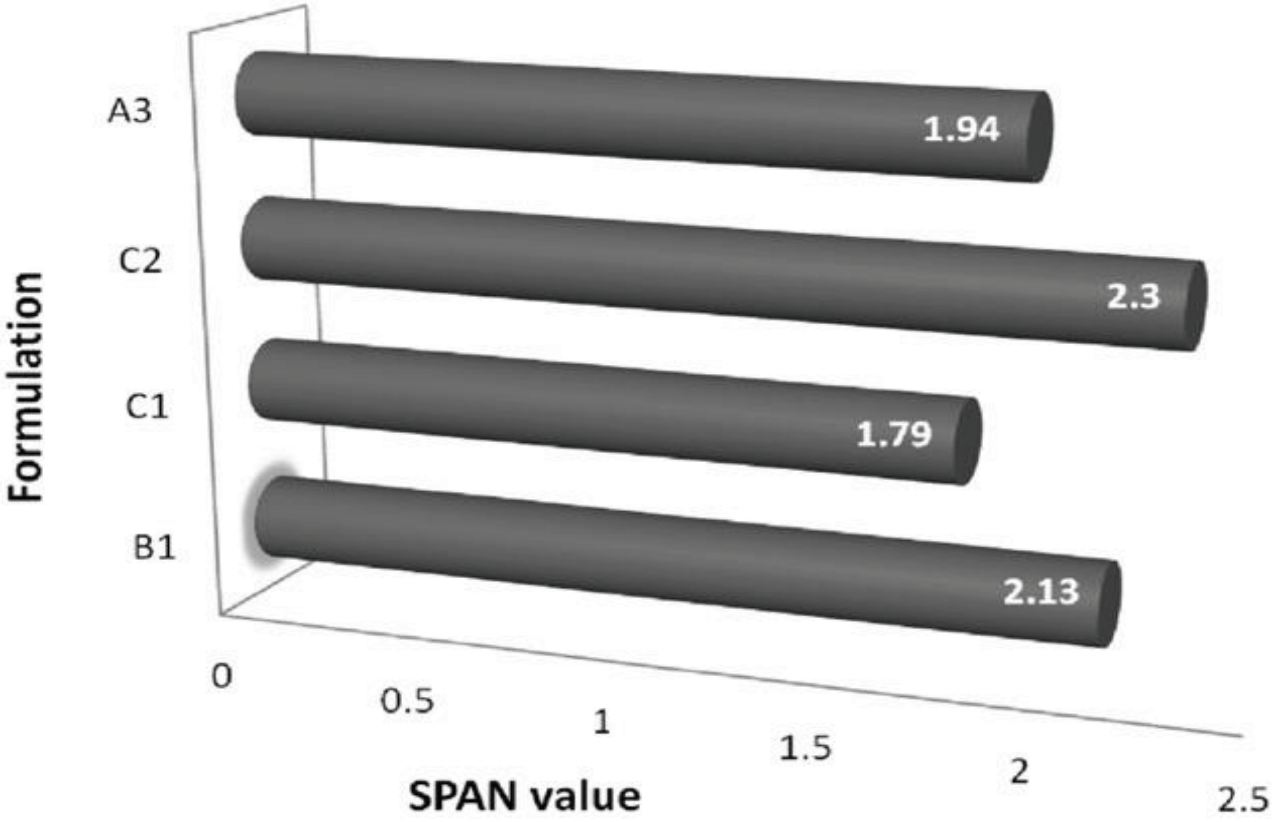

Figure 8. SPAN values of B1 and C1–2 suspensions, compared to the suspension A3

CONCLUSIONS

Particle size in suspensions for ocular drug delivery is a critical parameter determining the quality of the preparation. For this reason, the study of the influence of the technological parameters on the size of the microparticles is very important.

The results obtained from this study show that all the suspensions based on the drug/polyelectrolyte product of interaction are characterized by a positive mucoadhesivity, particularly those based on chondroitin sulfate. The addition of Carbopol obviously improves this property, but it determines a modification of particle size.

Furthermore, chondroitin sulfate coprecipitates the best characteristics in terms of particle size suitable for ocular administration.

As shown by comparison of dvs values, reduction in concentration of the solutions used to obtain the coprecipitates determines the formation of particles with smaller size but after a critical size reduction is achieved, agglomerates are formed, probably due to high surface energy. In the present case, the best formulation is characterized by 0.5% w/v concentration of drug and 0.25% w/v final concentration of polymer (A3).

A further improvement of the particle size characteristics was found with the addition of Tween 80 at the concentration of 0.1% w/v as surfactant, corresponding to T1 formulation. The presence of the surfactant also improves the resuspension properties of the formulation prepared and thus its conditions of use.

REFERENCES:

1. Teng W, Cappello J, Wu W. Physical crosslinking modulates sustained drug release from recombinant silk-elastin like protein polymer for ophthalmic applications. J Control Release. 2011;156:186–94.
2. Blondeau JM. Fluoroquinolones: mechanism of action, classification, and development of resistance. Surv Ophthalmol. 2004;49:S73–8.
3. Diamond JP, White L, Leeming JP, et al. Topical 0.3% ciprofloxacin, norfloxacin, and ofloxacin in treatment of bacterial keratitis: a new method for comparative evaluation of ocular drug penetration. Br J Ophthalmol. 1995;79:606–9.
4. Sanfilippo CM, Morrissey I, Janes R, Morris TW. Surveillance of the activity of aminoglycosides and fluoroquinolones against ophthalmic pathogens from Europe in 2010–2011. Curr Eye Res. 2015;22:1–9.
5. Montero MT, Vazquez JL, Hernandez-Borrell J, Keough KMW. 2. In: Carmona P, et al. (eds). Spectroscopy of biological molecules: Q2 modern trends. 2: Kluwer Academic Publishers. 1997:311–12.
6. Appelbaum PC, Hunter PA. The fluoroquinolone antibacterials: past, present, and future perspectives. Int J Antimicrob Agents. 2000; 16:5–15.
7. Campoli-Richards DM, Monk JP, Price A, et al. Ciprofloxacin. A review of its antibacterial activity, pharmacokinetic properties and therapeutic use. Drugs. 1988;35:373–447.
8. Mundada AS, Shrikhande BK. Formulation and evaluation of Ciprofloxacin hydrochloride soluble ocular drug insert. Curr Eye Res. 2008;33:469–75.
9. Parks DJ, Abrams DA, Sarfarazi FA, Katz HR. Comparison of topical ciprofloxacin to conventional antibiotic therapy in the treatment of ulcerative keratitis. Am J Ophthalmol. 1993;115:471–7.
10. Firestone BA, Dickason MA, Tran T. Solubility characteristics of three fluoroquinolone ophthalmic solutions in an in vitro tear model. Int J Pharm. 1998;164:119–28.
11. Abdelbary G, El-Gendy N. Niosome-encapsulated Gentamicin for ophthalmic controlled delivery. AAPS Pharm Sci Tech. 2008;9: 740–7.
12. Sintzel MB, Bernatchez SF, Tabatabay C, Gurny R. Biomaterials in ophthalmic drug delivery. Eur J Pharm Biopharm. 1996;42:358–74.

13. Rozier A, Mazuel C, Grove J, Plazonnet B. Gelrite: a novel, ionactivated, in situ gelling polymer for ophthalmic vehicles. Effect on bioavailability of Timolol. Int J Pharm. 1989;57:163–8.
14. Budai L, Hajdu M, Budai M, et al. Gels and liposomes in optimized ocular drug delivery: studies on Ciprofloxacin formulations. Int J Pharm 2007;343:34–40.
15. Kaur IP, Garg A, Singla AK, Aggarwal D. Vesicular systems in ocular drug delivery: an overview. Int J Pharm. 2004;269:1–14.
16. Hosny KM. Ciprofloxacin as ocular liposomal hydrogel. AAPS Pharm Sci Tech. 2010;11:241–6.
17. Taha EI, El-Anazi MH, Mel-Bagory I, Bayomi MA. Design of liposomal colloidal systems for ocular delivery of Ciprofloxacin. Saudi Pharm J. 2014;22:231–9.
18. Li H, Liu Y, Zhang Y, et al. Liposomes as a novel ocular delivery system for Brinzolamide: in vitro and in vivo studies. AAPS Pharm Sci Tech. 2015; Sep 3 [Epub ahead of print].
19. Chetoni P, Monti D, Tampucci S, et al. Liposomes as a potential ocular delivery system of Distamycin A. Int J Pharm. 2015;492: 120–6.
20. Abdelbary G. Ocular ciprofloxacin hydrochloride mucoadhesive chitosan-coated liposomes. Pharm Dev Technol. 2011;16:44–56.
21. Mahajan HS, Deshmukh SR. Development and evaluation of gelforming ocular films based on xyloglucan. Carbohydr Polym. 2015; 122:243–7.
22. Huang YY Chung TW. Microencapsulation of gentamicin in iodegradable PLA and/or PLA/PEG copolymer. J Microencapsul. 2001;18:457–65.
23. Giunchedi P, Conte U, Chetoni P, Saettone MF. Pectin microspheresas ophthalmic carriers for Piroxicam: evaluation in vitro and in vivo in albino rabbits. Eur J Pharm Sci. 1999;9:1–7.
24. Giunchedi P, Chetoni P, Conte U, Saettone MF. Albumin microspheres for ocular delivery of Piroxicam. Pharm Pharmacol Commun. 2000;6:149–53.
25. Gavini E, Chetoni P, Cossu M, et al. PLGA microspheres for the ocular delivery of a peptide drug, Vancomycin using emulsification/ spray-drying as the preparation method: in vitro/in vivo studies. Eur J Pharm Biopharm. 2004;57:207–12.
26. Rassu G, Gavini E, Jonassen H, et al. New chitosan derivatives for the preparation of Rokitamycin loaded microspheres designed for ocular or nasal administration. J Pharm Sci. 2009;98:4852–65.

27. Park CG, Kim MJ, Park M, et al. Nanostructured mucoadhesive microparticles for enhanced preocular retention. Acta Biomater. 2014;10:77–86.
28. Shinde UA, Shete JN, Nair HA, Singh KH. Design and characterization of chitosan-alginate microspheres for ocular delivery of azelastine. Pharm Dev Technol. 2014;19:813–23.
29. Addo RT, Yeboah KG, Siwale RC, et al. Formulation and characterization of atropine sulfate in albumin-chitosan microparticles for in vivo ocular drug delivery. J Pharm Sci. 2015;104:1677–90.
30. Cadinoiu AN, Peptu CA, Fache B, et al. Microparticulated systems based on chitosan and poly(vinyl alcohol) with potential ophthalmic applications. J Microencapsul. 2015;32:381–9.
31. Jani R, Gan O, Ali Y, et al. Ion exchange resins for ophthalmic delivery. J Ocul Pharmacol. 1994;10:57–67.
32. Li J, Liu H, Liu LL, et al. Design and evaluation of a brinzolamide drug-resin in situ thermosensitive gelling system for sustained ophthalmic drug delivery. Chem Pharm Bull. 2014;62:1000–8.
33. Qin F, Zeng L, Zhu Y, et al. Preparation and evaluation of a timolol maleate drug-resin ophthalmic suspension as a sustained-release formulation in vitro and in vivo. Drug Dev Ind Pharm. 2015;1–11. Sep 14:[Epub ahead of print].
34. Bonferoni MC, Chetoni P, Giunchedi P, et al. Carrageenan-gelatin mucoadhesive systems for ion-exchange based ophthalmic delivery: in vitro and preliminary in vivo studies. Eur J Pharm Biopharm 2004;57:465–72.
35. Sandri G, Bonferoni MC, Chetoni P, et al. Ophthalmic delivery systems based on drug-polymer-polymer ionic ternary interaction: in vitro and in vivo characterization. Eur J Pharm Biopharm. 2006;62:59–69.
36. Bonferoni MC, Sandri G, Gavini E, et al. Microparticle systems based on polymer-drug interaction for ocular delivery of ciprofloxacin I. In vitro characterization. J Drug Del Sci. Tech 2007;17:57–62.
37. Bonferoni MC, Sandri G, Chetoni P, et al. Microparticle systems based on polymer-drug interaction for ocular delivery of ciprofloxacin II. Precorneal residence times. J Drug Del Sci Tech. 2007;17:63–8.
38. Verschueren E, VanSantvliet L, Ludwig A. Evaluation of various carrageenans as ophthalmic viscolysers. STP Pharma Sci. 1996;6:203–10.

39. Moon JW, Lee HJ, Shin KC, et al. Short term effects of topical cyclosporine and viscoelastic on the ocular surfaces in patients with dry eye. Korean J Ophthalmol. 2007;21:189–94.
40. Baranowski P, Karolewicz B, Gajda M, Pluta J. Ophthalmic drug dosage forms: characterisation and research methods. Scientific World J. 2014;2014:861904. doi: 10.1155/2014/861904. Q3
41. Qi H, Chen W, Huang C, et al. Development of a poloxamer analogs/carbopol-based in situ gelling and mucoadhesive ophthalmic delivery system for puerarin. Int J Pharm. 2007;337:178–87.
42. Aburahma MH, Mahmoud AA. Biodegradable ocular inserts for sustained delivery of brimonidine tartarate: preparation and in vitro/in vivo evaluation. AAPS Pharm Sci Tech. 2011;12:1335–47.
43. Sandri G, Rossi S, Ferrari F, et al. Mucoadhesive and penetrationenhancement properties of three grades of hyaluronic acid usingporcine buccal and vaginal tissue, Caco-2 cell lines, and rat jejunum. J Pharm Pharmacol. 2004;56:1083–90.
44. Sandri G, Bonferoni MC, Ferrari F, et al. An in situ gelling buccal spray containing platelet lysate for the treatment of oral mucositis. Curr Drug Discov Technol. 2011;8:277–85.
45. Edmundson IC. 2. In: Bean HS, Carless JE, Beckett AH, eds. Advances in pharmaceutical sciences. Vol. 2. New York, NY: Q4 Academic Press;1967:2.
46. Gavini E, Rassu G, Muzzarelli C, et al. Spray-dried microspheres based on methylpyrrolidinone chitosan as new carrier for nasal administration of Metoclopramide,. Eur J Pharm Biopharm. 2008;68:245–52.
47. Rassu G, Gavini E, Spada G, Giunchedi P. Ketoprofen spray-dried microspheres based on Eudragit RS and RL: study of the manufacturing parameters. Drug Dev Ind Pharm. 2008;34:1178–87.
48. Sahoo S, Chakraborti CK Mishra SC. Qualitative analysis of controlled release Ciprofloxacin/Carbopol 934 mucoadhesive suspension. J Adv Pharm Technol Res. 2011;2:195–204.
49. Ammar HO, Salama HA, Ghorab M, Mahmoud AA. Nanoemulsion as a potential ophthalmic delivery system for dorzolamide hydrochloride. AAPS Pharm Sci Tech. 2009;10:808–19.

50. Yamaguchi M, Yasueda S, Isowaki A, et al. Formulation of an ophthalmic lipid emulsion containing an anti-inflammatory steroidal drug, difluprednate. Int J Pharm. 2005;301:121–8.
51. Alany RG, Tucker IG, Davies NM, Rades T. Characterizing colloidal structures of pseudoternary phase diagrams formed by oil/water/amphiphile systems. Drug Dev Ind Pharm. 2001;27:31–8.

GENERAL CONCLUSIONS:

In my PhD thesis the great potential of polysaccharides in wide areas of drug delivery was confirmed.

Composite pellets prepared by embedding o/w emulsions in microcrystalline cellulose could be considered a potential oral carrier of hydrophobic drugs such as furosemide and propranolol. The results of these studies revealed that drug, surfactant and oil/surfactant ratio affected droplet size, viscosity and ζ of emulsions as well as size, shape, and friability of microcrystalline pellets. Drug migration was more evident for the less lipophilic drug (furosemide) and for the lower oil/surfactant ratio.

Chitosan/glicerophosphate hydrogels could be considered a valid alternative to microspheres for transarterial embolization treatment of advanced stages of hepatocellular carcinoma. In addition, the strong electrostatic interaction between chitosan and indocyanine green can be exploited for intraoperative visualization of tumour nodules during hepatic resection.

Chitosan chloride-based microparticles were suitable for the nose-to-brain delivery of UDCA-AZT improving the drug-uptake into the central nervous system. The prodrug was rapidly released and then adsorbed from nasal mucosa of rats. Furthermore, nasal administration of UDCA-AZT loaded chitosan microparticles produced detectable amount of this prodrug in the cerebrospinal fluid of rats that could be relevant to achieve an anti-HIV activity.

Composite chitosan/alginate hydrogel with poly(lactic-co-glycolic acid) microspheres loaded with deferoxamine mesilate could be considered a novel strategy for the treatment of iron dysregulation diseases. This highly water soluble drug, can be encapsulated in biodegradable microspheres of poly(lactic-co-glycolic acid) but the co-formulation formulation with chitosan/alginate hydrogel is necessary in order to obtain sustained drug release: hydrogel is better capable to control the DFO release compared to PLGA microspheres.

Ocular infections from Gram-positive and Gram-negative bacteria could be treated with ciprofloxacin loaded chondroitin sulphate or lambda carrageenan microparticulate controlled delivery systems. The result of ionic interactions between ciprofloxacin and these polysaccharides are coprecipitates that can act as vehicles for the sustained release of this drug after being displaced by the mediums ions in the precorneal region.

LICENCE AGREEMENTS

SPRINGER LICENSE
TERMS AND CONDITIONS
Oct 22, 2015

This is a License Agreement between Andrea Salis ("You") and Springer ("Springer") provided by Copyright Clearance Center ("CCC"). The license consists of your order details, the terms and conditions provided by Springer, and the payment terms and conditions.

All payments must be made in full to CCC. For payment instructions, please see information listed at the bottom of this form.

License Number	3734280817309
License date	Oct 22, 2015
Licensed content publisher	Springer
Licensed content publication	AAPS PharmSciTech
Licensed content title	Relationships Between the Properties of Self-Emulsifying Pellets and of the Emulsions Used as Massing Liquids for Their Preparation
Licensed content author	Ioannis Nikolakakis
Licensed content date	Jan 1, 2014
Volume number	16
Issue number	1
Type of Use	Book/Textbook
Requestor type	Publisher
Publisher	Open University
Portion	Full text
Format	Print and Electronic
Will you be translating?	No
Print run	3
Author of this Springer article	Yes and you are the sole author of the new work
Order reference number	None
Title of new book	POLYSACCHARIDES AS DRUG DELIVERY SYSTEMS FOR DIFFERENT ADMINISTRATION ROUTES
Publisher	Open University
Author of new book	ANDREA SALIS
Expected publication date of new book	Jan 2016
Estimated size of new book (pages)	200
Total	0.00 EUR

Terms and Conditions

Introduction
The publisher for this copyrighted material is Springer Science + Business Media. By clicking "accept" in connection with completing this licensing transaction, you agree that the following terms and conditions apply to this transaction (along with the Billing and Payment terms and conditions established by Copyright Clearance Center, Inc. ("CCC"), at the time that you opened your Rightslink account and that are available at any time at http://myaccount.copyright.com).

Limited License
Springer Science + Business Media hereby grants to you a non-exclusive license to use this material, for the use as indicated in your inquiry. Licenses are for one-time use only with a maximum distribution equal to the number that you identified in the licensing process.

This License includes use in an electronic form, provided it's password protected, on intranet, or CD-Rom/E-book. For any other electronic use, please contact Springer at permissions.dordrecht@springer.com or permissions.heidelberg@springer.com

Although Springer holds copyright to the material and is entitled to negotiate on rights, this license is only valid, provided permission is also obtained from the author (address is given with the article/chapter) and provided it concerns original material which does not carry references to other sources (if material in question appears with credit to another source, authorization from that source is required as well).

Geographic Rights: Scope

Licenses may be exercised anywhere in the world.

Altering/Modifying Material: Not Permitted
However figures and illustrations may be altered minimally to serve your work. Any other abbreviations, additions, deletions and/or any other alterations shall be made only with prior written authorization of the author(s) and/or Springer Science + Business Media. (Please contact Springer at permissions.dordrecht@springer.com or permissions.heidelberg@springer.com)

Reservation of Rights
Springer Science + Business Media reserves all rights not specifically granted in the combination of (i) the license details provided by you and accepted in the course of this licensing transaction, (ii) these terms and conditions and (iii) CCC's Billing and Payment terms and conditions.

License Contingent on Payment
While you may exercise the rights licensed immediately upon issuance of the license at the end of the licensing process for the transaction, provided that you have disclosed complete and accurate details of your proposed use, no license is finally effective unless and until full payment is received from you (either by Springer Science + Business Media or by CCC) as provided in CCC's Billing and Payment terms and conditions. If full payment is not received by Due Date, then any license preliminarily granted shall be deemed automatically revoked and shall be void as if never granted. Further, in the event that you breach any of these terms and conditions or any of CCC's Billing and Payment terms and conditions, the license is automatically revoked and shall be void as if never granted. Use of materials as described in a revoked license, as well as any use of the materials beyond the scope of an unrevoked license, may constitute copyright infringement and Springer Science + Business Media reserves the right to take any and all action to protect its copyright in the materials.

Copyright Notice:
Please include the following copyright citation referencing the publication in which the material was originally published. Where wording is within brackets, please include verbatim.

"With kind permission from Springer Science+Business Media: <book/journal title, chapter/article title, volume, year of publication, page, name(s) of author(s), figure number(s), and any original (first) copyright notice displayed with material>."

Warranties
Springer Science + Business Media makes no representations or warranties with respect to the licensed material.

Indemnity
You hereby indemnify and agree to hold harmless Springer Science + Business Media and CCC, and their respective officers, directors, employees and agents, from and against any and all claims arising out of your use of the licensed material other than as specifically authorized pursuant to this license.

No Transfer of License
This license is personal to you and may not be sublicensed, assigned, or transferred by you to any other person without Springer Science + Business Media's written permission.

No Amendment Except in Writing
This license may not be amended except in a writing signed by both parties (or, in the case of Springer Science + Business Media, by CCC on Springer Science + Business Media's behalf).

Objection to Contrary Terms
Springer Science + Business Media hereby objects to any terms contained in any purchase order, acknowledgment, check endorsement or other writing prepared by you, which terms are inconsistent with these terms and conditions or CCC's Billing and Payment terms and conditions. These terms and conditions, together with CCC's Billing and Payment terms and conditions (which are incorporated herein), comprise the entire agreement between you and Springer Science + Business Media (and CCC) concerning this licensing transaction. In the event of any conflict between your obligations established by these terms and conditions and those established by CCC's Billing and Payment terms and conditions, these terms and conditions shall control.

Jurisdiction
All disputes that may arise in connection with this present License, or the breach thereof, shall be settled exclusively by the country's law in which the work was originally published.

Other terms and conditions:

v1.3

Questions? customercare@copyright.com or +1-855-239-3415 (toll free in the US) or +1-978-646-2777.

Andrea Salis <asalis@uniss.it>

RE: iedd20:Development of thermosensitive chitosan/glicerophospate injectable in situ gelling solutions for potential application in intraoperative fluorescence imaging and local therapy of hepatocellular carcinoma: a preliminary study

Academic Journals Society Permissions <society.permissions@tandf.co.uk> 26 ottobre 2015 11:55
A: Andrea Salis <asalis@uniss.it>

Our Ref: MD/IEDD/H257

26th October 2015

Dear Andrea Salis,

Thank you for your correspondence requesting permission to reproduce the following article published in our journal in your printed thesis and to be posted in your university's repository at the University of Sassari.

'Development of thermosensitive chitosan/glicerophospate injectable in situ gelling solutions for potential application in intraoperative fluorescence imaging and local therapy of hepatocellular carcinoma: a preliminary study' By Andrea Salis et al Expert Opinion on Drug Delivery Vol.12:10 (2015) pp.1583-1596

We will be pleased to grant permission on the sole condition that you acknowledge the original source of publication and insert a reference to the article on the Journals website:

This is the authors accepted manuscript of an article published as the version of record in Expert Opinion on Drug Delivery 2015 http://www.tandfonline.com/

Please note that this license does not allow you to post our content on any third party websites or repositories.

Thank you for your interest in our Journal.

Yours sincerely

Michelle Dickson – Permissions & Licensing Executive, Journals.

Routledge, Taylor & Francis Group.

4 Park Square, Milton Park, Abingdon, Oxon, OX14 4RN, UK.

Tel: +44 (0)20 7017 7413

Fax:+44 (0)20 7017 6336

Web: www.tandfonline.com

e-mail: Michelle.Dickson@tandf.co.uk

From: Andrea Salis [mailto:asalis@uniss.it]
Sent: 22 October 2015 16:29
To: Academic UK Non Rightslink
Subject: iedd20:Development of thermosensitive chitosan/glicerophospate injectable in situ gelling solutions for potential application in intraoperative fluorescence imaging and local therapy of hepatocellular carcinoma: a preliminary study

Permissions Request
Contact name: Andrea Salis
Street address: via lamarmora 116
Town: Nuoro
Postcode/ZIP code: 08100
Country: Italy
Contact telephone number: +393472446316
Contact email address: asalis@uniss.it
Article title: Development of thermosensitive chitosan/glicerophospate injectable in situ gelling solutions for potential application in intraoperative fluorescence imaging and local therapy of hepatocellular carcinoma: a preliminary study
Article DOI: 10.1517/17425247.2015.1042452
Author name: Andrea Salis, Giovanna Rassu, Maria Budai-Szűcs, Ilaria Benzoni, Erzsébet Csányi, Szilvia Berkó, Marcello Maestri, Paolo Dionigi, Elena P Porcu, Elisabetta Gavini, Paolo Giunchedi
Journal title: Expert Opinion on Drug Delivery
Volume number: 12
Issue number: 10
Year of publication: 2015
Page number(s): 200
Are you the sole author/editor of the new publication?: Yes
Are you requesting the full article?: Yes
If no, please supply extract and include number of word:
If no, please supply details of figure/table:
Name of publisher of new publication: UNIVERSITY OF SASSARI
Title of new publication: POLYSACCHARIDES AS DRUG DELIVERY SYSTEMS FOR DIFFERENT ADMINISTRATION ROUTES
Course pack: No
Number of Students:
Is print: Yes
Electronic: Yes
E-reserve: Yes
Period of use: Perpetual
Short loan library?: No
Thesis: Yes

To be reprinted in a new publication?: Yes
In print format: Yes
In ebook format?: Yes
ISBN:
Languages:
Distribution quantity:
Retail price:
Additional comments:

ELSEVIER LICENSE
TERMS AND CONDITIONS
Oct 27, 2015

This is a License Agreement between Andrea Salis ("You") and Elsevier ("Elsevier") provided by Copyright Clearance Center ("CCC"). The license consists of your order details, the terms and conditions provided by Elsevier, and the payment terms and conditions.

All payments must be made in full to CCC. For payment instructions, please see information listed at the bottom of this form.

Supplier	Elsevier Limited The Boulevard,Langford Lane Kidlington,Oxford,OX5 1GB,UK
Registered Company Number	1982084
Customer name	Andrea Salis
Customer address	via lamarmora 116 Nuoro, NU 08100
License number	3736961430650
License date	Oct 22, 2015
Licensed content publisher	Elsevier
Licensed content publication	Antiviral Research
Licensed content title	Nasal chitosan microparticles target a zidovudine prodrug to brain HIV sanctuaries
Licensed content author	Alessandro Dalpiaz,Marco Fogagnolo,Luca Ferraro,Antonio Capuzzo,Barbara Pavan,Giovanna Rassu,Andrea Salis,Paolo Giunchedi,Elisabetta Gavini
Licensed content date	Available online 30 September 2015
Licensed content volume number	n/a
Licensed content issue number	n/a
Number of pages	1
Start Page	None
End Page	None
Type of Use	reuse in a thesis/dissertation
Intended publisher of new work	other
Portion	full article
Format	both print and electronic
Are you the author of this	Yes

Elsevier article?	
Will you be translating?	No
Title of your thesis/dissertation	Polysaccharides as drug delivery systems for different administration routes
Expected completion date	Jan 2016
Estimated size (number of pages)	
Elsevier VAT number	GB 494 6272 12
Permissions price	0.00 USD
VAT/Local Sales Tax	0.00 USD / 0.00 GBP
Total	0.00 USD
Terms and Conditions	

INTRODUCTION

1. The publisher for this copyrighted material is Elsevier. By clicking "accept" in connection with completing this licensing transaction, you agree that the following terms and conditions apply to this transaction (along with the Billing and Payment terms and conditions established by Copyright Clearance Center, Inc. ("CCC"), at the time that you opened your Rightslink account and that are available at any time at http://myaccount.copyright.com).

GENERAL TERMS

2. Elsevier hereby grants you permission to reproduce the aforementioned material subject to the terms and conditions indicated.

3. Acknowledgement: If any part of the material to be used (for example, figures) has appeared in our publication with credit or acknowledgement to another source, permission must also be sought from that source. If such permission is not obtained then that material may not be included in your publication/copies. Suitable acknowledgement to the source must be made, either as a footnote or in a reference list at the end of your publication, as follows:

"Reprinted from Publication title, Vol /edition number, Author(s), Title of article / title of chapter, Pages No., Copyright (Year), with permission from Elsevier [OR APPLICABLE SOCIETY COPYRIGHT OWNER]." Also Lancet special credit - "Reprinted from The Lancet, Vol. number, Author(s), Title of article, Pages No., Copyright (Year), with permission from Elsevier."

4. Reproduction of this material is confined to the purpose and/or media for which permission is hereby given.

5. Altering/Modifying Material: Not Permitted. However figures and illustrations may be altered/adapted minimally to serve your work. Any other abbreviations, additions, deletions and/or any other alterations shall be made only with prior written authorization of Elsevier

Ltd. (Please contact Elsevier at permissions@elsevier.com)

6. If the permission fee for the requested use of our material is waived in this instance, please be advised that your future requests for Elsevier materials may attract a fee.

7. Reservation of Rights: Publisher reserves all rights not specifically granted in the combination of (i) the license details provided by you and accepted in the course of this licensing transaction, (ii) these terms and conditions and (iii) CCC's Billing and Payment terms and conditions.

8. License Contingent Upon Payment: While you may exercise the rights licensed immediately upon issuance of the license at the end of the licensing process for the transaction, provided that you have disclosed complete and accurate details of your proposed use, no license is finally effective unless and until full payment is received from you (either by publisher or by CCC) as provided in CCC's Billing and Payment terms and conditions. If full payment is not received on a timely basis, then any license preliminarily granted shall be deemed automatically revoked and shall be void as if never granted. Further, in the event that you breach any of these terms and conditions or any of CCC's Billing and Payment terms and conditions, the license is automatically revoked and shall be void as if never granted. Use of materials as described in a revoked license, as well as any use of the materials beyond the scope of an unrevoked license, may constitute copyright infringement and publisher reserves the right to take any and all action to protect its copyright in the materials.

9. Warranties: Publisher makes no representations or warranties with respect to the licensed material.

10. Indemnity: You hereby indemnify and agree to hold harmless publisher and CCC, and their respective officers, directors, employees and agents, from and against any and all claims arising out of your use of the licensed material other than as specifically authorized pursuant to this license.

11. No Transfer of License: This license is personal to you and may not be sublicensed, assigned, or transferred by you to any other person without publisher's written permission.

12. No Amendment Except in Writing: This license may not be amended except in a writing signed by both parties (or, in the case of publisher, by CCC on publisher's behalf).

13. Objection to Contrary Terms: Publisher hereby objects to any terms contained in any purchase order, acknowledgment, check endorsement or other writing prepared by you, which terms are inconsistent with these terms and conditions or CCC's Billing and Payment terms and conditions. These terms and conditions, together with CCC's Billing and Payment terms and conditions (which are incorporated herein), comprise the entire agreement between you and publisher (and CCC) concerning this licensing transaction. In the event of any conflict between your obligations established by these terms and conditions and those established by CCC's Billing and Payment terms and conditions, these terms and conditions

shall control.

14. Revocation: Elsevier or Copyright Clearance Center may deny the permissions described in this License at their sole discretion, for any reason or no reason, with a full refund payable to you. Notice of such denial will be made using the contact information provided by you. Failure to receive such notice will not alter or invalidate the denial. In no event will Elsevier or Copyright Clearance Center be responsible or liable for any costs, expenses or damage incurred by you as a result of a denial of your permission request, other than a refund of the amount(s) paid by you to Elsevier and/or Copyright Clearance Center for denied permissions.

LIMITED LICENSE

The following terms and conditions apply only to specific license types:

15. **Translation**: This permission is granted for non-exclusive world **English** rights only unless your license was granted for translation rights. If you licensed translation rights you may only translate this content into the languages you requested. A professional translator must perform all translations and reproduce the content word for word preserving the integrity of the article.

16. **Posting licensed content on any Website**: The following terms and conditions apply as follows: Licensing material from an Elsevier journal: All content posted to the web site must maintain the copyright information line on the bottom of each image; A hyper-text must be included to the Homepage of the journal from which you are licensing at http://www.sciencedirect.com/science/journal/xxxxx or the Elsevier homepage for books at http://www.elsevier.com; Central Storage: This license does not include permission for a scanned version of the material to be stored in a central repository such as that provided by Heron/XanEdu.

Licensing material from an Elsevier book: A hyper-text link must be included to the Elsevier homepage at http://www.elsevier.com . All content posted to the web site must maintain the copyright information line on the bottom of each image.

Posting licensed content on Electronic reserve: In addition to the above the following clauses are applicable: The web site must be password-protected and made available only to bona fide students registered on a relevant course. This permission is granted for 1 year only. You may obtain a new license for future website posting.

17. **For journal authors:** the following clauses are applicable in addition to the above:

Preprints:

A preprint is an author's own write-up of research results and analysis, it has not been peer-reviewed, nor has it had any other value added to it by a publisher (such as formatting,

copyright, technical enhancement etc.).

Authors can share their preprints anywhere at any time. Preprints should not be added to or enhanced in any way in order to appear more like, or to substitute for, the final versions of articles however authors can update their preprints on arXiv or RePEc with their Accepted Author Manuscript (see below).

If accepted for publication, we encourage authors to link from the preprint to their formal publication via its DOI. Millions of researchers have access to the formal publications on ScienceDirect, and so links will help users to find, access, cite and use the best available version. Please note that Cell Press, The Lancet and some society-owned have different preprint policies. Information on these policies is available on the journal homepage.

Accepted Author Manuscripts: An accepted author manuscript is the manuscript of an article that has been accepted for publication and which typically includes author-incorporated changes suggested during submission, peer review and editor-author communications.

Authors can share their accepted author manuscript:

- – immediately
    - via their non-commercial person homepage or blog
    - by updating a preprint in arXiv or RePEc with the accepted manuscript
    - via their research institute or institutional repository for internal institutional uses or as part of an invitation-only research collaboration work-group
    - directly by providing copies to their students or to research collaborators for their personal use
    - for private scholarly sharing as part of an invitation-only work group on commercial sites with which Elsevier has an agreement
- – after the embargo period
    - via non-commercial hosting platforms such as their institutional repository
    - via commercial sites with which Elsevier has an agreement

In all cases accepted manuscripts should:

- – link to the formal publication via its DOI
- – bear a CC-BY-NC-ND license - this is easy to do
- – if aggregated with other manuscripts, for example in a repository or other site, be shared in alignment with our hosting policy not be added to or enhanced in any way to appear more like, or to substitute for, the published journal article.

Published journal article (JPA): A published journal article (PJA) is the definitive final record of published research that appears or will appear in the journal and embodies all value-adding publishing activities including peer review co-ordination, copy-editing,

formatting, (if relevant) pagination and online enrichment.

Policies for sharing publishing journal articles differ for subscription and gold open access articles:

Subscription Articles: If you are an author, please share a link to your article rather than the full-text. Millions of researchers have access to the formal publications on ScienceDirect, and so links will help your users to find, access, cite, and use the best available version.

Theses and dissertations which contain embedded PJAs as part of the formal submission can be posted publicly by the awarding institution with DOI links back to the formal publications on ScienceDirect.

If you are affiliated with a library that subscribes to ScienceDirect you have additional private sharing rights for others' research accessed under that agreement. This includes use for classroom teaching and internal training at the institution (including use in course packs and courseware programs), and inclusion of the article for grant funding purposes.

Gold Open Access Articles: May be shared according to the author-selected end-user license and should contain a CrossMark logo, the end user license, and a DOI link to the formal publication on ScienceDirect.

Please refer to Elsevier's posting policy for further information.

18. **For book authors** the following clauses are applicable in addition to the above: Authors are permitted to place a brief summary of their work online only. You are not allowed to download and post the published electronic version of your chapter, nor may you scan the printed edition to create an electronic version. **Posting to a repository:** Authors are permitted to post a summary of their chapter only in their institution's repository.

19. **Thesis/Dissertation**: If your license is for use in a thesis/dissertation your thesis may be submitted to your institution in either print or electronic form. Should your thesis be published commercially, please reapply for permission. These requirements include permission for the Library and Archives of Canada to supply single copies, on demand, of the complete thesis and include permission for Proquest/UMI to supply single copies, on demand, of the complete thesis. Should your thesis be published commercially, please reapply for permission. Theses and dissertations which contain embedded PJAs as part of the formal submission can be posted publicly by the awarding institution with DOI links back to the formal publications on ScienceDirect.

Elsevier Open Access Terms and Conditions

You can publish open access with Elsevier in hundreds of open access journals or in nearly 2000 established subscription journals that support open access publishing. Permitted third

party re-use of these open access articles is defined by the author's choice of Creative Commons user license. See our open access license policy for more information.

Terms & Conditions applicable to all Open Access articles published with Elsevier:

Any reuse of the article must not represent the author as endorsing the adaptation of the article nor should the article be modified in such a way as to damage the author's honour or reputation. If any changes have been made, such changes must be clearly indicated.

The author(s) must be appropriately credited and we ask that you include the end user license and a DOI link to the formal publication on ScienceDirect.

If any part of the material to be used (for example, figures) has appeared in our publication with credit or acknowledgement to another source it is the responsibility of the user to ensure their reuse complies with the terms and conditions determined by the rights holder.

Additional Terms & Conditions applicable to each Creative Commons user license:

CC BY: The CC-BY license allows users to copy, to create extracts, abstracts and new works from the Article, to alter and revise the Article and to make commercial use of the Article (including reuse and/or resale of the Article by commercial entities), provided the user gives appropriate credit (with a link to the formal publication through the relevant DOI), provides a link to the license, indicates if changes were made and the licensor is not represented as endorsing the use made of the work. The full details of the license are available at http://creativecommons.org/licenses/by/4.0.

CC BY NC SA: The CC BY-NC-SA license allows users to copy, to create extracts, abstracts and new works from the Article, to alter and revise the Article, provided this is not done for commercial purposes, and that the user gives appropriate credit (with a link to the formal publication through the relevant DOI), provides a link to the license, indicates if changes were made and the licensor is not represented as endorsing the use made of the work. Further, any new works must be made available on the same conditions. The full details of the license are available at http://creativecommons.org/licenses/by-nc-sa/4.0.

CC BY NC ND: The CC BY-NC-ND license allows users to copy and distribute the Article, provided this is not done for commercial purposes and further does not permit distribution of the Article if it is changed or edited in any way, and provided the user gives appropriate credit (with a link to the formal publication through the relevant DOI), provides a link to the license, and that the licensor is not represented as endorsing the use made of the work. The full details of the license are available at http://creativecommons.org/licenses/by-nc-nd/4.0. Any commercial reuse of Open Access articles published with a CC BY NC SA or CC BY NC ND license requires permission from Elsevier and will be subject to a fee.

Commercial reuse includes:

- – Associating advertising with the full text of the Article
- – Charging fees for document delivery or access

- – Article aggregation
- – Systematic distribution via e-mail lists or share buttons

Posting or linking by commercial companies for use by customers of those companies.

20. **Other Conditions**:

v1.8

Questions? customercare@copyright.com or +1-855-239-3415 (toll free in the US) or +1-978-646-2777.

ELSEVIER LICENSE
TERMS AND CONDITIONS
Oct 29, 2015

This is a License Agreement between Andrea Salis ("You") and Elsevier ("Elsevier") provided by Copyright Clearance Center ("CCC"). The license consists of your order details, the terms and conditions provided by Elsevier, and the payment terms and conditions.

All payments must be made in full to CCC. For payment instructions, please see information listed at the bottom of this form.

Supplier	Elsevier Limited The Boulevard,Langford Lane Kidlington,Oxford,OX5 1GB,UK
Registered Company Number	1982084
Customer name	Andrea Salis
Customer address	via lamarmora 116 Nuoro, NU 08100
License number	3737570191447
License date	Oct 26, 2015
Licensed content publisher	Elsevier
Licensed content publication	Carbohydrate Polymers
Licensed content title	COMPOSITE CHITOSAN/ALGINATE HYDROGEL FOR CONTROLLED RELEASE OF DEFEROXAMINE: A SYSTEM TO POTENTIALLY TREAT IRON DYSREGULATION DISEASES
Licensed content author	Giovanna Rassu,Andrea Salis,Elena Piera Porcu,Paolo Giunchedi,Marta Roldo,Elisabetta Gavini
Licensed content date	Available online 23 October 2015
Licensed content volume number	n/a
Licensed content issue number	n/a
Number of pages	1
Start Page	None
End Page	None
Type of Use	reuse in a thesis/dissertation
Portion	full article
Format	both print and electronic
Are you the author of this Elsevier article?	Yes
Will you be translating?	No
Title of your thesis/dissertation	Polysaccharides as drug delivery systems for different administration routes
Expected completion date	Jan 2016
Estimated size (number of pages)	
Elsevier VAT number	GB 494 6272 12
Permissions price	0.00 USD

VAT/Local Sales Tax 0.00 USD / 0.00 GBP

Total 0.00 USD

Terms and Conditions

INTRODUCTION

1. The publisher for this copyrighted material is Elsevier. By clicking "accept" in connection with completing this licensing transaction, you agree that the following terms and conditions apply to this transaction (along with the Billing and Payment terms and conditions established by Copyright Clearance Center, Inc. ("CCC"), at the time that you opened your Rightslink account and that are available at any time at http://myaccount.copyright.com).

GENERAL TERMS

2. Elsevier hereby grants you permission to reproduce the aforementioned material subject to the terms and conditions indicated.

3. Acknowledgement: If any part of the material to be used (for example, figures) has appeared in our publication with credit or acknowledgement to another source, permission must also be sought from that source. If such permission is not obtained then that material may not be included in your publication/copies. Suitable acknowledgement to the source must be made, either as a footnote or in a reference list at the end of your publication, as follows:

"Reprinted from Publication title, Vol /edition number, Author(s), Title of article / title of chapter, Pages No., Copyright (Year), with permission from Elsevier [OR APPLICABLE SOCIETY COPYRIGHT OWNER]." Also Lancet special credit - "Reprinted from The Lancet, Vol. number, Author(s), Title of article, Pages No., Copyright (Year), with permission from Elsevier."

4. Reproduction of this material is confined to the purpose and/or media for which permission is hereby given.

5. Altering/Modifying Material: Not Permitted. However figures and illustrations may be altered/adapted minimally to serve your work. Any other abbreviations, additions, deletions and/or any other alterations shall be made only with prior written authorization of Elsevier Ltd. (Please contact Elsevier at permissions@elsevier.com)

6. If the permission fee for the requested use of our material is waived in this instance, please be advised that your future requests for Elsevier materials may attract a fee.

7. Reservation of Rights: Publisher reserves all rights not specifically granted in the combination of (i) the license details provided by you and accepted in the course of this licensing transaction, (ii) these terms and conditions and (iii) CCC's Billing and Payment terms and conditions.

8. License Contingent Upon Payment: While you may exercise the rights licensed immediately upon issuance of the license at the end of the licensing process for the transaction, provided that you have disclosed complete and accurate details of your proposed use, no license is finally effective unless and until full payment is received from you (either by publisher or by CCC) as provided in CCC's Billing and Payment terms and conditions. If full payment is not received on a timely basis, then any license preliminarily granted shall be deemed automatically revoked and shall be void as if never granted. Further, in the event that you breach any of these terms and conditions or any of CCC's Billing and Payment terms and conditions, the license is automatically revoked and shall be void as if never granted. Use of materials as described in a revoked license, as well as any use of the materials beyond the scope of an unrevoked license, may constitute copyright infringement and publisher reserves the right to take any and all action to protect its copyright in the materials.

9. Warranties: Publisher makes no representations or warranties with respect to the licensed material.

10. Indemnity: You hereby indemnify and agree to hold harmless publisher and CCC, and their respective officers, directors, employees and agents, from and against any and all claims arising out of your use of the licensed material other than as specifically authorized pursuant to this license.

11. No Transfer of License: This license is personal to you and may not be sublicensed, assigned, or transferred by you to any other person without publisher's written permission.

12. No Amendment Except in Writing: This license may not be amended except in a writing signed by both parties (or, in the case of publisher, by CCC on publisher's behalf).

13. Objection to Contrary Terms: Publisher hereby objects to any terms contained in any purchase order, acknowledgment, check endorsement or other writing prepared by you, which terms are inconsistent with these terms and conditions or CCC's Billing and Payment terms and conditions. These terms and conditions, together with CCC's Billing and Payment terms and conditions (which are incorporated herein), comprise the entire agreement between you and publisher (and CCC) concerning this licensing transaction. In the event of any conflict between your obligations established by these terms and conditions and those established by CCC's Billing and

Payment terms and conditions, these terms and conditions shall control.

14. Revocation: Elsevier or Copyright Clearance Center may deny the permissions described in this License at their sole discretion, for any reason or no reason, with a full refund payable to you. Notice of such denial will be made using the contact information provided by you. Failure to receive such notice will not alter or invalidate the denial. In no event will Elsevier or Copyright Clearance Center be responsible or liable for any costs, expenses or damage incurred by you as a result of a denial of your permission request, other than a refund of the amount(s) paid by you to Elsevier and/or Copyright Clearance Center for denied permissions.

LIMITED LICENSE

The following terms and conditions apply only to specific license types:

15. **Translation**: This permission is granted for non-exclusive world **English** rights only unless your license was granted for translation rights. If you licensed translation rights you may only translate this content into the languages you requested. A professional translator must perform all translations and reproduce the content word for word preserving the integrity of the article.

16. **Posting licensed content on any Website**: The following terms and conditions apply as follows: Licensing material from an Elsevier journal: All content posted to the web site must maintain the copyright information line on the bottom of each image; A hyper-text must be included to the Homepage of the journal from which you are licensing at http://www.sciencedirect.com/science/journal/xxxxx or the Elsevier homepage for books at http://www.elsevier.com; Central Storage: This license does not include permission for a scanned version of the material to be stored in a central repository such as that provided by Heron/XanEdu.

Licensing material from an Elsevier book: A hyper-text link must be included to the Elsevier homepage at http://www.elsevier.com . All content posted to the web site must maintain the copyright information line on the bottom of each image.

Posting licensed content on Electronic reserve: In addition to the above the following clauses are applicable: The web site must be password-protected and made available only to bona fide students registered on a relevant course. This permission is granted for 1 year only. You may obtain a new license for future website posting.

17. **For journal authors:** the following clauses are applicable in addition to the above:

Preprints:

A preprint is an author's own write-up of research results and analysis, it has not been peer-reviewed, nor has it had any other value added to it by a publisher (such as formatting, copyright, technical enhancement etc.).

Authors can share their preprints anywhere at any time. Preprints should not be added to or enhanced in any way in order to appear more like, or to substitute for, the final versions of articles however authors can update their preprints on arXiv or RePEc with their Accepted Author Manuscript (see below).

If accepted for publication, we encourage authors to link from the preprint to their formal publication via its DOI. Millions of researchers have access to the formal publications on ScienceDirect, and so links will help users to find, access, cite and use the best available version. Please note that Cell Press, The Lancet and some society-owned have different preprint policies. Information on these policies is available on the journal homepage.

Accepted Author Manuscripts: An accepted author manuscript is the manuscript of an article that has been accepted for publication and which typically includes author-incorporated changes suggested during submission, peer review and editor-author communications.

Authors can share their accepted author manuscript:

- – immediately
    - via their non-commercial person homepage or blog
    - by updating a preprint in arXiv or RePEc with the accepted manuscript
    - via their research institute or institutional repository for internal institutional uses or as part of an invitation-only research collaboration work-group
    - directly by providing copies to their students or to research collaborators for their personal use
    - for private scholarly sharing as part of an invitation-only work group on commercial sites with which Elsevier has an agreement
- – after the embargo period
    - via non-commercial hosting platforms such as their institutional repository

- via commercial sites with which Elsevier has an agreement

In all cases accepted manuscripts should:

- – link to the formal publication via its DOI
- – bear a CC-BY-NC-ND license - this is easy to do
- – if aggregated with other manuscripts, for example in a repository or other site, be shared in alignment with our hosting policy not be added to or enhanced in any way to appear more like, or to substitute for, the published journal article.

Published journal article (JPA): A published journal article (PJA) is the definitive final record of published research that appears or will appear in the journal and embodies all value-adding publishing activities including peer review co-ordination, copy-editing, formatting, (if relevant) pagination and online enrichment.

Policies for sharing publishing journal articles differ for subscription and gold open access articles:

Subscription Articles: If you are an author, please share a link to your article rather than the full-text. Millions of researchers have access to the formal publications on ScienceDirect, and so links will help your users to find, access, cite, and use the best available version.

Theses and dissertations which contain embedded PJAs as part of the formal submission can be posted publicly by the awarding institution with DOI links back to the formal publications on ScienceDirect.

If you are affiliated with a library that subscribes to ScienceDirect you have additional private sharing rights for others' research accessed under that agreement. This includes use for classroom teaching and internal training at the institution (including use in course packs and courseware programs), and inclusion of the article for grant funding purposes.

Gold Open Access Articles: May be shared according to the author-selected end-user license and should contain a CrossMark logo, the end user license, and a DOI link to the formal publication on ScienceDirect.

Please refer to Elsevier's posting policy for further information.

18. **For book authors** the following clauses are applicable in addition to the above: Authors are permitted to place a brief summary of their work online only. You are not allowed to download and post the published electronic version of your chapter, nor may you scan the printed edition to create an electronic version. **Posting to a repository:** Authors are permitted to post a summary of their chapter only in their institution's repository.

19. **Thesis/Dissertation**: If your license is for use in a thesis/dissertation your thesis may be submitted to your institution in either print or electronic form. Should your thesis be published commercially, please reapply for permission. These requirements include permission for the Library and Archives of Canada to supply single copies, on demand, of the complete thesis and include permission for Proquest/UMI to supply single copies, on demand, of the complete thesis. Should your thesis be published commercially, please reapply for permission. Theses and dissertations which contain embedded PJAs as part of the formal submission can be posted publicly by the awarding institution with DOI links back to the formal publications on ScienceDirect.

Elsevier Open Access Terms and Conditions

You can publish open access with Elsevier in hundreds of open access journals or in nearly 2000 established subscription journals that support open access publishing. Permitted third party re-use of these open access articles is defined by the author's choice of Creative Commons user license. See our open access license policy for more information.

Terms & Conditions applicable to all Open Access articles published with Elsevier:

Any reuse of the article must not represent the author as endorsing the adaptation of the article nor should the article be modified in such a way as to damage the author's honour or reputation. If any changes have been made, such changes must be clearly indicated.

The author(s) must be appropriately credited and we ask that you include the end user license and a DOI link to the formal publication on ScienceDirect.

If any part of the material to be used (for example, figures) has appeared in our publication with credit or acknowledgement to another

Dear Andrea Salis

Thank you for your correspondence requesting permission to reproduce the following article published in our journal in your printed thesis and to be posted in your university's repository University of Sassari.

'Engineered microparticles based on drug–polymer coprecipitates for ocular-controlled delivery of Ciprofloxacin: influence of technological parameters' By Elisabetta Gavini, Maria Cristina Bonferoni, Giovanna Rassu, Giuseppina Sandri, Silvia Rossi, Andrea Salis, Elena Piera Porcu, Paolo Giunchedi Drug Development and Industrial Pharmacy

We will be pleased to grant permission on the sole condition that you acknowledge the original source of publication and insert a reference to the article on the Journals website:

This is the authors accepted manuscript of an article published as the version of record in Drug Development and Industrial Pharmacy 2015 http://www.tandfonline.com/ http://dx.doi.org/10.3109/03639045.2015.1100201

Please note that this license does not allow you to post our content on any third party websites or repositories.

Thank you for your interest in our Journal.

Yours sincerely

Michelle Dickson – Permissions & Licensing Executive, Journals.

Routledge, Taylor & Francis Group.

4 Park Square, Milton Park, Abingdon, Oxon, OX14 4RN, UK.

Tel: +44 (0)20 7017 7413

Fax:+44 (0)20 7017 6336

Web: www.tandfonline.com

e-mail: Michelle.Dickson@tandf.co.uk

From: Andrea Salis [mailto:asalis@uniss.it]
Sent: 26 October 2015 11:18
To: Academic Journals Society Permissions
Subject: Re: iddi20:Engineered microparticles based on drug–polymer coprecipitates for ocular-controlled delivery of Ciprofloxacin: influence of technological parameters

AKNOWLEDGEMENTS

Thanks to Regione Autonoma Sardegna (RAS), Obiettivo competitività regionale e occupazione, Asse IV Capitale umano, Linea di Attività l.3.1, for supporting my PhD programme.